Contourite drifts and cold-water coral mounds in the Atlantic Moroccan coral province.
Origin, evolution and driving factors.

Thomas Vandorpe

Supervisor: Prof. Dr. David Van Rooij
Co-supervisor: Prof. Dr. Veerle Cnudde

Academic year 2016–2017

Submitted to the Faculty of Science of Ghent University
in fulfilment of the requirements for the degree of
Doctor of Science: Geology

Contourite drifts and cold-water coral mounds in the Atlantic Moroccan coral province

Origin, evolution and driving factors

Contourietdriften en koudwaterkoraalheuvels in de Atlantische Marokkaanse koraalprovincie

Oorsprong, evolutie en sturende factoren

Thomas Vandorpe

2017

Dissertation submitted for the degree of Doctor of Science: Geology

Supervisors: Prof. Dr. David Van Rooij & Prof. Dr. Veerle Cnudde

UNIVERSITEIT GENT

FACULTEIT WETENSCHAPPEN

Members of the examination committee:

Prof. Dr. S. Louwye (Ghent University, Belgium): chair

Prof. Dr. M. De Batist (Ghent University, Belgium): secretary

Prof. Dr. J. Hernández-Molina (Royal Holloway University London, United Kingdom)

Prof. Dr. D. Hebbeln (University of Bremen, Germany)

Dr. M. Van Daele (Ghent University, Belgium)

Prof. Dr. D. Van Rooij (Ghent University, Belgium): supervisor

Prof. Dr. V. Cnudde (Ghent University, Belgium): supervisor

To refer to this thesis: Vandorpe, T., 2017. Contourite drifts and cold-water coral mounds in the Atlantic Moroccan Coral Province: origin, evolution and driving factors. PhD thesis, Ghent University, Ghent, Belgium.

Research highlights

- **Topographic obstacles have a profound effect on sedimentation patterns**. When bottom currents encounter topographic obstacles, they focus and intensify, leading to sediment drifts at the base. Along the tectonic ridges of the Atlantic Moroccan margin, 11° is the threshold for sediment drift formation, while along the mud volcanoes, sediment drifts are present at the southern and/or northern side and are related to the size of the mud volcano.
- **Internal tides play an important role in the build-up of sediment drifts.** Although the sediment drifts along the Atlantic Moroccan margin were mainly driven by glacial water masses, internal tidal currents play an important role in their development. They are driving long-term bottom currents and consequently influence sediment drift deposition along the tectonic ridges and mud volcanoes. Sediment drifts created or influenced by internal tidal currents could be named tidal sediment drifts and a limited extent is proposed.
- **Coral mound build-up is related to climatic changes and interferes with its immediate surroundings.** The Atlantic Moroccan coral province is the largest discovered coral mound province in the world so far and possesses stratigraphic evidence, 10 different initiation horizons in the subsurface, of climate-dependant growth cycles of cold-water corals. Small-scale sediment drifts are created around some of the coral mounds, evidencing deviated and intensified bottom currents. This creates elevated fluxes of food particles and sediment towards the corals, allowing proliferation.
- **Diagnostic criteria for contourites could be developed based on CT analyses of sediment cores.** A workflow for analysing CT-scans, based on the grey values within the radiographs, of sediment cores has been developed which can aid in the discovery of diagnostic criteria to distinguish contourites from turbidites and pelagites. Higher Hounsfield unit values have been linked to more energetic sedimentation environments, related to the strength of the bottom currents at the time of deposition.

Table of content

List of figures

List of Tables

List of abbreviations

AAIW	Antarctic Intermediate Water
ADCP	Acoustic Doppler Current Profiler
AMCP	Atlantic Moroccan Coral Province
AUGC	Allochthonous Unit of the Gulf of Cádiz
AVO	Amplitude versus Offset
BQD	Base Quaternary Discontinuity
CDC	Contourite Depositional Complex
CDS	Contourite Depositional System
CT	X-ray Computed Tomography
CTD	Conductivity Temperature Depth
CWC	Cold-Water Coral
EAMVP	El Arraiche Mud Volcano Province
EMPT	Early Middle-Pleistocene Transition
GMV	Gemini Mud Volcano
HU	Hounsfield Unit
IODP	Integrated Ocean Discovery Program
LADCP	Lowered Acoustic Doppler Current Profiler
MIS	Marine Isotopic Stage
MOW	Mediterranean Outflow Water
MPR	Mid-Pleistocene Revolution
MS	Magnetic Susceptibility
MSCL	Multi Sensor Core Logger
NACW	North Atlantic Central Water
NADW	North Atlantic Deep Water
NASW	North Atlantic Surface Water
PDE	Pen Duick Escarpment
PVC	Poly Vinyl Chloride
R/V	Research Vessel
SBP	Sub-Bottom Profiler
SWIM	Southwestern Iberian Margin
TASYO	Transferencia Sedimentaria en Talud Y Mega-Olistostromas
TWT	Two-Way Travel time
XRF	X-Ray Fluorescence

Acknowledgments

David, jij hoort hier op de eerste plaats te staan. Zonder jou zou dit werk nooit afgeraakt zijn. Ik wil je extreem hard bedanken voor de mogelijkheid om dit doctoraat aan te vatten, de vele discussies die we gehad hebben en je immer wijze raad. Je was een geweldige promotor en dat 6 jaar lang!

Veerle en **Marc**, ook jullie hebben mij steeds met wijze raad bijgestaan. **Veerle**, bedankt voor de introductie tot het hele CT-gebeuren, de raad die je mij gaf en de discussies op het einde. **Tist**, ook jij hebt een wezenlijk aandeel in dit doctoraat. Die kleine opmerkingen die je gaf tijdens de lunch waardoor ik sommige zaken in twijfel trok of op een andere manier ging denken waren immer waardevol.

Hui, **Marta**, **Kainan**, **Zak**, **Shan**, **Carmen** en **Philipp**. Thanks for sharing the office with me. I am extremely grateful for all the little discussions we had (scientific and non-scientific) during our office-time. I will miss it a lot.

Stan, **Tim**, **Koen**, **Katrien, Elke, Nore** and **Wim**. Thanks for all those wonderful memories onboard the Belgica, Lutris or Garcia del Cid. You are great colleagues, whom it is a pleasure to work with on board of the scientific vessels.

The rest of the RCMG-gang. What a perfect work-environment you guys created. I will always remember the New Year dinners, the BBQ's, the croques-noons, … I will try to list all of you here, but I am sure that I will forget important people. An apology up front! **Agostina**, **David**, **Maikel**, **Oscar**, **Vasilis**, **Evelien**, **Katleen**, **Maarten**, **Thomas**, **Ann**, **Eleonora**, **Loïc**, **Dawei**, **Tine**, **Jean**-Pierre, **Marga**, **Seb**, **Lies**, **Jasper**, **Lieven**, **Willem**, **Mario**.

De rest van het AAP and ZAP van de vakgroep met wie het een plezier was om samen te werken. Wat een goed-geoliede machine zijn jullie! **Pieter**, **Tim**, **Julie**, **Koen**, **Elien**, **Mathijs**, **Stephen**, **Jacques**, **Thijs**, **Johan**, **Peter**, **Patrick**, **Eric**, **Kristine**.

Wim, **Marc** & **Kurt**, bedankt voor alle bijstand die jullie verleenden gedurende deze 6 jaar. Nooit hebben jullie laten blijken hoe belachelijk 1 van mijn vele administratieve of IT-gerelateerde vragen wel niet waren.

Javier, **Gemma**, **Pere**, **Elia**, **Peter**, **Marga**, **Dierk**, **Claudia**, **Isabel**, **Damien**, **Anxo**, **Ruth**, **Paulien**, **Ruth**, **Luis** and all the others who made sure that the marine/lacustrine campaigns will forever remain an unforgettable experience: Thanks you so much!!!!

The captains and crew of the R/V Belgica during the period 2011-2017. Thanks a lot for all the help during the campaigns we had on board of the vessel. Thanks a lot for your support to make the promotional video of the MiniMound-survey. You made those surveys unforgettable.

Also the captains and crews of the **research vessels** (R/V Belgica, R/V Pelagia, R/V Maria S. Merian, R/V Pelagia and R/V Sarmiento de Gamboa) who gathered the data used for this dissertation are acknowledged for their support!

Last (but not least) on the scientific front are the **reviewers** who helped improve the manuscripts related to chapters 4, 5 and 6. They improved the quality enormously and thereby the quality of this dissertation.

Op persoonlijk vlak moet ik mijn vriendin, Sharon, en **mijn ouders**, **familie** (**Jonas** en **Julie** vooral) en vrienden enorm bedanken. Ze waren er altijd voor mij en hebben op enkele moeilijke momenten mij er steevast bovenop geholpen.

Sharon, het laatste jaar van mijn doctoraat is soms niet van een leien dakje gelopen, maar je steunde mij desalniettemin in alles. Dat is enorm van jou en deed zo veel deugd! **Nico**, **Jelle**, **Wim** en **Borra**, de weekendjes waren geweldig, dat er nog vele mogen volgen! **Daf**, **Eveline**, **Thomas**, **Stefanie**, **Jamina**, **Nadim**, **Valerie**, **Nele**, **Charlotte**, **Charlotte** en **Jolien**, ook met jullie waren de weekends geweldig. Dit moet en zal een jaarlijkse traditie blijven. Aan alle andere vrienden die nog niet genoemd zijn (**Bock**, **Ward**, **Benjamin**, **Eva**, **Silke**, **GT**, …) ook een geweldige merci. Zonder jullie (en bijhorende café-bezoeken) had ik nooit zo rustig het einde van mijn doctoraat gehaald.

Hopelijk heb ik niemand vergeten (ook al ben ik zeker van wel). In ieder geval, ook aan jullie bedankt!

Samenvatting

Bodemstromingen werden voor het eerst beschreven in 1751, maar het duurde tot de jaren '50 en '60 van de vorige eeuw vooraleer ze de eigenschap werden toegedicht sedimenten te kunnen vervoeren en deze tegelijk af te zetten. Bodemstromingen komen voor in verschillende gedaantes; gaande van brede, continue, contour-volgende stromingen die een onderdeel zijn van de huidige thermohaliene circulatie tot kortstondige, episodische en semi-dagelijkse interne getijdenstromingen, geïnduceerd door het contactoppervlak tussen twee watermassa's met sterk verschillende eigenschappen. Zodoende bestrijken ze een heel breed spectrum en kunnen ze overal voorkomen, van de shelf tot de diepzee.

Contourieten zijn het product van bodemstromingen en worden tegenwoordig gedefinieerd als sedimenten afgezet of gedeeltelijk herwerkt door de blijvende actie van bodemstromingen. In wezen zijn ze een van de drie eindproducten van een continuüm van diepzeeafzettingen. De andere zijn turbidieten, resulterend van episodisch hellingafwaartse processen, en pelagieten, resulterend uit het verticaal bezinken van sediment in de waterkolom. Sedimentdriften zijn de morfologische eenheden waarin deels contourieten aanwezig zijn en komen voor in verschillende maten en gewichten, gaande van extensieve *'sheeted drifts'* tot kleinschalige *'patch drifts'*. Ze kunnen overal voorkomen waar voldoende sedimentaanvoer aanwezig is, waar bodemstromingen sterk genoeg zijn en waar de ruimte aanwezig is om sedimenten af te zetten. Contourieten worden gekenmerkt door verhoogde sedimentatiesnelheden en zijn aldus preferentiële sites voor paleoklimatologische en paleoceanografische studies.

Koudwaterkoralen zijn koralen die voorkomen in de diepzee en leven in afwezigheid van licht. Ze komen meestal voor op dieptes tussen 50 en 1000 m, maar er zijn specimen gevonden die voorkomen op 4000 m. Koudwaterkoralen kunnen koraalheuvels vormen, een samenhang van koraalfragmenten en sedimentpartikels, beide aangevoerd door bodemstromingen die ze door hun koraalskelet spoelen. Deze heuvels kunnen tot 200 m hoog uitgroeien en bestaan uit verschillende episodes van koraalgroei en periodes van voornamelijk (hemi-) pelagische sedimentatie. De groei van koudwaterkoralen is sterk afhankelijk van het klimaat en bijgevolg zijn ook koraalheuvels uitstekende locaties om de klimatologische veranderingen doorheen de tijd in het studiegebied te bestuderen.

Langs de Atlantisch Marokkaanse rand, ten zuiden van de Straat van Gibraltar komen zowel verschillende sedimentdriften als koraalheuvels voor. Bovendien zijn talrijke moddervulkanen, 2 tektonische ruggen en 2 transforme breuken aanwezig. Het samen voorkomen van sedimentdriften en koraalheuvels biedt een uitstekende opportuniteit om het Quartaire paleoklimaat van de Marokkaanse rand te achterhalen. Tegelijk biedt het voorkomen van verscheidene sedimentdriften langs topografische obstakels een uitgelezen kans om de invloed van topografische verhevenheden op driftafzettingen te bestuderen.

Het onderscheiden van contourieten en turbidieten in sedimentkernen is moeilijk door hun gelijkaardige eigenschappen en dus zijn er meer diagnostische criteria nodig om het onderscheid te kunnen maken. Het faciesmodel van contourieten berust voornamelijk op sedimentologische en lithologische criteria, terwijl het onderscheid op basis van deze criteria juist problematisch is. X-stralen computertomografie (CT) is een techniek die op een snelle en non-destructieve manier toelaat sedimentkernen te onderzoeken. Het gebruik van deze techniek in contourietonderzoek spitste zich tot nu toe vooral toe op het bestuderen van sedimentologische structuren, aangezien CT-beelden een scherp en contrasterend beeld van de kern kunnen geven. Nochtans biedt CT zoveel meer

mogelijkheden. Het kwantificeren van de grijswaarden, bekomen door de scans, laat toe om het contourietfacies op een geheel andere manier te definiëren en kan mogelijks een uitweg bieden in het determineren en onderscheiden van dit facies. De CT-beelden van 5 kernen van de noordelijke Golf van Cadiz en de Alboraanse Zee werden geanalyseerd met als doel hun contourietintervallen te kwantificeren en te beschrijven. Deze studie heeft als uiteindelijke doel diagnostische criteria te kunnen onderscheiden voor hun herkenning en zodoende beter turbidieten en contourieten te kunnen herkennen.

De methodes (**Hoofdstuk 3**) die gebruikt werden om de vooropgestelde doelen te bereiken bestaan voornamelijk uit geofysische methodes. Meer dan 3000 kilometer aan seismische profielen werden vergaard, gebruik makend van 2 verschillende bronnen, met name een SIG sparker en een ATLAS parametrische echosounder. De sparker kan grotere dieptes bereiken (tot 300 m in de ondergrond), terwijl de echosounder een hogere resolutie haalt (decimeterschaal). Beide datasets hadden een uitgebreide verwerking nodig alvorens ze konden worden geïnterpreteerd. De kartering van het gebied gebeurde aan de hand van twee multibeam datasets. De ene werd vergaard in 2002 door middel van een SIMRAD EM1002 systeem en de andere in 2008 gebruik makend van een Kongsberg EM300 systeem. Naast deze geofysische methodes werden er ook oceanografische metingen verricht. Hiervoor werden verschillende CTD (conductiviteit, temperatuur en diepte) profielen vergaard en ADCP (*acoustic Doppler current profiler*) metingen uitgevoerd. De eerste geven de fysische eigenschappen van de waterkolom, terwijl de laatste de stromingsrichting en –sterkte aanduiden. Tevens werden waterstalen genomen op verschillende dieptes en de nutriënteninhoud bepaald zodoende de verschillende watermassa's te kunnen onderscheiden. Sedimentkernen werden onderzocht aan de hand van een MSCL (*multi-sensor core logger*) en XRF (X-straal fluorescentie) toestel om de fysische (MSCL) en chemische (XRF) eigenschappen te achterhalen. Korrelgrootteanalyses werden uitgevoerd gebruik makend van een Malvern Masterseizer, een toestel dat de groottes meet aan de hand van laserdiffractie. Tenslotte werden de CT scans bekomen gebruikend makend van de medische SOMATOM scanner van het UZ Gent. De bekomen resolutie was 0.2x0.2x0.6 mm en de beelden werden gereconstrueerd gebruik makend van het '*J37 smooth medium*' algoritme.

De seismische stratigrafie van de Pen Duick en Renard noord driftsystemen werd toegelicht in **Hoofdstuk 4**. Hiervoor werd voornamelijk gebruik gemaakt van de seismische (sparker) en de multibeam dataset. Resultaten duiden aan dat er 5 verschillende eenheden onderscheiden kunnen worden, waarvan de 4 meest recente beïnvloed werden door bodemstromingen. Vanaf de start van het Quartair tot aan de EMPT (Vroeg Midden-Pleistocene transitie) bestond de sedimentatie aan de voet van de tektonische ruggen vooral uit *'sheeted drifts'*, terwijl vanaf de EMPT voornamelijk *'mounded drifts'* voorkomen. Vanaf de EMPT kunnen 10 subeenheden onderscheiden worden, die elk gelinkt werden aan glaciale periodes. De driften werden aanzienlijk beïnvloed door het omhoogkomen van de tektonische ruggen (tot aan de EMPT), aangeduid door het uitsterven van de reflectoren op de ruggen, en de uitvloei van modder uit de moddervulkanen, aangeduid door de kerstboomstructuur in de ondergrond. In de 'moat' aan de voet van de Pen Duick helling bevinden zich 7 koraalheuvels, die de stromingen beïnvloeden en de ligging van de 'moat' verplaatsen. Op hun beurt worden zij beïnvloed door de bodemstromingen aangezien ze een 'sediment' en 'koraal' kant bezitten. De stratigrafie van de driften duidt aan dat deze geen gelijkenissen vertoont met driften gelinkt aan het Mediterrane uitstroom water en bijgevolg moet de oorzaak van deze driften elders gezocht worden. Het AAIW (Antarctisch Intermediair Water) is een geschikte kandidaat door zijn bewezen aanwezigheid in de zuidelijke Golf van Cádiz.

De positie en sturende factoren van de verschillende driftsystemen in relatie tot de aanwezige watermassa's en bodemstromingen in de EAMVP (*El Arraiche mud volcano province*) werden

onderzocht in **Hoofdstuk 5**. Hiervoor werd opnieuw gebruik gemaakt van de multibeam en seismische (sparker) dataset, maar tevens van de oceanografische (CTD, ADCP en nutriënt-inhoud) metingen. Deze laatste toonden aan dat zowel NACW (Noord-Atlantisch Centraal Water) als AAIW aanwezig zijn langs de Atlantisch Marokkaanse rand. De stromingen waren hoofdzakelijk zuid-noord gericht, maar op de bodem was een complex patroon aanwezig, toegedicht aan de afbuiging van de bodemstromingen op de topografieën en de bewezen aanwezigheid van interne getijden. De positie van de driftsystemen langs de tektonische ruggen is bepaald door de steiltegraad van de ruggen, terwijl de driftsystemen langs de moddervulkanen (aan zowel de noord- als zuidzijde) ontstaan door de asymmetrische interne getijdenstromingen. Deze laatste kunnen ook erosieve componenten veroorzaken wanneer ze gedwongen worden door een nauwe passage te stromen. Tevens kunnen hierin *'patch drifts'* voorkomen. In de AMCP werd voor het eerst de link tussen steiltegraad en driftvoorkomen beschreven en werd het voorkomen van sedimentdriften voor het eerst aan interne getijdenstromingen gekoppeld. Deze conclusies kunnen bijdragen aan het verder begrijpen van de dynamische interacties tussen bodemstromingen en topografieën, waardoor mogelijks duizenden extra driften ontdekt kunnen worden.

De '*Atlantic Moroccan coral province'* (AMCP) is tot op heden de grootste ontdekte koraalprovincie ter wereld en is tevens de eerste koraalprovincie waar op grote schaal meerdere ontstaansniveaus kan aangetoond worden. Koraalheuvels werden in grote getale geobserveerd, zowel op de zeebodem als in de ondergrond. Hun spatiale en temporele evolutie werd besproken in **Hoofdstuk 6**. Hiervoor werd gebruik gemaakt van de seismische (zowel sparker als echosounder) en multibeam dataset. De heuvels zijn gemiddeld 20 meter hoog en ontwikkelden zich op verschillende tijdstippen, aangeduid door de aanwezigheid van minstens 10 ontstaansniveaus in de ondergrond. Sommige koraalheuvels spannen meerdere periodes, maar de meeste bleven relatief klein en werden begraven alvorens een nieuwe koraalgroeiperiode aanbrak. De 10 ontstaansniveaus werden tentatief gelinkt aan glaciale periodes vanaf de EMPT tot het heden, gezien de meerderheid van de ouderdommen (bekomen door absolute dateringen van koralen) uit dit gebied gelinkt zijn aan glaciale periodes. Deze link kan duiden op een sterk klimaat beïnvloede groei van koudwaterkoralen langs deze rand. Koraalheuvels lijken gegroepeerd voor te komen in de AMCP en dit kan verklaard worden door de afbuiging van bodemstromingen op koraalheuvels, wat leidt tot versterkte en meer gefocuste stromingen rond de koraalheuvel. Deze condities zijn ideaal voor andere koralen, aangezien ze lokaal een hogere flux aan voedsel en sediment (beide noodzakelijk voor hun groei) veroorzaken. Zodoende creëren koraalheuvels voor zichzelf een positief effect op de omgeving en dus de verdere ontwikkeling van koralen in de nabijheid.

Eenduidige onderscheidende eigenschappen om contourieten te herkennen in sedimentkernen zijn er nog niet. CT kan hierbij een grote hulp zijn, aangezien de eigenschappen van contourieten op basis van deze techniek nog niet in rekening werden gebracht bij hun identificatie. In **Hoofdstuk 7** werden 5 kernen geanalyseerd aan de hand van CT scans, XRF, MSCL en korrelgroottemetingen. Een stappenplan is opgesteld waarbij componenten worden onderscheiden op basis van het grijswaardenhistogram van de kern. De variaties van deze componenten doorheen de kern werden vergeleken met contourietintervallen en naast XRF, MSCL en korrelgrootte data geplot. Een directe link (op basis van deze 5 kernen) werd aangetoond tussen verhoogde Hounsfield eenheden (HU) en sterkere bodemstromingen (afgeleid van grovere korrelgroottes en een hogere ratio Zr/Al). Daarnaast kon een continue verhoging van de HU waarden worden vastgesteld naarmate meer energetische sedimentatie-omstandigheden heersten. Dit zet de link tussen HU waarden en bodemstromingen nog meer in de verf. Het analyseren van extra kernen uit verschillende sedimentatieomgevingen (contouriet-turbidiet-pelagiet) is echter noodzakelijk alvorens deze bevindingen bevestigd kunnen worden en de techniek algemeen toegepast.

De resultaten bekomen uit hoofdstukken 4-7 roepen enkele vragen op en onderlinge vergelijkingen leiden tot bemerkingen bij bestaande classificaties en definities. Deze vragen en bemerkingen zijn het onderwerp van **Hoofdstuk 8**. De stratigrafie bekomen in hoofdstukken 4 en 6 is niet in overeenstemming vanaf de EMPT. Dit kan aan meerdere oorzaken hebben. Twee voor de hand liggende oorzaken zijn het gebrek aan tektonische activiteit die bepaalde markers zou kunnen geven en het gebrek aan absolute dateringen van zowel de sedimentdriften als de koraalheuvels. Op basis van berekende sedimentatiesnelheden lijkt de koraalheuvelstratigrafie de meest plausibele, maar ook deze stratigrafie kan 1 of meerdere verkeerde ouderdom-diepte correlaties bevatten. Tevens is geopperd dat de AMCP de eerste regio is waar sedimentdriften direct gelinkt zijn aan interne getijdenstromingen. Voor de grotere 'mounded drifts' langs de tektonische ruggen zijn ze een helpende factor, maar voor de 'patch drifts' langs de moddervulkanen worden ze als enige bepalende factor naar voren geschoven, een primeur. Tevens is de opbouw van de sedimentdriften langs de tektonische ruggen deels te wijten aan de invloed van twee watermassa's die in dezelfde richting stromen. Opnieuw een bewijs dat contouriet afzettingssystemen wel degelijk kunnen ontstaan (of onderhouden worden) door meer dan één watermassa. Op basis van de kleine driftsystemen langs de moddervulkanen en koraalheuvels kon een nieuwe classificatie aangaande 'patch drifts' worden opgesteld. Het voorzetsel 'tidal' werd ook voorgesteld om sedimentdriften te beschrijven die (op zijn minst gedeeltelijk) door interne getijdenstromingen ontstaan of onderhouden worden. Voor deze 'tidal' sedimentdriften wordt een maximale omvang voorgesteld, zijnde het gebied waar effectief bodemstromingen invloed hadden op de sedimentatie. Anders zou een groot deel van de oceaanbodem bedekt zijn met sedimentdriften, wat geen weergave zou zijn van de realiteit waar stromings-beïnvloede sedimenten zich bevinden. Deze beperking wordt in de hand gewerkt door de observatie dat sedimentdriften kunnen ontstaan waar bodemstromingen afbuigen op verhevenheden boven een bepaalde steiltegraad (in dit geval 11°), wat zou betekenen dat een groot aantal extra kleinschalige driften kan ontdekt worden. Tenslotte worden de conclusies aangaande de CT analyses van contourietkernen in een breder daglicht gesteld. De differentiatie met turbidieten blijft moeilijk, aangezien ook turbidieten uit hoger-energetische omgevingen afgezet worden. Bijgevolg zijn extra analyses nodig alvorens algemene onderscheidende eigenschappen kunnen bekomen worden. Hiervoor zijn sedimentkernen nodig die zowel pelagieten, turbidieten als contourieten bevatten.

In **Hoofdstuk 9** worden de belangrijkste conclusies van deze thesis opgesomd. Deze behandelen (1) de klimaat gerelateerde groei van koudwaterkoralen en koraalheuvels in de AMCP, (2) de spatiale en temporele evolutie van de sedimentdriften in de EAMVP, (3) de link tussen oceanografische processen en driftafzettingen, (4) de classificatie en omvang van (vooral kleinschalige) sedimentdriften en (5) de analyse van sedimentkernen aan de hand van CT analyses. Daarnaast worden enkele mogelijke toekomstige onderzoeken voorgesteld die de bekomen resultaten kunnen uitdiepen en verifiëren. Deze bestaan voornamelijk uit het bekomen van sedimentkernen, langdurige oceanografische metingen uitvoeren, extra geofysische data vergaren en extra gerichte CT-analyses uitvoeren van sedimentkernen die turbidieten, contourieten en pelagieten bevatten.

Summary

Bottom currents were described for the first time in 1751, but it wasn't until the 1950's and 60's they were acknowledged for being able to transport and deposit sediments. Bottom currents can have a wide variety of shapes and sizes, ranging from broad, continuous, contour-following currents that are part of the global thermohaline circulation till ephemeral, episodic, semi-diurnal internal tidal currents, induced by the interface between two water masses with very different characteristics. As such, they cover a wide spectrum and can occur anywhere in the ocean, from the upper shelves till the abyssal depths.

Contourites result from bottom currents and are defined nowadays as sediments deposited or at least partly reworked by the persistent action of bottom currents. They are one of the three endmembers of a continuum of deep-sea deposits besides turbidites, resulting from episodic downslope processes, and pelagites, resulting from vertical settling of sediment particles in the water column. Sediment drifts are morphological units consisting (at least partly) of contourites and occur in many different shapes and sizes, ranging from extensive sheeted drifts till small-scale patch drifts. They can occur anywhere sufficient sediment is at their disposal, bottom currents are strong enough and ample accommodation space is present. Contourites are characterized by elevated sedimentation rates and are as such preferred sites for palaeoclimatic and palaeoceanographic research.

Cold-water corals are corals that live in the deep-sea in the absence of light. They occur mostly at depths between 50 and 1000 m, but specimen have been found at 4000 m. Cold-water corals have the ability to create cold-water coral mounds (hereafter called coral mounds), which are a combination of coral fragments and sediment particles. Both are delivered by bottom currents, which flush them through their framework. These coral mounds can reach heights exceeding 200 m and contain several periods of coral growth and periods of mainly (hemi-) pelagic sedimentation. The growth of cold-water corals is strongly depending upon climate and consequently, coral mounds are perfect features to study the effects of changing climate in the study area.

Along the Atlantic Moroccan margin, south of the Strait of Gibraltar, several sediment drifts and a large amount of coral mounds occur. Additionally, numerous mud volcanoes, two tectonic ridges and two transform faults are present. The co-occurrence of sediment drifts and coral mounds offers an excellent opportunity to unravel the Quaternary palaeoclimate of the Atlantic Moroccan margin. Furthermore, the occurrence of several sediment drifts along the topographic obstacles also provides the opportunity to study the effect of topographic obstacles on drift deposition.

The differentiation between contourites and turbidites in sediment cores is difficult due to their similar characteristics and consequently, more diagnostic criteria are required in order to discern them. The facies model of contourites mostly relies on sedimentological and lithological criteria, while the differentiation based on those criteria is problematic. X-ray computed tomography (CT) is a non-destructive method which allows to investigate sediment cores rather fast. The applications of this technique in contourite research mainly focused on sedimentological structures as X-ray radiographs yield a sharp and contrasting image of the sediment core. However, CT offers much more possibilities; quantification of the grey values, obtained from the radiographs, allows to define the contourite facies in an entirely different way and may offer a solution in determining and distinguishing this facies from turbidites and pelagites. The radiographs of 5 cores from the northern Gulf of Cádiz and the Alboran Sea were analysed to quantify and describe their contourite intervals in order to determine diagnostic criteria that can be used for their recognition in the sedimentary record.

The methods (**Chapter 3**) used to achieve the goals mainly consisted of geophysical methods. Over 3000 km of seismic profiles were gathered, using two different source, a SIG sparker and an ATLAS parametric echosounder. The sparker can reach greater depths (up till 300 m in the subsurface), while the echosounder achieves a higher resolution (decimetre-scale). Both datasets underwent extensive processing before they were interpreted. Multibeam maps were obtained based on two datasets, one gathered in 2002 using a SIMRAD E1002 system and one in 2008 using a Kongsberg EM300 system. Besides these geophysical methods, oceanographic measurements were performed as well. Several CTD (conductivity temperature depth) profiles and ADCP (acoustic Doppler current profiler) measurements were gathered. CTD profiles yield the physical properties of the water column, while ADCP measurements yield current direction and intensities. Additionally, water samples were gathered at specific depths and the nutrient content of these water samples were determined in order to define the water masses. Sediment cores were analysed using MSCL (multi-sensor core logger) and XRF (X-ray fluorescence) devices to ascertain the physical (MSCL) and chemical (XRF) composition. Grain-size analyses were performed using the Malvern Masterseizer, a device that measures grain sizes based on laser diffraction. Finally, CT scans were acquired using the medical SOMATOM scanner of the UZ Ghent hospital. The obtained resolution was 0.2x0.x0.6 mm and the images were reconstructed using the 'J37 smooth medium' algorithm.

The seismic stratigraphy of the Pen Duick and Renard north drift systems were discussed in **Chapter 4**. To achieve this goal the seismic (sparker) and multibeam dataset were mainly used. Results indicate that 5 different units could be discerned, off which the 4 most recent ones were influenced by bottom currents. From the base of the Quaternary till the Early-middle Pleistocene transition (EMPT), the sedimentation mainly consisted out of sheeted drifts, while from the EMPT onwards, mounded drifts occur. Between the seafloor and the EMPT boundary, 10 subunits could be differentiated, each linked to a glacial period. The sediment drifts were substantially influenced by the uplift of the tectonic ridges (till the EMPT), indicated by the pinch-out of the reflectors on the ridges, and the extrusion of mud from the mud volcanoes, indicated by the Christmas-tree structure in the subsurface. Seven coral mounds are situated in the moat at the foot of the Pen Duick escarpment. They influence the bottom currents and induce a shift in the position of the moat. In turn, the coral mounds are influenced by the bottom currents, as they contain a sediment and a coral side. The stratigraphy of the drift systems indicates no similarities with drifts linked to the Mediterranean outflow water and consequently, the water mass that is responsible for the drifts systems originates elsewhere. The AAIW (Antarctic Intermediate Water) is a suitable candidate due to its proven presence in the southern Gulf of Cádiz.

The position and the driving factors behind the different drift systems related to the prevailing water masses and bottom currents in the EAMVP (El Arraiche mud volcano province) were investigated in **Chapter 5**. To achieve this goal, not only the multibeam and seismic (sparker) data were used, but also the oceanographic measurements (CTD, ADCP and nutrient content). The latter indicated that both NACW (North Atlantic Central Water) and AAIW are present along the Moroccan Atlantic margin. The currents are mainly directed south-north, but along the seafloor, a more complex pattern is present, related to the deviation of bottom currents on the topographies and the proven presence of internal tides. The position of the drift systems along the tectonic ridges is determined by the steepness of the ridges, while the drift systems along the mud volcanoes (both at their northern and southern side) originate due to the asymmetric internal tidal currents. The latter are also capable of creating erosional features when forced to pass through a narrow gateway. Patch drifts may occur in those erosional features. The link between the steepness of the bounding topographic features and drift occurrence has been described for the first time, as well as sediment drifts resulting from internal tidal currents. The conclusions may contribute to our understanding of the dynamic interactions between bottom

currents and topographies, which may lead to the discovery of thousands of additional drift systems all over the world.

The Atlantic Moroccan coral province (AMCP) is up till now the largest discovered coral mound province in the world as well as the first coral province where several initiation horizons are evidenced on such a broad scale. Ubiquitous coral mounds were observed on top of the seafloor as well as in the subsurface and their spatial and temporal evolution is discussed in **Chapter 6**. To achieve this goal, the seismic (both sparker and echosounder) and multibeam dataset have been studied. The coral mounds are on average 20 m high and developed during different epochs, indicated by the presence of at least 10 initiation levels in the subsurface. Some coral mounds span several epochs, but most of them remained rather small and were buried before the successive period of coral mound initiation and aggradation started. The 10 initiation levels were tentatively linked to glacial periods from the EMPT till present, given the majority of the ages (obtained by absolute datings of coral rubble) from this area are linked to glacial stages. This link indicates the strong climatic dependence of cold-water corals along this margin. Coral mounds seem to occur grouped in the AMCP, which may be explained by the deviation of bottom currents on coral mounds, resulting in more focused and intensified bottom currents around the coral mounds. These conditions are ideal for other cold-water corals, as a higher flux of food particles and sediment (both prerequisites for coral mound growth) is caused by this mechanism. As such, coral mounds exert a positive effect on their environment and induce the further development of cold-water corals in the vicinity.

Unambiguous distinctive criteria to recognize contourites in sediment cores have not yet been discovered. CT may prove to be a big asset to achieve this goal, given the characteristics of contourites based on CT scans have not yet been considered in their identification. In **Chapter 7**, five cores were analysed using CT, XRF, MSCL and grain-size measurements after which a workflow was created, allowing to discern components of the core based on the grey values histogram. The variations of these components throughout the core were compared to known contourite intervals and plotted beside XRF, MSCL and grain size data. A direct link (based on these 5 cores) between Hounsfield unit (HU) values and more vigorous bottom currents (derived from grain sizes and elevated ratios of Zr/Al) was discovered. Also a gradual increase in HU values with increasing energetic sedimentation environments was established, further highlighting the link between bottom currents and HU values. Analysing additional sediment cores from different locations is required though before this technique could be generally applied.

The results obtained from chapters 4-7 invoke several questions and mutual comparisons induce remarks regarding the current classifications and definitions. These questions and remarks are the subject of **Chapter 8**. The stratigraphies obtained in chapters 4 and 6 do not agree from the EMPT onwards. This may be caused by several factors, off which the two most important ones are the lack of tectonic activity (yielding possible markers) and the lack of absolute datings from the sediment drifts and coral mounds. Based on calculated sedimentation rates (resulting from both stratigraphies), the coral mound stratigraphy seems the most plausible, although one or several erratic age-depth correlations may be present nonetheless. The AMCP is the first region in the world where sediment drifts are linked directly to internal tidal currents. For the larger mounded drifts along the tectonic ridges, they are merely a helping factor, but for the patch drifts along the mud volcanoes, they are considered to be the sole cause. Moreover, the build-up of the sediment drifts along the tectonic ridges is related to two water masses containing bottom currents flowing in the same direction. Consequently, these drifts could support the hypothesis that contourite depositional systems may originate from (or be maintained by) more than one water mass. A new classification scheme for patch drifts was proposed based on the small drift systems along the mud volcanoes and coral mounds in

the AMCP. Additionally, the preposition 'tidal' was proposed to describe sediment drifts that are (at least partially) the result of or are maintained by internal tidal currents. A maximum extent has been proposed for these tidal sediment drifts (i.e. the area where bottom current influence can be recognized in the sedimentary record) since otherwise a large part of the ocean floor would be covered with sediment drifts, which would not represent the location of bottom-current influenced deposits. As sediment drifts can result from the deviation of bottom currents on topographic obstacles surpassing a certain steepness-threshold (11° in the AMCP), a large amount of additional (small-scale) sediment drifts could be discovered in the world's oceans, further strengthening the need of a limited extent for at least (tidal) patch drifts. Finally, the conclusions regarding CT-analyses of contourite cores are put into a broader perspective. The differentiation between contourites and turbidites remains difficult though as turbidites also originate from high-energetic depositional environments. Consequently, additional analyses are required before general diagnostic characteristics can be obtained. To achieve this goal, sediment cores are required that contain well-defined and well-studied pelagites, turbidites and contourites.

In **Chapter 9**, the main conclusions of this thesis are summarized. The conclusions are grouped into 5 main topics: (1) the climatic growth phases of cold-water corals and coral mounds in the AMCP, (2) the spatial and temporal evolution of sediment drifts in the EAMVP, (3) the link between oceanographic processes and drift deposits, (4) the classification and extent of (mostly small-scale) sediment drifts and (5) the analysis of sediment cores using CT-analyses. Moreover, several possible future research topics are proposed, which would enable to extent and verify some of the conclusions resulting from this thesis. They consist mainly of acquiring sediment cores, conducting long-term oceanographic measurements and acquiring additional geophysical data as well as specific CT-analyses of sediment cores containing turbidites, contourites and pelagites.

Chapter 1

Introduction

Chapter 1 – Introduction

1. Bottom currents

Bottom currents can occur in a wide range of geological settings: from the abyssal depths (Faugères et al., 1999; Uenzelmann-Neben and Gohl, 2012) to the continental shelves (Roque et al., 2012; Preu et al., 2013) and even in lakes (Gilli et al., 2004; Heirman et al., 2012, Van Daele et al., 2016). They were first described in 1751 by observations of very cold waters at subtropical locations by English slave-trading ships and in 1797, Benjamin Thompson connected them to cold currents, coming from the poles (Rahmstorf, 2006). In 1908, Johan Sandström first described the properties of wind-driven and thermal-driven circulation based on tank experiments (Sandström, 1908) resulting in the confirmation of the distinction between these two types of circulation. By the 1920s, the term thermohaline circulation (displayed in Figure 1.1) was established by including salinity into the thermal-driven circulation (Rahmstorf, 2006). However, it was not until the late 1950s and early 1960s that bottom currents were considered being able to transport sediment and deposit them at another place (Heezen, 1959; Heezen and Hollister, 1964).

Sediments influenced by bottom currents were first recognized in the 1960's based on deep-sea bottom photographs of current ripples (Heezen et al., 1966; Rebesco et al., 2014) and were initially exclusively associated with thermohaline currents. Sedimentary deposits resulting from bottom currents are called sediment drifts (e.g. McCave and Tucholke, 1986) and the current-controlled/ current-affected sediments within sediment drifts are called contourites (Stow et al., 2002; Rebesco et al., 2005). Especially the deposits along the eastern North American margin, shaped by the western boundary undercurrent, received the dominant attention (Schneider et al., 1967; McCave and Tucholke, 1986). From then onwards, gradually a larger variety of sediment drifts, both in small or large scale, have been discovered (Egloff and Johnson, 1975; McCave and Tucholke, 1986; Flood and Shor, 1988; Faugères and Stow, 1993b; Llave et al., 2001; Hernández-Molina et al., 2011) and as a consequence they are nowadays known to occur in a wide variety of settings (Dalrymple et al., 1992; Locker and Laine, 1992; Viana et al., 1998; Gilli et al., 2004; Maldonado et al., 2005; Chen et al., 2016) and are linked to deep (McCave and Carter, 1997), intermediate (Van Rooij et al., 2010; Preu et al., 2013) and shallow water masses (Vandorpe et al., 2011).

Any along-slope bottom current strong enough to transport and subsequently deposit sediment may in theory create a contourite. Whether an along-slope current is capable of transporting sediment depends on the strength of the current and the nature of the sediment. Muddy and silty sediments can be displaced by bottom currents of 8 cm/s with depositional bedforms being created from 10 cm/s and erosional bedforms from 35 cms/s onwards, while sandy sediments require higher flow intensities, respectively 10 cm/s, 15 cm/s and 50 cm/s (Stow et al., 2009).
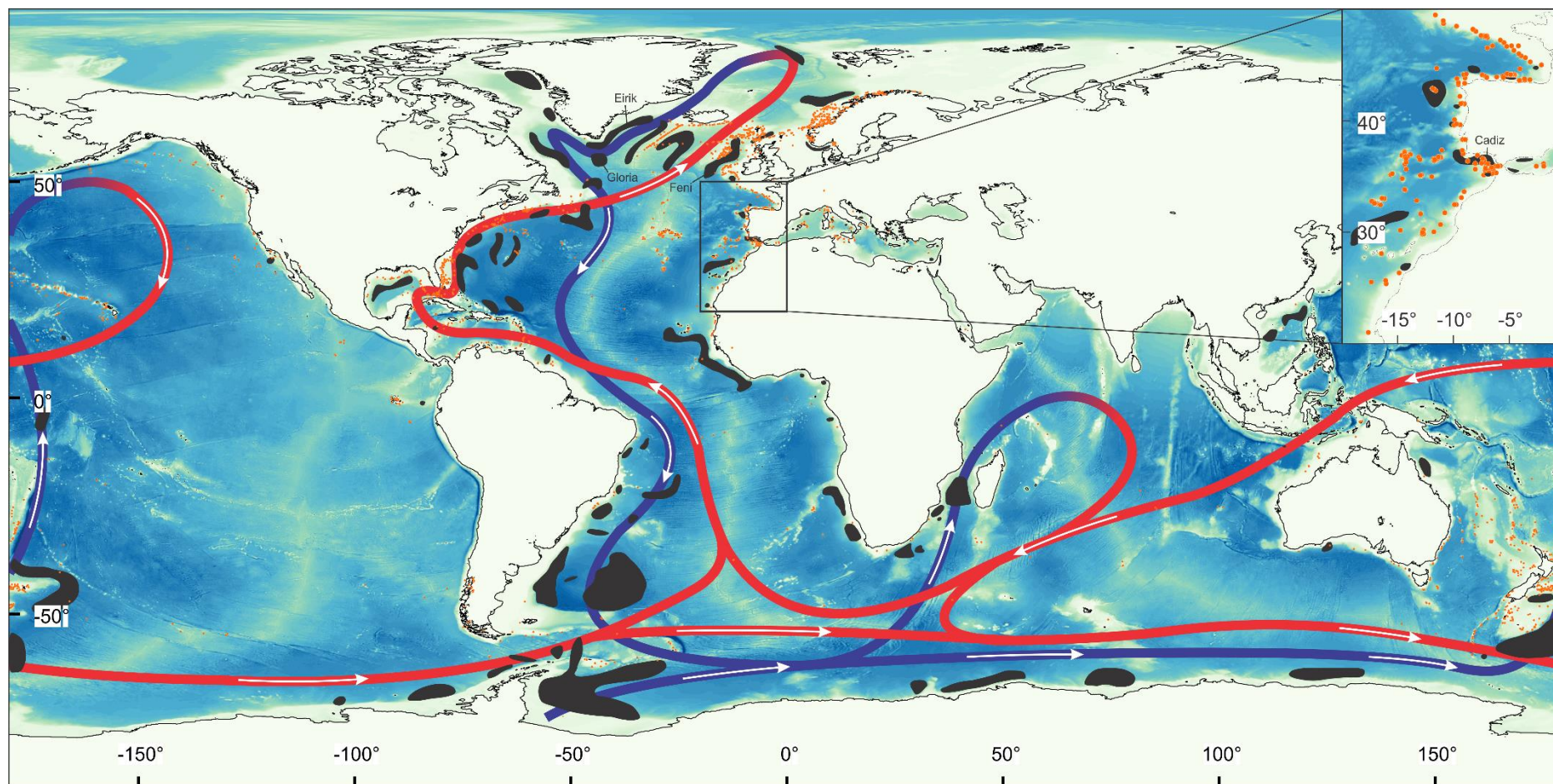
Figure 1.1: Overview map of the location of the main sediment drifts (indicated in black and obtained from Rebesco et al. (2014)), the occurrence of Scleractinia, Octocorralia, Zoanthidae and Filifera CWC (indicated in orange and obtained from Freiwald et al. (2005)) and the global thermohaline circulation pattern shown in blue (cold currents) and red (warm currents) lines. The inset shows the occurrence of CWC and sediment drifts in the vicinity of the research area.

Tectonic processes influence the position of sediment drifts to a large extent as can be observed in the northern Gulf of Cádiz where the location of the depositional and erosional features is controlled by the interaction with the bathymetry, which is in turn controlled by tectonic forces (Hernández-Molina, et al., 2006; Roque et al., 2012; Stow et al., 2013; Hernández-Molina et al., 2016). The deflection of bottom currents on topographic obstacles may create several flow filaments, each being able to create their own erosional (and depositional) features. Some of the best-studied examples are present in the Gulf of Cádiz where the erosional features created by the flow filaments have been used in order to reconstruct the palaeo-circulation of the bottom currents (García et al., 2009). In some areas, contourite deposits are encountered solely around topographic obstacles, e.g. around a 20 km long seamount in the South China Sea (Chen et al., 2013) or around the 60 km long Le Danois Bank in the Bay of Biscay (Van Rooij et al., 2010). Smaller features are also known to be neighbored by contourite deposits, e.g. the on average 1 km wide mud volcanoes in the Alboran Sea (Somoza et al., 2012; Lo Iacono et al., 2014) or the 0.5 to 2 km wide cold-water coral mounds in the Porcupine Seabight (Van Rooij et al., 2007). In all of these regions, background bottom current velocities are mostly below 10 cm/s, e.g. around 1-2 cm/s in the Le Danois region (Van Rooij et al., 2010), between 2 and 5 cm/s in the Porcupine Seabight (Van Rooij et al., 2007), below 10 cm/s around the West Melilla mounds (Lo Iacono et al., 2014) and between 5 and 12 cm/s in the Ceuta drift (Pistek et al., 1985). Nearly all of these velocities are below the threshold for transporting sediment (Stow et al., 2009), indicating that the deflection of the bottom currents increases the velocities, crossing the mobilization-threshold of sediments (Turnewitsch et al., 2013). Deflected bottom currents lead to a more focused, faster and more erosive bottom current (Borenäs et al., 2002; Wåhlin, 2004; Figure 1.2A), allowing erosion at the foot of the obstacle and deposition at the side, leading to (small-scale) contourite deposits. The discovery of this phenomenon has led to a shift from studying large-scale drifts (Schneider et al., 1967; McCave and Tucholke, 1986; Maldonado et al., 2005) to smaller-scale drifts (Verdicchio and Trincardi, 2008; Van Rooij et al., 2010; Palomino et al., 2011; Chen et al., 2013; Rebesco et al., 2013).
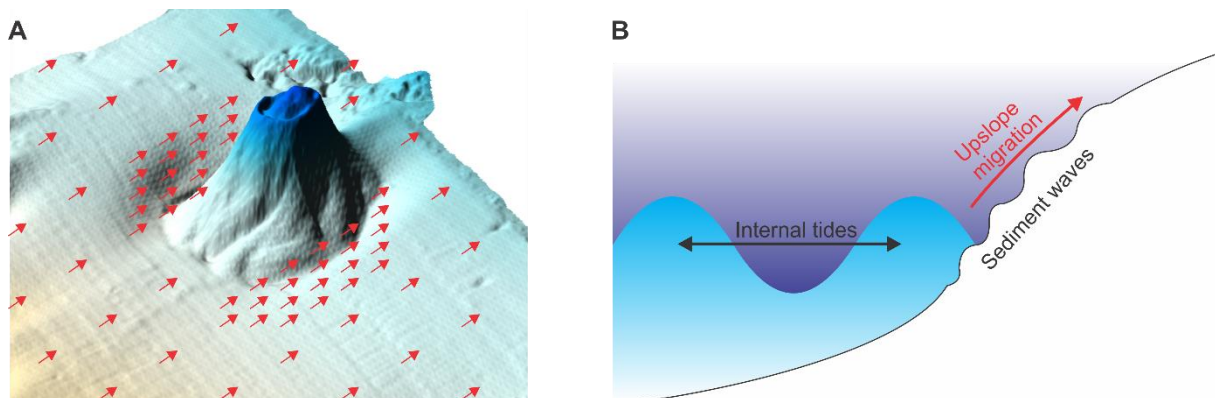
Figure 1.2: A) Simplified model of deflected bottom currents. A larger amount of arrows indicate increased bottom current speeds. B) Schematic representation of internal tides and the associated sediment waves on a continental slope.

Over the years, it became clear that not only long-term bottom currents were responsible for the creation of contourite deposits, but also intermittent high-frequency currents, like internal tidal currents, are capable of creating contourites. The pycnocline is the interface between two water masses of different densities and is characterized by internal nepheloid layers, which can be up to 100-150 meters high (Mienis et al., 2012; Ribó et al., 2013) and contain over 0.5 mg/l suspended sediment concentrations (Ribó et al., 2013). The pycnocline is responsible for the formation of the internal tidal

currents, which when encountering the continental slope can cause resuspension of sediment (Cacchione and Drake, 1986; Ribó et al., 2015; Figure 1.2B). As a result, they can reshape the seafloor by causing re-sedimentation on the continental slope (Ribbe and Holloway, 2001), mostly upslope prograding internal waves (Ribó et al., 2016; Symons et al., 2016; Figure 1.2B) or by creating contourite terraces. Examples of contourite terraces can be found along the Argentinian Margin (Hernández-Molina et al., 2009; Preu et al., 2013) and in the Alboran Sea (Ercilla et al., 2016) whereas sediment waves have been found in the Gulf of Valencia (Ribó et al., 2016) or along the Conrad Rise in the southern Indian Ocean (Oiwane et al., 2014).

The additional mechanisms that allow the creation and build-up of contourites led to re-evaluate the idea that current speed is the main factor controlling sediment deposition (Turnewitsch et al., 2013). As a consequence, the definition of a contourite has been broadened and they are now considered to be sediments deposited or substantially reworked by the persistent action of (any type of) bottom current (Rebesco et al., 2005; 2014).

The study area of this thesis, the Atlantic Moroccan continental margin, is under the influence of two main water masses, i.e. the North Atlantic Central Water (NACW) and the Antarctic Intermediate Water (AAIW) (Van Rooij et al., 2011). Bottom current velocites remain mostly below 10 cm/s, although excursions up to 30 cm/s (Mienis et al., 2012) are registered close to the topographic obstacles (Van Rensbergen et al., 2005). Also internal tides are known to occur (Martins and Vitorino, 2012; Mienis et al., 2012). **As a consequence, the region between the Strait of Gibraltar and 35°N is investigated to better understand the interaction between the drift systems, the topographic obstacles and the various oceanographic processes**. The role of the different topographic obstacles on drift deposition will be assessed by constructing a morpho-sedimentary map. The processes that create these small-scale contourite deposits can be used in order to identify the origin of similar drift systems all over the world.

2. Contourites and sediment drifts

Contourites (Figure 1.3) are one of three endmembers in a continuum of deep-sea sedimentary deposits besides pelagites and turbidites (Rebesco et al., 2014). They correspond to the three main processes that take place in oceans: along-slope bottom flows (resulting in contourites), settling of pelagic particles (pelagites) and downslope density currents (turbidites). As a consequence, they are being recognized more and more in the marine geological record, with most of the discoveries being made in the Atlantic Ocean (Faugères and Stow, 1993b; Rebesco et al., 2014) as most of the research so far focused on this region. Increasing numbers of contourite deposits are being recognized though in the Mediterranean Sea (Alonso and Ercilla, 2003; Verdicchio and Trincardi, 2008; Ercilla et al., 2016), the South China Sea (Chen et al., 2014; 2016), the southern Atlantic Ocean (Flood and Shor, 1988; Hernández-Molina et al., 2009; Preu et al., 2013) and both the Antarctic and Arctic Margins (Maldonado et al., 2005; Hernández-Molina et al., 2006). However, some regions are still in dire need of contourite research, e.g. the Indian Ocean (Faugères et al., 1999) and the Pacific Ocean (Cacchione et al., 1988). A recent summary by Rebesco et al. (2014) yielded 116 "contourite areas" (Figure 1.1), but many more areas will most likely be discovered and described in the coming years due to two main reasons. Firstly, Smith and Sandwell (2004) pointed out that only a few percent of the ocean floor is mapped by high-resolution mapping techniques and even less is covered by seismic profiles. Consequently, acquiring new datasets or re-interpreting old ones will result in the discovery and

description of new contourite drifts. Secondly, the increased attention for and exposure of contourites in the geological community may prove an onset towards the re-interpretation of older datasets. For example, the initial difficulties in discerning contourite and turbidite deposits (Hollister, 1697; Hollister and Heezen, 1972; Piper, 1972; Bouma and Hollister, 1973) will have resulted in the classification of many contourites as turbidite deposits and needs to be adjusted as a consequence.
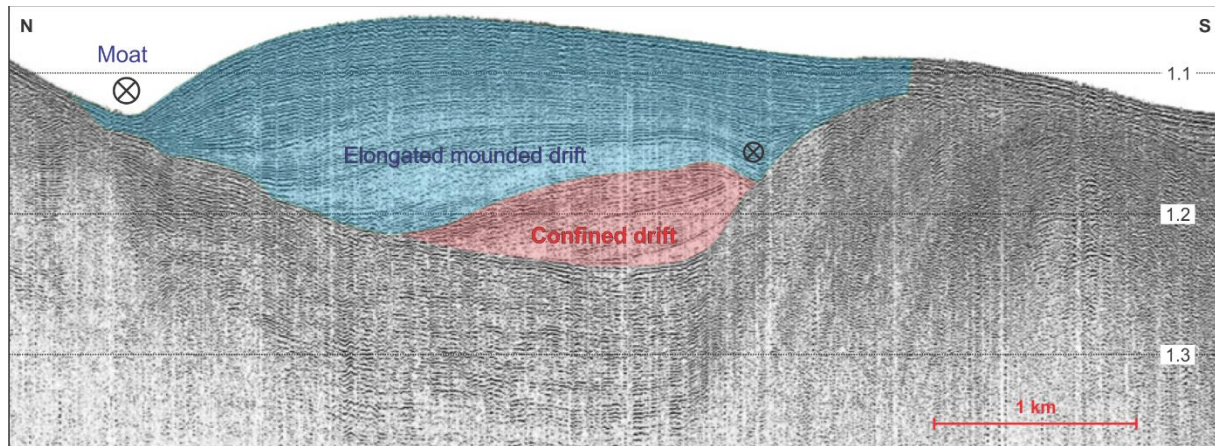
Figure 1.3: Typical contourite drift from the Le Danois area, southern Bay of Biscay (Van Rooij et al. 2010). Depths are in milliseconds two-way travel time.

The depositional part of a contourite drift usually has higher sedimentation rates (20-30 cm/ky with exceptions up to 100 cm/ky or more) compared to the surrounding areas (several cm/ky), creating thicker deposits (up to 2 km; Bryn et al., 2005; Rebesco et al., 2014). Due to the higher sedimentation rates, climatic and oceanographic changes may be preserved in higher resolution in contourite deposits and as a consequence, they are preferred sites for palaeoceanographic studies. The morphology and stacking pattern of a contourite drift, imaged by seismic techniques can indicate the direction of the palaeo-currents and when these currents picked up or slowed down (Lobo et al., 2000; Hernández-Molina et al., 2006; Van Rooij et al., 2010; Preu et al., 2013). The deflection against topographic obstacles and the adjacent development of a moat can also be visualized and interpreted (Palomino et al., 2011; Chen et al., 2014). On the other hand, sediment cores from contourite drifts may yield valuable information on the palaeo-climate (Llave et al., 2006; Toucanne et al., 2007). Besides the importance of contourites in palaeoceanographic and palaeo-climatic studies, the grain-size sorting effect of bottom currents and the resulting economic potential of these deposits as reservoir systems or seals may also not be underestimated (Viana et al., 2007; Brackenridge et al., 2013; Rebesco et al., 2014). In addition, as contourites are usually fine-grained, have a high water content and low permeability values, they can easily form over-pressured gliding plains (Rebesco et al., 2005) which may become gravitationally instable and create submarine landslides (Bryn et al., 2005; Elliott et al., 2010; Martorelli et al., 2016). The study of contourite deposits is as a consequence crucial in terms of slope stability, especially for the positioning of submarine installations.

Contourite (drifts) can be classified based on their lithological, sedimentological and morphological characteristics. Their lithological content varies from clay to gravel (Viana et al., 1998; Stow and Faugères, 2008; Verdicchio and Trincardi, 2008) and they can contain biogenic, terrigenous and volcanic compositions, although a combination is ubiquitous (Stow et al., 2008). Contourites can be discerned from neighbouring (hemi-) pelagic deposits by their different texture and fabric. Pelagic deposits are usually poorly-sorted, heavily bioturbated and can contain small horizons of different

lithologies, while contourites are usually rather well sorted (Stow et al., 2002). Several sedimentary structures can be preserved within the contourite deposits when intense bioturbation was absent and include laminations, stratifications and erosive scarps (Stow and Faugères, 2008; Stow et al., 2009). These structures are indicative for the velocities of the bottom current at the time of deposition (Stow et al., 2009). The sedimentological classification of contourite deposits consists of clastic, calcareous and chemogenic types. The first two include muddy, silty, sandy and gravel contourites, while the latter consists of manganiferous and gravel-lag contourites (Stow and Faugères, 2008; Rebesco et al., 2014). Bottom current reworked sands (Shanmugam, 2012, 2013) are classified as clastic contourites.
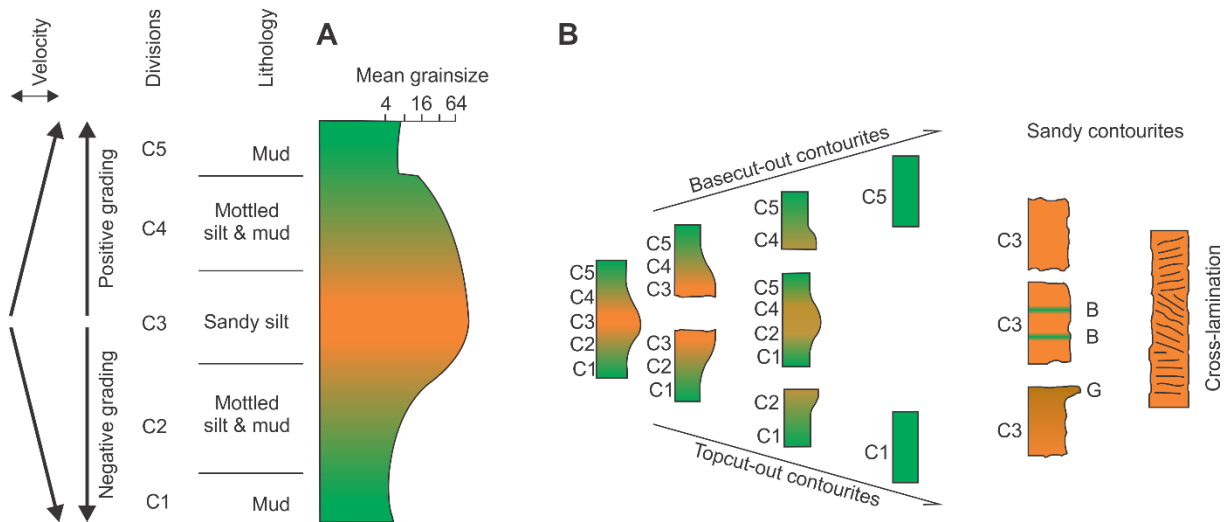
Figure 1.4: Bottom current velocity, grading, divisions and lithology of a typical contourite sequence (A) based on the Faugères et al. (1984) and Gonthier et al. (1984) facies model. (B) Adaptations to the basic model, where basecut-out and topcut-out contourites are considered as well as several sandy contourite facies. B: bioturbation, G: gravel horizon. Figure adapted from Faugères and Stow (2008).

The combination of lithological and sedimentological properties resulted in the contourite facies model of Faugères et al. (1984) and Gonthier et al. (1984). The model was updated by Stow and Faugères (2008) and consists of a coarsening and fining-up sequence. Five facies (C1-C5) are part of the typical contourite sequence, while basecut-out (contourites developed on top of a discontinuity) and topcut-out contourites (contourites topped by a discontinuity) are also considered (Figure 1.4). The model largely applies to muddy and silty contourites and not to sandy contourites where bioturbation is largely absent, which is an important factor of the facies model. Although several facies are presented for sandy contourites, the model (Figure 1.4) does not consider traction sedimentary features, diagnostic for sandy contourites (Shanmugam, 2012, 2013). Moreover, Mulder et al. (2013) pointed out that the contourite sequences of the facies model may only partly reflect changes in bottom current velocities, but also reflect changes in the supply of coarser material. As a consequence, no unique contourite facies model can be composed, although the model of Mutti and Carminati (2012), which discerns 6 facies and includes muddy, silty and sandy features is more comprehensive. The studies, used for discerning contourite facies displayed in the facies model (Figure 1.4), are uniquely based on sedimentological studies (Faugères et al., 1984; Gonthier et al., 1984; Faugères and Stow, 1993a; Rebesco et al., 2005; Llave et al., 2006; Stow and Faugères, 2008; Shanmugam, 2012, 2013; Stow et al., 2013). Innovative techniques, such as X-ray computed tomography (CT) are not considered yet in this model, even though this method (which combines geochemical, porosity and grain size data) already yielded some promising initial results in differentiating contourites from (hemi)-pelagites, turbidites and ice-rafted debris layers (Mena et al., 2015). In addition, CT can be

performed on un-split cores, is non-destructive (not hindering additional research) and is performed rather fast (scanning 1 m of sediment requires about 10 minutes). **Therefore, this thesis attempts to contribute to the characterization of typical contourite sequences using CT-radiographs in order to improve the diagnostic criteria for identifying contourite facies.**

In terms of morphology, a distinction is made between depositional and erosional features. The most recent morphological classification scheme for contourite drift deposits defines eight different depositional members (Rebesco et al., 2014): elongated mounded drifts (both separated and detached), sheeted drifts (both plastered and abyssal), channel-related drifts, confined drifts, patch drifts (both sheeted and mounded), infill drifts, fault-controlled drifts and mixed drift systems (Figure 1.5). Overlap between these endmembers exists and contourite drifts may evolve laterally from one morphology into another (e.g. from sheeted to mounded drift deposits).

Bottom currents do not only create depositional, but also erosional features. Areal erosional features include terraces and abraded surfaces (Brackenridge et al., 2013; Preu et al., 2013), while linear features consist of contourite channels, moats and marginal valleys (scours) (Hernández-Molina et al., 2008; García et al., 2009). Moats originate due to localized non-deposition or erosion beneath the flow path of a bottom current and are preferentially associated to elongated mounded separated drifts (Hernández-Molina et al., 2008), meaning they are usually oriented alongslope. Contourite channels are elongated erosional depressions created by vigorous bottom currents and can be oriented oblique or parallel to the slope. Marginal valleys are created by flow instabilities due to the action of bottom currents that hit a topographic obstacle and induce erosion on the other side of that obstacle (García et al., 2009). Furrows are erosional features as well, but are (except for some cases) rather small (up to a couple of kilometers), less incised and much narrower compared to contourite channels (Rebesco et al., 2014). Their origin is linked to detached filaments of bottom currents.
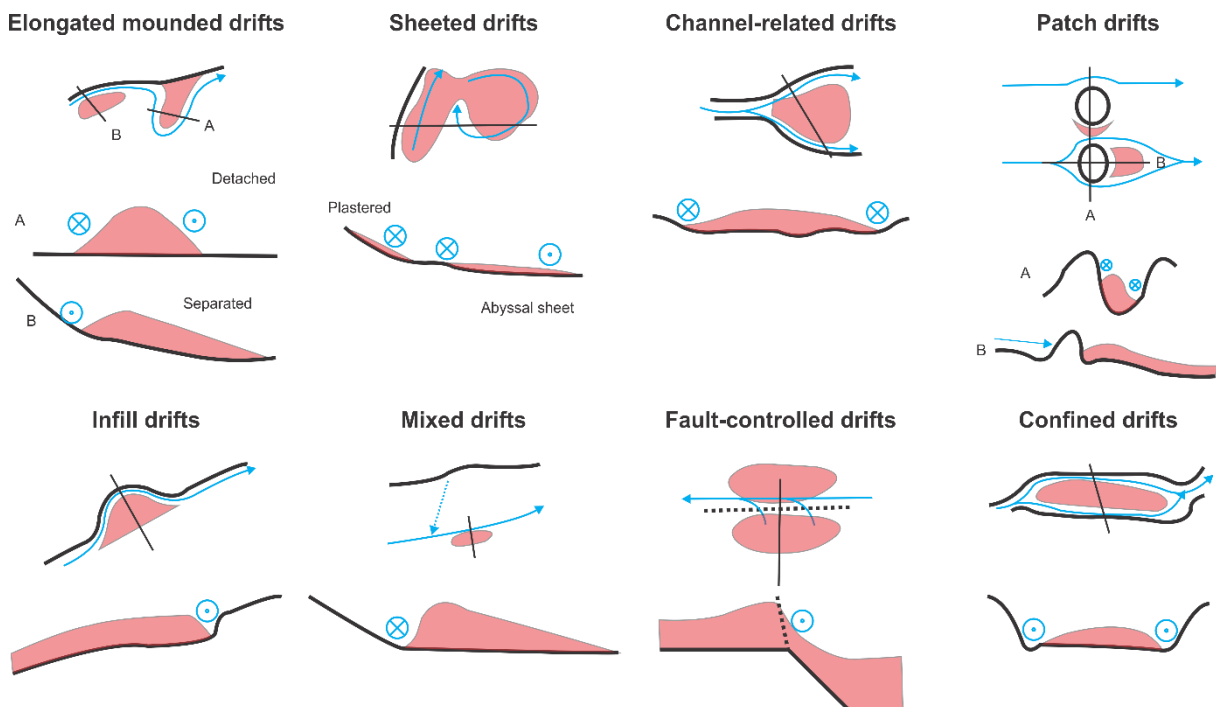
Figure 1.5: Classification of sediment drifts based on the morphology observed in seismic profiles. Adapted from Rebesco (2005) and Hernández-Molina et al. (2008).

The association of various erosional and depositional features, shaped by the alongslope bottom currents, create a contourite depositional system (CDS; Hernàndez-Molina et al., 2008; 2009), while contourite depositional complexes (CDC) are considered to be CDS's which are connected and originate from the same water mass (Hernàndez-Molina et al., 2008).

The most-studied CDS is situated in the northern Gulf of Cadiz and is shaped by the Mediterranean Outflow Water (MOW) (Llave et al., 2001; Hernández-Molina et al., 2006; Llave et al., 2007; García et al., 2009; Hernández-Molina, 2009; Hernández-Molina et al., 2011; Llave et al., 2011; Brackenridge et al., 2013; Stow et al., 2013). The MOW is a warm and saline water mass that flows out of the Mediterranean Sea via the Gibraltar Strait and continues as an intermediate water mass (500 to 1400 meters water depth) along the Southern Iberian slope due to Coriolis deflection (Iorga and Lozier, 1999; Serra et al., 2010; Hernández-Molina et al., 2011; Figure 1.6). The MOW is composed of mainly Levantine Intermediate Water and small amounts of Western Mediterranean Deep Water (Bryden and Stommel, 1984). After its exit out of the Strait of Gibraltar, the MOW is split up into two main branches (the upper and lower Mediterranean cores) due to seafloor topographies and the resulting frictional effects (Iorga and Lozier, 1999; Borenäs et al., 2002; Hernández-Molina et al., 2006). The upper core is the least dense core and flows along the shelf edge at depths of 500 to 800 meters until Cape Saint Vincent (Ambar et al., 1999). The lower core is the most saline core and flows at depths of 750 to 1400 meters to the west-northwest. It is the main water flux and is heavily affected by the seafloor morphology. Due to this influence, the lower core splits up into three major branches (from north to south): the intermediate, the principal and the southern branch (Figure 1.6; Nelson et al., 1993; García, 2002). At Cape Saint Vincent, the MOW can detach and create eddy structures, called meddies (Mediterranean eddies), which flow both west- and southwards (Richardson et al., 2000; Ambar et al., 2008). Due to frictional effects and detached flow filaments, current velocities within the MOW decrease from >1 m/s after its exit out of the Strait of Gibraltar to 20-30 cm/s at Cape Saint Vincent (Baringer and Price, 1997; Hernández-Molina et al., 2006).

Hernández-Molina et al. (2006) defined five sectors in the Cádiz CDS: the proximal scours and ribbons sector, the overflow sedimentary lobe sector, the channels and ridges sector, the contourite depositional sector and the submarine canyon sector (Figure 1.6). The "proximal scour and ribbons sector" contains only erosional features and sand deposits due to the extremely high bottom current velocities of the MOW close to the Strait of Gibraltar (close to 1 m/s). The overflow sedimentary lobe sector is located seaward of the first sector and consists of sandy and muddy sedimentary lobes and wave-fields. Several furrows are present as well (García, 2002; Figure 1.6). The channels and ridges sector is located in the central part of the Cádiz CDS, in between two branches of the MOW (Figure 1.6). A combination of neo-tectonic activity and strong bottom currents shaped this region, resulting in the presence of several contourite channels (García, 2002) over a buried contourite drift system (Hernández-Molina et al., 2006). The contourite drift sector is located at the northwestern middle slopes, along the Iberian margin and is characterized by the presence of mainly mounded, elongated and sheeted drift deposits: the Faro-Albufeira, the Bartolomeu Dias and the Faro-Cádiz drift systems (Figure 1.6). Apart from the different contourite drifts, several contourite channels and moats are present in this sector as well (Llave et al., 2001). The fifth sector is the submarine canyons sector and is located close to the Cape Saint Vincent (Figure 1.6). Several canyons (Portimao, Lagos, Sagres and San Vincente) cut through the sheeted drift deposits (called Portimao, Lagos and Sagres drifts, Figure 1.6). Considering the complex nature of the Cádiz CDS and the combination of several drifts and

erosional features, several hundreds of kilometers apart (Figure 1.6), one might wonder whether the Cadiz CDS should not be called the Cadiz contourite depositional complex …
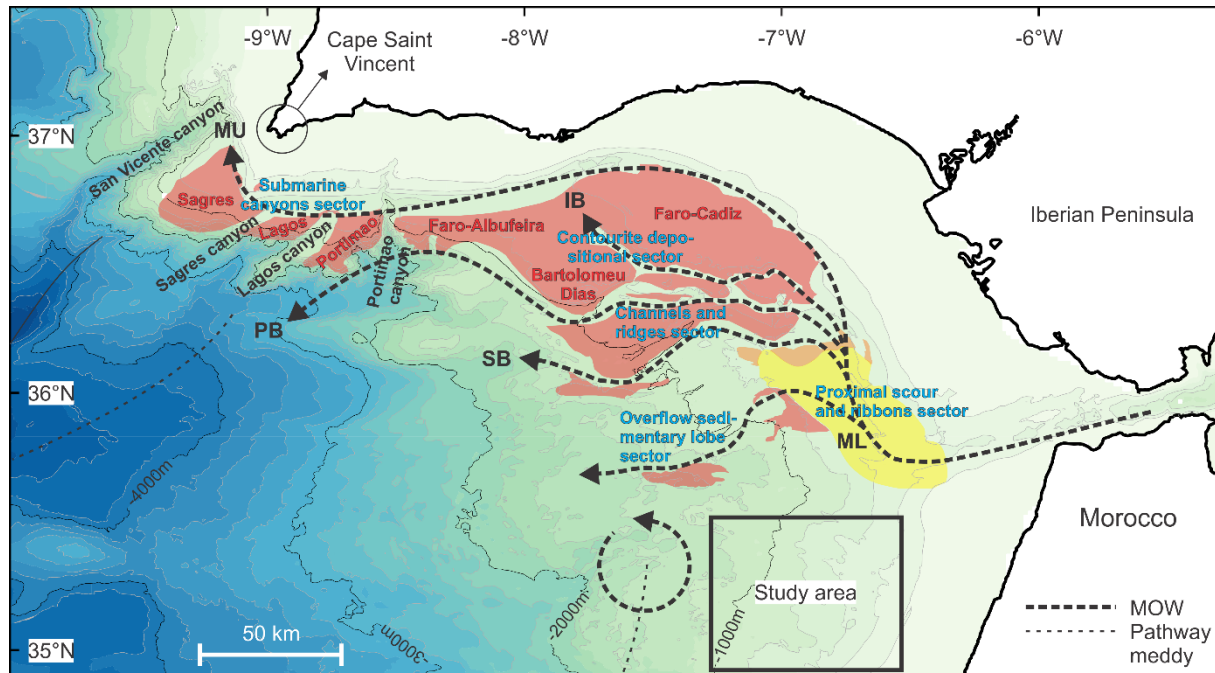
Figure 1.6: Water masses with their associated (bottom) currents. Mediterranean pathways have been derived from Iorga and Lozier (1999) and the meddy pathway (centered around 1200 m) from Ambar et al. (2008). The largest sediment drifts of the Cádiz CDS are labelled in red and the different sectors in blue. The erosional features are indicated in yellow (abrasive surfaces and rock outcrops) and orange (sand dune fields). The location of the features of the Cádiz CDS have been obtained from Hernández-Molina et al. (2006). MU: Mediterranean Upper Core, ML: Mediterranean Lower Core, IB: Intermediate Branch, PB: Principal Branch, SB: Southern Branch.

Most of the CDS's that serve as a base for the classification schemes (Figure 1.1), e.g. Gloria drift in the North Atlantic (McCave and Tucholke, 1986), the Faro drift in the Gulf of Cadiz (Llave et al., 2001), the Eirik drift off southern Greenland (Artur et al., 1989) or the Feni drift in the Rockall Trough (McCave and Tucholke, 1986), are rather complex, usually extensive (Stow et al., 2002) and they all result from the global thermohaline circulation. As a result, small, topography-driven contourite drifts, to which the scientific attention is shifting (Van Rooij et al., 2010; Vandorpe et al., 2011; Ercilla et al., 2016; Martorelli et al., 2016), are not considered and consequently, specific criteria for identifying them may be absent in the different classification schemes. Therefore, studying these small-scale contourite drifts may prove to be very important. Additionally, they may shed new insights on the interaction between bottom currents and topographic obstacles (Turnewitsch et al., 2013). For these two reasons, the drift systems along the Moroccan Atlantic margin (Van Rooij et al., 2011) are the focus of this study as they are situated within a dynamic region containing tectonic ridges (Medialdea et al., 2009), mud volcanoes (Van Rensbergen et al., 2005) and cold-water coral (CWC) mounds (Foubert et al., 2008; Van Rooij et al., 2011), all influencing the position and development of the contourite drifts.

This thesis attempts to unravel the spatial and temporal evolution of the drift systems, the involved (palaeo-) oceanographic processes and the interplay with and influence of mud extrusion and tectonic activity on contourite deposition. By studying the small-scale drift deposits in this area, more insight in the general formation and maintenance mechanisms of drift systems can be acquired and this insight may be applied to locate and understand similar small-scale contourite deposits worldwide.

3. Cold-Water Corals and coral mounds

Bottom currents are not only essential for contourites, but they are also of the utmost importance for the development and "maintenance" of deep-water ecosystems, especially with respect to CWC mounds (hereafter called coral mounds). The most recent paper describing the important link between the two was published last year (Hebbeln et al., 2016) and emphasizes that both are extremely depending on sediment input, have a wide-spread co-occurrence (for the moment mostly observed in the North Atlantic, Figure 1.1) and provide a high-resolution palaeo-environmental record (although of differing temporal resolutions). Elevated bottom currents can deliver more food particles (zoo- and phytoplankton, protozoans and bacteria) to CWC, allowing them to thrive (Mienis et al., 2012). The supply of sediments is one of the most important parameters controlling mound aggradation and is delivered to the CWC's by bottom currents (Hebbeln et al., 2016), enabling the co-occurrence of coral mounds and sediment drifts. When coral mounds and contourite drifts occur together (De Mol et al., 2002; Van Rooij et al., 2007; Hübscher et al., 2010; Van Rooij et al., 2011), they provide the possibility of analysing the palaeo-environmental setting much more comprehensively (Hebbeln et al., 2016).

During the last 15 years, CWC research experienced a boost resulting in a steadily increasing knowledge regarding their environmental requirements and preferences, their ecology and physiology, their recent spatial distribution and their temporal occurrence (Freiwald and Roberts, 2005; Roberts et al., 2006; Roberts, 2009; Wienberg and Titschack, 2016; Hebbeln et al., 2016).

Corals are usually associated in one's mind to warm tropical environments, shallow waters and colorful fishes. However, since the 18th century, CWC's are known to occur in deeper water settings as well, ranging from 50 to 1000 meters water depth (with exceptions up to depths of 4000 m; Roberts et al., 2006). CWC belong to the phylum Cnidaria, comprising Scleractinia (stony corals), Octocorallia (soft corals), Antipatharia (black corals) and Stylasteridae (hydrocorals), are azooxanthellate (meaning they have no symbiotic link with dinoflagellates) and often form colonies, providing suitable habitats for many other species (Freiwald and Roberts, 2005; Roberts et al., 2006). CWC's occur all over the world, but most of the discoveries have been done in the North Atlantic (Figure 1.1), probably due to the high intensity of research in this region (Freiwald et al., 2004). They occur on continental shelves and slopes, on oceanic banks, on seamounts and mid-oceanic ridges and on artificial structures (e.g. ship wrecks) (Freiwald et al., 2004).

Figure 1.7: Left, Lophelia Pertusa corals from the Sula reef along the Norwegian shelf; right, Madrepora Oculata from the Santa Maria di Leuca reef from the Ionian Sea (Freiwald et al., 2004).

Of particular interest are framework-forming scleractinian CWC, such as *Lophelia pertusa* and *Madrepora oculata*, as they have the capability to form small to large reefs (Roberts et al., 2006),

possibly leading to the development of huge coral mounds which can be up to 300 meters high as observed for the Rockall Trough off Ireland (van Weering et al., 2003; Mienis et al., 2006; de Haas et al., 2009). The temporal development of coral mounds often is discontinuous with recurring periods of CWC colonization and mound aggradation alternating with periods of coral demise and possible mound erosion (Wienberg and Titschack, 2016). Coral mounds are the result of an interplay between sustained phases of CWC growth and concurrent sediment input, with the sediments being entrapped within the coral framework (known as baffling effect; Huvenne et al., 2009; Titschack et al., 2009) and thus stabilizing the biogenic construction. Over time, this can result in mound aggradation rates of up to 1600 cm/ka as identified for Norwegian coral mounds (Titschack et al., 2015). During periods of coral demise, the mounds might by covered solely by (hemi-) pelagic sediments, which later on may act as an instable layer and could induce slumping, widening the mound at the base (Eisele et al., 2008).
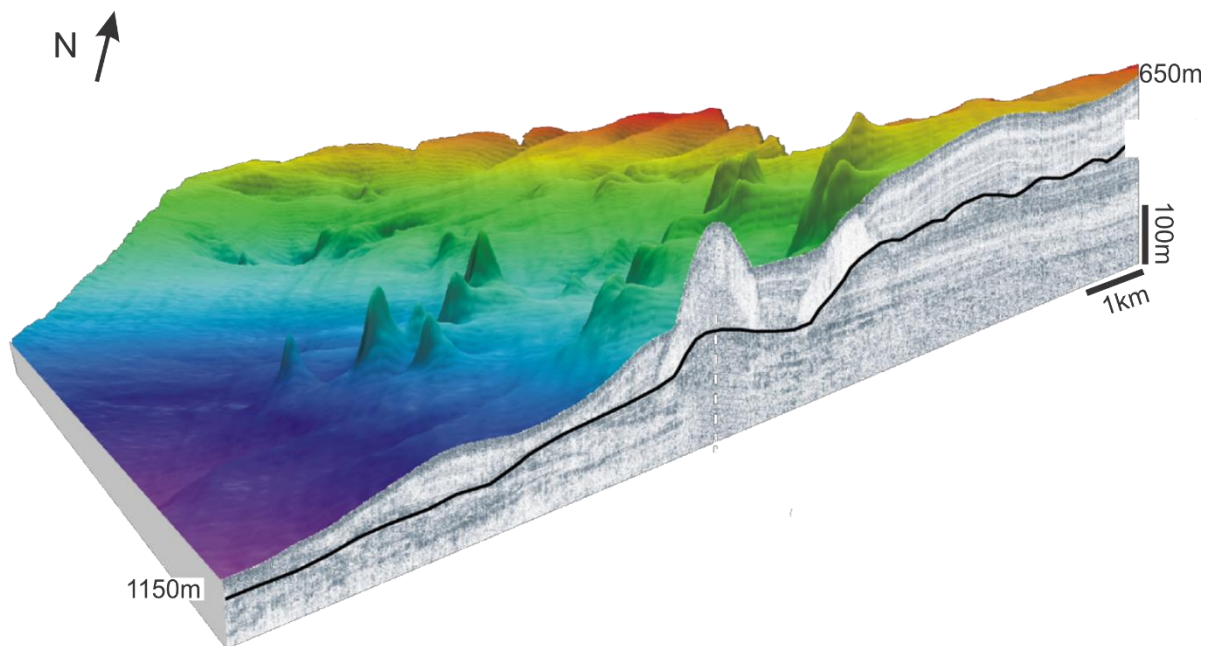
Figure 1.8: Multibeam bathymetry and seismic profile through the Challenger mound in the Porcupine Basin. The black reflector indicates the rooting horizon, which is the local RD1 unconformity. Modified after Thierens et al. (2013).

Coral mounds exhibit a wide variety of shapes, ranging from conical, oval, elongated and ridge-like to even V-like shapes (Wheeler et al., 2007). Coral mounds occur as individual mounds or cluster to form coral provinces, which may consist of thousands of mounds (Glogowski et al., 2015). When they are arranged in clusters or provinces, coral mounds are usually confined to certain depth intervals, creating slope-parallel chains as a consequence (Colman et al., 2005; Wheeler et al., 2007; Wienberg and Titschack, 2016).

As most of the CWC's discovered so far are situated in the North Atlantic (Figure 1.1), also most of the coral mounds are situated in the same region. Coral mounds are widely distributed in the North Atlantic Ocean, where they occur on shelves (eastern Florida, Scotland and Norway) and along the continental margins (Porcupine Seabight, Rockall Bank, Morocco, Mauritania) mainly being confined to water depths of 200 to 1000 m (Wienberg and Titschack, 2016 and references therein). Although continental slopes and shelves are the main environments in which coral mounds occur, more and more coral mounds are being discovered on submarine topographies or on canyon flanks, expanding our knowledge about their occurrence (Van Rooij et al., 2011; Sánchez et al., 2014; Somoza et al.,

2014). They can become rather high (>100 m), as for example in the Porcupine Basin and the Rockall Trough (De Mol et al., 2002; Huvenne et al., 2003; Dorschel et al., 2005; Mienis et al., 2007; Eisele et al., 2008; van der Land et al., 2014) or remain rather small (several to tens of meters high) as seen for the Moira mounds (Porcupine Basin; Wheeler et al., 2007) and along the Moroccan margin (Foubert et al., 2008; Wienberg et al., 2009). The dimensions of the coral mounds depend on environmental controls and sediment input.

Environmental control for mound aggradation first and foremost depends on a complex set of suitable environmental conditions and a suitable substrate that allow the CWC's to settle, grow and develop into large thriving reefs. Important are distinct ranges for seawater temperature (-1.8°C to 14.9°C), salinity (31.7 – 38.8) and dissolved oxygen concentration (3 - 7.2 ml/l) as well as a high net primary production (Davies et al., 2008; Davies and Guinotte, 2011). Additionally, several other chemical and biological parameters such as the pH, the aragonite saturation state and concentrations of dissolved and particulate organic matter were indicated to play an important role in the occurrence of CWC (Davies et al., 2008; Davies and Guinotte, 2011). Given that the physical setting fits the CWC requirements, the availability of sufficient food particles and distinct hydrodynamic processes (geostrophic currents, local bottom currents, internal waves, …) to deliver the food particles to the corals or enrich food around them (nepheloid layers) are the most important parameters (Mienis et al., 2007; Mienis et al., 2012; Hebbeln et al., 2016). Even under erosive conditions for the surrounding areas, coral mounds can still aggrade (Thierens et al., 2013) as sediments delivered by vigorous bottom currents are entrapped or baffled within the coral framework (Huvenne et al., 2009; Titschack et al., 2009; Hebbeln et al., 2016).

More strict ranges for especially temperature and oxygen seem to exist for mound aggradation compared to CWC growth (Wienberg and Titschack, 2016), as solitary CWC's are very common in the world's oceans and do not always build up coral mound structures. Sediment input and baffling capacity also play a crucial role as it stabilizes the structure and allows aggradation. These last two parameters are hard to assess due to the lack of appropriate data on the subject (Wienberg and Titschack, 2016). It is very important that a balanced interplay between the different parameters exists in order for coral mounds being able to aggrade.

The existing knowledge on buried mounds along the Moroccan margin so far was restricted to a rather small area within and south of the El Arraiche mud volcano province. As the number of discovered exposed coral mounds along the Moroccan Atlantic margin increased steadily with every new mapping survey/expedition (by now comprising a very large area bordered by the El Arraiche mud volcano province in the north and the 35°N latitude in the south; henceforth be called the Atlantic Moroccan Coral Province, AMCP), it is most likely that also many more buried mounds are present in the area. **The goal of this thesis is to make a first assessment on the amount and dimensions of the buried mounds along the Moroccan Atlantic margin and to unravel how many initiation events are present.** Finally, the link between the bottom currents (and as a consequence sediment drifts) and the coral mounds will be investigated in order to improve our understanding of the coupling between both geological phenomena. Moreover, as coral mounds consist of periods of mound aggradation and coral demise (Wienberg and Titschack, 2016), the question that arises is "**Can a clear climatic and oceanographic signal be determined in the growth phases of the coral mounds in the AMCP?**". By studying these small coral mounds, new and improved insights may be gathered regarding initiation phases of coral mounds, not only in the AMCP, but worldwide.

Research objectives

This dissertation will endeavor to answer four main research questions, by focusing on sediment drifts and coral mounds in the AMCP and sediment cores from contourites from the Alboran Sea and northern Gulf of Cádiz. The AMCP is introduced in **Chapter 2**, while the methods used to accomplish these research objectives are be discussed in **Chapter 3**.

1. How do tectonic processes and mud volcano activity influence the evolution of the drift systems in the AMCP? Do other processes/obstacles interfere with the spatial and temporal evolution of the small-scale drift systems? These research questions will be answered in **chapter 4** by composing the stratigraphy of 3 main drift systems in the region and comparing their evolution.
2. The role of topographic obstacles on the location of sediment drifts and the influence of various oceanographic processes on drift development will be assessed in **chapter 5** by focusing on the sediment drifts in the AMCP. An oceanographic characterization of the region will be conducted and compared (together with the position of the topographic obstacles) to the location of sediment drifts.
3. The amount, dimensions, initiation levels, aggradation periods and controlling factors of the coral mounds in the AMCP are the main subjects of **Chapter 6**. An initial assessment of these parameters may lead to the detection of climatic and/or oceanographic patterns in their growth phases.
4. Additional diagnostic criteria for discerning contourites from turbidites and/or pelagites are still needed. A method that did not yield any criteria so far, but may aid in discerning these deposits is CT. In **Chapter 7**, four cores from various contourite settings in the Gulf of Cádiz and the Alboran Sea are characterized in order to improve the diagnostic criteria for identifying contourite facies.

Since contourites are characterized by elevated sedimentation rates and higher water contents they are more prone to become gravitationally unstable and fail (Rebesco et al., 2005; Laberg and Camerlenghi, 2008). As a consequence, it is advised to investigate contourites in order to assess the locations of deep-sea constructions (military constructions, pipelines, cables). By studying the small-scale drift deposits in the AMCP, new insights will be gathered on where they occur, especially regarding their link with seafloor-topographies, and how they evolve. The results obtained in the AMCP may consequently lead to more specific diagnostic criteria, beneficial for industrial applications.

Elevated sedimentation rates may not be beneficial for the stability of the sediment, but they are for palaeo-climate studies, as higher-resolution records can be obtained. Consequently, contourites are preferred sites for palaeo-climatic research and their identification may be of great value for the climatic record of certain regions, especially if those regions lack other archives. The coral mound research in the AMCP might shed new insights on the climatic growth patterns of coral mounds and is consequently also important for climate research. By studying both records in the same region, their complementarity can be investigated and a more complete record of the Atlantic Moroccan margin can be obtained. In times when even the most important world leaders question climate change, additional research on how certain regions respond to climatic changes and how organisms (in this case CWC) dealt with this is always a plus. It will give policy makers less ammunition to fight this phenomenon.

The last research question (distinguishing contourites from turbidites and pelagites) may have important industrial and scientific applications. If criteria are developed which allow to distinguish both

facies based on CT (which is a time- and cost-efficient method), determining the origin of sediment cores will take a lot less time, enabling nimble assessments on their potential. This potential can be either industrial, e.g. reservoir rocks, or purely scientific, e.g. climate research.

References

Alonso, B., Ercilla, G., 2003. Small turbidite systems in a complex tectonic setting (SW Mediterranean Sea): morphology and growth patterns. Marine and Petroleum Geology 19, 1225-1240.

Ambar, I., Armi, L., Bower, A., Ferreira, T., 1999. Some aspects of time variability of the Mediterranean Water off south Portugal. Deep Sea Research Part I: Oceanographic Research Papers 46, 1109-1136.

Ambar, I., Serra, N., Neves, F., Ferreira, T., 2008. Observations of the Mediterranean Undercurrent and eddies in the Gulf of Cadiz during 2001. Journal of Marine Systems 71, 195-220.

Artur, M.A., Srivastava, S.P., Kaminski, M., Jarrad, R., Osler, J., 1989. Seismic stratigraphy and history of deep circulation and sediment drift development in Baffin Bay and the Labrador Sea., in: Srivastava, S.P., Arthur, M., Clement, B. (Eds.), Proceedings of the Ocean Drilling Program, Scientific Results, College Station, pp. 957-988.

Baringer, M.O.N., Price, J.F., 1997. Momentum and Energy Balance of the Mediterranean Outflow. Journal of Physical Oceanography 27, 1678-1692.

Borenäs, K.M., Wåhlin, A.K., Ambar, I., Serra, N., 2002. The Mediterranean outflow splitting—a comparison between theoretical models and CANIGO data. Deep Sea Research Part II: Topical Studies in Oceanography 49, 4195-4205.

Bouma, A.H., Hollister, C.D., 1973. Deep ocean basin sedimentation, in: Middleton, G.V., Bouma, A.H. (Eds.), Turbidites and Deep-water Sedimentation. SEPM Pacific Section Short Course. SEPM, Anaheim, CA, pp. 79-118.

Brackenridge, R.E., Hernández-Molina, F.J., Stow, D.A.V., Llave, E., 2013. A Pliocene mixed contourite–turbidite system offshore the Algarve Margin, Gulf of Cadiz: Seismic response, margin evolution and reservoir implications. Marine and Petroleum Geology 46, 36-50.

Bryden, H.L., Stommel, H., 1984. Limiting processes that determine basic features of the circulation in the mediterranean-sea. Oceanologica Acta 7, 289-296.

Bryn, P., Berg, K., Stoker, M.S., Haflidason, H., Solheim, A., 2005. Contourites and their relevance for mass wasting along the Mid-Norwegian Margin. Marine and Petroleum Geology 22, 85-96.

Cacchione, D., Schwab, W., Noble, M., Tate, G., 1988. Internal tides and sediment movement on Horizon Guyot, Mid-Pacific Mountains. Geo-Marine Letters 8, 11-17.

Cacchione, D.A., Drake, D.E., 1986. Nepheloid layers and internal waves over continental shelves and slopes. Geo-Marine Letters 6, 147-152.

Chen, H., Xie, X., Van Rooij, D., Vandorpe, T., Huang, L., Guo, L., Su, M., 2013. Depositional characteristics and spatial distribution of deep-water sedimentary systems on the northwestern middle-lower slope of the Northwest Sub-Basin, South China Sea. Marine Geophysical Research 34, 239-257.

Chen, H., Xie, X., Van Rooij, D., Vandorpe, T., Su, M., Wang, D., 2014. Depositional characteristics and processes of alongslope currents related to a seamount on the northwestern margin of the Northwest Sub-Basin, South China Sea. Marine Geology 355, 36-53.

Chen, H., Xie, X., Zhang, W., Shu, Y., Wang, D., Vandorpe, T., Van Rooij, D., 2016. Deep-water sedimentary systems and their relationship with bottom currents at the intersection of Xisha Trough and Northwest Sub-Basin, South China Sea. Marine Geology.

Colman, J.G., Gordon, D.M., Lane, A.P., Forde, M.J., Fitzpatrick, J.J., 2005. Carbonate mounds off Mauritania, Northwest Africa: status of deep-water corals and implications for management of fishing and oil exploration activities, in: Freiwald, A., Roberts, J.M. (Eds.), Cold-Water Corals and Ecosystems. Springer, Berlin, Heidelberg, pp. 417-441.

Dalrymple, R.W., LeGresley, E.M., Fader, G.B.J., Petrie, B.D., 1992. The western Grand Banks of Newfoundland: Transgressive Holocene sedimentation under the combined influence of waves and currents. Marine Geology 105, 95-118.

Davies, A.J., Guinotte, J.M., 2011. Global Habitat Suitability for Framework-Forming Cold-Water Corals. PLoS ONE 6, e18483.

Davies, A.J., Wisshak, M., Orr, J.C., Roberts, M.J., 2008. Predicting suitable habitat for the cold-water coral Lophelia pertusa (Scleractinia). Deep Sea Research Part I: Oceanographic Research Papers 55, 1048-1062.

de Haas, H., Mienis, F., Frank, N., Richter, T.O., Steinacher, R., Stigter, H., Land, C., Weering, T.C.E., 2009. Morphology and sedimentology of (clustered) cold-water coral mounds at the south Rockall Trough margins, NE Atlantic Ocean. Facies 55, 1-26.

De Mol, B., Van Rensbergen, P., Pillen, S., Van Herreweghe, K., Van Rooij, D., McDonnell, A., Huvenne, V., Ivanov, M., Swennen, R., Henriet, J.P., 2002. Large deep-water coral banks in the Porcupine Basin, southwest of Ireland. Marine Geology 188, 193-231.

Dorschel, B., Hebbeln, D., Rüggeberg, A., Dullo, W.-C., Freiwald, A., 2005. Growth and erosion of a cold-water coral covered carbonate mound in the Northeast Atlantic during the Late Pleistocene and Holocene. Earth and Planetary Science Letters 233, 33-44.

Egloff, J., Johnson, G.L., 1975. Morphology and structure of the southern Labrador Sea. Can. J. Earth Sci. 12, 2111-2133.

Eisele, M., Hebbeln, D., Wienberg, C., 2008. Growth history of a cold-water coral covered carbonate mound — Galway Mound, Porcupine Seabight, NE-Atlantic. Marine Geology 253, 160-169.

Elliott, G.M., Shannon, P.M., Haughton, P.D.W., Øvrebø, L.K., 2010. The Rockall Bank Mass Flow: Collapse of a moated contourite drift onlapping the eastern flank of Rockall Bank, west of Ireland. Marine and Petroleum Geology 27, 92-107.

Ercilla, G., Juan, C., Hernández-Molina, F.J., Bruno, M., Estrada, F., Alonso, B., Casas, D., Farran, M.l., Llave, E., García, M., Vázquez, J.T., D'Acremont, E., Gorini, C., Palomino, D., Valencia, J., El Moumni, B., Ammar, A., 2016. Significance of bottom currents in deep-sea morphodynamics: An example from the Alboran Sea. Marine Geology 378, 157-170.

Faugères, J.-C., Gonthier, E., Stow, D.A.V., 1984. Contourite drift molded by deep Mediterranean outflow. Geology 12, 296-300.

Faugères, J.-C., Stow, D.A.V., Imbert, P., Viana, A., 1999. Seismic features diagnostic of contourite drifts. Marine Geology 162, 1-38.

Faugères, J., Stow, D.A.V., 1993a. Bottom-current-controlled sedimentation: A synthesis of the contourite problem. Sedimentary Geology 82, 287-297.

Faugères, J.C., Stow, D.A.V., 1993b. Contourite drift types and their distribution in the North and South Atlantic Ocean basins. Sedimentary Geology 82, 189-203.

Faugères, J.C., Stow, D.A.V., 2008. Contourite drifts: Nature, Evolution and Controls, in: Rebesco, M., Camerlenghi, A. (Eds.), Contourites. Elsevier, pp. 259-288.

Flood, R.D., Shor, A.N., 1988. Mudwaves in the Argentine basin and their relation to regional bottom circulation patterns. Deep Sea Research 35, 943-972.

Foubert, A., Depreiter, D., Beck, T., Maignien, L., Pannemans, B., Frank, N., Blamart, D., Henriet, J.-P., 2008. Carbonate mounds in a mud volcano province off north-west Morocco: Key to processes and controls. Marine Geology 248, 74-96.

Freiwald, A., Fosså, J.H., Grehan, A., Koslow, T., Roberts, J.M., 2004. Cold-water Coral reefs, UNEP-WCMC, Cambridge, UK.

Freiwald, A., Roberts, J.M., 2005. Cold-Water Corals and Ecosystems. Springer, Heidelberg.

Freiwald, A., Rogers, A., Hall-Spencer, J., 2005. Global distribution of cold-water corals (version 2). Update of the dataset in Freiwald et al. (2004), UNEP World Conservation Monitoring Centre, Cambridge (UK). http://data.unepwcmc.org/datasets/3.

García, M., 2002. Caracterización morfológica del sistema de canales y valles submarinos del talud medio del Golfo de Cádiz (SO de la Peninsula Iberica): Implecaciones oceanográficas., Facultad de Ciencias de l Mar. Univ. Cádiz, Cádiz, p. 114.

García, M., Hernández-Molina, F.J., Llave, E., Stow, D.A.V., Léon, R., Fernández-Puga, M.C., Diaz del Río, V., Somoza, L., 2009. Contourite erosive features caused by the Mediterranean Outflow Water in the Gulf of Cadiz: Quaternary tectonic and oceanographic implications. Marine Geology 257, 24-40.

Gilli, A., Anselmetti, F.S., Ariztegui, D., Beres, M., McKenzie, J.A., Markgraf, V., 2004. Seismic stratigraphy, buried beach ridges and contourite drifts: the Late Quaternary history of the closed Lago Cardiel basin, Argentina (49°S). Sedimentology 52, 1-23.

Glogowski, S., Dullo, W.C., Feldens, P., Liebetrau, V., Reumont, J., Hühnerbach, V., Krastel, S., Wynn, R.B., Flögel, S., 2015. The Eugen Seibold coral mounds offshore western Morocco: oceanographic and bathymetric boundary conditions of a newly discovered cold-water coral province. Geo-Marine Letters 35, 257-269.

Gonthier, E.G., Faugères, J.-C., Stow, D.A.V., 1984. Contourite facies of the Faro Drift, Gulf of Cadiz. Geological Society, London, Special Publications 15, 275-292.

Hebbeln, D., Van Rooij, D., Wienberg, C., 2016. Good neighbours shaped by vigorous currents: Cold-water coral mounds and contourites in the North Atlantic. Marine Geology, 171-185.

Heezen, B.C., 1959. Dynamic Processes of Abyssal Sedimentation: Erosion, Transportation, and Redeposition on the Deep-sea floor. Geophysical Journal of the Royal Astronomical Society 2, 142-172.

Heezen, B.C., Hollister, C., 1964. Deep-sea current evidence from abyssal sediments. Marine Geology 1, 141-174.

Heezen, B.C., Hollister, C.D., Ruddiman, W.F., 1966. Shaping of the continental rise by deep geostrophic currents. Science 152, 502-508.

Heirman, K., De Batist, M., Arnaud, F., De Beaulieu, J.-L., 2012. Seismic stratigraphy of the late Quaternary sedimentary infill of Lac d'Armor (Kerguelen archipelago): a record of glacier retreat, sedimentary mass wasting and southern Westerly intensification. Antarctic Science 24, 608-618.

Hernández-Molina, F.J., 2009. Los Sistemas Deposicionales Contorníticos: ejemplos alrededor del Margen Ibérico, in: Flor Rodríguez, G., Gallastegui, J., Flor Blanco, G., Martín Llaneza, J. (Eds.), Nuevas contribuciones al margen Ibérico Atlántico 2009, Oviedo, pp. xxi-xxiv.

Hernández-Molina, F.J., Larter, R.D., Rebesco, M., Maldonado, A., 2006. Miocene reversal of bottom water flow along the Pacific Margin of the Antarctic Peninsula: Stratigraphic evidence from a contourite sedimentary tail. Marine Geology 228, 93-116.

Hernández-Molina, F.J., Llave, E., Stow, D.A.V., 2008. Continental slope contourites, in: Rebesco, M., Camerlenghi, A. (Eds.), Contourites. Elsevier, *Developments in Sedimentology*, ELSEVIER, pp. 379-407.

Hernández-Molina, F.J., Llave, E., Stow, D.A.V., García, M., Somoza, L., Vázquez, J.T., Lobo, F.J., Maestro, A., Díaz del Río, V., León, R., Medialdea, T., Gardner, J., 2006. The contourite depositional system of the Gulf of Cádiz: A sedimentary model related to the bottom current activity of the Mediterranean outflow water and its interaction with the continental margin. Deep Sea Research Part II: Topical Studies in Oceanography 53, 1420-1463.

Hernàndez-Molina, F.J., maldonado, A., Stow, D.A.V., 2008. Abyssal plain contourites, in: Rebesco, M., Camerlenghi, A. (Eds.), Contourites. Elsevier, pp. 347-378.

Hernández-Molina, F.J., Paterlini, M., Violante, R., Marshall, P., de Isasi, M., Somoza, L., Rebesco, M., 2009. Contourite depositional system on the Argentine Slope: An exceptional record of the influence of Antarctic water masses. Geology 37, 507-510.

Hernández-Molina, F.J., Serra, N., Stow, D.A.V., Llave, E., Ercilla, G., Van Rooij, D., 2011. Along-slope oceanographic processes and sedimentary products around the Iberian margin. Geo-Mar Lett (in press).

Hernández-Molina, F.J., Sierro, F.J., Llave, E., Roque, C., Stow, D.A.V., Williams, T., Lofi, J., Van der Schee, M., Arnáiz, A., Ledesma, S., Rosales, C., Rodríguez-Tovar, F.J., Pardo-Igúzquiza, E., Brackenridge, R.E., 2016. Evolution of the gulf of Cadiz margin and southwest Portugal contourite depositional system: Tectonic, sedimentary and paleoceanographic implications from IODP expedition 339. Marine Geology 377, 7-39

Hollister, C.D., 1697. Sediment distribution and deep circulation in the western North Atlantic. Columbia University, New York.

Hollister, C.D., Heezen, B.C., 1972. Geological effects of ocean bottom currents: Western Northern Atlantic, in: Gordon, A.I. (Ed.), Studies in physical Oceanography. Gordon and Breach, New York, pp. 37-66.

Hübscher, C., Dullo, C., Flögel, S., Titschack, J., Schönfeld, J., 2010. Contourite drift evolution and related coral growth in the eastern Gulf of Mexico and its gateways. International Journal of Earth Sciences 99, 191-206.

Huvenne, V.A.I., De Mol, B., Henriet, J.P., 2003. A 3D seismic study of the morphology and spatial distribution of buried coral banks in the Porcupine Basin, SW of Ireland. Marine Geology 198, 5-25.

Huvenne, V.A.I., Van Rooij, D., De Mol, B., Thierens, M., O'Donnell, R., Foubert, A., 2009. Sediment dynamics and palaeo-environmental context at key stages in the Challenger cold-water coral mound

formation: Clues from sediment deposits at the mound base. Deep Sea Research Part I: Oceanographic Research Papers 56, 2263-2280.

Iorga, M.C., Lozier, M.S., 1999. Signatures of the Mediterranean outflow from a North Atlantic climatology: 1. Salinity and density fields. Journal of Geophysical Research: Oceans 104, 25985-26009.

Llave, E., Hernández-Molina, F.J., Somoza, L., Díaz-del-Río, V., Stow, D.A.V., Maestro, A., Alveirinho Dias, J.M., 2001. Seismic stacking pattern of the Faro-Albufeira contourite system (Gulf of Cadiz): a Quaternary record of paleoceanographic and tectonic influences. Marine Geophysical Research 22, 487-508.

Llave, E., Hernández-Molina, F.J., Somoza, L., Stow, D.A.V., Díaz Del Río, V., 2007. Quaternary evolution of the contourite depositional system in the Gulf of Cadiz. Geological Society, London, Special Publications 276, 49-79.

Llave, E., Matias, H., Hernández-Molina, F., Ercilla, G., Stow, D., Medialdea, T., 2011. Pliocene–Quaternary contourites along the northern Gulf of Cadiz margin: sedimentary stacking pattern and regional distribution. Geo-Marine Letters 31, 377-390.

Llave, E., Schönfeld, J., Hernández-Molina, F.J., Mulder, T., Somoza, L., Díaz del Río, V., Sánchez-Almazo, I., 2006. High-resolution stratigraphy of the Mediterranean outflow contourite system in the Gulf of Cadiz during the late Pleistocene: The impact of Heinrich events. Marine Geology 227, 241-262.

Lo Iacono, C., Gràcia, E., Ranero, C.R., Emelianov, M., Huvenne, V.A.I., Bartolomé, R., Booth-Rea, G., Prades, J., Ambroso, S., Dominguez, C., Grinyó, J., Rubio, E., Torrent, J., 2014. The West Melilla cold water coral mounds, Eastern Alboran Sea: Morphological characterization and environmental context. Deep Sea Research Part II: Topical Studies in Oceanography 99, 316-326.

Lobo, F.J., Hernández-Molina, F.J., Somoza, L., Rodero, J., Maldonado, A., Barnolas, A., 2000. Patterns of bottom current flow deduced from dune asymmetries over the Gulf of Cadiz shelf (southwest Spain). Marine Geology 164, 91-117.

Locker, S.D., Laine, E.P., 1992. Paleogene-Neogene depositional history of the middle U.S. Atlantic continental rise: mixed turbidite and contourite depositional systems. Marine Geology 103, 137-164.

Maldonado, A., Barnolas, A., Bohoyo, F., Escutia, C., Galindo-Zaldívar, J., Hernández-Molina, J., Jabaloy, A., Lobo, F.J., Nelson, C.H., Rodríguez-Fernández, J., Somoza, L., Vázquez, J.-T., 2005. Miocene to Recent contourite drifts development in the northern Weddell Sea (Antarctica). Global and Planetary Change 45, 99-129.

Martins, I., Vitorino, J., 2012. Physical processes affecting the El-Arraiche mud volcano Field (NW Moroccan Margin), HERMIONE Final Meeting, Carvoeiro.

Martorelli, E., Bosman, A., Casalbore, D., Falcini, F., 2016. Interaction of down-slope and along-slope processes off Capo Vaticano (southern Tyrrhenian Sea, Italy), with particular reference to contourite-related landslides. Marine Geology 378, 43-55.

McCave, I.N., Carter, L., 1997. Recent sedimentation beneath the Deep Western Boundary Current off northern New Zealand. Deep Sea Research Part I: Oceanographic Research Papers 44, 1203-1237.

McCave, I.N., Tucholke, B.E., 1986. Deep current-controlled sedimentation in the western North Atlantic, in: McCreggor, B.A. (Ed.), The western North Atlantic region. The geological society of America, pp. 451-468.

Medialdea, T., Somoza, L., Pinheiro, L.M., Fernández-Puga, M.C., Vázquez, J.T., León, R., Ivanov, M.K., Magalhaes, V., Díaz-del-Río, V., Vegas, R., 2009. Tectonics and mud volcano development in the Gulf of Cádiz. Marine Geology 261, 48-63.

Mena, A., Francés, G., Pérez-Arlucea, M., Aguiar, P., Barreiro-Vázquez, J.D., Iglesias, A., Barreiro-Lois, A., 2015. A novel sedimentological method based on CT-scanning: Use for tomographic characterization of the Galicia Interior Basin. Sedimentary Geology 321, 123-138.

Mienis, F., De Stigter, H.C., De Haas, H., Van der Land, C., Van Weering, T.C.E., 2012. Hydrodynamic conditions in a cold-water coral mound area on the Renard Ridge, southern Gulf of Cadiz. Journal of Marine Systems 96–97, 61-71.

Mienis, F., de Stigter, H.C., White, M., Duineveld, G., de Haas, H., van Weering, T.C.E., 2007. Hydrodynamic controls on cold-water coral growth and carbonate-mound development at the SW and SE Rockall Trough Margin, NE Atlantic Ocean. Deep Sea Research Part I: Oceanographic Research Papers 54, 1655-1674.

Mienis, F., van Weering, T., de Haas, H., de Stigter, H., Huvenne, V., Wheeler, A., 2006. Carbonate mound development at the SW Rockall Trough margin based on high resolution TOBI and seismic recording. Marine Geology 233, 1-19.

Mulder, T., Hassan, R., Ducassou, E., Zaragosi, S., Gonthier, E., Hanquiez, V., Marchès, E., Toucanne, S., 2013. Contourites in the Gulf of Cadiz: a cautionary note on potentially ambiguous indicators of bottom current velocity. Geo-Marine Letters 33, 357-367.

Mutti, E., Carminati, M., 2012. Deep-Water Sands of the Brazilian Offshore Basins. AAPG Search and Discovery. article 30219 http://www.searchanddiscovery.com/documents/2012/30219mutti/ndx_mutti.pdf.

Nelson, H.C., Baraza, J., Maldonado, A., 1993. Mediterranean undercurrent sandy contourites, Gulf of Cadiz, Spain. Sedimentary Geology 82, 103-131.

Oiwane, H., Ikehara, M., Suganuma, Y., Miura, H., Nakamura, Y., Sato, T., Nogi, Y., Yamane, M., Yokoyama, Y., 2014. Sediment waves on the Conrad Rise, Southern Indian Ocean: Implications for the migration history of the Antarctic Circumpolar Current. Marine Geology 348, 27-36.

Palomino, D., Vázquez, J.-T., Ercilla, G., Alonso, B., López-González, N., Díaz-del-Río, V., 2011. Interaction between seabed morphology and water masses around the seamounts on the Motril Marginal Plateau (Alboran Sea, Western Mediterranean). Geo-Marine Letters 31, 465-479.

Piper, D.J.W., 1972. Sediments of the Middle Cambrian Burgess Shale, Canada. Lethaia 5, 169-175.

Pistek, P., de Strobel, F., Montanari, C., 1985. Deep-sea circulation in the Alboran Sea. Journal of Geophysical Research 90, 4969-4976.

Preu, B., Hernández-Molina, F.J., Violante, R., Piola, A.R., Paterlini, C.M., Schwenk, T., Voigt, I., Krastel, S., Spiess, V., 2013. Morphosedimentary and hydrographic features of the northern Argentine margin: The interplay between erosive, depositional and gravitational processes and its conceptual implications. Deep Sea Research Part I: Oceanographic Research Papers 75, 157-174.

Rahmstorf, 2006. Thermohaline Ocean Circulation, in: Elias, S.A. (Ed.), Encyclopedia of Quaternary Sciences, Amsterdam.

Rebesco, M., Hernández-Molina, F.J., van Rooij, D., Wåhlin, A., 2014. Contourites and associated sediments controlled by deep-water circulation processes: State of the art and future considerations. Marine Geology.

Rebesco, M., Richard, C.S., Cocks, L.R.M., Ian, R.P., 2005. Sedimentary environments: Contourites, Encyclopedia of Geology. Elsevier, Oxford, pp. 513-528.

Rebesco, M., Wåhlin, A., Laberg, J.S., Schauer, U., Beszczynska-Möller, A., Lucchi, R.G., Noormets, R., Accettella, D., Zarayskaya, Y., Diviacco, P., 2013. Quaternary contourite drifts of the Western Spitsbergen margin. Deep Sea Research Part I: Oceanographic Research Papers 79, 156-168.

Ribbe, J., Holloway, P.E., 2001. A model of suspended sediment transport by internal tides. Continental Shelf Research 21, 395-422.

Ribó, M., Puig, P., Muñoz, A., Lo Iacono, C., Masqué, P., Palanques, A., Acosta, J., Guillén, J., Gómez Ballesteros, M., 2016. Morphobathymetric analysis of the large fine-grained sediment waves over the Gulf of Valencia continental slope (NW Mediterranean). Geomorphology 253, 22-37.

Ribó, M., Puig, P., Salat, J., Palanques, A., 2013. Nepheloid layer distribution in the Gulf of Valencia, northwestern Mediterranean. Journal of Marine Systems 111–112, 130-138.

Ribó, M., Puig, P., van Haren, H., 2015. Hydrodynamics over the Gulf of Valencia continental slope and their role in sediment transport. Deep Sea Research Part I: Oceanographic Research Papers 95, 54-66.

Richardson, P.L., Bower, A.S., Zenk, W., 2000. A census of Meddies tracked by floats. Progress In Oceanography 45, 209-250.

Roberts, J.M., 2009. Cold-Water Coral Reefs, in: Steele, J.H., Turekian, K.K., Thorpe, S.A. (Eds.), Encyclopedia of Ocean Sciences (Second Edition). Academic Press, Oxford, pp. 615-625.

Roberts, J.M., Wheeler, A.J., Freiwald, A., 2006. Reefs of the Deep: The Biology and Geology of Cold-Water Coral Ecosystems. Science 312, 543-547.

Roque, C., Duarte, H., Terrinha, P., Valadares, V., Noiva, J., Cachão, M., Ferreira, J., Legoinha, P., Zitellini, N., 2012. Pliocene and Quaternary depositional model of the Algarve margin contourite drifts (Gulf of Cadiz, SW Iberia): Seismic architecture, tectonic control and paleoceanographic insights. Marine Geology 303–306, 42-62.

Sánchez, F., González-Pola, C., Druet, M., García-Alegre, A., Acosta, J., Cristobo, J., Parra, S., Ríos, P., Altuna, Á., Gómez-Ballesteros, M., Muñoz-Recio, A., Rivera, J., del Río, G.D., 2014. Habitat characterization of deep-water coral reefs in La Gaviera Canyon (Avilés Canyon System, Cantabrian Sea). Deep Sea Research Part II: Topical Studies in Oceanography 106, 118-140.

Sandström, J.W., 1908. Dynamische Versuche mit Meerwasser. Annalen der Hydrographie und Maritimen Meteorologie 36, 6-23.

Schneider, E.D., Fox, P.J., Hollister, C.D., Needham, H.D., Heezen, B.C., 1967. Further evidence of contour currents in the Western North Atlantic. Earth and Planetary Science Letters 2, 351-359.

Serra, N., Ambar, I., Boutov, D., 2010. Surface expression of Mediterranean Water dipoles and their contribution to the shelf/slope-open ocean exchange. Ocean Science Discussions 6, 191-209.

Shanmugam, G., 2012. New perspectives on deep-water sandstones: origin, recognition, initiation and reservoir quality. Handbook of Petroleum Exploration and Production. Elsevier, Amsterdam.

Shanmugam, G., 2013. New perspectives on deep-water sandstones: Implications. Petroleum Exploration and Development 40, 316-324.

Smith, W.H.F., Sandwell, D.T., 2004. Conventional bathymetry, bathymetry from space, and geodetic altimetry. Oceanography 17, 8-23.

Somoza, L., Ercilla, G., Urgorri, V., León, R., Medialdea, T., Paredes, M., Gonzalez, F.J., Nombela, M.A., 2014. Detection and mapping of cold-water coral mounds and living Lophelia reefs in the Galicia Bank, Atlantic NW Iberia margin. Marine Geology 349, 73-90.

Somoza, L., Medialdea, T., León, R., Ercilla, G., Vázquez, J.T., Farran, M.l., Hernández-Molina, J., González, J., Juan, C., Fernández-Puga, M.C., 2012. Structure of mud volcano systems and pockmarks in the region of the Ceuta Contourite Depositional System (Western Alborán Sea). Marine Geology 332–334, 4-26.

Stow, D.A.V., Faugères, J.-C., Howe, J.A., Pudsey, C.J., Viana, A.R., 2002. Bottom currents, contourites and deep-sea sediment drifts: current state-of-the-art. Geological Society, London, Memoirs 22, 7-20.

Stow, D.A.V., Faugères, J.C., 2008. Chapter 13 Contourite Facies and the Facies Model, in: Rebesco, M., Camerlenghi, A. (Eds.), Developments in Sedimentology. Elsevier, pp. 223-256.

Stow, D.A.V., Hernández-Molina, F.J., Alvarez Zarikian, C.A., and the Expedition 339 Scientists. 2013. Expedition 339 of the riserless drilling platform Ponta Delgada, Azores (Portugal), to Lisbon, Portugal Sites U1385–U1391 16 November 2011–16 January 2012, Proceedings IODP, 339. Integrated Ocean Drilling ProgramManagement International, Tokyo.

Stow, D.A.V., Hernández-Molina, F.J., Llave, E., Bruno, M., García, M., Díaz del Rio, V., Somoza, L., Brackenridge, R.E., 2013. The Cadiz Contourite Channel: Sandy contourites, bedforms and dynamic current interaction. Marine Geology 343, 99-114.

Stow, D.A.V., Hernández-Molina, F.J., Llave, E., Sayago-Gil, M., Díaz del Río, V., Branson, A., 2009. Bedform-velocity matrix: The estimation of bottom current velocity from bedform observations. Geology 37, 327-330.

Stow, D.A.V., Hunter, S., Wilkinson, D., Hernández-Molina, F.J., 2008. The nature of Contourite deposition, in: Rebesco, M., Camerlenghi, A. (Eds.), Developments in sedimentology: Contourites. Elsevier, Oxford, pp. 143-156.

Symons, W.O., Sumner, E.J., Talling, P.J., Cartigny, M.J.B., Clare, M.A., 2016. Large-scale sediment waves and scours on the modern seafloor and their implications for the prevalence of supercritical flows. Marine Geology 371, 130-148.

Thierens, M., Browning, E., Pirlet, H., Loutre, M.F., Dorschel, B., Huvenne, V.A.I., Titschack, J., Colin, C., Foubert, A., Wheeler, A.J., 2013. Cold-water coral carbonate mounds as unique palaeo-archives: the Plio-Pleistocene Challenger Mound record (NE Atlantic). Quaternary Science Reviews 73, 14-30.

Titschack, J., Baum, D., De Pol-Holz, R., López Correa, M., Forster, N., Flögel, S., Hebbeln, D., Freiwald, A., 2015. Aggradation and carbonate accumulation of Holocene Norwegian cold-water coral reefs. Sedimentology 62, 1873-1898.

Titschack, J., Thierens, M., Dorschel, B., Schulbert, C., Freiwald, A., Kano, A., Takashima, C., Kawagoe, N., Li, X., 2009. Carbonate budget of a cold-water coral mound (Challenger Mound, IODP Exp. 307). Marine Geology 259, 36-46.

Toucanne, S., Mulder, T., Schönfeld, J., Hanquiez, V., Gonthier, E., Duprat, J., Cremer, M., Zaragosi, S., 2007. Contourites of the Gulf of Cadiz: A high-resolution record of the paleocirculation of the Mediterranean outflow water during the last 50,000 years. Palaeogeography, Palaeoclimatology, Palaeoecology 246, 354-366.

Turnewitsch, R., Falahat, S., Nycander, J., Dale, A., Scott, R.B., Furnival, D., 2013. Deep-sea fluid and sediment dynamics—Influence of hill- to seamount-scale seafloor topography. Earth-Science Reviews 127, 203-241.

Uenzelmann-Neben, G., Gohl, K., 2012. Amundsen Sea sediment drifts: Archives of modifications in oceanographic and climatic conditions. Marine Geology 299–302, 51-62.

Van Daele, M., Bertrand, S., Meyer, I., Moernaut, J., Vandoorne, W., Siani, G., Tanghe, N., Ghazoui, Z., Pino, M., Urrutia, R., De Batist, M., 2016. Late Quaternary evolution of Lago Castor (Chile, 45.6°S): Timing of the deglaciation in northern Patagonia and evolution of the southern westerlies during the last 17 kyr. Quaternary Science Reviews 133, 130-146.

van der Land, C., Eisele, M., Mienis, F., de Haas, H., Hebbeln, D., Reijmer, J.J.G., van Weering, T.C.E., 2014. Carbonate mound development in contrasting settings on the Irish margin. Deep Sea Research Part II: Topical Studies in Oceanography 99, 297-306.

Van Rensbergen, P., Depreiter, D., Pannemans, B., Moerkerke, G., Van Rooij, D., Marsset, B., Akhmanov, G., Blinova, V., Ivanov, M., Rachidi, M., Magalhaes, V., Pinheiro, L., Cunha, M., Henriet, J.-P., 2005. The El Arraiche mud volcano field at the Moroccan Atlantic slope, Gulf of Cadiz. Marine Geology 219, 1-17.

Van Rooij, D., Blamart, D., De Mol, L., Mienis, F., Pirlet, H., Wehrmann, L.M., Barbieri, R., Maignien, L., Templer, S.P., de Haas, H., Hebbeln, D., Frank, N., Larmagnat, S., Stadnitskaia, A., Stivaletta, N., van Weering, T., Zhang, Y., Hamoumi, N., Cnudde, V., Duyck, P., Henriet, J.P., 2011. Cold-water coral mounds on the Pen Duick Escarpment, Gulf of Cadiz: The MiCROSYSTEMS project approach. Marine Geology 282, 102-117.

Van Rooij, D., Blamart, D., Richter, T., Wheeler, A., Kozachenko, M., Henriet, J.P., 2007. Quaternary sediment dynamics in the Belgica mound province, Porcupine Seabight: ice-rafting events and contour current processes. International Journal of Earth Sciences 96, 121-140.

Van Rooij, D., Iglesias, J., Hernández-Molina, F.J., Ercilla, G., Gomez-Ballesteros, M., Casas, D., Llave, E., De Hauwere, A., Garcia-Gil, S., Acosta, J., Henriet, J.P., 2010. The Le Danois Contourite Depositional System: Interactions between the Mediterranean Outflow Water and the upper Cantabrian slope (North Iberian margin). Marine Geology (2010) 274, 1-20.

van Weering, T.C.E., de Haas, H., de Stigter, H.C., Lykke-Andersen, H., Kouvaev, I., 2003. Structure and development of giant carbonate mounds at the SW and SE Rockall Trough margins, NE Atlantic Ocean. Marine Geology 198, 67-81.

Vandorpe, T., Van Rooij, D., Stow, D., Henriet, J.-P., 2011. Pliocene to Recent shallow-water contourite deposits on the shelf and shelf edge off south-western Mallorca, Spain. Geo-Marine Letters 31, 391-403.

Verdicchio, G., Trincardi, F., 2008. Mediterranean shelf-edge muddy contourites: examples from the Gela and South Adriatic basins. Geo-Marine Letters 28, 137-151.

Viana, A.R., Almeida, W., Jr, Nunes, M.C.V., Bulhoes, E.M., 2007. The economic importance of contourites. Geological Society, London, Special Publications 276, 1-23.

Viana, A.R., Faugères, J.C., Stow, D.A.V., 1998. Bottom-current-controlled sand deposits -- a review of modern shallow- to deep-water environments. Sedimentary Geology 115, 53-80.

Wåhlin, A., 2004. Topographic advection of dense bottom water. Journal of Fluid Mechanics 510, 95-104.

Wheeler, A.J., Beyer, A., Freiwald, A., de Haas, H., Huvenne, V.A.I., Kozachenko, M., Olu-Le Roy, K., Opderbecke, J., 2007. Morphology and environment of cold-water coral carbonate mounds on the NW European margin. International Journal of Earth Sciences 96, 37-56.

Wienberg, C., Hebbeln, D., Fink, H.G., Mienis, F., Dorschel, B., Vertino, A., Correa, M.L., Freiwald, A., 2009. Scleractinian cold-water corals in the Gulf of Cádiz—First clues about their spatial and temporal distribution. Deep Sea Research Part I: Oceanographic Research Papers 56, 1873-1893.

Wienberg, C., Titschack, J., 2016. Framework-Forming Scleractinian Cold-Water Corals Through Space and Time: A Late Quaternary North Atlantic Perspective, in: Rossi, S., Bramanti, L., Gori, A., Orejas, C. (Eds.), Marine Animal Forests: The ecology of Benthic Biodiversity Hotspots. Springer International Publishing Switzerland.

Chapter 2

Setting

Campaign 2: Le Danois - Belgica (2011)

Chapter 2 - Setting

The AMCP, Atlantic Moroccan Coral Province (35°N to 35°30'N and 6°30'W to 7°10'W; Figure 2.1), is situated within the northern part of the Atlantic Moroccan continental margin and contains several topographic obstacles, including tectonic ridges (Medialdea et al., 2009), mud volcanoes (Van Rensbergen et al., 2005) and coral mounds (Foubert et al., 2008). The northern part of the AMCP, containing the Renard and Vernadsky ridges as well as nine mud volcanoes is called the El Arraiche Mud Volcano Province (EAMVP; Figure 2.1). The morphology of the ridges and mud volcanoes and the position of the coral mounds is linked to the geological evolution of the southern Gulf of Cádiz (Somoza et al., 2002; Medialdea et al., 2004). As a consequence, it is an ideal region to investigate the effect of topographic obstacles of various sizes on bottom currents.
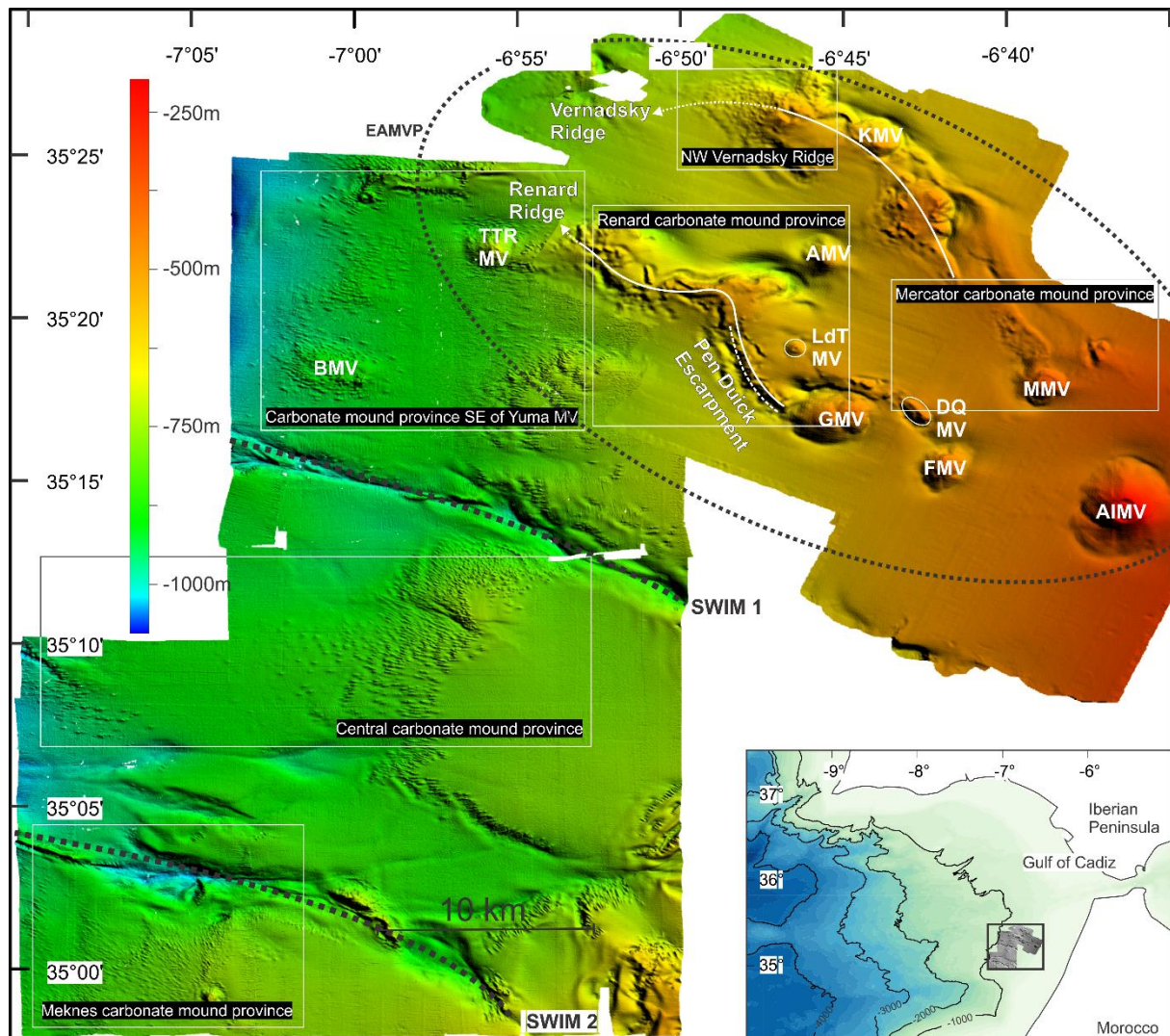
Figure 2.1: Overview of the AMCP, including the EAMVP, indicating the tectonic ridges (Renard and Vernadsky), the two extensional faults (SWIM 1 & 2), the nine mud volcanoes (white abbreviations) and the carbonate mound provinces (white rectangles). AIMV: Al Idrissi Mud Volcano, AMV: Adamastor Mud Volcano, BMV: Becks Mud Volcano, DQMV: Don Quichote Mud Volcano, EAMVP: El Arraiche Mud Volcano Field, FMV: Fiuza Mud Volcano, GMV: Gemini Mud Volcano, KMV: Kidd Mud Volcano, LdTMV: Lazarillo del Torme Mud Volcano, SWIM: Southwestern Iberian Margin.

The proximity of the region to the Strait of Gibraltar allows studying the influence of Mediterranean waters in the southern Gulf of Cádiz as well as the influence of the detected AAIW (Van Rooij et al., 2011; Mienis et al., 2012). The exact location of both water masses is rather poorly constrained and needs to be clarified in order to study the influence of both water masses on the various drift systems. In addition, the presence of internal tides (Van Rooij et al., 2011; Martins and Vitorino, 2012; Mienis et al., 2012) allows studying the effects of these oceanographic features on the sedimentological evolution.

1. Geology

1.1. Tectonic evolution

The present-day structure and geomorphology of the Gulf of Cádiz is the result of several episodes of rifting, extension and compression from the Triassic onwards (Maldonado et al., 1999; Medialdea et al., 2004; Figure 2.2). The movements include European-African plate convergence, dextral strike-slip convergence (mainly along the Azores-Gibraltar arc) and westward migration of the Betic - Rifian arc and Alboran domain (Dewey et al., 1989; Rosenbaum et al., 2002; Medialdea et al., 2009).

Extensional forces governed the region during Triassic and Late Cretaceous times due to the breakup of Pangea, with the opening of the Neo-Thetys and the Central Atlantic as a result (Heymann, 1989; Medialdea et al., 2009). Continued Jurassic spreading induced the separation of the African and Iberian margins, initially created during the Triassic, while a triple junction occurred between Africa, Iberia and North America during the Late Cretaceous (Mauffret et al., 1989; Maldonado et al., 1999). The Iberian plate got attached to Africa in the Late Cretaceous, but again detached during the Middle Eocene to Middle Miocene (Srivastava et al., 1990; Roest and Srivastava, 1991). The Azores-Gibraltar fracture zone became an active plate boundary between Africa and Iberia during that time as well (Figure 2.3).

From the Late Oligocene to Late Miocene, the Gulf of Cádiz experienced about 200 km of north-south convergence (African and Eurasian plates), leading to the development of the Alboran Sea as a back-arc basin (Comas et al., 1992). The westward migration of the orogenic front of the Gibraltar arc (and the Alboran domain) led to the development of two orogenic belts: the Betic cordillera on the Iberian margin and the Rif cordillera on the African margin (Dewey et al., 1989; Flinch, 1993; Figure 2.3). Associated foreland basins of both cordillera are the Guadalquivir and the Rharb Basin (Figure 2.3). The westward movement of the Alboran domain also led to the radial emplacement of a large olistostrome unit in the Gulf of Cádiz, called the Allochtonous Unit of the Gulf of Cádiz (AUGC; Dewey et al., 1989; Maldonado et al., 1999; Medialdea et al., 2004; Figure 2.3). The AUGC extends from the Iberian and Moroccan margins till the Horseshoe and Seine abyssal plains and consists of a series of westward imbricated thrusts (Figure 2.3) cutting through a thick sedimentary package (about 2.75 km; Maldonado et al., 1999). From the Late Miocene onwards, convergence (about 50 km) shifted to a northwest-southeast direction (Dewey et al., 1989). Post-Tortonian reorganisation induced extensional collapse of the AUGC along NW-SE extensional faults (of which both SWIM (south-western Iberian margin) faults in the research area are an example; Figure 2.3), tectonic subsidence and diapiric processes (Flinch et al., 1996; Medialdea et al., 2004; Fernández-Puga et al., 2007). The diapiric structures are mainly rooted in the AUGC and developed isolated morphological highs and ridge systems (e.g. the Guadalquivir diapiric ridge; Fernández-Puga et al., 2007). Although the tectonic activity decreased at the end of the Lower Pliocene and the margin evolved to a more stable phase (Medialdea et al., 2009), Quaternary uplift and reactivation of diapiric structures in the Gulf of Cádiz

have been observed (Fernández-Puga et al., 2007). The Renard and Vernadsky Ridges, bounded by lystric faults (Flinch, 1993), are thought to originate due to a local compressive regime that started about 2.4 Ma ago, in contrast to the general extensional regime in the Gulf of Cádiz (Van Rensbergen et al., 2005). These compressional forces induced the dissolution of an allochtonous salt body, located at least 1000 m in the subsurface (Perez-Garcia et al., 2011). Reactivation of these salt-tectonic forces caused the continued uplift of the Vernadsky ridge and in turn fuelled the mud volcanoes in the region (Perez-Garcia et al., 2011).
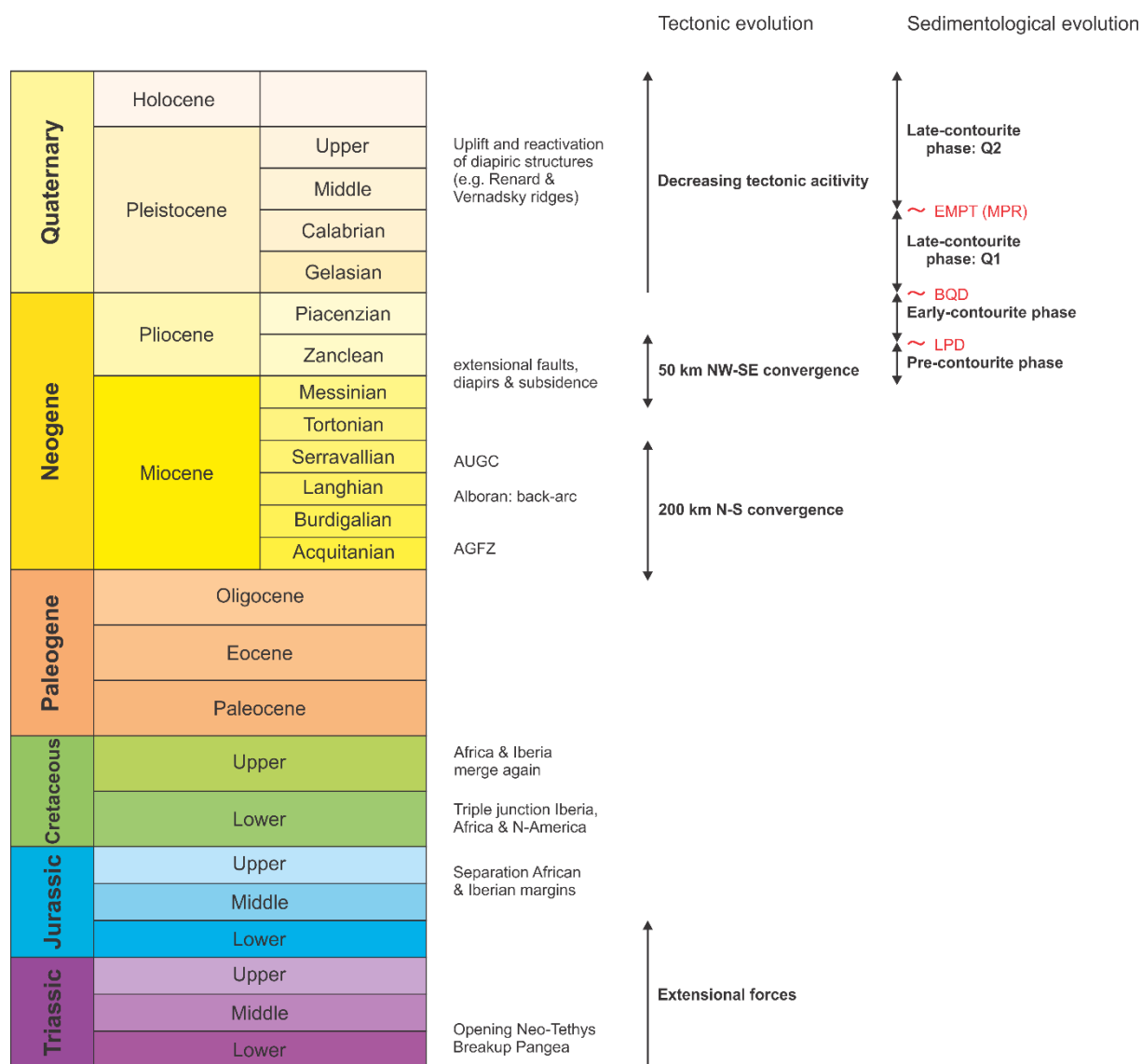
Figure 2.2: Stratigraphic table indicating the various tectonic and sedimentological changes in the southern Gulf of Cádiz. AGFZ: Azores-Gibraltar Fracture Zone; AUGC: Allochthonous Unit of the Gulf of Cádiz; EMPT: Early-Middle Pleistocene Transition; MPR: Middle-Pleistocene Revolution; BQD: Base Quaternary Discontinuity; LPR: Lower Pliocene Discontinuity.

The sedimentation in the Gulf of Cádiz (Figure 2.2) on top of the olistostrome unit is controlled by regional tectonic forces, eustatic variations and bottom current activity (Maldonado et al., 1999; Llave et al., 2011). Maldonado et al. (1999) discerned 4 main units above the olistostrome unit. The lower unit is Messinian in age and consists of clays and interbedded fine-grained sand lenses. This unit drapes the irregularities of the underlying deposits. The second unit is Lower Pliocene in age and can be up to several hundred of meters thick between the diapiric ridges. The lithologies encountered within this

unit comprise clays and interbedded sandy clays, both of hemipelagic origin. The first expressions of contourite drifts systems in the northern Gulf of Cádiz are present within this unit (Maldonado et al., 1999; Llave et al., 2011; Brackenridge et al., 2013). The third unit is Upper Pliocene in age and consists of clays and sands of hemipelagic and contouritic origin. In the southern Gulf of Cádiz, thicknesses can be up to 1000 m (Maldonado et al., 1999). The final and upper unit is Upper Pliocene and Quaternary in age and is composed of several subunits, controlled by the structure of the margin, the sediment source and the eustatic variations (Rodero et al., 1999). Llave et al. (2011) published a similar stratigraphy on the northern Gulf of Cádiz contourite depositional system, comprising four units in three phases. The pre-contourite phase, ranging from 5.6 to 4.2 Ma (Lower Pliocene discontinuity), contains unit P1 and the sediments are hemipelagic and pelagic in origin. The early contourite phase, ranging from 4.2 to 2.4 Ma (Base Quaternary discontinuity) contains unit P2 and has a sheeted drift origin. Finally, the late-contourite phase, lasting from 2.6 Ma till present contains units Q1 and Q2. They are separated by the Mid-Pleistocene boundary, a boundary that was recently updated to the Early-Middle Pleistocene Transition (EMPT; Head et al., 2008). The EMPT indicates the transition from obliquity controlled to eccentricity controlled climatic cycles. Units Q1 and Q2 are characterized by mounded elongated and separated drifts.

1.2. Mud volcanism

The sedimentary cover on top of the AUGC is Neogene in age and is pierced by numerous mud volcanoes, salt diapirs, diapiric ridges and other fluid escape features, such as pockmarks (Somoza et al., 2003; Medialdea et al., 2009). Mud volcano build up is related to over-pressured fluid muds rising to the surface as a consequence of compressional tectonics (Medialdea et al., 2009). This happens in two stages with diapirism and small-scale tectonic processes creating ideal pathways for migration of gas towards the surface as a first step (Maldonado et al., 1999; Medialdea et al., 2004; Medialdea et al., 2009). Possible sources are biogenic gas from Miocene shales and thermogenic gas from the AUGC (Medialdea et al., 2009). Secondly, fault-controlled extrusion of fluids and mud flows helps build up the edifices of the mud volcanoes (Pinheiro et al., 2003; Van Rensbergen et al., 2005; Medialdea et al., 2009). Circular depressions are usually present around the mud volcanoes and originate due to subsidence (subsidence rims; Camerlenghi et al., 1995) or result from the interaction of the mud volcano with bottom currents (Somoza et al., 2002). A combination of both processes is suggested by Van Rensbergen et al. (2005).

Most mud volcanoes in the Gulf of Cádiz are located within the offshore Betic - Rifian domain of the accretionary wedge (Medialdea et al., 2004). The mud volcanoes are grouped into fields: the Guadalquivir ridge field and the TASYO (Transferencia Sedimentaria en Talud Y Mega-Olistostromas) field at the offshore prolongation of the Guadalquivir Basin (Betic foreland basin) and the Spanish-Moroccan field at the offshore prolongation of the Rharb basin (the Rifian foreland basin). The Spanish-Moroccan field contains the EAMVP, which itself contains 9 mud volcanoes (Figure 2.1) ranging from 1 to 5.5 km in width and 45 m to 255 m in height (Somoza et al., 2003; Van Rensbergen et al., 2005; Hebbeln et al., 2008). The base of the mud volcanoes in the EAMVP is assigned to the regional Upper Pliocene unconformity and correlation with the industrial LAR-1 well yielded an age of 2.4 Ma (Van Rensbergen et al., 2005). A forth cluster is present at deeper water depths and is called the deep Portuguese margin field (Medialdea et al., 2009; Figure 2.3).
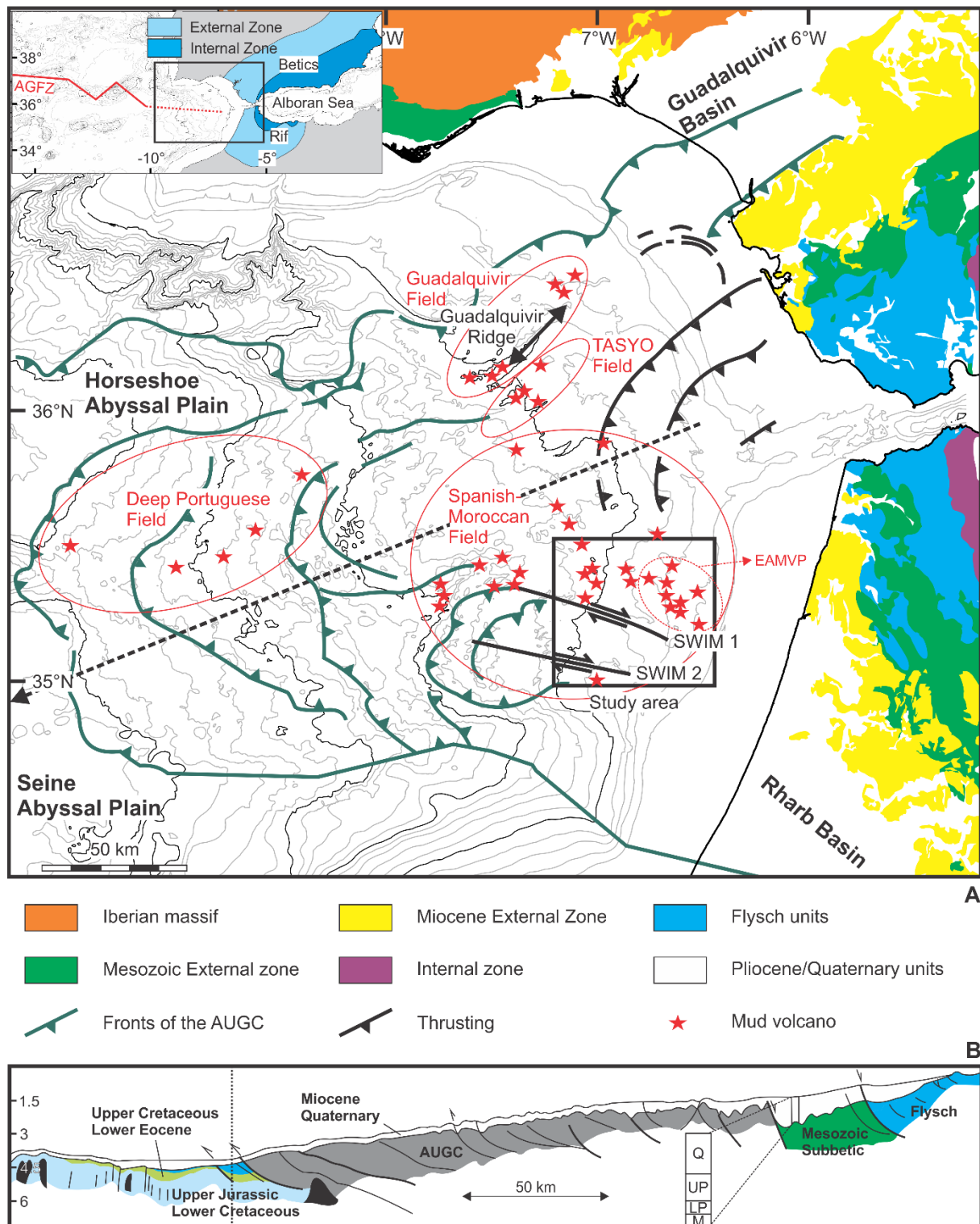
Figure 2.3: Geological setting of the Gulf of Cádiz, based on Medialdea et al. (2009). A. The deformation zones of the AUGC are indicated by dark green lines. The mud volcanoes are indicated by red stars and those of the study area have been updated. The inset in the upper left corner shows the Betic and Rifian chains with both their internal and external zones. These are displayed in greater detail on the big map. The dashed black line in the middle of the Gulf of Cádiz indicates the location of the simplified cross-section. B. Simplified cross-section through the Gulf of Cádiz. The depths are indicated in kilometers. The dotted line indicates the end of the profile on the map above. Diapirs are shown in black. AGFZ: Azores-Gibraltar Fault Zone, AUGC: Allochtonous Unit of the Gulf of Cádiz, EAMVP: El Arraiche Mud Volcano Province, LP: Lower Pliocene, M: Miocene, Q: Quaternary, SWIM: Southwest Iberian Margin, UP: Upper Pliocene.

The mud volcanoes originate due to Neogene compressional tectonics which induced sediment liquefaction at shallow depths (max 2 km; Flinch, 1993; Medialdea et al., 2004; Hensen et al., 2007). The transformation from smectite to illite and the accompanied dehydration is the most common source of fluids (Pinheiro et al., 2003). The fluids dissolve the top of the salt body and induce sediment fluidization and mobilization, which then migrate upwards and feed the mud volcanoes at the seafloor (Perez-Garcia et al., 2011). Build-up of the mud volcanoes in the Gulf of Cádiz occurred through successive extrusions of mud and yielded Christmas-tree structures in the subsurface (Somoza et al., 2003; Van Rensbergen et al., 2005). Perez-Garcia et al. (2011) showed that for the Mercator and a neighbouring buried mud volcano, 4 extrusions took place.

1.3. Cold-water corals and coral mounds

In the southern Gulf of Cádiz, no living specimen of cold water corals (CWC's) are encountered (Foubert et al., 2008; Van Rooij et al., 2011), however isolated patches of fossil coral and coral rubble are abundant (Wienberg et al., 2009) indicating past periods of proliferation. Most of these occurrences are found in the vicinity or on top of topographic obstacles (Pinheiro et al., 2003; Somoza et al., 2003; Foubert et al., 2008; Hebbeln et al., 2008). Wienberg et al. (2010) indicated that coral growth in the Gulf of Cádiz mainly occurred during glacial periods, although *Madrepora Oculata* shows a higher resilience to abrupt environmental changes compared to *Lophelia Pertusa* (Wienberg et al., 2009). In the southern Gulf of Cádiz, many of the CWC's are encountered on small mounds in the vicinity of large topographic obstacles (Foubert et al., 2008) and are the result of framework-forming Scleractinian CWC (Wienberg and Titschack, 2015). So-called "juvenile" (with respect to size, around 30 m high) coral mounds occur on top of the Pen Duick escarpment (PDE), e.g. Alpha, Beta and Gamma mound (Foubert et al., 2008; Frank et al., 2009; De Mol et al., 2011; Van Rooij et al., 2011). The position on top of a topographic height puts them in the pathway of elevated bottom currents, which may increase their food and sediment supply (Van Rooij et al., 2011), both prerequisites for coral mound growth (Hebbeln et al., 2016; Wienberg and Titschack, 2016). Moreover, the hardgrounds (carbonate crusts) that developed on top of the PDE due to stratigraphic migration (along Miocene strata) of hydrocarbons can provide the ideal place for settlement of CWC (Van Rooij et al., 2011). Finally, diagenetic processes are responsible for internal geochemical changes (aragonite dissolution and carbonate precipitation), adding to their stability, but also to the "resetting" of their palaeo-environmental recording capability (Pirlet et al., 2010).

The coral mounds occur in clusters and provinces, four of which were delineated in the Atlantic Moroccan continental margin by Foubert et al. (2008). In this study, these provinces have been bundled into one Renard carbonate mound province (Figure 2.1). In 2008, Hebbeln et al. (2008) discovered another four provinces, yielding five large carbonate mound provinces in the AMCP (Figure 2.1).

2. Oceanography

In the Gulf of Cádiz, 5 water masses are known to occur (Figure 2.4): the North Atlantic Surface Water (NASW, 0-100 m), the NACW (100-600 m), the AAIW (600-1500 m), the MOW and the North Atlantic Deep Water (NADW, beneath 1500 m) (Machín, et al., 2006; Ambar et al., 2008; Louarn and Morin, 2011). Within the southern part of the Gulf of Cádiz, the MOW occurs as meddies and has Si-values between 10 and 15 µmol/l and PO_4-values between 0.39 and 0.7 µmol/l (Richardson et al., 2000; Cabecadas et al., 2002).

NASW represents the upper 100 meters of the water column and consists of modified NACW. The NACW is characterized by a linear decrease in temperature (16°-12°C) and salinity (36.25-35.5; Criado-Aldeanueva et al., 2006; Louarn and Morin, 2011) and very low nutrient values; Si-values are usually below 10 µmol/L and PO_4-values between 0.7 and 1 µmol/L (Cabecadas et al., 2002; Machín et al., 2006a; Machín et al., 2006b). The general flow direction of the NACW is from west to east in the Gulf of Cádiz. NACW recirculates along the African coast due to deflection of a coastal upwelling zone and splits up along the Iberian margin, where one branch flows directly into the Mediterranean Sea (Pelegrí et al., 2005; Machín et al., 2006; Figure 2.4). The general circulation pattern of these upper two water masses (NACW and NASW) is anticyclonic, as they are part of the Azores current, which is in turn part of the north-eastern Atlantic circulation (Machín et al., 2006).

Although intensive mixing with under- and overlying water masses makes the direct recognition of AAIW problematic, it is known to flow cyclonically along the African coast (entering the Gulf of Cádiz in the southwest and exiting it in the northwest) at water depths between 600 and 1500 m (Louarn and Morin, 2011, Figure 2.4). Typical nutrient values are in the range of 10.9 - 11.9 µmol/l for Si and between 1.1 and 1.5 µmol/l for PO_4 (Cabecadas et al., 2002; Louarn and Morin, 2011). Below 1500 meters, NADW is present, and flows from south to north in the Gulf of Cádiz (Figure 2.4), along the Atlantic margin. It is characterized by low salinities (<35.5) and temperatures (<8° C; Louarn and Morin, 2011), although its nutrient content is very high with Si-values above 15 µmol/l and PO_4-values between 1 and 1.5 µmol/l (Cabecadas et al., 2002; Machín et al., 2006).

At present, MOW does not occur along the Renard Ridge, as Mediterranean waters are not observed above 700 meters water depth (Mienis et al., 2012) and CTD (conductivity, temperature, depth) data do not indicate their presence (Van Rooij et al., 2011). However, meddies are known to transport MOW south of the Strait of Gibraltar (Richardson et al., 2000; Ambar et al., 2008) and the MOW is strongly influenced by glacial-interglacial alternations, with a stronger MOW during glacial periods (Toucanne et al., 2007). Consequently, the influence of the MOW in the region cannot be excluded, certainly as Van Rooij et al. (2011) and Foubert et al. (2008) inferred the possibility of an intensified glacial MOW, being able to reach the PDE through enhanced meddy activity.
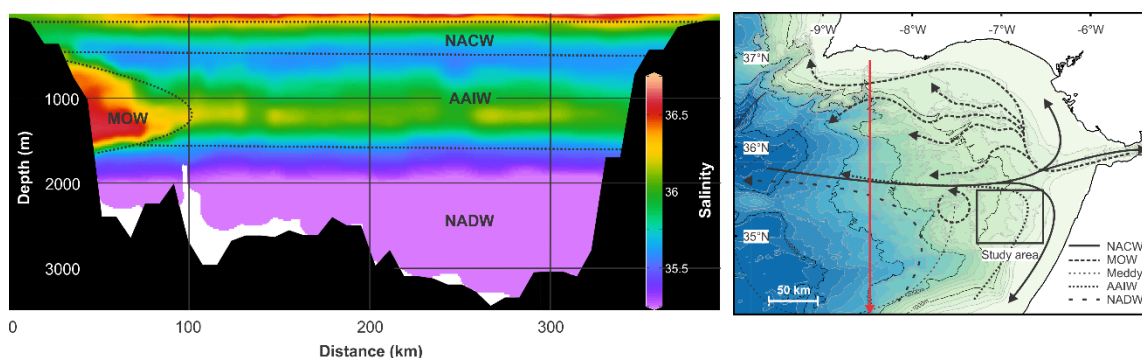
Figure 2.4: N-S oceanographic transect (left, Ocean Data View) and their different flow paths (right) within the Gulf of Cádiz. Five water masses are present: North Atlantic Surface Water (not indicated) occupies the upper 100 meters of the water column. NACW: North Atlantic Central Water; AAIW: Antarctic Intermediate Water; MOW: Mediterranean Outflow Water; NADW: North Atlantic Deep Water.

References

Ambar, I., Serra, N., Neves, F., Ferreira, T., 2008. Observations of the Mediterranean Undercurrent and eddies in the Gulf of Cadiz during 2001. Journal of Marine Systems 71, 195-220.

Brackenridge, R.E., Hernández-Molina, F.J., Stow, D.A.V., Llave, E., 2013. A Pliocene mixed contourite–turbidite system offshore the Algarve Margin, Gulf of Cadiz: Seismic response, margin evolution and reservoir implications. Marine and Petroleum Geology 46, 36-50.

Cabecadas, G., José Brogueira, M., Goncalves, C., 2002. The chemistry of Mediterranean outflow and its interactions with surrounding waters. Deep Sea Research Part II: Topical Studies in Oceanography 49, 4263-4270.

Camerlenghi, A., Cita, M.B., Vedova, B.D., Fusi, N., Mirabile, L., Pellis, G., 1995. Geophysical evidence of mud diapirism on the Mediterranean Ridge accretionary complex. Marine Geophysical Researches 17, 115-141.

Comas, M.C., García-Dueñas, V., Jurado, M.J., 1992. Neogene tectonic evolution of the Alboran Sea from MCS data. Geo-Marine Letters 12, 157-164.

Criado-Aldeanueva, F., García-Lafuente, J., Vargas, J.M., Del Río, J., Vázquez, A., Reul, A., Sánchez, A., 2006. Distribution and circulation of water masses in the Gulf of Cadiz from in situ observations. Deep Sea Research Part II: Topical Studies in Oceanography 53, 1144-1160.

De Mol, L., Hilário, A., Van Rooij, D., Henriet, J.P., 2011. Habitat mapping of a cold-water coral mound on Pen Duick escarpment (Gulf of Cadiz), in: harris, P., Baker, E. (Eds.), Seafloor morphology as benthic habitat. Elsevier, pp. 645-654.

Dewey, J.F., Helman, M.L., Knott, S.D., Turco, E., Hutton, D.H.W., 1989. Kinematics of the western Mediterranean. Geological Society, London, Special Publications 45, 265-283.

Fernández-Puga, M.C., Vázquez, J.T., Somoza, L., Díaz del Rio, V., Medialdea, T., Mata, M.P., León, R., 2007. Gas-related morphologies and diapirism in the Gulf of Cádiz. Geo-Marine Letters 27, 213-221.

Flinch, J.F., 1993. Tectonic evolution of the Gibraltar Arc. Rice University, Houston, Texas, p. 381.

Flinch, J.F., Bally, A.W., Wu, S.G., 1996. Emplacement of a passive-margin evaporitic allochton in the Betic Cordillera of Spain. Geology 24, 67-70.

Foubert, A., Depreiter, D., Beck, T., Maignien, L., Pannemans, B., Frank, N., Blamart, D., Henriet, J.-P., 2008. Carbonate mounds in a mud volcano province off north-west Morocco: Key to processes and controls. Marine Geology 248, 74-96.

Frank, N., Ricard, E., Lutringer-Paquet, A., van der Land, C., Colin, C., Blamart, D., Foubert, A., Van Rooij, D., Henriet, J.-P., de Haas, H., van Weering, T., 2009. The Holocene occurrence of cold water corals in the NE Atlantic: Implications for coral carbonate mound evolution. Marine Geology 266, 129-142.

Head, M.J., Pillans, B., Farquhar, S.A., 2008. The Early–Middle Pleistocene Transition: characterization and proposed guide for the defining boundary. Episodes 31, 255-259.

Hebbeln, D., Van Rooij, D., Wienberg, C., 2016. Good neighbours shaped by vigorous currents: Cold-water coral mounds and contourites in the North Atlantic. Marine Geology, 171-185.

Hebbeln, D., Wienberg, C., Participants, C., 2008. Report and preliminary results of RV Pelagia cruise 64PE284, Cold-water corals in the Gulf of Cádiz and on Coral Patch Seamont, Portimao-Portimao, 18.02-09.03.2008. Reports of the Department of Geosciences (GeoB) of the University of Bremen, University of Bremen, Germany, p. 90.

Hensen, C., Nuzzo, M., Hornibrook, E., Pinheiro, L.M., Bock, B., Magalhães, V.H., Brückmann, W., 2007. Sources of mud volcano fluids in the Gulf of Cadiz—indications for hydrothermal imprint. Geochimica et Cosmochimica Acta 71, 1232-1248.

Heymann, M.A.W., 1989. Tectonic and Depositional History of the Moroccan Continental Margin, in: Tankard, A.J., Balkwill, H.R. (Eds.), Extensional Tectonics and Stratigraphy of the Northern Atlantic Margins. Am. Assoc. Pet. Geol. and Can. Geol. Found. AAPG Mem, pp. 323-340.

Llave, E., Matias, H., Hernández-Molina, F., Ercilla, G., Stow, D., Medialdea, T., 2011. Pliocene–Quaternary contourites along the northern Gulf of Cadiz margin: sedimentary stacking pattern and regional distribution. Geo-Marine Letters 31, 377-390.

Louarn, E., Morin, P., 2011. Antarctic Intermediate Water influence on Mediterranean Sea Water outflow. Deep Sea Research Part I: Oceanographic Research Papers 58, 932-942.

Machín, F., Hernández-Guerra, A., Pelegrí, J.L., 2006a. Mass fluxes in the Canary Basin. Progress In Oceanography 70, 416-447.

Machín, F., Pelegrí, J.L., Marrero-Díaz, A., Laiz, I., Ratsimandresy, A.W., 2006b. Near-surface circulation in the southern Gulf of Cádiz. Deep Sea Research Part II: Topical Studies in Oceanography 53, 1161-1181.

Maldonado, A., Somoza, L., Pallarés, L., 1999. The Betic orogen and the Iberian-African boundary in the Gulf of Cadiz: geological evolution (central North Atlantic). Marine Geology 155, 9-43.

Martins, I., Vitorino, J., 2012. Physical processes affecting the El-Arraiche mud volcano Field (NW Moroccan Margin), HERMIONE Final Meeting, Carvoeiro.

Mauffret, A., Mougenot, D., Miles, P.R., Malod, J.A., 1989. Results from Multichannel Reflection Profiling of the Tagus Abyssal Plain (Portugal). Comparison with the Canadian Margin, in: Tankard, A.J., Balkwill, H.R. (Eds.), Extensional Tectonics and Stratigraphy of the Northern Atlantic Margins. Am. Assoc. Pet. Geol. and Can. Geol. Found. AAPG Mem, pp. 379-393.

Medialdea, T., Somoza, L., Pinheiro, L.M., Fernández-Puga, M.C., Vázquez, J.T., León, R., Ivanov, M.K., Magalhaes, V., Díaz-del-Río, V., Vegas, R., 2009. Tectonics and mud volcano development in the Gulf of Cádiz. Marine Geology 261, 48-63.

Medialdea, T., Vegas, R., Somoza, L., Vázquez, J.T., Maldonado, A., Día-del-Río, V., Maestro, A., Córdoba, D., Fernández-Puga, M.C., 2004. Structure and evolution of the "Olistostrome" complex of the Gibraltar Arc in the Gulf of Cádiz (eastern Central Atlantic): evidence from two long seismic cross-sections. Marine Geology 209, 173-198.

Mienis, F., De Stigter, H.C., De Haas, H., Van der Land, C., Van Weering, T.C.E., 2012. Hydrodynamic conditions in a cold-water coral mound area on the Renard Ridge, southern Gulf of Cadiz. Journal of Marine Systems 96–97, 61-71.

Pelegrí, J.L., Arístegui, J., Cana, L., González-Dávila, M., Hernández-Guerra, A., Hernández-León, S., Marrero-Díaz, A., Montero, M.F., Sangrà, P., Santana-Casiano, M., 2005. Coupling between the open ocean and the coastal upwelling region off northwest Africa: water recirculation and offshore pumping of organic matter. Journal of Marine Systems 54, 3-37.

Perez-Garcia, C., Berndt, C., Klaeschen, D., Mienert, J., Haffert, L., Depreiter, D., Haeckel, M., 2011. Linked halokinesis and mud volcanism at the Mercator mud volcano, Gulf of Cadiz. Journal of Geophysical Research: Solid Earth 116, n/a-n/a.

Pinheiro, L.M., Ivanov, M.K., Sautkin, A., Akhmanov, G., Magalhães, V.H., Volkonskaya, A., Monteiro, J.H., Somoza, L., Gardner, J., Hamouni, N., Cunha, M.R., 2003. Mud volcanism in the Gulf of Cadiz: results from the TTR-10 cruise. Marine Geology 195, 131-151.

Pirlet, H., Wehrmann, L.M., Brunner, B., Frank, N., Dewanckele, J.A.N., Van Rooij, D., Foubert, A., Swennen, R., Naudts, L., Boone, M., Cnudde, V., Henriet, J.-P., 2010. Diagenetic formation of gypsum and dolomite in a cold-water coral mound in the Porcupine Seabight, off Ireland. Sedimentology 57, 786-805.

Richardson, P.L., Bower, A.S., Zenk, W., 2000. A census of Meddies tracked by floats. Progress In Oceanography 45, 209-250.

Rodero, J., Pallarés, L., Maldonado, A., 1999. Late Quaternary seismic facies of the Gulf of Cadiz Spanish margin: depositional processes influenced by sea-level change and tectonic controls. Marine Geology 155, 131-156.

Roest, W.R., Srivastava, S.P., 1991. Kinematics of the plate boundaries between Eurasia, Iberia, and Africa in the North Atlantic from the Late Cretaceous to the present. Geology 19, 613-616.

Rosenbaum, G., Lister, G.S., Duboz, C., 2002. Relative motions of Africa, Iberia and Europe during Alpine orogeny. Tectonophysics 359, 117-129.

Somoza, L., Díaz del Río, V., León, R., Ivanov, M., Fernández-Puga, M.C., Gardner, J.M., Hernández-Molina, F.J., Pinheiro, L.M., Rodero, J., Lobato, A., Maestro, A., Vázquez, J.T., Medialdea, T., Fernández-Salas, L.M., 2003. Seabed morphology and hydrocarbon seepage in the Gulf of Cádiz mud volcano area: Acoustic imagery, multibeam and ultra-high resolution seismic data. Marine Geology 195, 153-176.

Somoza, L., Gardner, J.M., Díaz-del-Río, V., Vázquez, J.T., Pinheiro, L.M., Hernández-Molina, F.J., parties, T.A.s.s., 2002. Numerous methane gas-related sea floor structures identified in Gulf of Cadiz. Eos, Transactions American Geophysical Union 83, 541-549.

Srivastava, S.P., Schouten, H., Roest, W.R., Klitgord, K.D., Kovacs, L.C., Verhoef, J., Macnab, R., 1990. Iberian plate kinematics: a jumping plate boundary between Eurasia and Africa. Nature 344, 756-759.

Toucanne, S., Mulder, T., Schönfeld, J., Hanquiez, V., Gonthier, E., Duprat, J., Cremer, M., Zaragosi, S., 2007. Contourites of the Gulf of Cadiz: A high-resolution record of the paleocirculation of the Mediterranean outflow water during the last 50,000 years. Palaeogeography, Palaeoclimatology, Palaeoecology 246, 354-366.

Van Rensbergen, P., Depreiter, D., Pannemans, B., Henriet, J.-P., 2005. Seafloor expression of sediment extrusion and intrusion at the El Arraiche mud volcano field, Gulf of Cadiz. Journal of Geophysical Research: Earth Surface 110, F02010.

Van Rensbergen, P., Depreiter, D., Pannemans, B., Moerkerke, G., Van Rooij, D., Marsset, B., Akhmanov, G., Blinova, V., Ivanov, M., Rachidi, M., Magalhaes, V., Pinheiro, L., Cunha, M., Henriet, J.-P., 2005. The El Arraiche mud volcano field at the Moroccan Atlantic slope, Gulf of Cadiz. Marine Geology 219, 1-17.

Van Rooij, D., Blamart, D., De Mol, L., Mienis, F., Pirlet, H., Wehrmann, L.M., Barbieri, R., Maignien, L., Templer, S.P., de Haas, H., Hebbeln, D., Frank, N., Larmagnat, S., Stadnitskaia, A., Stivaletta, N., van Weering, T., Zhang, Y., Hamoumi, N., Cnudde, V., Duyck, P., Henriet, J.P., 2011. Cold-water coral mounds on the Pen Duick Escarpment, Gulf of Cadiz: The MiCROSYSTEMS project approach. Marine Geology 282, 102-117.

Wienberg, C., Frank, N., Mertens, K.N., Stuut, J.-B., Marchant, M., Fietzke, J., Mienis, F., Hebbeln, D., 2010. Glacial cold-water coral growth in the Gulf of Cádiz: Implications of increased palaeo-productivity. Earth and Planetary Science Letters 298, 405-416.

Wienberg, C., Hebbeln, D., Fink, H.G., Mienis, F., Dorschel, B., Vertino, A., Correa, M.L., Freiwald, A., 2009. Scleractinian cold-water corals in the Gulf of Cádiz—First clues about their spatial and temporal distribution. Deep Sea Research Part I: Oceanographic Research Papers 56, 1873-1893.

Wienberg, C., Titschack, J., 2016. Framework-Forming Scleractinian Cold-Water Corals Through Space and Time: A Late Quaternary North Atlantic Perspective, in: Rossi, S., Bramanti, L., Gori, A., Orejas, C. (Eds.), Marine Animal Forests: The ecology of Benthic Biodiversity Hotspots. Springer International Publishing Switzerland.

Chapter 3

Methods

Chapter 3 – Methods

The bulk of the data acquired within this dissertation are geophysical (single channel sparker reflection seismic, parasound and multibeam bathymetric data), although some datasets are sediment core-related (grain-size measurements, computed tomography images, chemical and physical content of the sediment core) or oceanographic datasets (current measurements and properties of the water column). The general applied methodologies used in this dissertation will be discussed in this chapter, while the specific settings (and/or materials) for each of the datasets will be discussed in the specific chapters. However, a table containing all used datasets is given below (Table 3.1).

Device	Year	Description	Amount	Origin
Sparker	2002	Single-channel seismic profiles	480 km	R/V Belgica
	2005	Single-channel seismic profiles	1120 km	R/V Belgica
	2007	Single-channel seismic profiles	900 km	R/V Belgica
	2009	Single-channel seismic profiles	605 km	R/V Belgica
	2013	Single-channel seismic profiles	1000 km	R/V Belgica
Airgun	2005	Multi-channel seismic profile	20 km	R/V Pelagia
Parasound	2014	Single-channel seismic profiles	1430 km	R/V Maria S. Merian
SIMRAD E1002	2002	Bathymetric data	700 km²	R/V Belgica
KongsbergEM300	2006	Bathymetric data	1200 km²	R/V Pelagia
Nutrient	2009	Si, PO_4 and NO_x content of water samples	36 station	NRP A. Gago Coutinho
LADCP	2013	Current directions and intensities	9 stations	R/V Belgica
CT	2015	3D non-destructive radiographs of cores	5 cores	UZ Ghent
XRF		Chemical content of cores	5 cores	CSIC/IGME
MSCL		Geophysical properties of cores	5 cores	CSIC/IGME
Grain size		Grain-size measurements of cores	5 cores	CSIC/IGME

Table 3. 1: Summary of the data used for this dissertation. Detailed information can be found in Chapters 4-7. AMCP: Atlantic Moroccan coral Province, CT: X-ray computed tomography, EAMVP: El Arraiche mud volcano province, LADCP: lowered acoustic Doppler profiler, MSCL: multi-sensor core logger, XRF: X-ray fluorescence .

1. Reflection seismic profiling

1.1. Acquisition

Single channel seismic reflection profiles from the Atlantic Moroccan coral province (AMCP) have been obtained using a SIG sparker source (operating at 600 J; frequency range between 900 and 1400 Hz) and a sub-bottom profiler (SBP) ATLAS Parasound (type 70; frequency range between 0.5 and 6 kHz) in order to visualize the contourite drifts and coral mounds.

The sparker system consists of a power supply, the sparker electrodes themselves (100 electrodes) and a streamer, consisting of 10 hydrophones, each 0.5 m apart (Figure 3.1). The capacitor within the power supply discharges electrical energy (ranging from 100 to 600 J) through the 100 electrodes (Reynolds, 2011) after which the seawater is ionized between the tips of the electrodes and the frame, creating hydrogen bubbles which then implode, causing the typical sparker pulse (Reynolds, 2011). The best pulse shape is created when a large amount of electrodes is present.

A parametric echosounder uses two main primary frequencies (18 kHz and 20.5 - 23.5 kHz) resulting in the generation of a secondary frequency generated in the central part of the beam. The interaction

between both simultaneously transmitted frequencies induces two secondary waves equal to the difference and the sum of the two primary frequency waves, this is called the "parametric effect" (Lurton, 2002). The result is the creation of acoustic waves with both a low frequency and a small transmit/receive array. The advantage lies in the fact that both penetration and accuracy can be achieved due to the narrow beam width (Lurton, 2002). The disadvantage however is the poor penetration of the signal (maximum 200 m compared to 500 m for the sparker signal).

Seismic profiles originate due to the partial reflection of the acoustic signal at the boundary between two media with different acoustic impedances (i.e. the product of the seismic velocity and the density of each layer); the higher the difference in acoustic impedance, the higher the reflection coefficient will be and the stronger the reflector will appear in the seismic profile (Reynolds, 2011). After the reflection of the seismic pulse at an interface, it can be detected by a receiver (hydrophones in the case of the sparker signal (Figure 3.1), transducers in the case of parasound signal) and the difference in time between the emission and acquisition of the signal is expressed in seconds Two-Way-Travel Time (TWT). If the velocity of the seismic pulse in the subsurface is known, the depths in seconds TWT can be converted into meters. The vertical resolution of the profile depends on the wavelength of the seismic signal, scattering and spherical divergence and is controlled by the source; the horizontal resolution depends on the cruising speed and the shot interval as well as the Fresnel zone (Reynolds, 2011). The Fresnel zones is the part of the reflector from which energy is returned within half of the wavelength of the initial signal. The vertical resolution of the sparker data is about 1 m, while the vertical resolution of the parasound data is down to several decimeter. Horizontal resolutions are in the range of 3.5 to 5 m for the sparker, while the parasound achieved a horizontal resolutions of 5 to 8 m.

Figure 3.1: Components of the sparker system. Upper left: power supply with the cable towards the sparker indicated. Lower left: Sparker containing 100 electrodes. Right: streamer with 10 electrodes (red), each 0.5 m apart.

1.2. Processing

Raw seismic profiles (acquired in the SEG-Y format), usually need processing in order to increase signal-to-noise ratios, amplify and improve the signal quality. Several processing steps are applied to the profiles, depending on their source (sparker or parasound).

A seismic wave loses energy as it propagates away from its source. To correct for this, a **spherical divergence correction** is applied. The loss of energy can be calculated and a gain correction function can be calculated as a consequence and applied to the profile (Aki and Richards, 1980; Wang and McCowan, 1989). The only disadvantage is that noise will be amplified as well.

In order to remove unnecessary frequencies (i.e. not resulting from the main frequency of the acoustic pulse) from the frequency spectrum (Figure 3.2A), a **bandpass-filter** can be applied. This bandpass filter has a low-pass and a high-pass filter (Figure 3.2B). The former can remove high-frequency noise, while the latter is able to remove the effect of ship-generated noise. As the geologically significant reflection signals are always gathered around the main frequency of the source signal, the values of the low- and high-pass filter can be chosen accordingly.
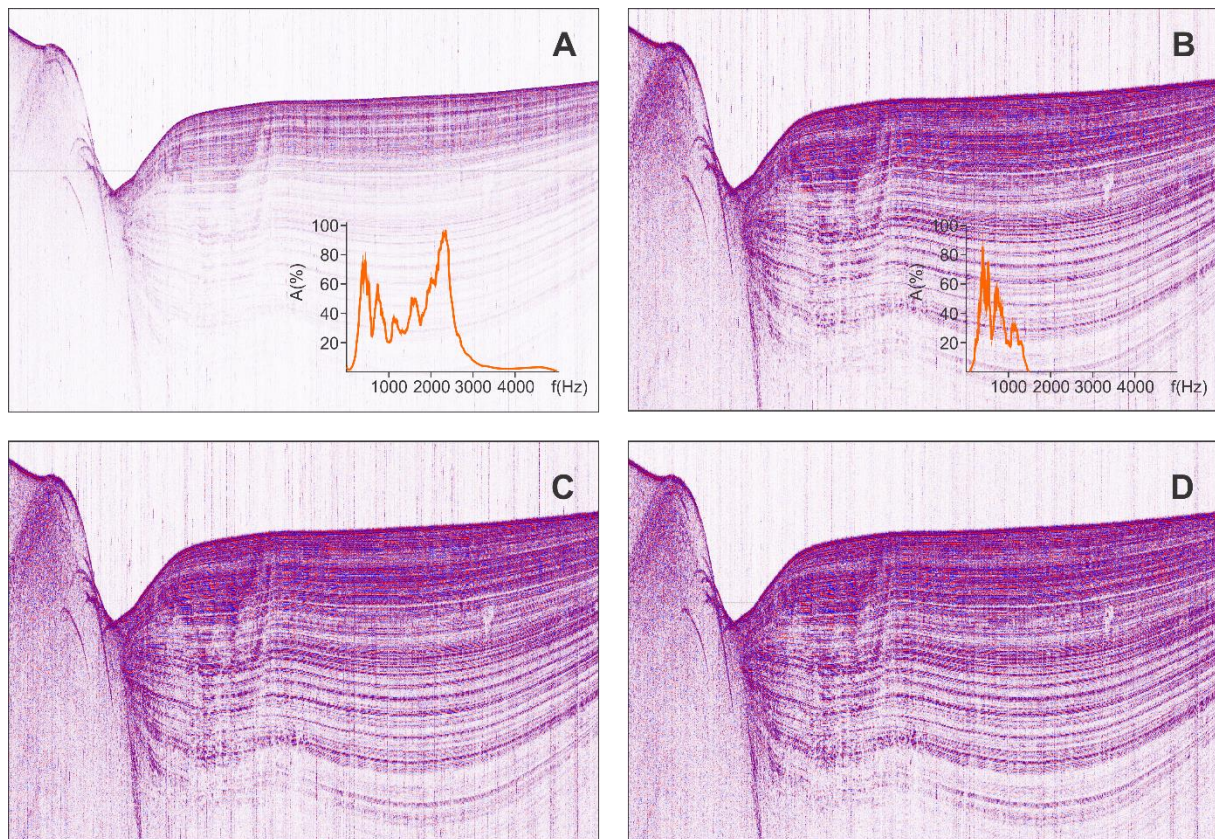
Figure 3.2: Seismic profile from the AMCP showing the different processing steps. A. raw profile with the amplitude spectrum in orange. B. The profile after a bandpass-filter (cutting at 75 Hz (0%) and 150 Hz (100%) for the low-pass filter and at 1250 Hz (100%) and 1500 Hz (0%) as a high-pass filter). C. The profile after applying a swell filter. D. The profile after applying the burst noise removal.

Static corrections are made to take into account the effect of travel times of irregular or changing topography. In the case of single channel marine seismic profiles, static corrections are needed due to the action of surface waves which induce vertical ship-movements. These give a distorted image of the reflectors and will give incoherent events. The static correction applied on these profiles is a swell-filter (Figure 3.2C). An average of every 5, 7 or 9 (depending on the wave amplitude during recording)

traces is calculated and the difference between each trace and its running average is obtained. This difference (either positive or negative) is added to the trace and a smoothed, swell-corrected profile is obtained with more coherent events in the subsurface. Caution has to be taken to not take too many traces into account when calculating the average, as relevant small geological features may be smoothened this way.

Burst noise can usually be observed as small abnormally strong reflections, not reflecting a geological boundary. It is an electronic noise that occurs in semiconductors and can be edited out by applying a **burst noise removal**. The burst noise removal processing step calculates the average amplitude of several traces for every depth interval and searches for these parts of the traces which horizontally are deviant by a fixed percentage (usually 50%). The values for the reflections are replaced by the averages and the burst noise is removed in this way (Figure 3.2D).

A seismic attribute is any quantity measured or calculated from seismic data and can be divided into physical (e.g. envelope and instantaneous phase) and geometrical (dip, azimuth and discontinuity) attributes (Subrahmanyam and Rao, 2008). Evidently, amplitude, phase and frequency are also seismic attributes. For this dissertation, the Hilbert transform itself has been calculated (using seismic processing software) from the parasound data by using the formula:

$$H(t) = \frac{1}{\pi} \int\limits_{-\infty}^{\infty} \frac{f(x)}{t - x} dx$$

In this formula, H(t) is the Hilbert transform, f(x) is the real seismic trace and t is time. The Hilbert transform can be regarded as the projection of a seismic trace onto the imaginary plane, resulting from the complex trace (Hardage, 2010). This complex trace has to be regarded as a mathematical expression within the complex domain and arises from the combination of the real and imaginary trace (Figure 3.3). This attribute highlights main seismic features and allows improved visualization of discontinuities, faults and sequence boundaries (Subrahmanyam and Rao, 2008; Figure 3.4).
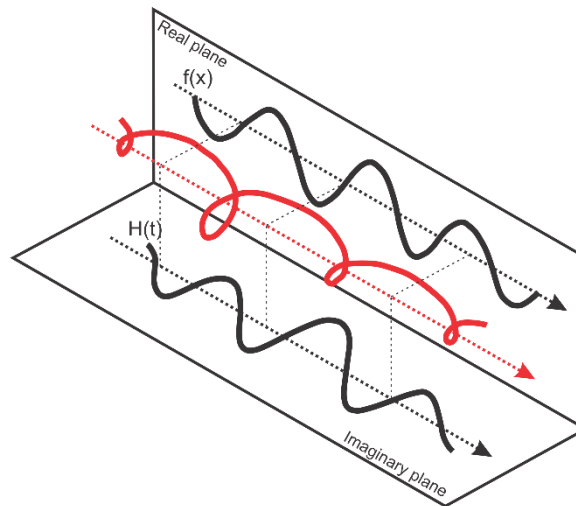
Figure 3.3: Visualization of the real trace f(x), complex trace (red) and the Hilbert transform H(t) on the imaginary plane. Adapted from Hardage (2010).
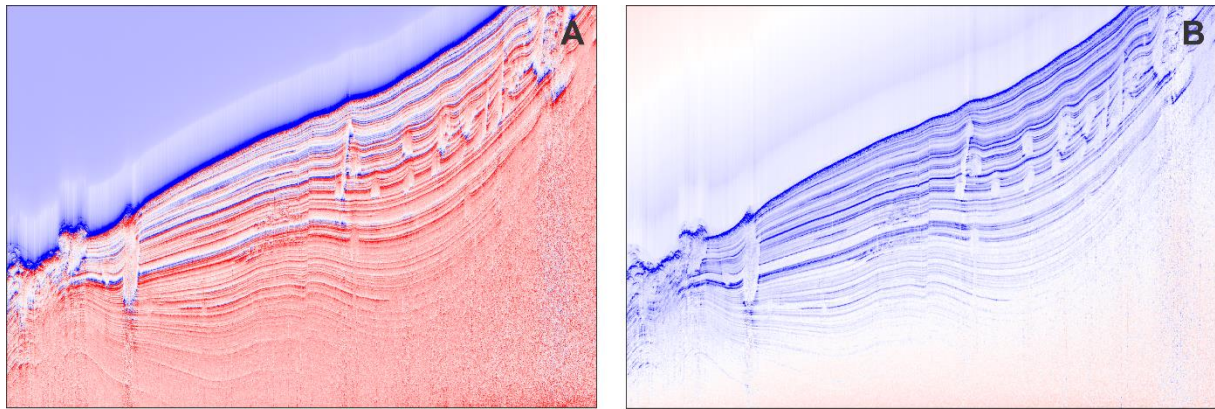
Figure 3.4: A. Unprocessed parasound profile. B. Parasound profile after applying the Hilbert transform.

2. Multibeam bathymetry

Multibeam bathymetry is an ideal tool to map the seafloor morphology. The depth of the seafloor is measured by emitting acoustic pulses from transducers positioned close to the ocean surface (usually below the hull of the vessel) and wait for their reflected arrival. The technique is similar to the seismic profiling technique, only the frequencies are much higher, usually in the order of 12 to 400 kHz, depending on the water depth. Moreover, multiple beams are emitted at the same time (nowadays mostly about 250 beams), which results in a large area that can be covered by one single swath profile: 750 m in shallow waters (<500 m) and 500 m in depths exceeding 500 m to reduce signal deterioration and noise (Van Rensbergen et al., 2005).

Two main corrections need to be applied when acquiring deep-water multibeam data: motion and sound velocity corrections. The first correction is based on the simultaneous recording of the motions of a ship (roll, pitch and heave) by a motion-sensor and applying these corrections to the acquired data. The second correction results from the varying velocities of the acoustic wave within different water masses: denser waters will be characterized by higher velocities. As a consequence, detailed profiles of the water column need to be obtained in order to exactly know the sound velocities and obtain the correct depths.

Processing of the multibeam data was performed by Van Rensbergen et al. (2005) by using the Kongsberg packages Merlin and Neptune.

3. Hydrographic measurements

3.1. CTD

Conductivity, Temperature, Depth (CTD) measurements are performed by lowering sensors (the CTD onboard the R/V Belgica contained a temperature, conductivity, turbidity, pressure and oxygen sensor) mounted on a frame down to the bottom of the ocean and pulling them back up. This results in two measurements of the aforementioned properties of the water column, namely the down- and up-cast. As each water mass usually has different characteristics, the water masses at that exact location can be determined. The disadvantage of this method is that variations (tidal, seasonal, yearly and higher order) of water mass properties are not measured. Several recurring measurements (e.g. yo-yo measurements) can be a solution to overcome this problem. In this dissertation, the measurements from numerous campaigns, stored in the world ocean database (https://www.nodc.noaa.gov/OC5/WOD/pr_wod.html, 05/02/2013), are put together in order to pinpoint which water masses are present in the southern Gulf of Cádiz.

3.2. LADCP

An Acoustic Doppler Current Profiler (ADCP) measures the direction and intensities of currents present within the depth range (max 150 m) of the ADCP frequency (in this case a 300 kHz RDI Teledyne ADCP). During the 2013 "COMIC" campaign, an ADCP was attached to the CTD frame of R/V Belgica, allowing the synchronous acquisition of both CTD and ADCP data (Figure 3.5). ADCP measurements are based on the emission of 4 high-frequency sonar signals (emitted by the transducers), which are scattered/reflected by particles carried by the ocean currents. The transducers of an ADCP are positioned in a JANUS configuration (two transducers in a forward and two in a backward position, with an angle of 20-30° from the vertical axis). This is needed in order to accurately calculate the resulting vector of the currents, for which at least 3 signals are needed. This means that one of the transducers can fail without endangering the measurements.

Processing of the acquired Lowered ADCP (LADCP) data was carried out using an extensive Matlab script, developed by the Lamont Doherty Earth Observatory. For this script, 2 types of data are necessary, the LADCP data themselves and the magnetic declination data. The latter is important as the directions and intensities are obtained with respect to the magnetic north and have to be recalculated compared to the geographic north. The magnetic declination can either be calculated or derived from the geographical location (as was done in this case). Optional datasets to calibrate the LADCP data are CTD time series, GPS time series, shipboard ADCP data and CTD profiles. A summary on how to process the data can be found in Thurnherr (2005). The resulting velocities that are obtained are given in two directions: north-south and east-west. By combining these two speeds, the resulting vector can be calculated.
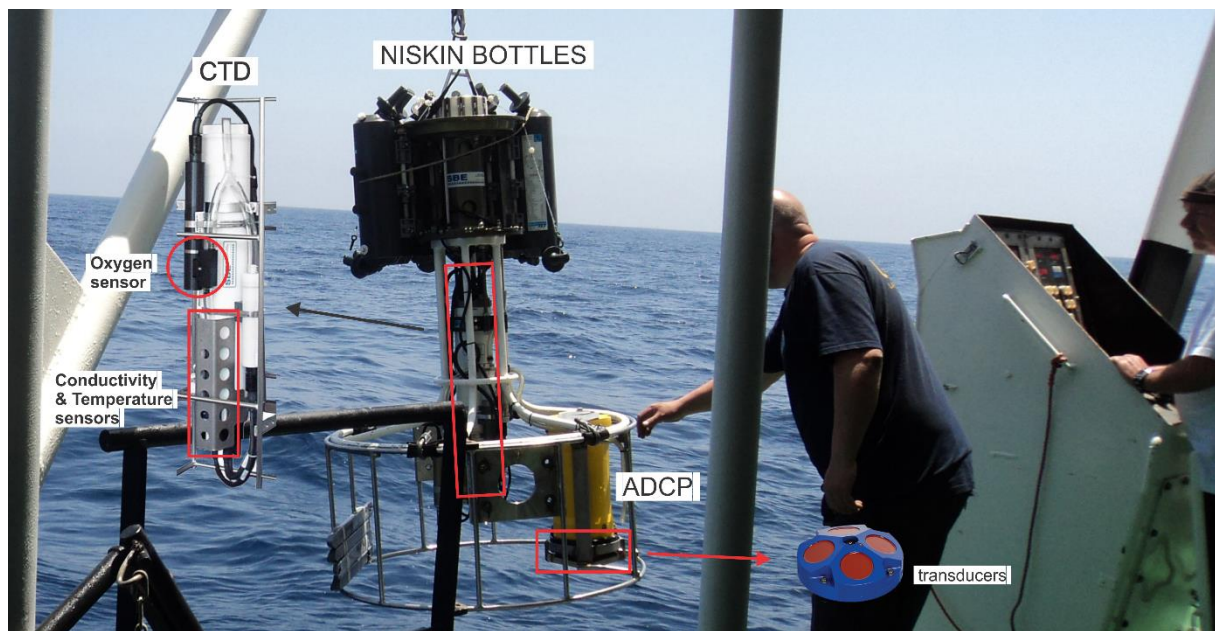
Figure 3.5: Oceanographic equipment on board of the R/V Belgica during the 2013 "COMIC" campaign. CTD: Conductivity, Temperature, Depth; ADCP: Acoustic Doppler Current Profiler.

3.3. Nutrient concentrations

Water masses can be discerned based on their physical properties (temperature and conductivity, measured by CTD), but also based on their nutrient content, e.g. Si, NO_3, and PO_4 (Cabecadas et al., 2002; Braga et al., 2008; Kovačević et al., 2012; McGrath et al., 2012; Palma et al., 2012). These properties can not only indicate which water masses are present, but also the amount of mixing that occurred between them (e.g. Pérez et al., 2001; You et al., 2003; Louarn and Morin, 2011; Bostock et

al., 2013). Nutrient contents of water masses are measured by taking water samples at different levels using NISKIN bottles (Figure 3.5). These bottles can be closed at the desired water depth, capturing the water sample. These samples are stored frozen before being analyzed in the lab.

4. Cores

4.1. Acquisition

Gravity cores are acquired by lowering a PVC liner within a steel barrel, topped by a heavy weight and closed by a core catcher, down to the seafloor and make it penetrate the sediments due to its rapid descent (Figure 3.6). Sediment cores up to 10 meters can be obtained this way, depending on the nature of the sediments. Once the gravity core is retrieved, it can be split in half or stored as a whole. If a core contains CWC's, it cannot be split on the vessel and is stored as a whole. A CWC-core has to be frozen at -20°C for at least a day (until it is completely frozen) after which it is cut in two using a stone saw (Figure 3.7).
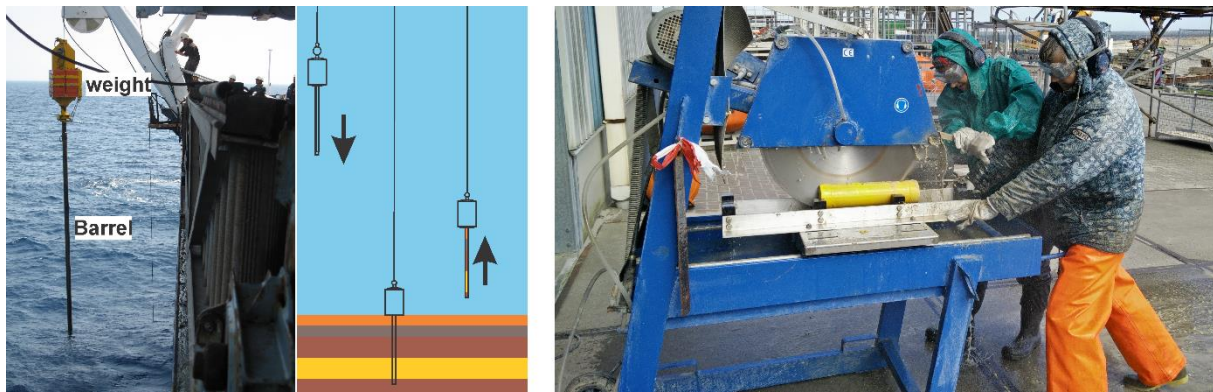
Figure 3.6: Left: picture from the Marion Dufresne when a gravity core was being prepared to go down to the seafloor (picture courtesy of Susana Lebreiro). Middle: The mechanism of the gravity core. Right: Cutting of a CWC-filled core (picture courtesy of Tim Collart).

4.2. Multi-Sensor Core Logger (MSCL)

A MSCL is a device measuring several geophysical properties at very high resolution (down to mm-scale) along-core. The Ghent University MSCL measures magnetic susceptibility (MS), gamma density, core thickness and contains a spectrophotometer, analyzing the colors of the core (Figure 3.7).

MS is the degree of magnetization of a material, measured by inducing an external magnetic field. Positive MS values indicate para-, ferro-, ferri- or antiferromagnetic sediments, while negative MS values indicate diamagnetic sediments. MS is used a lot in palaeoclimate studies, as it indicates changes in the amount of magnetic minerals and their composition (Stoner et al., 1996) and glacial/interglacial changes (Robinson et al., 1995).

Gamma density measures the amount of absorption of gamma-rays by the sediment core and is used to calculate the bulk density of the sediment. The gamma-rays are emitted from a ^{137}Cs source in a narrow collimated beam. The energy level (0.662 MeV) at which the rays are emitted makes sure that the primary mechanism for attenuation is Compton scattering. The attenuation is therefore related to the core thickness (measured) and electron density. To derive the density of the material from the gamma density, a calibration is performed in which a liner containing water and an aluminum plate of varying thickness is measured. Gamma density is a measure for porosity and lithological changes.

The Konica Minolta color spectrophotometer is mounted on the MSCL and measures the reflectance of the visible light (360-740 nm) in steps of 10 nm and calculates from these measurments the luminosity (L*, ranging from 0, black, to 100, white), a* (positive red; negative green) and b* (positive yellow ; negative blue) values of the core on a 1 mm band along the axis of the core (Nederbragt and Thurow, 2004). This method is frequently used in palaeoceanographic studies (Rogerson et al., 2006). Also, a high-resolution image through line-scan imaging can be obtained. The advantage compared to area camera's lies in the fact that uneven lighting is omitted using line scan.
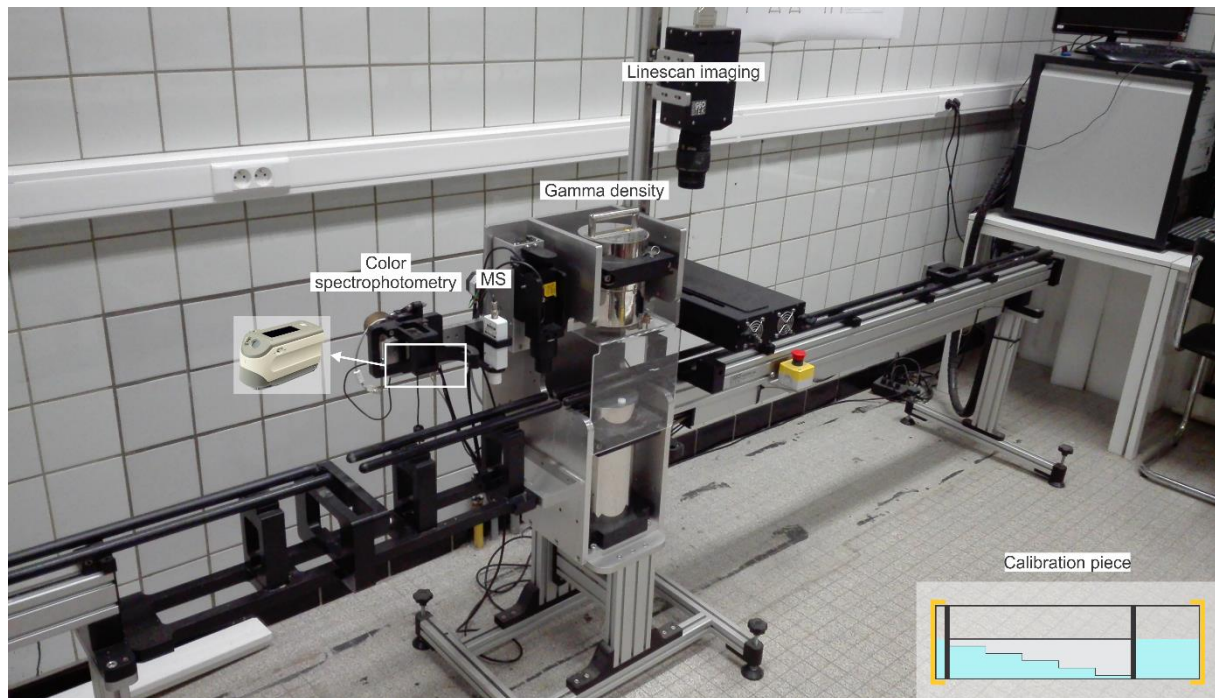
Figure 3.7: the Ghent University MSCL containing a linescan imaging system and the gamma density, MS and colour spectrophotometry devices (the latter is not mounted on the system at the moment the picture was taken and has been added later). A schematic representation of the calibration piece (for the gamma density) is displayed in the lower right part of the figure.

4.3. X-Ray Fluorescence (XRF) core scanning

XRF is a non-destructive high-resolution method to obtain a qualitative and semi-quantitative assessment of the main element distribution of the upper few mm of a narrow band of a sediment core (Figure 3.8). High-energetic X-rays are generated by heating a Rh, W, Mo or Cr target and are bombarded towards the sediment. Due to the high energies of the bombarding X-rays, electrons from the inner orbitals may be emitted and replaced by electrons from outer orbitals. The energy that is released during this process (fluorescence) is proportional to the difference in energy between the two orbitals and hence to the specific atom. By repeating this measurement along the vertical axis of the core, the down-core variation of the element distribution can be obtained. XRF is a semi-quantitative method, meaning that the counts only represent relative variations in concentration. In order to compare down-core variations, ratios between different elements (e.g. Ca/Fe, Ti/Al, Sr/Ca) are calculated, removing the effects of (among others) density and water content (Weltje and Tjallingii, 2008).

The ratio's resulting from XRF-measurements have a wide array of applications, summarized in Rothwell and Croudace (2015), e.g. Ca/Fe for carbonate stratigraphy or variations in terrigenous sediment supply, Ca/Al for variations in biogenic versus terrigenous contributions, Ba/Ti for productivity and Br/Cl for the presence of organic-rich layers.
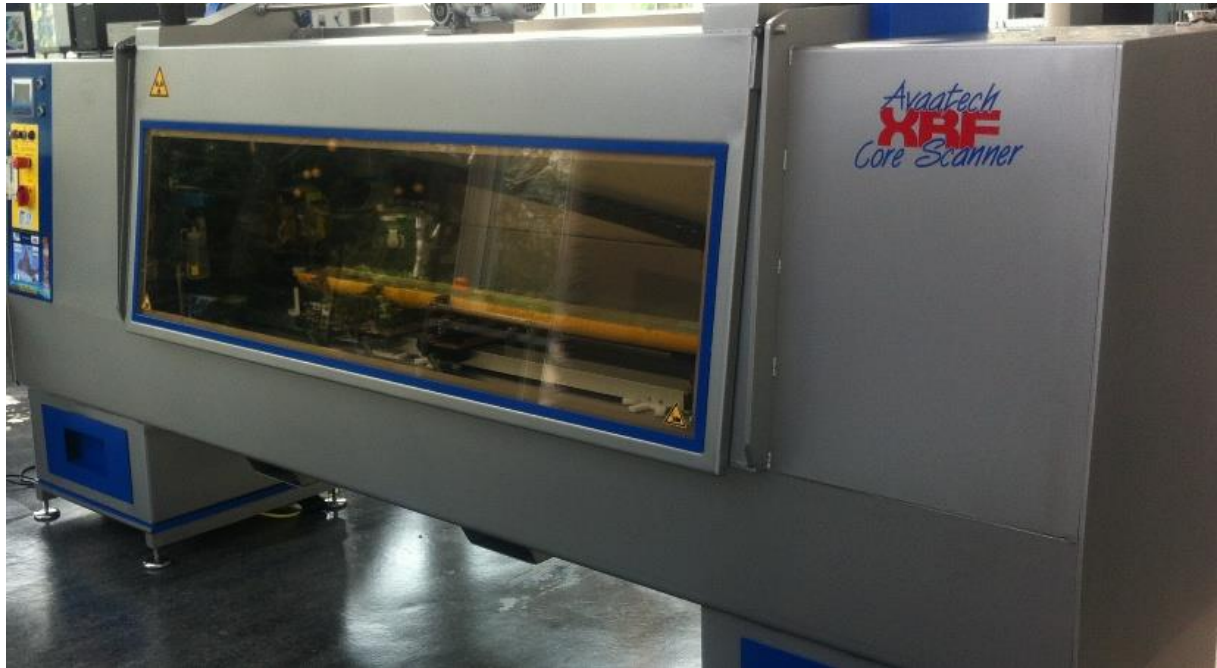
Figure 3.8: Avaatech XRF core scanner, similar to the one used at the Royal NIOZ (picture courtesy of AVAATECH, 27/10/2016).

4.4. Grain-size measurements

Grain-size measurements were performed using the Malvern Mastersizer 3000, a device that can measure grains with a size ranging from 0.01 µm up to 3500 µm, using two different lasers: the red light (633 nm) and the blue light (470 nm) (Figure 3.9). The advantage by also using the blue light is that the instrument is more sensitive to smaller particles, increasing the range of that can be measured. The Mastersizer uses light scattering to calculate the particle-size distribution of the sample. In general, smaller particles will scatter light at wide angles with low intensities, while larger particles will scatter light at narrow angles with high intensities (Figure 3.9). The particle-size distributions are calculated based on the Mie theory, which always keeps in mind that not only scattering may happen, but also absorption, diffraction and refraction.
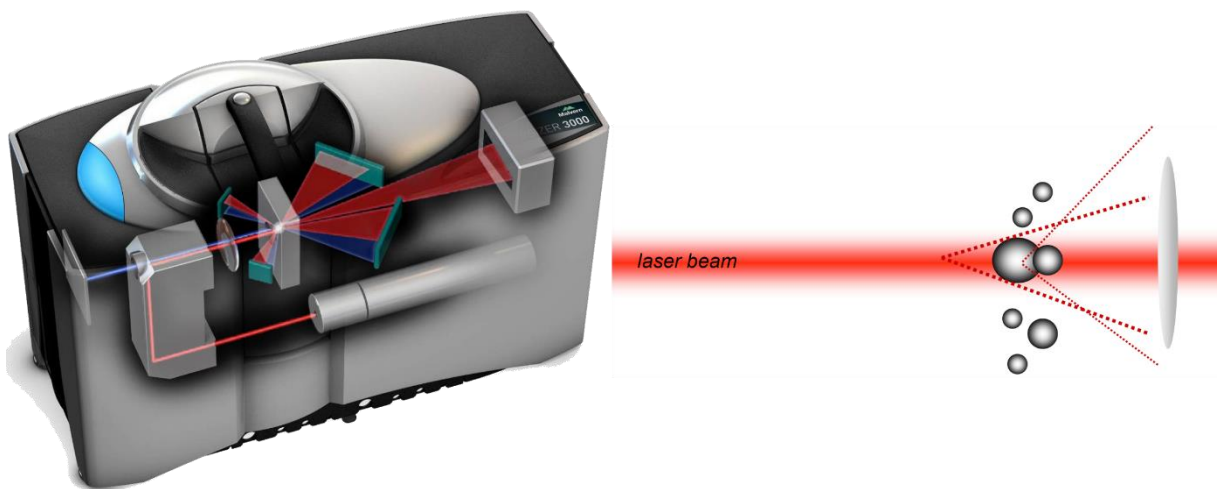
Figure 3.9: Left: Malvern Mastersizer 3000 with red and blue lasers, reaching different detectors. Right: Scattering of particles with different sizes. Modified from Sysmex (2014).

5. X-ray Computed Tomography (CT) scans

CT is a non-destructive technique enabling researchers to visualize and characterize the variation of X-ray attenuation in 3 dimensions within an object (Brabant et al., 2011). X-ray images are gathered based on the absorption of X-rays by material, depending on the initial energy. This is expressed in Beer's law:

$$I = I_0 e^{-\int \mu(S) dS}$$

Where I_0 is the incident beam intensity and $\mu(S)$ is the local attenuation coefficient along the raypath S. The X-ray attenuation is dependent on the density, thickness and the composition (effective atomic number) of the object (Cnudde and Boone, 2013). Four major processes occur when an X-ray passes through the material: Compton (incoherent) scattering, Rayleigh (coherent) scattering, photoelectric effect and pair production. It is not possible to differentiate between the various interaction processes when an X-ray passes through a medium in practical CT scans, however due to the energies used in medical CT-scans (50-120 keV), the photoelectric effect will be the most important process causing attenuation (Ketcham and Carlson, 2001). In this dissertation, the local attenuation coefficient is given in Hounsfield units (HU; Zatz, 1981; Freeman, 2010), a quantitative scale for radio-densities, calibrated based on the absorption of X-rays by distilled water (0 HU) and air (-1000 HU) and is be calculated by:

$$HU = 1000 \, x \, \frac{\mu - \mu_{water}}{\mu_{water} - \mu_{air}}$$

Caution has to be taken when interpreting the CT scans, as several artefacts (e.g. beam hardening; star, line, ring and outlining artefacts; partial volume effects) may arise.

All CT scans processed in this dissertation are the result of medical scans, which usually have a high signal-to-noise ratio due to the large and sensitive detector elements. In the "SOMATON Definition Flash" scanner of the Ghent University Hospital, the sediment core is positioned in between the X-ray source and the detector and the source is rotating around the sample (Figure 3.10). Digital radiographs from all angles can be taken from the core and a digital slice is reconstructed based on the radiographs from all angles using the SAFIRE reconstruction software. In this way, a 3D view of the interior of the core can be obtained without actually disturbing the sediment (Figure 3.10). CT-images of sediment core sections may display features not visible with the naked eye or on core-pictures, such as distinct layers, bioturbation, cracks, and weathering effects (e.g. Dewanckele et al., 2014).

Figure 3.10: Left: Sediment core on the scanning table. The source and detector are positioned within the cylinder and rotate around the sample. Right: view on the acquisition software, with radiograph (A), individual slice (B) and input parameters (C). Pictures courtesy of Maarten Van Daele.

References

Aki, K., Richards, P.G., 1980. Quantitative seismology. Theory and methods.

AVAATECH, 27/10/2016. http://www.avaatech.com/#.

Bostock, H.C., Sutton, P.J., Williams, M.J.M., Opdyke, B.N., 2013. Reviewing the circulation and mixing of Antarctic Intermediate Water in the South Pacific using evidence from geochemical tracers and Argo float trajectories. Deep Sea Research Part I: Oceanographic Research Papers 73, 84-98.

Brabant, L., Vlassenbroeck, J., Witte, Y.D., Cnudde, V., Boone, M.N., Dewanckele, J., Hoorebeke, L.V., 2011. Three-Dimensional Analysis of High-Resolution X-Ray Computed Tomography Data with Morpho+. Microscopy and microanalysis 17, 252-263.

Braga, E.S., Chiozzini, V.C., Berbel, G.B.B., Maluf, J.C.C., Aguiar, V.M.C., Charo, M., Molina, D., Romero, S.I., Eichler, B.B., 2008. Nutrient distributions over the Southwestern South Atlantic continental shelf from Mar del Plata (Argentina) to Itajaí (Brazil): Winter–summer aspects. Continental Shelf Research 28, 1649-1661.

Cabecadas, G., José Brogueira, M., Goncalves, C., 2002. The chemistry of Mediterranean outflow and its interactions with surrounding waters. Deep Sea Research Part II: Topical Studies in Oceanography 49, 4263-4270.

Cnudde, V., Boone, M.N., 2013. High-resolution X-ray computed tomography in geosciences: A review of the current technology and applications. Earth-Science Reviews 123, 1-17.

Dewanckele, J., De Kock, T., Fronteau, G., Derluyn, H., Vontobel, P., Dierick, M., Van Hoorebeke, L., Jacobs, P., Cnudde, V., 2014. Neutron radiography and X-ray computed tomography for quantifying weathering and water uptake processes inside porous limestone used as building material. Materials Characterization 88, 86-99.

Freeman, T., 2010. The Mathematics of Medical Imaging: A Beginner's Guide, Undergraduate Texts in Mathematics and Technology. Springer.

Hardage, B., 2010. Thin Is In: Here's a Helpful Attribute. AAPG Explorer.

Ketcham, R.A., Carlson, W.D., 2001. Acquisition, optimization and interpretation of X-ray computed tomographic imagery: applications to the geosciences. Comput. Geosci. 27, 381-400.

Kovačević, V., Manca, B.B., Ursella, L., Schroeder, K., Cozzi, S., Burca, M., Mauri, E., Gerin, R., Notarstefano, G., Deponte, D., 2012. Water mass properties and dynamic conditions of the Eastern Mediterranean in June 2007. Progress In Oceanography 104, 59-79.

Louarn, E., Morin, P., 2011. Antarctic Intermediate Water influence on Mediterranean Sea Water outflow. Deep Sea Research Part I: Oceanographic Research Papers 58, 932-942.

Lurton, X., 2002. An introduction to underwater acoustics: principles and applications. Springer Science & Business Media.

McGrath, T., Nolan, G., McGovern, E., 2012. Chemical characteristics of water masses in the Rockall Trough. Deep Sea Research Part I: Oceanographic Research Papers 61, 57-73.

Nederbragt, A.J., Thurow, J.W., 2004. Digital Sediment Colour Analysis as a Method to Obtain High Resolution Climate Proxy Records, in: Francus, P. (Ed.), Image Analysis, Sediments and Paleoenvironments. Springer Netherlands, Dordrecht, pp. 105-124.

Palma, C., Lillebø, A.I., Borges, C., Souto, M., Pereira, E., Duarte, A.C., Abreu, M.P.d., 2012. Water column characterisation on the Azores platform and at the sea mounts south of the archipelago. Marine Pollution Bulletin 64, 1884-1894.

Pérez, F.F., Mintrop, L., Llinás, O., Glez-Dávila, M., Castro, C.G., Alvarez, M., Körtzinger, A., Santana-Casiano, M., Rueda, M.J., Ríos, A.F., 2001. Mixing analysis of nutrients, oxygen and inorganic carbon in the Canary Islands region. Journal of Marine Systems 28, 183-201.

Reynolds, J.M., 2011. An introduction to applied and environmental geophysics, 2nd edition. Wiley-Blackwell, West Sussex.

Robinson, S.G., Maslin, M.A., McCave, I.N., 1995. Magnetic susceptibility variations in Upper Pleistocene deep-sea sediments of the NE Atlantic: Implications for ice rafting and paleocirculation at the Last Glacial Maximum. Paleoceanography 10, 221-250.

Rogerson, M., Weaver, P.P.E., Rohling, E.J., Lourens, L.J., Murray, J.W., Hayes, A., 2006. Colour logging as a tool in high-resolution palaeoceanography. Geological Society, London, Special Publications 267, 99-112.

Rothwell, R.G., Croudace, I.W., 2015. Twenty Years of XRF Core Scanning Marine Sediments: What Do Geochemical Proxies Tell Us?, in: Croudace, I.W., Rothwell, R.G. (Eds.), Micro-XRF Studies of Sediment Cores: Applications of a non-destructive Tool for the Environmental Sciences. Springer Science, Dordrecht.

Stoner, J.S., Channell, J.E.T., Hillaire-Marcel, C., 1996. The magnetic signature of rapidly deposited detrital layers from the Deep Labrador Sea: Relationship to North Atlantic Heinrich layers. Paleoceanography 11, 309-325.

Subrahmanyam, D., Rao, P.H., 2008. Seismic Attributes - A Review, 7th International Conference and Exposition on Petroleum Geophysics, Hyderabad, India, pp. 398-404.

Sysmex, 2014. Laser diffractie Malvern Masterseizer 3000. User Training, pp. 57.

Thurnherr, A.M., 2005. How to process LADCP data with the LDEO software.

Van Rensbergen, P., Depreiter, D., Pannemans, B., Henriet, J.-P., 2005. Seafloor expression of sediment extrusion and intrusion at the El Arraiche mud volcano field, Gulf of Cadiz. Journal of Geophysical Research: Earth Surface 110, F02010.

Van Rensbergen, P., Depreiter, D., Pannemans, B., Moerkerke, G., Van Rooij, D., Marsset, B., Akhmanov, G., Blinova, V., Ivanov, M., Rachidi, M., Magalhaes, V., Pinheiro, L., Cunha, M., Henriet, J.-P., 2005. The El Arraiche mud volcano field at the Moroccan Atlantic slope, Gulf of Cadiz. Marine Geology 219, 1-17.

Wang, D.Y., McCowan, D.W., 1989. Sperical divergence correction for seismic reflection data using slant stacks. Geophysics 54, 563-569.

Weltje, G.J., Tjallingii, R., 2008. Calibration of XRF core scanners for quantitative geochemical logging of sediment cores: Theory and application. Earth and Planetary Science Letters 274, 423-438.

You, Y., Lutjeharms, J.R.E., Boebel, O., de Ruijter, W.P.M., 2003. Quantification of the interocean exchange of intermediate water masses around southern Africa. Deep Sea Research Part II: Topical Studies in Oceanography 50, 197-228.

Zatz, I.M., 1981. Basic principles of computed tomography scanning, in: Newton, T.H., Potts, D.G. (Eds.), Radiology of the skull and brain. Mosby, St. Louis.

Chapter 4

Seismic Stratigraphy

Campaign 4: Valencia Trough - Garcia del Cid (2011)

Chapter 4 – Seismic stratigraphy of the El Arraiche drift systems

This chapter is based on:

Vandorpe, T., Van Rooij, D., de Haas, H., 2014. Stratigraphy and paleoceanography of a topography-controlled contourite drift in the Pen Duick area, southern Gulf of Cádiz. Marine Geology 349, 136-151.

Abstract

The northern part of the Gulf of Cádiz has and still is receiving a lot of attention from the scientific community due to (amongst others) the recent IODP Expedition 339. In contrast, its southern part, or the Moroccan margin has received far less attention, although mud volcanoes, diapiric ridges and cold-water corals are present in this region. The El Arraiche mud volcano field is characterized by a compressive regime creating several ridges and assisting the migration of hydrocarbon fluids towards the seabed surface. This study presents seismic and multibeam evidence for the existence of several contourite drifts at water depths between 550 and 750 m along the southwestern flank of the Renard and Vernadsky Ridges, within the El Arraiche Mud Volcano field. From the onset of the Quaternary, when the ridges started to lift and the local mud volcanism initiated, contouritic deposition was initiated at the foot of both topographic obstacles. Initially, fairly low-velocity bottom currents gave rise to sheeted drift deposits, affected by the uplift of the ridges or by mud extrusion from nearby mud volcanoes. From the Middle Pleistocene onwards, separated mounded drift deposits were formed due to intensified bottom currents. An Antarctic Intermediate Water origin is inferred as driving mechanism for the drift development, although glacial conditions are not yet well constrained. The influence of Mediterranean Outflow Water (MOW) cannot be substantiated here. Moreover, the changes recorded within this contourite drift differ from the MOW-dominated contourite depositional system in the northern Gulf of Cádiz, as drift deposits only occur as early as the base of the Quaternary (compared to the Early Pliocene for the north) and mounded drift deposits only occur from the Middle Pleistocene onwards (compared to the Early Pleistocene). Cold-water coral mounds have been observed within and on top of the sedimentary sequence at the foot of the Pen Duick Escarpment. This implies that environmental conditions in which cold-water corals thrive were not necessarily restricted to the top of the Pen Duick Escarpment.

Keywords: Gulf of Cádiz, Contourite drifts, Renard and Vernadsky Ridge, Gemini mud volcano, Antarctic Intermediate Water

Contribution: DVR and HDH acquired the data and TVD processed and interpreted them. The paper was written by TVD and revised by DVR and HDH.

1. Introduction

The Pen Duick drift in the EAMVP has been briefly described by Van Rooij et al. (2011). As the focus of that paper was on coral mounds, the proposed stratigraphy was preliminary and based on a single seismic profile. A detailed stratigraphy of the drift system is useful though, as the contourite drift is located within the vicinity of several well-studied coral mounds (Foubert et al., 2008; Wienberg et al., 2009; Pirlet et al., 2010; Templer et al., 2011; Wehrmann et al., 2011) and can yield an additional perspective on the palaeoceanographic evolution of the area, since coral mound growth is a discontinuous process (Wienberg and Titschack, 2016). Consequently, the geophysical seismic dataset that consists of several dense grids covering the mud volcanoes and one closely spaced grid southwest of the Gemini mud volcano (GMV) and the PDE (Figure 4.1), is used to study the stratigraphy and palaeo-environment of the contourite drifts. The first part of this dissertation focusses on the seismic stratigraphy and lateral variation of the drift systems as well as the water masses involved in their buildup and maintenance.

2. Material and methods

Within the framework of the R/ V Belgica "CADIPOR" cruises (2001, 2005 and 2007), the "Pen Duick" campaign (2009) and the "COMIC" campaign (2013) in the southern Gulf of Cádiz, over 1500 km (Figure 4.1) high-resolution single channel sparker seismic profiles have been acquired. A SIG sparker (80 electrodes in 2001, 100 electrodes in 2013 and 120 electrodes in 2005, 2007 and 2009) has been used, with a shot interval of 2 s (3 s in 2009). The energies reached 500 J and a 8 kHz sampling frequency (10 kHz in 2013) has been used. A record length between 1.6 s TWT and 2.5 s TWT (depending on the shot interval and water depth) was obtained. The profiles were acquired with acquisition velocities within the range of 3 to 4 knots.

All seismic profiles have been processed using the DECO Geophysical RadexPro processing software. A swell filter, bandpass filter (Butterworth type, low cut at 200 Hz, low-cut slope of 24 dB/s and high cut at 1500 Hz, high-cut slope of 36 dB/s), burst noise removal and amplitude corrections (spherical divergence correction) have been applied.

The multibeam data (700 km² in total; Figure 4.2), recorded during the CADIPOR I cruise (2001) has been obtained using the SIMRAD EM1002 system, extended with a deep water module, permanently installed on the R/V Belgica. The swath width was 500 m above 500 m water depth and 750 m below. The data have been corrected and cleaned using Kongsberg's Merlin and Neptune packages. The footprint at 400 m water depth is 15x15 m. This dataset was already extensively described with respect to the main geomorphological features and mud volcanoes within Van Rensbergen et al. (2005).

Profile M2005_105 (Figure 4.3) has been acquired by the R/V Pelagia in 2006 within the framework of the ESF EuroDIVERSITY MiCROSYSTEMS project. Three airguns (10, 20 and 40 cubic inch volume) were used and towed in a frame at respectively 1.3, 1.8 and 2.0 m depth. The guns were towed 37 m behind the stern of the ship and fired every 5 s at a pressure of 100 bars, resulting in an average distance between the shots of 10.5 m (4.2 knots sailing speed). The streamer (towed at a depth of 1 m below surface) consists of four 63 m long sections with 6 channels each. Each channel has 10 Teledyne T2 hydrophones (interval of 1 m). The data were recorded by the Geo-Resources Geo-Trace 24 hard- and software system, consisting of a 24 channel digital pre-amplification system. The record length was 2.0 s TWT and the sampling interval 0.5 ms. During recording, a bandpass filter (30 Hz high pass and 700 Hz low pass) was applied. On board, the lines were stacked and a preliminary migration has been performed.
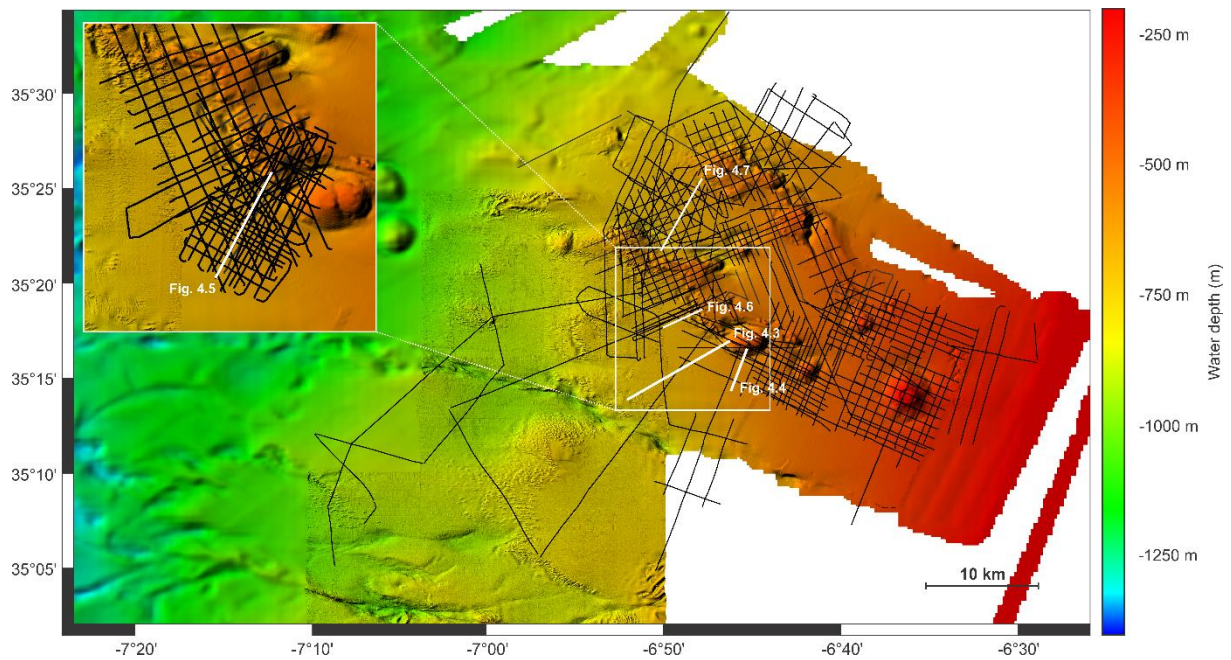
Figure 4.1: Overview of the seismic dataset used in this study. The inset shows the 2009 "Pen Duick" campaign data. Multibeam background data include the GEBCO and SWIM (Zitellini et al., 2009) datasets. The profiles used in this chapter are indicated in white, although a more detailed position is displayed in Figure 4.2.

3. Results

3.1. Geomorphology

The study area extends from 35.50° N to 35.25° N and 6.90° W to 6.70° W (Figure 4.2). Within the investigated area, the multibeam data show the presence of the Renard Ridge (about 100-150 m above the surrounding seafloor) and the Vernadsky Ridge (80-120 m above the surrounding seafloor), five mud volcanoes (e.g. GMV, about 150 m high), coral mounds (on top of the ridges, e.g. alpha, beta and gamma mounds; De Mol et al., 2011; Van Rooij et al., 2011) and 6 mounded features along the foot of the PDE. They have a diameter between 200 and 300 m and are between 5 and 10 m high.

Several semi-continuous channels, between 3 and 10 km long and with widths varying between 200 and 1500 m, are present along the foot of the ridges (Figure 4.2). The moat along the PDE is the longest one and stretches from the southeastern part of the GMV till the northwestern part of the PDE. The first 2 km of this channel have an east-west orientation, following the southern border of the GMV. Here, the most pronounced expression of the channel is observed with depth differences up to 15 m. Then, it changes to a south-southeast to north-northwest orientation for 8 km, following the base of the GMV and PDE, respectively. When the channel passes the boundary between the GMV and the PDE, the depth decreases to about 5 m, after which it increases again along the PDE. Along the PDE, the depth of this channel varies between 5 and 15 m, with a gradual decrease in expression towards the first of the six mounded features. Along these mounded features, two channels are observed: one that continues along the foot of the PDE and increases in depth, to former values of about 15 m and a second one WSW of the mounded features (depths of about 15 m). Both gradually lose their expression towards the northwest (Figure 4.2). The channel along the northern part of the Renard Ridge is about 4 km long, very deep (up till 75 m) and has a general ENE-WSW orientation. The deepest part of the channel is observed in the middle (Figure 4.2). Further west, a very deep incisive channel is observed of about 4.5 km long and up till 200 m deep. The channel follows the orientation of the Renard Ridge (locally being E-W) and is partly squeezed between the ridge and the Adamastor mud volcano (Figure

61

4.2). The channel along the Vernadsky Ridge has the weakest expression of the three (Figure 4.2). It has a SE-NW orientation, is about 3 km long and usually only about 5 m deep.
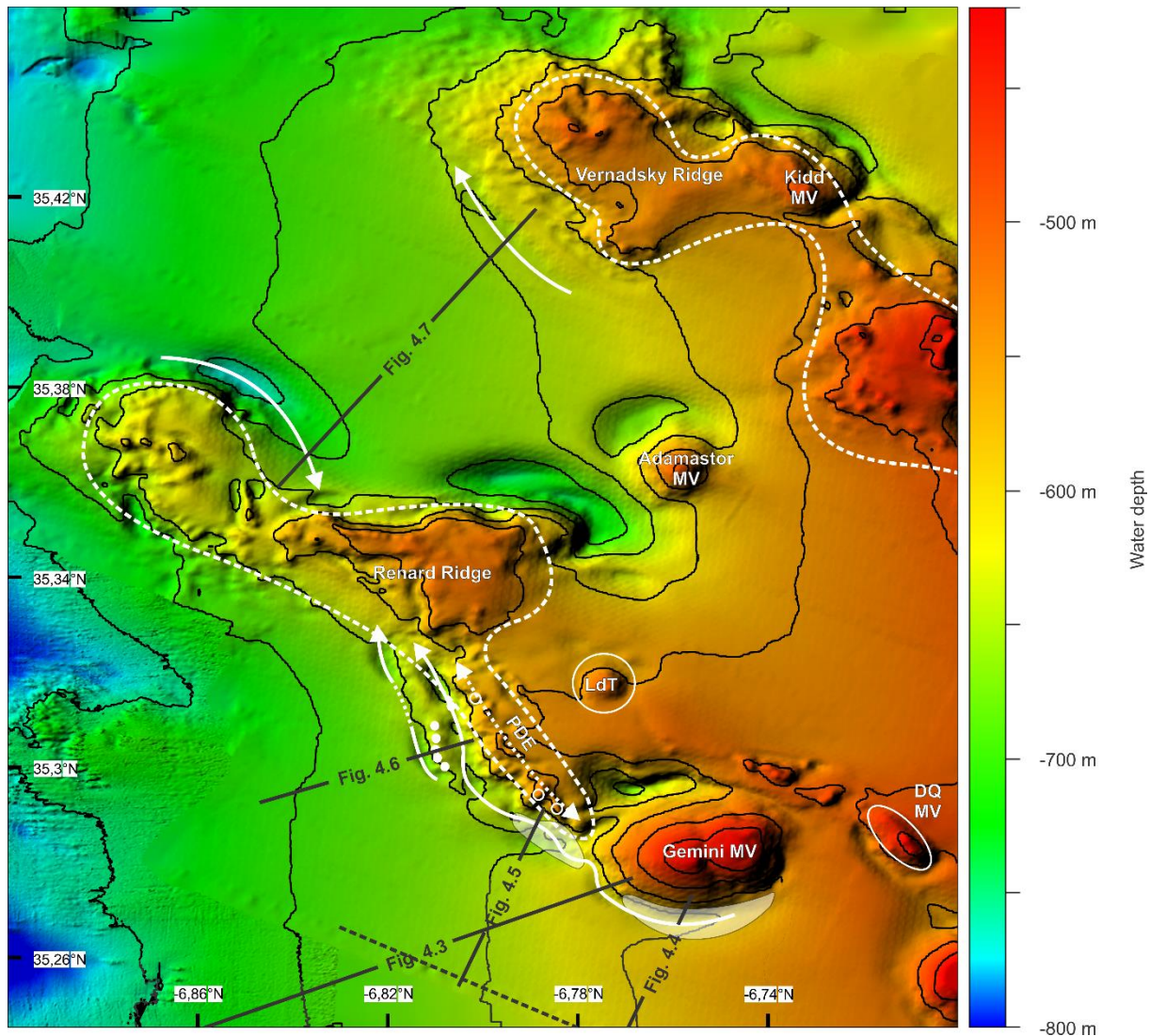
Figure 4.2: Topographic features in the Pen Duick area (Renard and Vernadsky ridge in white dashed lines, PDE in white dashed double arrow) and location of the discussed seismic profiles. The black dashed line in the south of the region shows the westernmost part of the connection profile to the region described by Maad et al. (2010); This profile (although not presented in this chapter) has been used to correlate unit Q2 (Maad et al., 2010) with the Pen Duick region. The full white dots indicate the six presumed mounds at the base of the PDE, while the white circles indicate alpha (southernmost), beta (central) and gamma (northernmost) coral mound (Van Rooij et al., 2011). The white arrows indicate the position of the moats and the presumed flow-paths of the bottom currents. The semi-transparent white plains indicate the position of the mud extrusions within the Pen Duick drift. LdT: Lazarillo del Torres (mud volcano), DQ: Don Quichote, PDE: Pen Duick escarpment. Multibeam bathymetry from Van Rensbergen et al. (2005).

3.2. Seismic stratigraphy

Based on the sparker seismic profiles (Figure 4.4Figure 4.5Figure 4.6Figure 4.7) and the multichannel airgun profile (Figure 4.3), 5 seismic stratigraphic units can be discerned, separated by 4 discontinuities D1 to D4. Due to the lower penetration of the sparker source (about 400 ms TWT, while at least 800 ms TWT for the airgun), mostly only 4 of the 5 units can be observed on the higher-frequency sparker profiles. In between the Renard and Vernadsky ridges, some profiles (e.g. Figure 4.7) do show D4, although very faintly. The Renard and Vernadsky Ridges and the mud volcanoes may be considered as the acoustic basement, but in the other parts of the region, no actual acoustic basement is observed.

This is due to the attenuation of the signal in the rather thick sedimentary package. Reflections can be distinguished in the sparker profiles down to depths of about 1200 ms TWT (Figure 4.4Figure 4.5Figure 4.6Figure 4.7) and down to 1700 ms TWT in the airgun profile (Figure 4.3). Below this depth, the multiple inhibits any further observations. Figure 4.3 shows that (semi-) continuous deposits of units 1 to 5 are bounded in this area by the PDE or GMV in the northeast and a palaeohigh in the southwest. Between the Renard and Vernadsky Ridges, both ridges constitute the boundaries of units 1-5 (Figure 4.7). The palaeohigh rises to 150 to 200 ms beneath the seafloor (Figure 4.3). Its seismic facies consists of very chaotic, discontinuous reflections of varying intensity. This facies differs from the seismic facies within the mud volcanoes in the fact that the palaeohigh still contains sparse reflections, while the mud volcanoes and tectonic ridges display an almost acoustically transparent facies (Figure 4.4Figure 4.5Figure 4.6Figure 4.7).

3.2.1. Unit 5

Unit 5 (visible on Figure 4.3 and slightly on Figure 4.7) consists of low-amplitude semi-continuous reflections at the base and more continuous, slightly higher amplitude reflections at the top. On top of the palaeohigh (Figure 4.3), the unit is intersected by many normal faults. Unit 5 displays a more low-angle onlap onto the PDE, while on the palaeohigh, a higher angle of onlap is observed (Figure 4.3). The top of the unit is incised deeply (± 60 ms TWT) along the GMV. The thicknesses of unit 5 vary between 150 ms TWT on top of the palaeohigh and up to 550 ms TWT in the centre of Figure 4.3. The maximum thickness cannot be calculated, as the multiple inhibits the observation of the lower boundary (Figure 4.3).

Unit 5 and a small part of unit 4 are affected by 2 distinct fault patterns: one major fault is located in the centre of the basin between the PDE and the palaeohigh and at least nine smaller ones to the west-southwest of this large fault (Figure 4.3). The large fault (about 750 m long and a dip of about 50-55°) is a west-dipping normal fault with offsets of 10 ms TWT at its top (about 1250 ms TWT), evolving to zero offsets at 1450 ms TWT. Deeper down, the offset cannot be determined anymore due to a chaotic seismic expression. The smaller faults are west-dipping normal faults with offsets inferior to 5 ms TWT. The activity along the faults stops within the lower part of unit 4.

3.2.2. Unit 4

The boundary between units 5 and 4 is erosive, evidenced by the incision into unit 5 along the GMV (Figure 4.3) and by the downlap of deposits of unit 4 onto unit 5 deposits along the Vernadsky Ridge (Figure 4.7). Unit 4 consists out of low to medium-amplitude, continuous reflections at the base and medium-amplitude, continuous reflections at the top (Figure 4.4Figure 4.5Figure 4.7). Overall, slightly mounded deposits are present along the GMV (Figure 4.4), PDE (Figure 4.5) and both Renard and Vernadsky Ridges (Figure 4.7). Moderately mounded (compared to the upper units) deposits in the upper parts of this unit northwest of the Renard Ridge are observed (Figure 4.7). Unit 4 fills a small incision at the intersection along the GMV, (only visible on Figure 4.3). The base of the incision contains discontinuous, slightly chaotic deposits, while more continuous deposits arise on top.
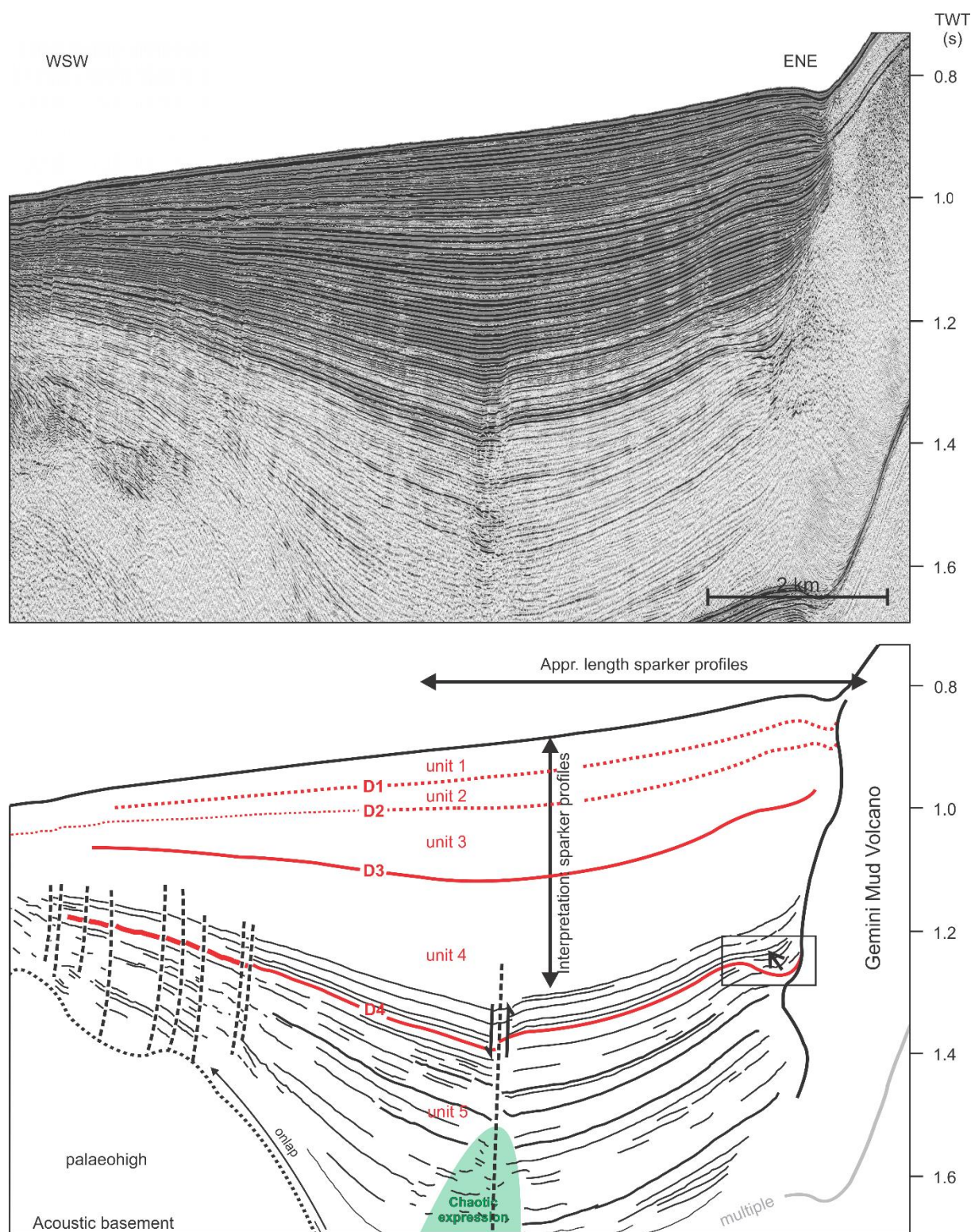
Figure 4.3: Multichannel airgun seismic profile (and interpretation) displaying 5 seismic stratigraphic units. The interpretations of unit 5 and the upper part of unit 4 are shown in detail, whereas the detail of the upper units is displayed in Figure 4.4Figure 4.5Figure 4.6. A large fault is present in the center of the profile and smaller ones to the southwest. The lower part of the large fault is concealed by a chaotic reflection expression. The small arrow in the ENE indicates the infill progradation of the depression (within the black box).
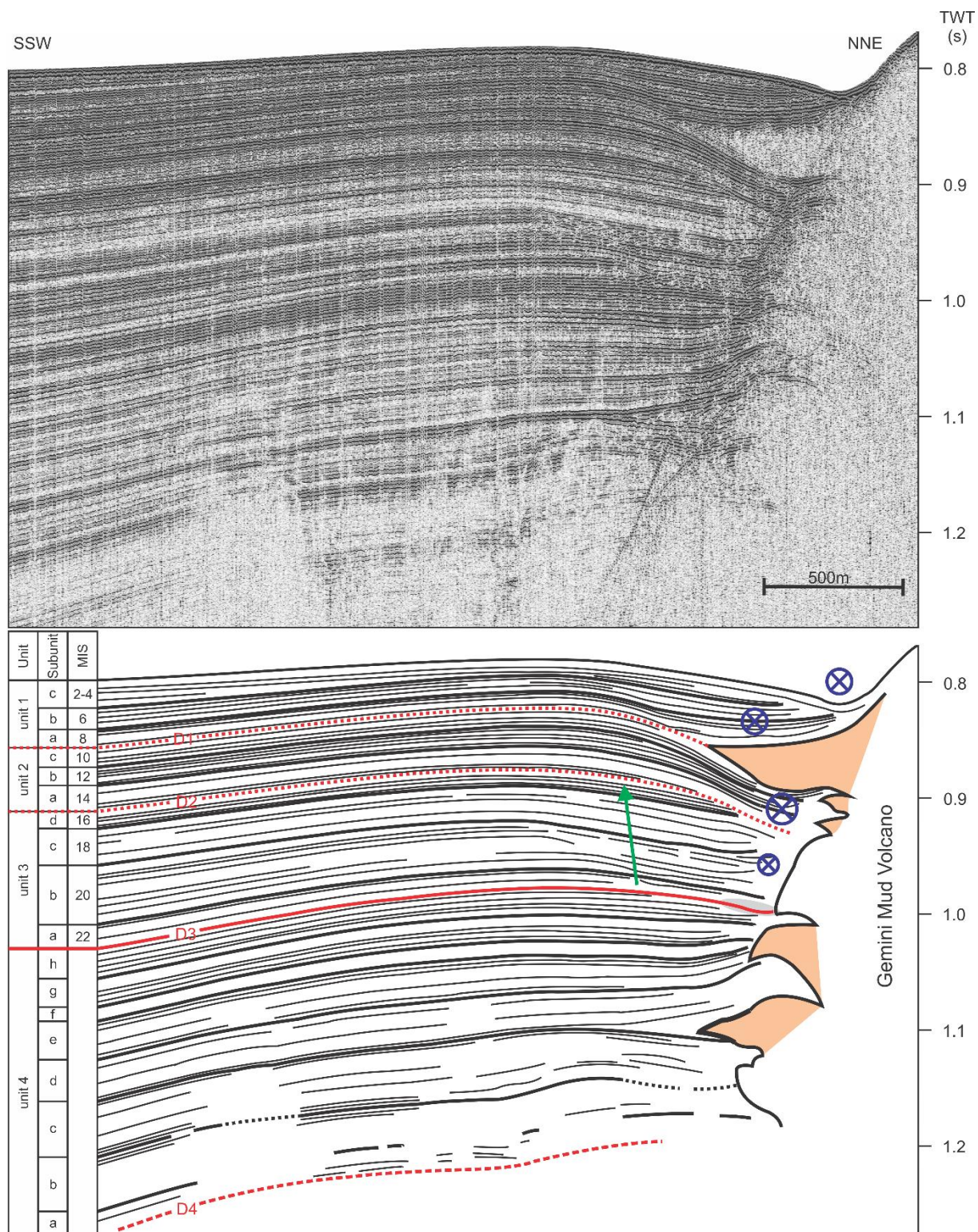
Figure 4.4: Single channel sparker seismic profile (and interpretation) perpendicular to the GMV, displaying 4 out of 5 units. The lower boundary of unit 4 is based on correlation with other profiles. Relative bottom current intensities are indicated by the size of the bottom current symbol, whereas the green arrow shows the increasing convex nature of the sediments of unit 3. The orange surfaces near the GMV indicate outflow lobes of the mud volcano. The table at the left side of the figure summarizes the units, subunits and interpreted marine isotopic stages (MIS).
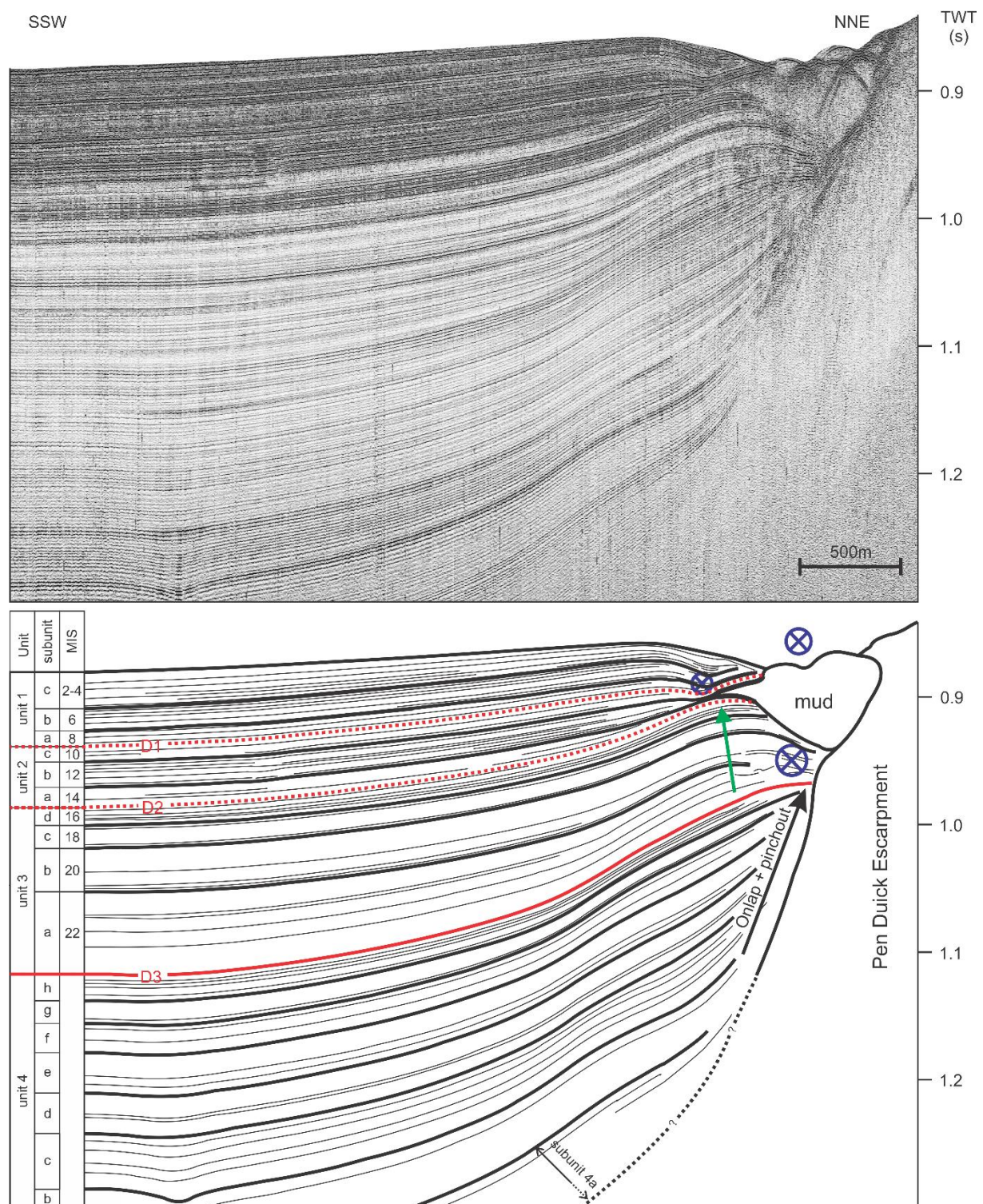
Figure 4.5: Single channel sparker seismic profile (and interpretation) perpendicular to the PDE, displaying 4 out of 5 units. The green arrow indicates the increase in mounded nature of the sediments in unit 3. The table at the left side of the figure summarizes the units, subunits and interpreted MIS. Relative current intensities are indicated by the size of the current symbol.

Unit 4 contains eight small subunits, each one about 25 to 35 ms TWT thick (Figure 4.4Figure 4.5Figure 4.7), all occurring within a cyclic pattern. All subunits display high amplitude reflections at their base and lower amplitudes on top (Figure 4.4Figure 4.5). Subunit c has slightly higher amplitude deposits, compared to the other 7 subunits. Generally, all subunits are conformable, but they pinch out near the ridges (Figure 4.5Figure 4.7), evidenced by the uplift of individual reflections and a decrease in

thickness of the subunits towards the ridges. The pinch-out is most pronounced at the base of unit 4 and gradually diminishes upwards along the PDE. The deposits along the Renard Ridge display a smaller degree of onlap, while along the Vernadsky Ridge, pinch-out can be observed further up the sedimentary sequence (Figure 4.7). Along the GMV, a different pattern is observed: the boundaries between the subunits display small erosional features. At the base of unit 4, the first evidence of a Christmas-tree structure appears (Figure 4.4). This pattern of mud extrusions disrupts the sedimentation at the foot of GMV and can be observed in all other units as well. The reflections on top of these extrusions display a convex pattern (Figure 4.4). The faults affecting unit 5 also disrupt the basal sediments of unit 4, but the small depression, caused by the central large normal fault, is gradually flattened throughout this unit (Figure 4.3 andFigure 4.5). The thicknesses generally vary between 200 and 250 ms TWT. The thicknesses are reduced due to the presence of the palaeohigh (Figure 4.3).

3.2.3.Unit 3

Units 4 and 3 are separated by a subtle angular unconformity. South of the PDE and GMV, small-scale erosion affects the deposits, but these small depressions are filled within unit 3 (Figure 4.4Figure 4.5). North of the Renard Ridge, the deposits of unit 4 are partly eroded and a small moat is present near the ridge (Figure 4.7). Near the Renard Ridge, unit 3 has low-amplitude reflections at its base and moderate-amplitude reflections at its top (Figure 4.5Figure 4.7). Near the GMV, unit 3 consists of mostly high-amplitude reflections with a low-amplitude part in the middle of the unit (Figure 4.4). Four subunits are present in this unit. The variability in amplitudes of the different subunits is rather low (although some high-amplitude reflections are present) and they can be distinguished by small angular unconformities (visible along both ridges). A moat is present along all of the topographic features, with mounded sediments on their sides. The moat along the PDE and GMV is about 150 m wide and re-incises itself continuously into underlying sediments, causing an increase in channel depth upwards (5 to 20 ms TWT). Deeper incisions are present along the PDE (Figure 4.4Figure 4.5). The moat north of the Renard Ridge is up to 500 m wide and shows incision depths up to 75 ms TWT (Figure 4.7), while the moat north of the Vernadsky Ridge is rather small (up to 100 m wide and only several ms TWT deep, Figure 4.7).

Along the northernmost part of PDE, unit 3 has a different appearance: very high amplitudes at the base, moderate in the middle and high again at the top (Figure 4.6). Also, no evidence of a moat along the PDE is observed here; the sedimentation pattern is obscured due to the presence of one of the mounded features and the associated diffraction hyperbola.

Several large (20-30 ms TWT high and up to 200 m wide) and small (<10 ms TWT high and less than 50 m wide) mounded features are present within this unit (Figure 4.6Figure 4.7). They have an acoustically almost transparent appearance. The large mounded structures along the PDE originate at the same stratigraphic level, which is 15 to 25 ms TWT above the base of unit 3 (Figure 4.6), while those north of the Renard Ridge seem to have at least 3 initiation horizons (Figure 4.7). The deposits on top of these mounded features are characterized by a concave geometry.

The thicknesses are fairly constant and vary around 100 ms TWT. Only along the mounded features at the foot of the ridges, 70 ms TWT of sediment is present (Figure 4.4Figure 4.5).
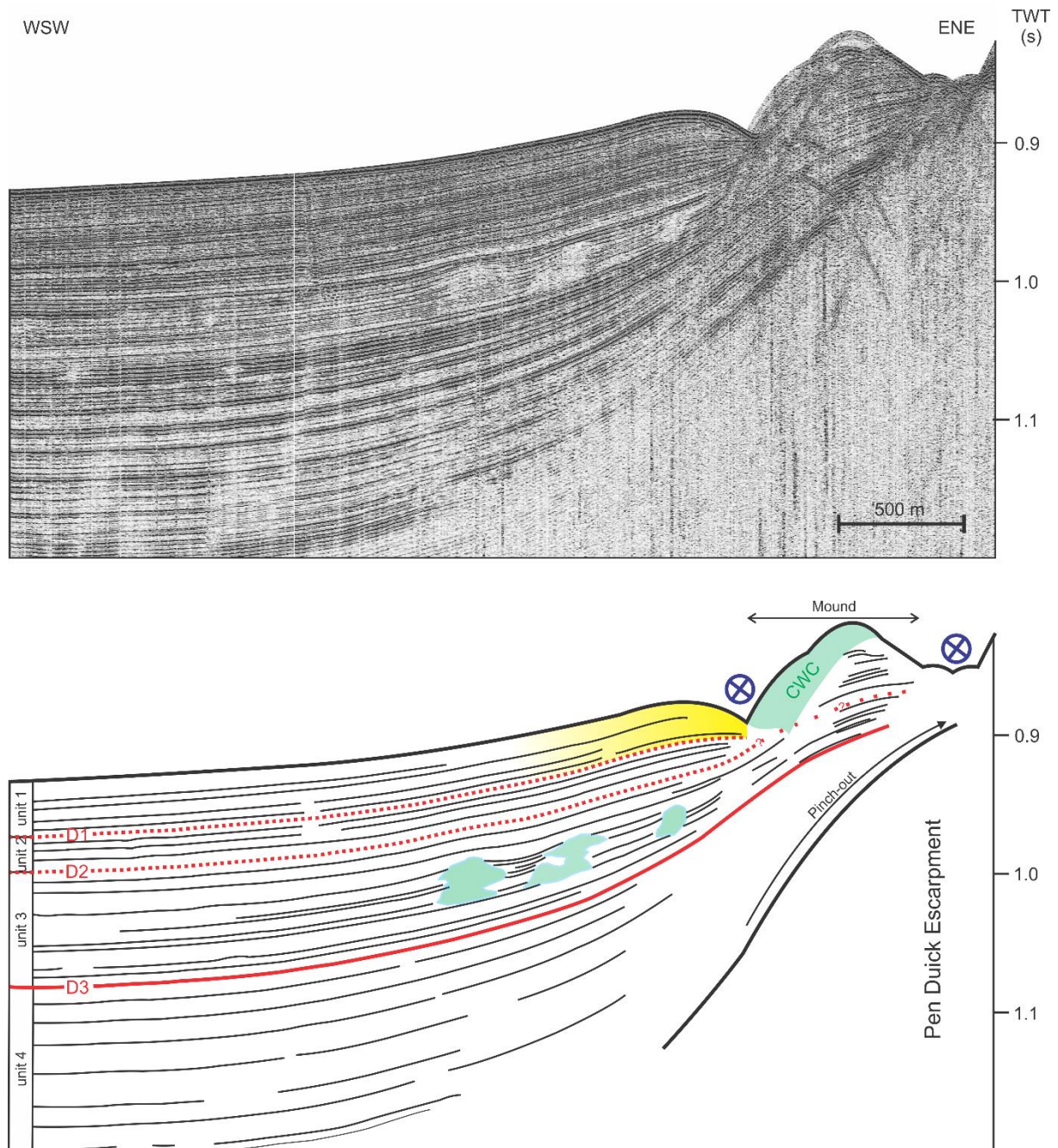
Figure 4.6: Single channel sparker seismic profile (and interpretation) perpendicular to the PDE, across one of the mounded features at its foot (Figure 4.2). The green shaded areas within units 3 and 1 indicate respectively buried and surfacing coral mounds. The yellow part of unit 1 illustrates the location of the mounded sediment drift WSW of the coral mound.

3.2.4.Unit 2

The boundary between units 3 and 2 (D2) is the most erosive of the entire sedimentary sequence. Up to 25 ms TWT (along the PDE and GMV) or up to 50 ms TWT (north of the Renard Ridge) sediments of unit 3 are eroded, creating a huge moat along the ridges. Along the Vernadsky Ridge, the erosion is less intense (Figure 4.7). The moats, which are present throughout the entire unit, are filled differently along the Renard Ridge and the GMV (Figure 4.4Figure 4.5Figure 4.7). Along the GMV, continuous high-amplitude reflections are encountered within the moat, while just outside the reflections have a concave appearance. In the rest of the unit, high-amplitude, dipping, continuous deposits are present (Figure 4.5Figure 4.7). Along the PDE, a nearly reflection-free triangular shaped block is encountered

within the moat. This block has a small run-out up to 50 ms TWT thick and 300 m long. Figure 4.2 shows the position of these deposits.

Based on small erosional surfaces and changes in acoustic appearance, 3 subunits are discerned within unit 2. The lowermost subunit (15-20 ms TWT thick) contains lower amplitudes compared to the upper two subunits (Figure 4.4Figure 4.5Figure 4.7). Within the upper subunit, near the PDE, a moat (about 100 m wide and only a few ms TWT deep) is observed about 750 m southwest of the PDE (Figure 4.5). Due to the thinning of this unit towards the north (comparison between Figure 4.4Figure 4.5Figure 4.6), the subunits are no longer discernible in Figure 4.6. Unit 2 is the thinnest of the sedimentary sequence with values varying around 50 ms TWT. At the position of the triangular shaped block, thicknesses are reduced to zero (Figure 4.5).

3.2.5.Unit 1

A partly erosive boundary separates units 2 and 1, although it is less erosive compared to D2. Along the GMV, a large concave extrusion (up to 800 m wide and 40 ms TWT deep) is observed (Figure 4.4).

A moat is present along the topographies, although the geometry changes. Along the GMV, PDE and Renard Ridge, the channel is rather wide (about 800 m) and 20 ms (GMV and PDE) or 100 ms (Renard Ridge) TWT deep, while the moat along the Vernadsky Ridge is only 200 m wide and 5 ms TWT deep. Along the PDE, a smaller channel (200 m wide and 10 ms TWT deep) is present SSW of the triangular shaped deposits within the lower two subunits (1a and b). However, within the upper subunit (1c), this channel, again positioned along the foot of the PDE has widened to 1 km and is just about 25 ms TWT deep (Figure 4.5). Along the northern part of the PDE, a second channel occurs just southwest of the mounded features at the base of the PDE. This channel is 150 m wide and up to 15 ms TWT deep. Southwest of this second channel, mounded sediments are observed which pass into conformable sheet-like deposits.

In total, 3 subunits are present, discernible through small angular unconformities. All subunits consist of high-amplitude, continuous reflections. In Figure 4.6, the subunits are again not discernible due to the decreases in thickness. Unit 1 is larger than unit 2: on average 50 to 55 ms TWT (Figure 4.4Figure 4.5Figure 4.7). The mounded features near the base of the PDE displays remarkable seismic features: its WSW side contains chaotic, very low-amplitude reflections, while its ENE side displays short horizontal, continuous reflections which seem to be a prolongation of the underlying sedimentation (Figure 4.6). Within the moat north of the Renard Ridge, a small patch of sediments is present (Figure 4.7).

4. Discussion

4.1. Sedimentary processes

4.1.1.Initiation (unit 5)

The deposits of unit 5 drape the acoustic basement and gently flatten the deepest parts. The settling of sedimentary particles in absence of strong currents, resulting in hemipelagic deposits (depending on the amount of biogenic material), is proposed as the main depositional mechanism. However, a minor downslope (earthquake-triggered?) component may be present given that palaeo-topographies are flattened. Unit 5 and the base of unit 4 are affected by faults: several smaller faults at the flanks of the palaeohigh and a large normal fault in between the palaeohigh and the PDE. These faults may be due to the compressional regime in the region (Van Rensbergen et al., 2005). However, as there is only one profile showing these features, they cannot be mapped and as a consequence, the actual orientation and direction cannot be derived. The palaeohigh resembles the compressional tectonic

ridges (Vernadsky and Renard) and may also be a compressional ridge that does not reach the present-day seafloor and is covered by sediments as a consequence.
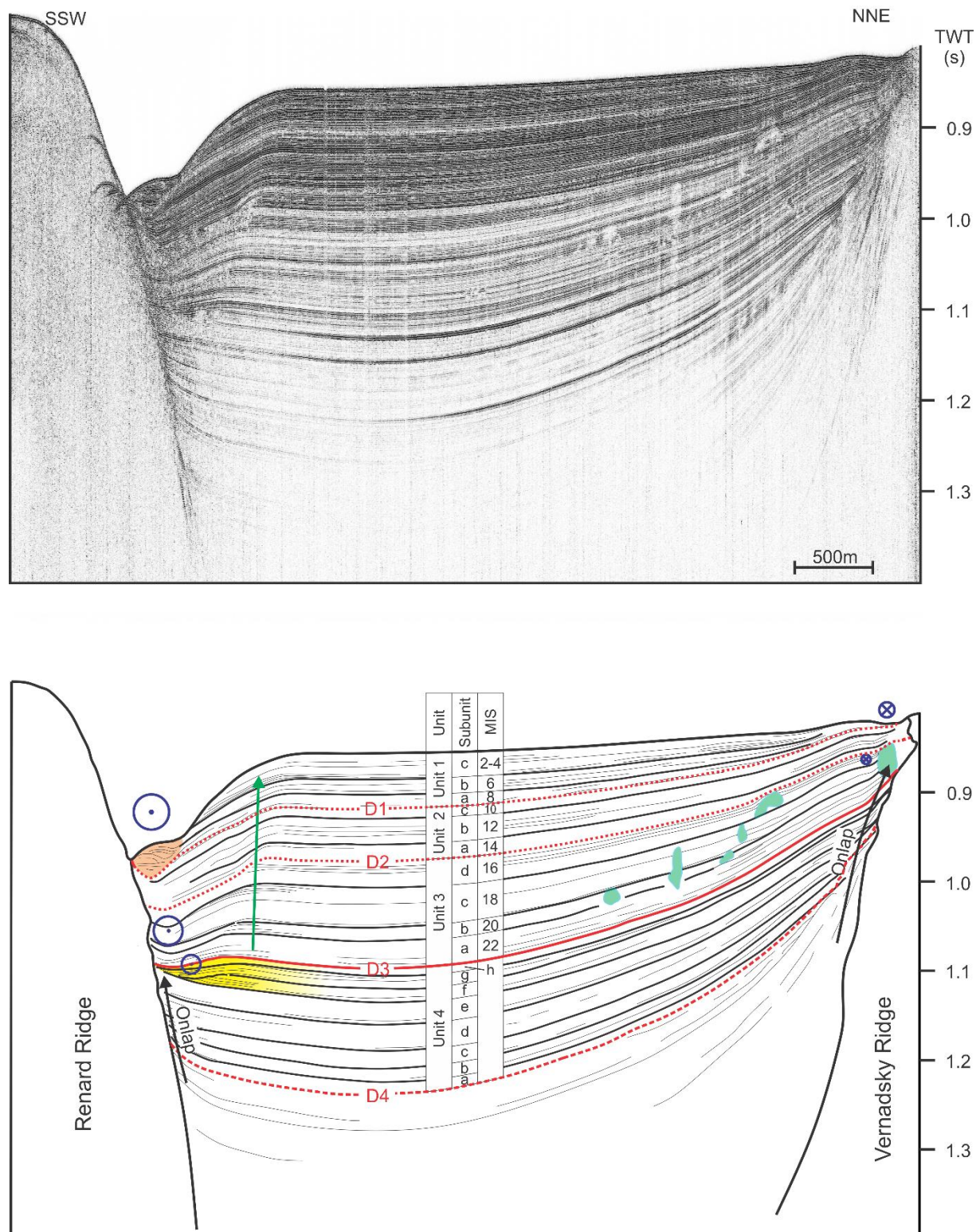
Figure 4.7: Single channel sparker seismic profile between the Renard and Vernadsky Ridges (position see Figure 4.2) showing all discerned subunits. The green features close to the Vernadsky Ridge are coral mounds, the yellow colored field indicates mounded deposits in unit 4 and the orange block at the foot of the Renard Ridge indicates sediments deposited within the moat. The table in the middle of the figure summarizes the units, subunits and interpreted MIS. Relative current intensities are indicated by the size of the current symbol.

4.1.2.Sheeted drift (unit 4)

From unit 4 onwards, very gradually, sheeted and detached mounded drift deposits develop parallel to the local relief.

Unit 4 mostly consists of horizontal, continuous, slightly mounded deposits along most of the PDE and slightly onlapping, semi-horizontal deposits along the northern part of the PDE and in between the Renard Ridge and Vernadsky Ridge (Figure 4.7). When the mounded geometry is present, it increases towards the top of the unit (Figure 4.4Figure 4.5Figure 4.7) and indicates together with the fairly uniform thickness, the aggradational stacking pattern and the location along steep slopes towards slope sheeted drift deposits (Faugères and Stow, 2008). When the mounded geometry is absent, hemipelagic deposits are present and no influence of bottom currents can be inferred. The upper part of unit 4 along the Renard Ridge is an exception to this, as clear mounded deposits alongside a moat are present (Figure 4.7). In this area, mounded drift deposits are observed for the first time, indicating faster-flowing bottom currents along this part of the Renard Ridge; mounded drift deposits are present throughout the area from units 3 onwards. This implies important horizontal variations in current strength along the ridges.

The presence of out-pinching strata, in an onlap configuration, onto the PDE, Renard Ridge and Vernadsky Ridge within the entire unit suggests a syn-lift sedimentation, affected by the uplift of these topographic features, as suggested by Van Rooij et al. (2011). Similarly, syntectonic sedimentation has been observed to the east of the study area by Maad et al. (2010). For the deposits along the PDE and Renard Ridge, the uplift gradually reduces towards the top of unit 4 and is not noticeable anymore in younger deposits. A slightly different story can be told for the Vernadsky Ridge, as uplift seems to continue after D3 (Figure 4.7), although onlap also gradually reduces above this discontinuity. This indicates the local effect of the ruling compressional forces, as neighbouring ridges show different uplift characteristics. The Renard Ridge is an extension of the Larache Ridge, which originates due to anticlinal folds along which fluid expulsion takes place (Maad et al., 2010). The uplift of the ridges (such as the Larache Ridge) has been attributed to compressional stresses (Somoza et al., 2003; Maad et al., 2010), originating from the NW-SE convergence of the African and Eurasian plates (Maldonado et al., 1999; Medialdea et al., 2009). As a consequence, the compressional forces, uplifting the Renard Ridge, must have diminished throughout and stopped at the top of unit 4 in this area, while those accounting for the uplift of the Vernadsky Ridge continued for some time after. The (eventual) cessation of the uplift must be a local effect, as the African-Eurasian convergence is still ongoing.

4.1.3.Mounded drift: units 3-1

Within the sedimentary sequence, the most striking change is the evolution from horizontal or slightly mounded and onlapping (except along the GMV) deposits (unit 4) into upslope prograding, mounded deposits with a moat along all of the topographic obstacles (units 3 to 1, Figure 4.4Figure 4.5Figure 4.7). Mounded drifts are associated with higher bottom current velocities (between 10 and 30 cm/s; Stow et al., 2008), compared to sheeted drifts (10 cm/s), which were described to be present within unit 4 along the GMV and PDE. The bottom current intensities also increase during the deposition of unit 3 as the depth of the moat (5 to 20 ms TWT along PDE/GMV and 10 to 50 ms TWT along the Renard Ridge) and the expression of the associated sediment drift mound increases (Figure 4.4Figure 4.5Figure 4.7). This can be interpreted as the evolution from the initiation of mounded drifts towards a continuous presence of stronger bottom currents within the moats, resulting into a gradual change from non-depositional (lower parts of unit 3) into erosional action (upper parts of unit 3). Along the northern part of the PDE, a typical moat and associated drift mound is absent and hemipelagic sedimentation is present (Figure 4.6). This can be interpreted as a lateral decline in bottom current strength. The decline in thickness of unit 3 from southeast to northwest along the PDE and GMV

illustrates the lateral change in sedimentation pattern: mounded drift deposits are thicker and occur in the southeastern part, whereas the hemipelagic sediments are thinner and occur in the northwest. Also along the Renard Ridge, lateral changes are observed, as the present-day moat has very different incision depths (Figure 4.2). Along the Vernadsky Ridge, the mounded drift deposits are less expressed, but not absent (Figure 4.7), implying slower flowing bottom currents along this ridge (compared to the Renard Ridge and PDE/GMV).

Three mound-like structures, originating at the same stratigraphic level (Figure 4.6) and six structures originating at different levels (Figure 4.7) have been observed within unit 3. They closely resemble buried coral mounds discussed by Huvenne et al. (2003) and Lo Iacono et al. (2014) and are therefore classified as such. The occurrence of coral mounds in this part of the study area implies that environmental conditions (food supply, prevention to burial) were right during at least a certain amount of time for CWC to flourish (Foubert et al., 2008; Wienberg et al., 2009; Wienberg et al., 2010).

An erosive boundary separates units 3 and 2 (Figure 4.4Figure 4.5Figure 4.7). Unit 2 is characterized by a larger (and along GMV wider) moat, except for the northern part of the PDE. In this area, the moat is still absent, indicating the continuing lateral decline in bottom current intensity. The erosive nature of the moat (by now even along the Vernadsky Ridge, Figure 4.7) indicates stronger bottom currents, capable of eroding more sediment. A large mud extrusion is observed at the base of subunit 2c (Figure 4.4). This has the same seismic characteristics as, and is positioned at the same stratigraphic level as, the triangular deposits in Figure 4.5. These similarities as well as the position of the triangular deposits near the GMV indicate a muddy origin for the triangular deposits as well, extruded at the same period. The separate patches of mud (Figure 4.2) may be the consequence of two different pathways, certainly as the GMV actually consists of two mud volcanoes within one mud cone (Van Rensbergen et al., 2005). After the large mud extrusion, the depocentre shifted SSW-wards, indicated by the relocation of the moat and mounded sediments for about 500 m (Figure 4.4Figure 4.5). Along the GMV, this relocation only occurs at the base of unit 1, whereas along the PDE this already occurred within subunit 2c.

Unit 1 consists of elongate mounded drift deposits along all of the topographies, even along the northern part of the PDE and south of the Vernadsky Ridge (Figure 4.4Figure 4.5Figure 4.6Figure 4.7). This indicates focussed bottom currents along all of the topographies, strong enough to create drift deposits. Along the GMV, only on the present-day seafloor, a narrow, deep moat occurs again directly SSW of the GMV and not more to the southwest as for subunits 1a and 1b (Figure 4.4). The same is observed along the PDE, a narrow but deep moat is present about 500 m SSW of the escarpment for subunits 1a and 1b (Figure 4.5) and on the present-day seafloor, the position of the moat shifted back to the foot of the PDE.

The occurrence of semi-buried coral mounds, recognized at the base of the northern part of the PDE, is a most peculiar feature (Figure 4.6). In morphology (width, height, shape) they resemble the coral mounds observed on top of the PDE (Foubert et al., 2008; Van Rooij et al., 2011). However, the presence of continuous reflections facing the PDE side of these mounded features, resembling the sedimentation below, contradicts a full CWC origin. Given the fact that the WSW part of the mound contains a seismic facies resembling the buried mounds of unit 3 (Figure 4.6) and the ENE part contains continuous, parallel, horizontal reflections, a dual origin for the mounded features is proposed. CWC started to settle at the base of unit 1, near the PDE, where gradually a mound was built against which sediment was deposited, provided by the bottom current along the PDE (inset Figure 4.8). This created these "hybrid" mounds, consisting of both a sedimentary (ENE) and coral mound (WSW) part. This implies that conditions for CWC to thrive were favourable at the foot of the PDE in this region. However, further investigations are required to further reveal and understand the exact nature and origin of these features. A small moat along the WSW part of the mounds implies a bottom current

flowing along them. A bottom current flows on the WSW flank of the mounds (probably due to their presence) and separated mounded drift deposits are present (Figure 4.6). Whether the bottom current flowing along the GMV and PDE splits or a second bottom current, unrelated to the first one, is present, cannot be derived from the present dataset (Figure 4.2).

4.2. Chronostratigraphy

The spatial and temporal distribution of the El Arraiche drifts indicates a depositional history including several changes in sedimentation pattern. Two major (D4, D3) and two minor transitions (D2, D1) are recorded as unconformities separating the depositional sequences. D4 marks the initiation of the drift deposition (at least along the PDE and GMV), while from D3 the transition from sheeted to elongated mounded drifts is initiated. D2 and D1 indicate changes within the elongated mounded drift deposits. These alterations have been compared to surrounding regions in order to construct a possible chronostratigraphy. Maad et al. (2010) discussed the seismic stratigraphy of the northwestern Moroccan Atlantic continental shelf based on sparker seismic data. Their unit Q2 is considered to have a Middle to Upper Pleistocene age (correlation with well LAR-A1, 25 km east-southeast of the study area from this chapter). The correlation (through connecting seismic profiles) of this unit to the investigated region reveals that at least units 3, 2 and 1 are within that age range.

Petrographic studies of mud breccia clasts show that the Al Idrissi mud volcano field is situated on an Upper Miocene-Pliocene sedimentary basin (Akhmanov et al., 2003; Pinheiro et al., 2003), implying that the sedimentary deposits described in this paper are of Plio-Pleistocene age. The mud volcanoes appeared 2.4 Ma ago (Van Rensbergen et al., 2005) or 2.6 Ma according to Perez-Garcia et al. (2011), implying that the entire contourite drift (units 4 to 1) is post-Pliocene in age and only unit 5 has a possible Pliocene age. Moreover, the basal unconformity, discussed by Van Rensbergen et al. (2005) and Perez-Garcia et al. (2011), is set at an age of 2.6 Ma, which could plausibly correlate with D4. This implies that discontinuity D4 could coincidentally be associated with the base Quaternary discontinuity (BQD), set at 2.588 Ma (Gibbard et al., 2010).

During the Quaternary, the Early-Middle Pleistocene Revolution (EMPT) is the most important palaeoceanographic change in the entire North-Atlantic Ocean, coeval with the switch to a "full" glacial mode with 100 ka eccentricity cyclicity (Shackleton et al., 1990; Paillard, 1998; Marino et al., 2009). In many contourite systems, this is accompanied by an increase in sedimentation rates (Van Rooij et al., 2010; Roque et al., 2012; Müller-Michaelis et al., 2013), mostly evidenced by higher amplitude reflections (Hernández-Molina et al., 2006; Llave et al., 2007; Van Rooij et al., 2007). A similar observation has been made here; a transition from sheeted to elongate mounded drift deposits and a gradual increase in amplitudes of the reflections throughout units 3, 2 and 1 (Figure 4.4Figure 4.5Figure 4.6Figure 4.7). Therefore, discontinuity D3 may tentatively be correlated to the EMPT (0.9 Ma).

The continental shelves and upper slopes are more prone to eustatic sea-level variations compared to deep-water environments. Hence, in response, bottom currents fluctuate more in these shallow water regions (Hernández-Molina et al., 2002; Verdicchio and Trincardi, 2008; Ridente et al., 2009). The upper three units display features which can be attributed to climatic variations: a cyclic pattern of progradational subunits (onto the PDE, GMV, Renard Ridge or Vernadsky Ridge) with reflections of varying amplitudes. In nearby regions (Alboran Sea, northern Gulf of Cádiz), the majority (65-80%) of the sediment is deposited during regressive and lowstand periods (Hernández-Molina et al., 2002). Except for the upper parts of the sedimentary column (Van Rooij et al., 2011), no overall sedimentation rates are known yet for this region. Hence, the subunits have been tentatively linked to glacial marine isotopic stages (MIS). This correlation has been applied before along the Adriatic margin by Ridente et al. (2009) and along the southwestern Mallorca shelf by Vandorpe et al. (2011). The ten discerned

subunits from the EMPT to Recent can be correlated to the ten (even) MIS (Lisiecki and Raymo, 2005; Figure 4.4Figure 4.5Figure 4.7). A periodicity of 80 to 120 ky is obtained due to this correlation, which is in agreement with the obliquity pacing hypothesis proposed by Huybers (2007), stating that glacial cycles vary by 80 or 120 ka in the late-Pleistocene by skipping one or two obliquity beats. As a result, D2 and D1 could be linked to MIS 15 (about 575 ka) and 9 (about 325 ka) respectively.
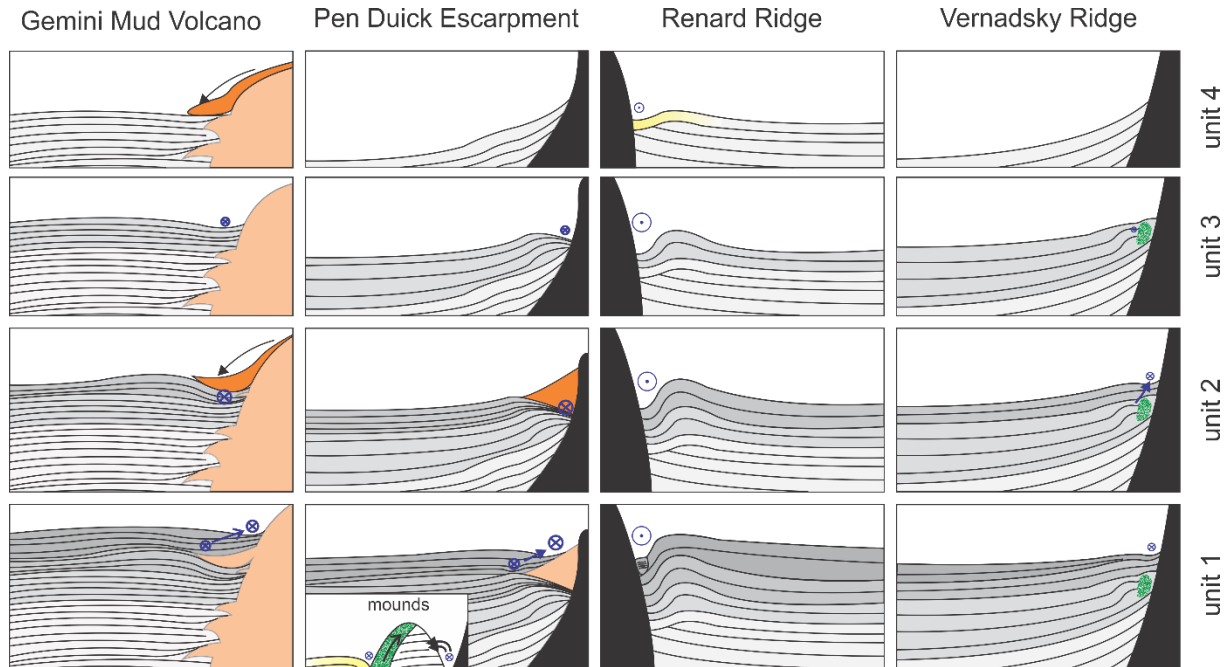
Figure 4.8: Summarizing sketches of the El Arraiche contourite drift evolution. The relative bottom current intensities are indicated by the size of the current symbol. Dark orange zones indicate active mud flow extrusions from the GMV, yellow colors indicate mounded drift growth at unusual locations and the green areas indicate coral mounds. The inset sketch within unit 1 along the PDE shows the build-up of the coral mounds at the foot of the PDE.

Based on this tentative chronostratigraphy and the average measured thicknesses (the conversion into metric scale is based on a theoretical seismic velocity of 1650 m/s within the sediment), the sedimentation rate for the period between BQD and EMPT (unit 4) is 10.8 cm/ka and between EMPT and Recent (units 3 to 1) 17.0 cm/ka. These rates are close to or within the range of theoretical values for sediment drifts: 3-10 cm/ka for sheeted drifts (unit 4) and 5-30 cm/ka for mounded drifts (units 3 to 1; Stow et al., 2008) and are close to the sedimentation rates determined by Wienberg et al. (2009). Van Rooij et al. (2011) obtained a sedimentation rate of 8-14 cm/s for MIS3, which is compatible with the calculated values. Also, the increase in sedimentation rate after the EMPT is consistent with the aforementioned enhanced sedimentation rates. This tentative chronostratigraphy also points out some differences in uplift of the ridges throughout the entire Gulf of Cádiz. Whereas the Cádiz and Guadalquivir ridges are reactivated during the EMPT and MIS 6, changing the sedimentation pattern in the Guadalquivir and Huelva drifts (Llave et al., 2007), the PDE does not show signs of uplift during these periods (Figure 4.5). Indeed, uplift would have stopped in this region around the EMPT (difference between Renard and Vernadsky Ridge), implying that timing of compression may vary locally within the Gulf of Cádiz.

4.3. Comparison to the northern Gulf of Cádiz palaeoceanography

When comparing the depositional history of the El Arraiche drifts to other systems along upper continental slopes of the Northeast Atlantic Ocean (Cádiz and Le Danois CDS), several resemblances and differences can be identified (Figure 4.9). While in the Cádiz and Le Danois CDS, drift deposits are present from the Pliocene onwards, the El Arraiche area only contains Quaternary drift deposits

(except for the upper three subunits of unit 4 along the Renard Ridge; Figure 4.7). After the EMPT, an intensification of bottom currents and an accompanying growth of the CDS occurs in all drift systems, expressed by a severe growth phase of the mounded drift deposits in the Cádiz and Le Danois drifts (Van Rooij et al., 2010; Llave et al., 2011; Roque et al., 2012; Brackenridge et al., 2013) and by the evolution from sheeted to mounded drift deposits in the El Arraiche area (Figure 4.4Figure 4.5Figure 4.7). A final intensification stage is observed in the Cádiz CDS at about MIS 12 (Llave et al., 2007; Marchès et al., 2010; Llave et al., 2011; Roque et al., 2012), while in the El Arraiche drifts, this intensification is tentatively set at MIS 15. The boundary at MIS 9 observed in the El Arraiche drifts is not encountered in the other systems. The vast above-mentioned differences in evolution between MOW-controlled CDS's and the El Arraiche drifts suggest that the MOW is not likely to be the main driving force behind the formation or shaping of the El Arraiche drifts. Although the MOW is present within the area as meddies (Ambar et al., 2008), it is not observed along the topographic obstacles (only in deeper water settings; Figure 4.10). During glacial periods, MOW flows at even greater depths (García et al., 2009) and therefore, its presence at the foot of the Renard Ridge and Vernadsky Ridge during glacials is not likely neither.

Figure 4.9: Comparison of the evolution of the El Arraiche drifts with MOW-controlled drifts in the northern Gulf of Cádiz (Roque et al., 2012; Brackenridge et al., 2013) and the Bay of Biscay (Van Rooij et al., 2010). Red boxes represent pre-contourite deposits, yellow boxes signify sheeted drifts and green is used for mounded drift deposits. BQD: Base Quaternary Discontinuity, LPR: Lower Pliocene Revolution, MIS: Marine Isotopic Stage, EMPT: Early-Middle Pleistocene Revolution, UPD: Upper Pleistocene Discontinuity.

A more suitable and plausible candidate may be the AAIW. It enters the Gulf of Cádiz in the south and flows along the African coast towards the north, before being outcompeted by the MOW (Machín et al., 2006; Louarn and Morin, 2011). CTD data from Van Rooij et al. (2011) and Mienis et al. (2012) indicate the presence of AAIW at the foot of the escarpment, while NACW is present on top. The absence of MOW, the proved presence of AAIW and the depth range in which the Pen Duick drift occurs (Figure 4.10), favours towards a recent AAIW-influence. Most of the sediment is inferred to be deposited during glacial periods and the production of AAIW is known to increase during colder periods (e.g. during the last glacial maximum (Makou et al., 2010; Wainer et al., 2012) and during Heinrich events (Jung et al., 2011)), leading to thicker deposits along the Argentinian margin (Voigt et al., 2013). These arguments support the idea of an AAIW-origin of the El Arraiche drifts, even during glacial periods. However, the northern extent of the glacial AAIW is not yet fully known (Oppo and Curry, 2005, 2012); its presence north of 27°S is not yet proven. This implies that glacial north Atlantic

intermediate water, known to occur in this region and present down till depths of about 2200 m (Marchitto and Broecker, 2006), might as well be involved in the origin of the El Arraiche drifts.

Mienis et al. (2012) showed the presence of northeast-directed currents at the foot of the PDE. This is in agreement with the observed seismic characteristics and geomorphology of the Pen Duick drift. A moat is present along the PDE and GMV, indicating a bottom current along both topographies. This bottom current has been active throughout the entire Quaternary (Figure 4.4Figure 4.5Figure 4.6), depositing sediment SSW of the GMV and PDE. Taking into account the pathway of the bottom current and the Coriolis deflection to the right in the northern hemisphere, the bottom current is inferred to have a northeast-ward direction. The CTD data and the flow direction at the foot of the topographies together hint towards a bottom current coming from the south, being deflected by the GMV and PDE and which continues to flow along the bases of the topographies due to Coriolis deflection. No bottom current directions are available from the region between the Renard and Vernadsky Ridge, but the position of the moats (Figure 4.2) and the Coriolis deflection infer a bottom current from west to east along the Renard Ridge and from east to west along the Vernadsky Ridge (Figure 4.2). Higher velocities due to deflection against small-scale topographies (such as seamounts, mud volcanoes, escarpments, …) are commonly described (Stow et al., 2009; Hernández-Molina et al., 2011; Rebesco et al., 2014). Taking into account the fact that bottom currents are on average 8 cm/s on the plain at the foot of the PDE (Mienis et al., 2012) and that drift deposits solely occur along the topographies, the El Arraiche drifts are excellent examples of obstacle-related contourite systems.
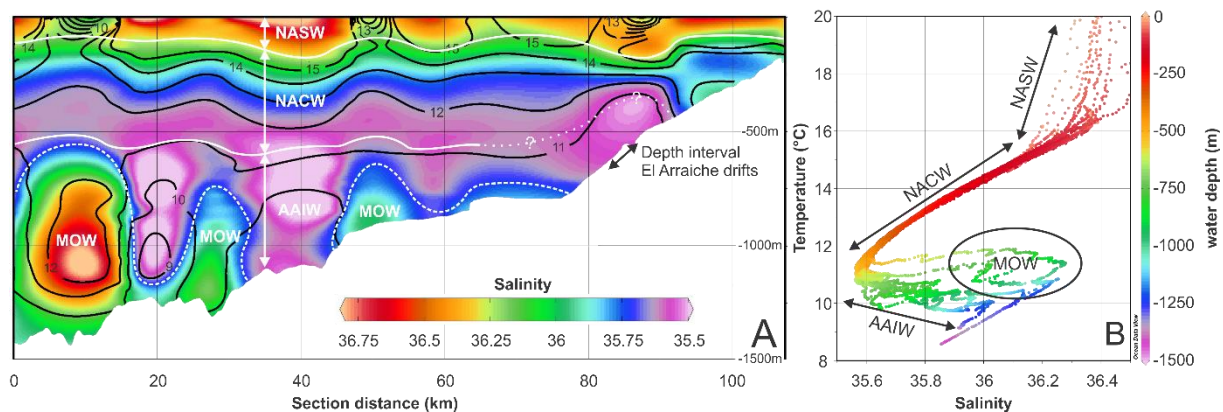
Figure 4.10: A) Salinity (colors) and temperature (contours, °C) transect, 10–15 km south of the GMV and PDE. The data were obtained from the world ocean database (World Ocean Database, 05/02/2013). B) Salinity-temperature diagram of all available CTD stations along the profile.

5. Conclusions

Based on high-resolution sparker single-channel seismic profiles, an airgun multi-channel seismic profile and multibeam data, several contourite drifts along the Renard and Vernadsky Ridges and GMV have been described in terms of sedimentary evolution and palaeoceanography. Five main conclusions may be drawn from this study:

1. The El Arraiche drifts are excellent examples of obstacle-related drifts as they occur in an area with general low-intensity bottom currents. Bottom currents are deflected against the topographies and build a contourite drift along them, parallel to the local relief.

2. The El Arraiche drifts originate at the start of the Quaternary, creating sheeted drift deposits (unit 4). The bottom currents intensified after the EMPT, leading to the deposition of separated mounded drift deposits (unit 3 to 1). A general intensification of bottom currents is inferred from the EMPT to present.

3. The presence of the GMV interferes with the drift deposits: several extrusions are recorded within the sedimentary sequence leading to a Christmas-tree structure along the mud volcano. The presence of a large block of mud along both PDE and GMV within unit 2 indicates a large eruption in that period.

4. The El Arraiche drifts have a possible AAIW-origin which would make them the most northern expression of AAIW within the Atlantic Ocean. Evidence (both drift architecture and CTD data) for the presence of MOW at the foot of the topographies is not present.

5. Coral mounds have been found within and on top of the El Arraiche drift. This means that not only on top of the Renard and Vernadsky Ridges, environmental conditions were right for CWC to flourish, but also at their bases. The "hybrid" mounds at the food of the PDE were active from the base of unit 1 (about 71 ka). The presence of the buried mounds within unit 3 indicates that also in the past, periods with conditions favourable for coral mound growth were present.

References

World Ocean Database, 05/02/2013. http://www.nodc.noaa.gov/OC5/WOD09/pr_wod09.html.

Akhmanov, G., Ivanov, M., Henriet, J.P., Sarantzev, E.S., 2003. The El Arraiche mud volcano field and its "exotic" mud volcano deposits recovere during the TTR-12 cruise in the Gulf of Cadiz, in: Marani, M., Akhmanov, G., Suzyumov, A. (Eds.), Geological and biological processes at deep-sea European margins and oceanic basins. UNESCO, Bologna, Italy, pp. 9-10.

Ambar, I., Serra, N., Neves, F., Ferreira, T., 2008. Observations of the Mediterranean Undercurrent and eddies in the Gulf of Cadiz during 2001. Journal of Marine Systems 71, 195-220.

Brackenridge, R.E., Hernández-Molina, F.J., Stow, D.A.V., Llave, E., 2013. A Pliocene mixed contourite–turbidite system offshore the Algarve Margin, Gulf of Cadiz: Seismic response, margin evolution and reservoir implications. Marine and Petroleum Geology 46, 36-50.

De Mol, L., Hilário, A., Van Rooij, D., Henriet, J.P., 2011. Habitat mapping of a cold-water coral mound on Pen Duick escarpment (Gulf of Cadiz), in: harris, P., Baker, E. (Eds.), Seafloor morphology as benthic habitat. Elsevier, pp. 645-654.

Faugères, J.C., Stow, D.A.V., 2008. Contourite drifts: Nature, Evolution and Controls, in: Rebesco, M., Camerlenghi, A. (Eds.), Contourites. Elsevier, pp. 259-288.

Foubert, A., Depreiter, D., Beck, T., Maignien, L., Pannemans, B., Frank, N., Blamart, D., Henriet, J.-P., 2008. Carbonate mounds in a mud volcano province off north-west Morocco: Key to processes and controls. Marine Geology 248, 74-96.

García, M., Hernández-Molina, F.J., Llave, E., Stow, D.A.V., León, R., Fernández-Puga, M.C., Díaz del Río, V., Somoza, L., 2009. Contourite erosive features caused by the Mediterranean Outflow Water in the Gulf of Cadiz: Quaternary tectonic and oceanographic implications. Marine Geology 257, 24-40.

Gibbard, P.L., Head, M.J., Walker, M.J.C., 2010. Formal ratification of the Quaternary System/Period and the Pleistocene Series/Epoch with a base at 2.58 Ma. Journal of Quaternary Science 25, 96-102.

Hernández-Molina, F.J., Larter, R.D., Rebesco, M., Maldonado, A., 2006. Miocene reversal of bottom water flow along the Pacific Margin of the Antarctic Peninsula: Stratigraphic evidence from a contourite sedimentary tail. Marine Geology 228, 93-116.

Hernández-Molina, F.J., Serra, N., Stow, D.A.V., Llave, E., Ercilla, G., Van Rooij, D., 2011. Along-slope oceanographic processes and sedimentary products around the Iberian margin. Geo-Mar Lett 32, 315-341.

Hernández-Molina, F.J., Somoza, L., Vazquez, J.T., Lobo, F., Fernández-Puga, M.C., Llave, E., Díaz-del Río, V., 2002. Quaternary stratigraphic stacking patterns on the continental shelves of the southern Iberian Peninsula: their relationship with global climate and palaeoceanographic changes. Quaternary International 92, 5-23.

Huvenne, V.A.I., De Mol, B., Henriet, J.P., 2003. A 3D seismic study of the morphology and spatial distribution of buried coral banks in the Porcupine Basin, SW of Ireland. Marine Geology 198, 5-25.

Huybers, P., 2007. Glacial variability over the last two million years: an extended depth-derived agemodel, continuous obliquity pacing, and the Pleistocene progression. Quaternary Science Reviews 26, 37-55.

Jung, S.J.A., Kroon, D., Ganssen, G., Peeters, F., Ganeshram, R., 2011. Southern Hemisphere intermediate water formation and the bi-polar seesaw. Pages News 18, 36-38.

Lisiecki, L.E., Raymo, M.E., 2005. A Plio-Pleistocene stack of 57 globally distributed benthic delta 18O records. Paleoceanography 20, PA1003.

Llave, E., Hernández-Molina, F., Stow, D.V., Fernández-Puga, M., García, M., Vázquez, J., Maestro, A., Somoza, L., Díaz del Río, V., 2007. Reconstructions of the Mediterranean Outflow Water during the quaternary based on the study of changes in buried mounded drift stacking pattern in the Gulf of Cadiz. Marine Geophysical Researches 28, 379-394.

Llave, E., Hernández-Molina, F.J., Somoza, L., Stow, D.A.V., Díaz Del Río, V., 2007. Quaternary evolution of the contourite depositional system in the Gulf of Cadiz. Geological Society, London, Special Publications 276, 49-79.

Llave, E., Matias, H., Hernández-Molina, F., Ercilla, G., Stow, D., Medialdea, T., 2011. Pliocene–Quaternary contourites along the northern Gulf of Cadiz margin: sedimentary stacking pattern and regional distribution. Geo-Marine Letters 31, 377-390.

Lo Iacono, C., Gràcia, E., Ranero, C.R., Emelianov, M., Huvenne, V.A.I., Bartolomé, R., Booth-Rea, G., Prades, J., Ambroso, S., Dominguez, C., Grinyó, J., Rubio, E., Torrent, J., 2014. The West Melilla cold water coral mounds, Eastern Alboran Sea: Morphological characterization and environmental context. Deep Sea Research Part II: Topical Studies in Oceanography 99, 316-326.

Louarn, E., Morin, P., 2011. Antarctic Intermediate Water influence on Mediterranean Sea Water outflow. Deep Sea Research Part I: Oceanographic Research Papers 58, 932-942.

Maad, N., Le Roy, P., Sahabi, M., Gutscher, M.-A., Hssain, M., Babonneau, N., Rabineau, M., Lanoë, B.V.V., 2010. Seismic stratigraphy of the NW Moroccan Atlantic continental shelf and Quaternary deformation at the offshore termination of the southern Rif front. Comptes Rendus Geoscience 342, 731-740.

Machín, F., Hernández-Guerra, A., Pelegrí, J.L., 2006. Mass fluxes in the Canary Basin. Progress In Oceanography 70, 416-447.

Makou, M.C., Oppo, D.W., Curry, W.B., 2010. South Atlantic intermediate water mass geometry for the last glacial maximum from foraminiferal Cd/Ca. Paleoceanography 25, PA4101.

Maldonado, A., Somoza, L., Pallarés, L., 1999. The Betic orogen and the Iberian-African boundary in the Gulf of Cadiz: geological evolution (central North Atlantic). Marine Geology 155, 9-43.

Marchès, E., Mulder, T., Gonthier, E., Cremer, M., Hanquiez, V., Garlan, T., Lecroart, P., 2010. Perched lobe formation in the Gulf of Cadiz: Interactions between gravity processes and contour currents (Algarve Margin, Southern Portugal). Sedimentary Geology 229, 81-94.

Marchitto, T.M., Broecker, W.S., 2006. Deep water mass geometry in the glacial Atlantic Ocean: A review of constraints from the paleonutrient proxy Cd/Ca. geochemistry, geophysics, Geosystems 7, Q12003.

Marino, M., Maiorano, P., Lirer, F., Pelosi, N., 2009. Response of calcareous nannofossil assemblages to paleoenvironmental changes through the mid-Pleistocene revolution at Site 1090 (Southern Ocean). Palaeogeography, Palaeoclimatology, Palaeoecology 280, 333-349.

Medialdea, T., Somoza, L., Pinheiro, L.M., Fernández-Puga, M.C., Vázquez, J.T., León, R., Ivanov, M.K., Magalhaes, V., Díaz-del-Río, V., Vegas, R., 2009. Tectonics and mud volcano development in the Gulf of Cádiz. Marine Geology 261, 48-63.

Mienis, F., De Stigter, H.C., De Haas, H., Van der Land, C., Van Weering, T.C.E., 2012. Hydrodynamic conditions in a cold-water coral mound area on the Renard Ridge, southern Gulf of Cadiz. Journal of Marine Systems 96–97, 61-71.

Müller-Michaelis, A., Uenzelmann-Neben, G., Stein, R., 2013. A revised Early Miocene age for the instigation of the Eirik Drift, offshore southern Greenland: Evidence from high-resolution seismic reflection data. Marine Geology 340, 1-15.

Oppo, D.W., Curry, W.B., 2005. Glacial water mass geometry and the distribution of delta 13C of CO2 in the western Atlantic Ocean. Paleoceanography 20.

Oppo, D.W., Curry, W.B., 2012. Deep Atlantic Circulation during the Last Glacial Maximum and deglaciation. Nature Education Knowledge 3 (10):1.

Paillard, D., 1998. The timing of Pleistocene glaciations from a simple multiple-state climate model. Nature 391, 378-381.

Perez-Garcia, C., Berndt, C., Klaeschen, D., Mienert, J., Haffert, L., Depreiter, D., Haeckel, M., 2011. Linked halokinesis and mud volcanism at the Mercator mud volcano, Gulf of Cadiz. Journal of Geophysical Research: Solid Earth 116, n/a-n/a.

Pinheiro, L.M., Ivanov, M.K., Sautkin, A., Akhmanov, G., Magalhães, V.H., Volkonskaya, A., Monteiro, J.H., Somoza, L., Gardner, J., Hamouni, N., Cunha, M.R., 2003. Mud volcanism in the Gulf of Cadiz: results from the TTR-10 cruise. Marine Geology 195, 131-151.

Pirlet, H., Wehrmann, L.M., Brunner, B., Frank, N., Dewanckele, J.A.N., Van Rooij, D., Foubert, A., Swennen, R., Naudts, L., Boone, M., Cnudde, V., Henriet, J.-P., 2010. Diagenetic formation of gypsum and dolomite in a cold-water coral mound in the Porcupine Seabight, off Ireland. Sedimentology 57, 786-805.

Rebesco, M., Hernández-Molina, F.J., van Rooij, D., Wåhlin, A., 2014. Contourites and associated sediments controlled by deep-water circulation processes: State of the art and future considerations. Marine Geology.

Ridente, D., Trincardi, F., Piva, A., Asioli, A., 2009. The combined effect of sea level and supply during Milankovitch cyclicity: Evidence from shallow-marine $\delta^{18}O$ records and sequence architecture (Adriatic margin). Geology 37, 1003-1006.

Roque, C., Duarte, H., Terrinha, P., Valadares, V., Noiva, J., Cachão, M., Ferreira, J., Legoinha, P., Zitellini, N., 2012. Pliocene and Quaternary depositional model of the Algarve margin contourite drifts (Gulf of Cadiz, SW Iberia): Seismic architecture, tectonic control and paleoceanographic insights. Marine Geology 303–306, 42-62.

Shackleton, N.J., Berger, A., Peltier, W.R., 1990. An alternative astronomical calibration of the lower Pleistocene timescale based on ODP Site 677. Transactions of the Royal Society of Edinburgh, Earth Sciences 81, 251-261.

Somoza, L., Díaz del Río, V., León, R., Ivanov, M., Fernández-Puga, M.C., Gardner, J.M., Hernández-Molina, F.J., Pinheiro, L.M., Rodero, J., Lobato, A., Maestro, A., Vázquez, J.T., Medialdea, T., Fernández-Salas, L.M., 2003. Seabed morphology and hydrocarbon seepage in the Gulf of Cádiz mud volcano area: Acoustic imagery, multibeam and ultra-high resolution seismic data. Marine Geology 195, 153-176.

Stow, D.A.V., Hernández-Molina, F.J., Llave, E., Sayago-Gil, M., Díaz del Río, V., Branson, A., 2009. Bedform-velocity matrix: The estimation of bottom current velocity from bedform observations. Geology 37, 327-330.

Stow, D.A.V., Hunter, S., Wilkinson, D., Hernández-Molina, F.J., 2008. The nature of contourite deposition, in: Rebesco, M., Camerlenghi, A. (Eds.), Contourites. Elsevier.

Templer, S.P., Wehrmann, L.M., Zhang, Y., Vasconcelos, C., McKenzie, J.A., 2011. Microbial community composition and biogeochemical processes in cold-water coral carbonate mounds in the Gulf of Cadiz, on the Moroccan margin. Marine Geology 282, 138-148.

Van Rensbergen, P., Depreiter, D., Pannemans, B., Moerkerke, G., Van Rooij, D., Marsset, B., Akhmanov, G., Blinova, V., Ivanov, M., Rachidi, M., Magalhaes, V., Pinheiro, L., Cunha, M., Henriet, J.-P., 2005. The El Arraiche mud volcano field at the Moroccan Atlantic slope, Gulf of Cadiz. Marine Geology 219, 1-17.

Van Rooij, D., Blamart, D., De Mol, L., Mienis, F., Pirlet, H., Wehrmann, L.M., Barbieri, R., Maignien, L., Templer, S.P., de Haas, H., Hebbeln, D., Frank, N., Larmagnat, S., Stadnitskaia, A., Stivaletta, N., van Weering, T., Zhang, Y., Hamoumi, N., Cnudde, V., Duyck, P., Henriet, J.P., 2011. Cold-water coral mounds on the Pen Duick Escarpment, Gulf of Cadiz: The MiCROSYSTEMS project approach. Marine Geology 282, 102-117.

Van Rooij, D., Blamart, D., Richter, T., Wheeler, A., Kozachenko, M., Henriet, J.P., 2007. Quaternary sediment dynamics in the Belgica mound province, Porcupine Seabight: ice-rafting events and contour current processes. International Journal of Earth Sciences 96, 121-140.

Van Rooij, D., Iglesias, J., Hernández-Molina, F.J., Ercilla, G., Gomez-Ballesteros, M., Casas, D., Llave, E., De Hauwere, A., Garcia-Gil, S., Acosta, J., Henriet, J.P., 2010. The Le Danois Contourite Depositional System: Interactions between the Mediterranean Outflow Water and the upper Cantabrian slope (North Iberian margin). Marine Geology (2010) 274, 1-20.

Vandorpe, T., Van Rooij, D., Stow, D., Henriet, J.-P., 2011. Pliocene to Recent shallow-water contourite deposits on the shelf and shelf edge off south-western Mallorca, Spain. Geo-Marine Letters 31, 391-403.

Verdicchio, G., Trincardi, F., 2008. Shallow-water Contourites, in: Rebesco, M., Camerlenghi, A. (Eds.), Contourites. Elsevier, *Developments in Sedimentology*, pp. 409-433.

Voigt, I., Henrich, R., Preu, B.M., Piola, A.R., Hanebuth, T.J.J., Schwenk, T., Chiessi, C.M., 2013. A submarine canyon as a climate archive — Interaction of the Antarctic Intermediate Water with the Mar del Plata Canyon (Southwest Atlantic). Marine Geology 341, 46-57.

Wainer, I., Goes, M., Murphy, L.N., Brady, E., 2012. Changes in the intermediate water mass formation rates in the global ocean for the Last Glacial Maximum, mid-Holocene and pre-industrial climates. Paleoceanography 27, PA3101.

Wehrmann, L.M., Templer, S.P., Brunner, B., Bernasconi, S.M., Maignien, L., Ferdelman, T.G., 2011. The imprint of methane seepage on the geochemical record and early diagenetic processes in cold-water coral mounds on Pen Duick Escarpment, Gulf of Cadiz. Marine Geology 282, 118-137.

Wienberg, C., Frank, N., Mertens, K.N., Stuut, J.-B., Marchant, M., Fietzke, J., Mienis, F., Hebbeln, D., 2010. Glacial cold-water coral growth in the Gulf of Cádiz: Implications of increased palaeo-productivity. Earth and Planetary Science Letters 298, 405-416.

Wienberg, C., Hebbeln, D., Fink, H.G., Mienis, F., Dorschel, B., Vertino, A., Correa, M.L., Freiwald, A., 2009. Scleractinian cold-water corals in the Gulf of Cádiz—First clues about their spatial and temporal distribution. Deep Sea Research Part I: Oceanographic Research Papers 56, 1873-1893.

Wienberg, C., Titschack, J., 2016. Framework-Forming Scleractinian Cold-Water Corals Through Space and Time: A Late Quaternary North Atlantic Perspective, in: Rossi, S., Bramanti, L., Gori, A., Orejas, C. (Eds.), Marine Animal Forests: The ecology of Benthic Biodiversity Hotspots. Springer International Publishing Switzerland.

Chapter 5

Sedimentation pattern & Oceanography

Chapter 5 – El Arraiche sedimentation pattern and Oceanography

This chapter is based on:

Abstract

The completion of IODP expedition 339 within the Cádiz contourite depositional system, along the southern Iberian margin (which was created and maintained by the Mediterranean Outflow Water) has brought increased amounts of attention to this natural contourite laboratory. In contrast, a lot less attention is given to the southern Gulf of Cádiz despite the ubiquitous presence of tectonic ridges, small contourite deposits, mud volcanoes and coral mounds. The El Arraiche Mud Volcano province (EAMVP) is located in the southern Gulf of Cádiz and is characterized by an extensional regime, creating two tectonic ridges named Renard and Vernadsky. Also, nine mud volcanoes and numerous coral mounds are present in this area.

The northward flowing bottom currents are deflected by the topographic obstacles and flow in a westward direction at the foot of the NW-SE-oriented Renard Ridge. Calculations indicate that this bottom current is capable of turning around the tip of the Renard Ridge and continue its path along its northern edge. The locations of the contourite deposits at the foot of the Renard Ridge are controlled by the steepness of the ridge: slopes of more than 12° are associated to contourite deposits, while less steep ones merely show hemipelagic deposits. The moats around the mud volcanoes originate due to a combination of subsidence and the action of bottom currents, as the seismic data show separated mounded drift deposits perpendicular to the moats as well as subsidence rims. Some mud volcanoes have a less incised northern and a deeper southern moat, which indicates eastward flowing bottom currents. This orientation is consistent with the shoreward component of the internal tides, which flow vigorously in this area with peaks of speed over 30 cm/s. The integration of geophysical and hydrographic datasets in the EAMVP sheds new light on the dynamic nature of the interaction of bottom currents and topographic features.

Author contributions: The acquisition of the 2013 seismic data was performed (amongst others) by TVD, DVR, IM and MG. DH delivered the multibeam data south of the EAMVP. The seismic data were processed and interpreted by TVD. The oceanographic data were processed by TVD, Carlos Borges (IH Lisbon) and IM and interpreted by TVD. The paper was written by TVD and revised by DVR, JV, IM, DH and MG.

1. Introduction

As outlined in the previous chapter, the EAMVP contains several genetically linked contourite drifts, but the geophysical dataset (Figure 5.1) covers a wide variety of geological features: contourite drifts, mud volcanoes, coral mounds and tectonic features. The dense network of seismic profiles and the accompanying multibeam dataset does not only allow studying the seismic stratigraphy of the various drifts, but also their position and present expression. In this chapter, the causal properties for the development of the small-scale topography-controlled drifts and their relation with the current oceanographic setting will be investigated. The latter will be conducted by adding several current and water property measurements. The controlling factors of the El Arraiche drift systems may shed new insights on similar drifts worldwide.

2. Material and methods

The multibeam data consist of three datasets: the SWIM compilation dataset (Zitellini et al., 2009), a dataset recorded during the 2001 "CADIPOR" campaign on board of R/V Belgica and one recorded during the 64PE284 campaign on board of R/V Pelagia in 2008. The CADIPOR data were obtained using the SIMRAD EM1002 system, equipped with a deep water module. The swath width was 500 m above 500 m water depth and 750 m below. Kongsberg's Merlin and Neptune packages have been used to clean and correct the data. The 64PE284 dataset was acquired using a Kongsberg EM300 (31.5 kHz) system. The sweep-angle from port to starboard was maximum 2x65 degrees, with sometimes a restriction to 2x55 degrees. The obtained grid has a cell size of 15 by 15 m and no post-processing was performed onboard. Both datasets were combined on top of the SWIM multibeam compilation dataset (Figure 5.2).
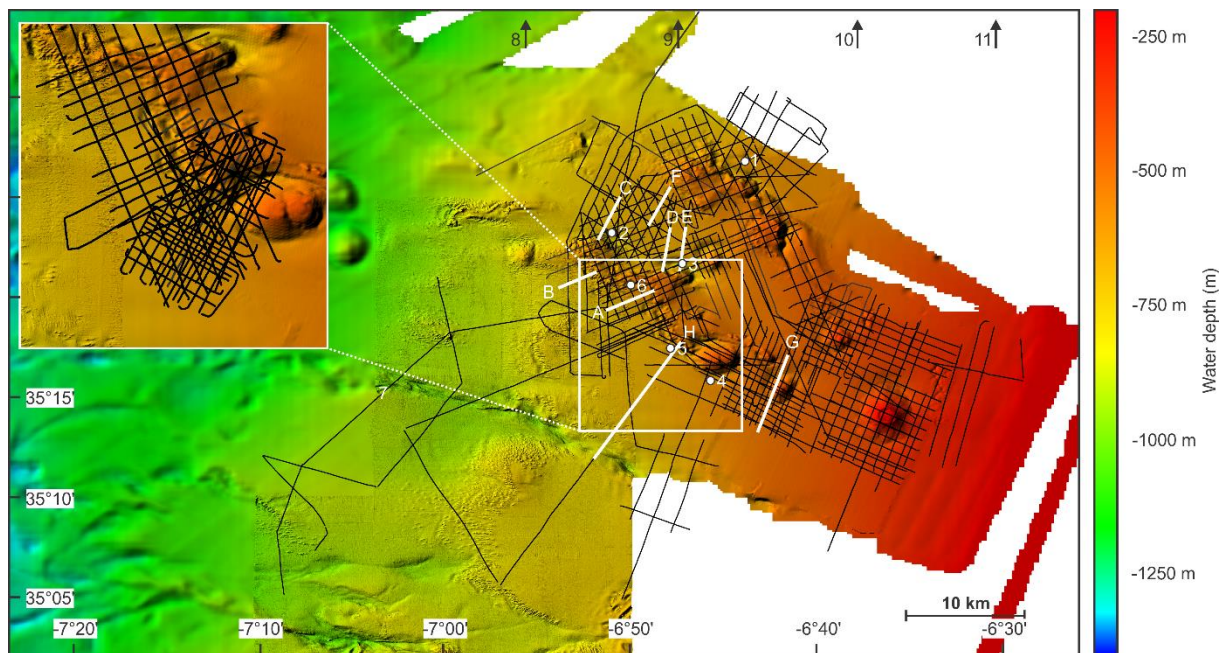
Figure 5.1: Overview of the seismic dataset. The inset shows the 2009 "Pen Duick" campaign data. Multibeam background data include the GEBCO and SWIM (Zitellini et al., 2009) datasets. The described profiles of Figure 5.3 are indicated in white and the CTD/LADCP stations are indicated by white circles. Stations 8, 9, 10 and 11 are located at 35°39'N.

The seismic data include over 1500 km of high-resolution single channel sparker reflection seismic profiles that were acquired between 2001 and 2013 during the CADIPOR, Pen Duick and COMIC campaigns on board of R/V Belgica (Figure 5.1). The characteristics of the SIG sparker, used during these campaigns, varied from year to year. The amount of electrodes changed from 80 (2001) over 100

(2013) to 120 (2005, 2007 and 2009). The shot interval was mostly 2 s (2001, 2005, 2007 and partly in 2013), while 1 s (shallow profiles in 2013) and 3 s (2009) also occur. The energy was always 500 J and sampling frequency 8 kHz, except in 2013 when it was 10 kHz. The record length varied between 1.6 s and 2.5 s, depending on the water depth and shot interval. Sailing speeds were always maintained between 3 and 4 knots.

The seismic data were processed using the DECO geophysical processing software RadexPro. All profiles underwent bandpass filtering (Butterworth, 200 Hz and 24dB/s to 1500 Hz and 36 dB/s), a swell filter, a 2D spike removal (burst noise removal) and an amplitude correction (spherical divergence correction).

The LADCP data were acquired during the R/V Belgica COMIC cruise (2013; Figure 5.1). The system consisted of a 300 kHz broadband Teledyne RDI ADCP from Instituto Hidrográfico (Portuguese Hydrographic Office – IH) and was installed in a downward looking configuration on the R/V Belgica CTD frame. The system was set up with 45 cells of each 5 m cell size, an ensemble interval of 2 s and 3 pings per ensemble. This enabled a maximum reach of 91 m, a blank distance of 1.76 m and a standard deviation of 1.64 cm/s. Processing of the LADCP data was performed using Lamont-Doherty East Observatory Matlab scripts (Thurnherr, 2005). No vessel mounted ADCP data from R/V Belgica was used to constrain the LADCP data. Calibration was performed based on the bottom detection method. The first 3 profiles were calibrated with the available CTD data, the remaining 8 (4-11) were not calibrated due to the high amount of spikes in the CTD data. These CTD data were acquired using a SeaBird SBE 9 plus probe with a temperature, pressure, conductivity and dissolved oxygen sensor.

In order to identify the water masses that comprise the EAMVP, the nutrient content of the water column was obtained. This dataset was compiled during the "IHPT2009-HERM02" cruise on board of the NRP Almirante Gago Coutinho, conducted by IH in the framework of the HERMIONE (E7) program. The water samples were vacuum filtered onboard using polycarbonate filters of 0.45 μm and kept frozen (below -20°C) until analyzed. The nutrient concentrations were determined using a Skalar SANplus Segmented Flow Auto Analyzer. NO_x was determined according to the Strickland and Parsons (1972) method and PO_4 according to the Murphy and Riley (1962) method. The limits of detection are 0.17 for NO_x, 0.33 for NH_3, 0.067 for PO_4 and 0.1 for SiO_2.

3. Results

The contourite deposits were classified based on their geometry (mounded, elongated, sheeted or plastered) and their acoustic character (transparent or not, layered vs chaotic, high vs low amplitude and continuity of the reflections). The criteria for recognition have been summarized recently by Rebesco et al. (2014). Sheeted drift deposits are characterized by continuous, low to high amplitude slightly mounded reflectors in absence of a clear moat. The sheeted drift deposits have been discussed by Vandorpe et al. (2014) and only occur in the Pen Duick drift where they are heavily affected by the uplift of the escarpment. The mounded drift deposits are accompanied by a well-defined moat and are usually characterized by mounded, continuous and high-amplitude reflectors (Figure 5.3b, c, d, f and h). Except for the Pen Duick drift, all mounded drift deposits are present on top of (hemi-) pelagites and can be distinguished by the presence of a moat. (Hemi-) pelagic deposits are characterized by continuous, nearly horizontal, low to medium amplitude deposits which may be affected by the uplift of the ridges (Figure 5.3a). Depths have been converted from seconds two-way-travel time to meters by using a constant velocity of 1500 m/s and are displayed in Figure 5.3.
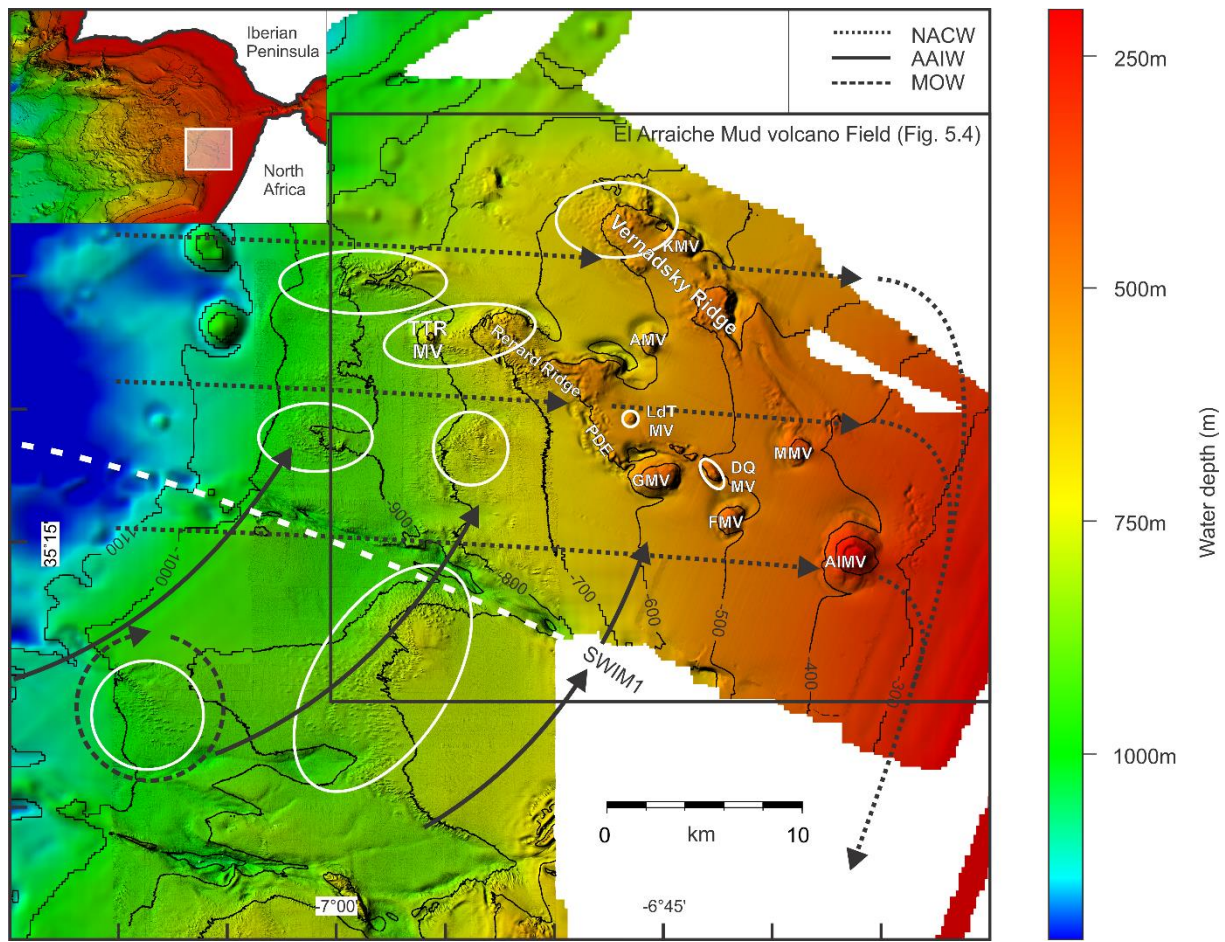
Figure 5.2: Multibeam map of the broader research area in the southern Gulf of Cádiz with contour lines every 100 m. All of the topographic obstacles are named on the map: the Vernadsky and Renard tectonic ridges and all of the mud volcanoes. Coral mound fields are indicated by the white ovals. The general direction of the currents and their water masses has been indicated based on Criado-Aldeanueva et al. (2006), Machín et al. (2006), Ambar et al. (2008) and Louarn and Morin (2011). The black box indicates the area characterized in Figure 5.4. NACW = North Atlantic Central Water, AAIW = Antarctic Intermediate Water, MOW = Mediterranean Outflow Water, AIMV = Al Idrissi mud volcano, AMV = Adamastor mud volcano, DQMV = Don Quijote mud volcano, FMV = Fiúza mud volcano, GMV = Gemini mud volcano, KMV = Kidd mud volcano, LdTMV = Lazarillo de Tormes mud volcano. The SWIM compilation dataset (Zitellini et al., 2009) has been used as a background.

3.1. Morpho-sedimentary characterization

3.1.1. Depositional features

The morpho-sedimentary map (Figure 5.4) was created based on the multibeam (Figure 5.2) and seismic datasets (Figure 5.3). They show two tectonic ridges with an acoustically nearly transparent facies (Figure 5.3a, b, c, d, e and f). Seven smaller isolated bedrock outcrops are also observed between the Lazarillo de Tormes and Don Quijote mud volcanoes and to the west of the Renard Ridge. Many coral mounds can be observed both on top and at the foot of these bedrock outcrops. They can be over 200 m in diameter and up to 15 m high (Figure 5.3b). Their seismic facies is mostly acoustically transparent and weak layering can be observed in the subsurface. They have a distinct broad conical shape and are characterized by the presence of many diffraction hyperbola (Figure 5.3b). Apart from the surfacing coral mounds, many subsurface mounds can be recognized as well (Figure 5.3b & f). They are also acoustically transparent and can reach up to a height of 150 m.

The mud volcanoes in this area have been described in detail by Van Rensbergen et al. (2005). They are between 25 and 255 m high and between 800 m and 6 km wide. The smallest one is Don Quijote and the largest one Al Idrissi mud volcano.

The mud volcanoes are completely acoustically transparent. Along their edges depressions are observed and a Christmas-tree structure is created in the neighboring sediments (Figure 5.3g). The biggest mud volcano, Al Idrissi has a depositional tail on its eastern side: sediment has accumulated up to 25 m high. Also Fiuza mud volcano has a (less pronounced) depositional tail of 5-10 m (Figure 5.2).

The seismic data indicate the presence of several mounded deposits rising up to 10 m above the surrounding seafloor (Figure 5.3b, c, f & g). They are characterized as mounded drift deposits, laterally associated to deep moats (>10 m) along the topographic obstacles. The contourite deposits have been named Pen Duick drift, Renard South drift, Renard North drift and Vernadsky South drift (Figure 5.4). The Pen Duick drift contains about 150 m of mounded drift deposits below which sheeted drift deposits occur (Vandorpe et al., 2014). On average, the present-day moat is about 10 to 15 m deep and the mounded part of the drift rises 5 to 8 m above the surrounding seafloor (Vandorpe et al. 2014). The moat is the longest one present in the EAMVP: about 5 km. The Renard South drift is relatively small and contains 100-150 m of slightly mounded drift deposits on top of hemipelagic sediments (Figure 5.3b). The moat is 1 to 1.5 km long, about 20 m deep and the mounded part rises about 10 m above the surrounding seafloor. The Renard North drift is composed of 130 m of mounded drift deposits (Figure 5.3c). The drift has a 50 to 75 m deep, 750 m wide moat of about 3 km length. A gentle transition into hemipelagic deposits occurs to the west. A small patch drift is observed within a deep incision (about 100 m) between the Renard Ridge and the Adamastor mud volcano. This patch is about 500 m wide and 15 m high (Figure 5.3e). Slightly northward dipping reflectors are deposited on top of horizontal ones in this patch (inset Figure 5.3e). The Vernadsky South drift is composed of 70 m of moun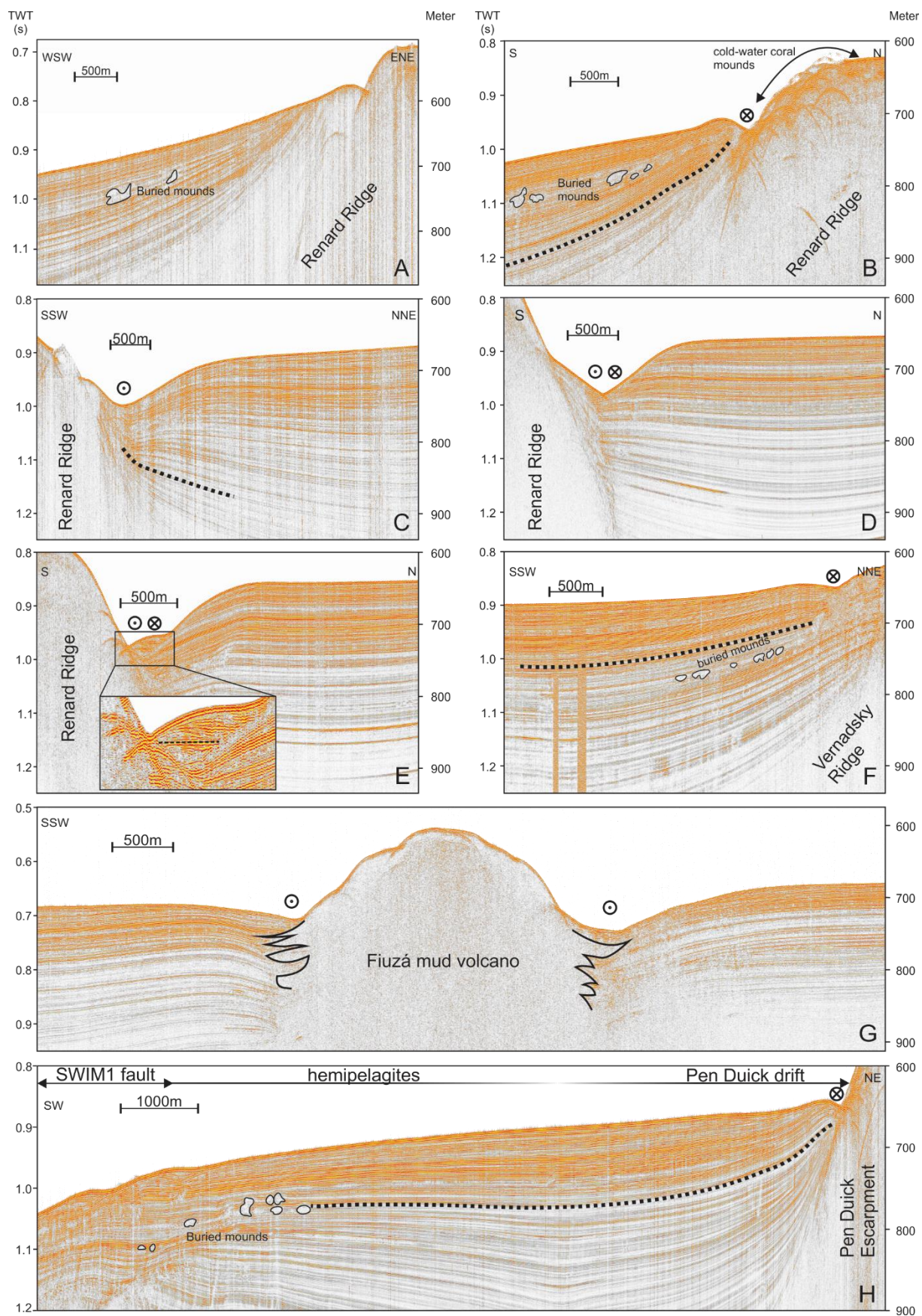ded drift deposits (Figure 5.3f). The associated moat is about 2.5 km in length and only 5 m deep. Along the Kidd, Fiuza, Mercator and Al Idrissi mud volcanoes, several mounded drift deposits are present. For Fiuza and Al Idrissi, both at their northern and southern edges drift deposits are present (Figure 5.3g). These drift deposits can be up to 115 m (e.g. Fiuza mud volcano, Figure 5.3g).

The lateral transition between contouritic (Figure 5.3b, c, d, e and f) and non-contouritic (Figure 5.3a) deposits can be very abrupt: within a few 100 m, the geometry of the sediment can change. Perpendicular to the channel, the transition is more gradual and contourite deposits progressively pass into hemipelagic sediments (Figure 5.3h). Away from ridges, mud volcanoes, contourite drifts or coral mounds, only hemipelagic sediments occur. Along the Renard and Vernadsky Ridge sediments pinch out towards them (Figure 5.3a, b & f).

Figure 5.3: Seismic profiles of the EAMVP with scales both in TWT (s) and m based on a conversion of 1500m/s. Dashed black lines indicate the boundary between mounded drifts and underlying deposits. a: profile perpendicular to the Renard Ridge with uplifted hemipelagic deposits. b. Profile perpendicular to the Renard South drift with a 20 m deep moat and both surfacing and buried coral mounds. c. Profile perpendicular to the Renard North drift with a wide, deep moat. d. Profile perpendicular to the Renard Ridge showing a very erosive channel in horizontal hemipelagic deposits. e. Profile 500 m east of profile D showing the same erosive channel. Here, a small patch-like drift is observed in the channel (see inset). f. profile perpendicular to the Vernadsky Ridge displaying the Vernadsky South drift. A small moat is present and several buried mounds occur in the subsurface. g. Profile across the Fiúza Mud Volcano with a deeper southern and a less deep northern moat. On both sides of the mud volcano, a Christmas-tree structure can be observed. h. Profile perpendicular to the Pen Duick escarpment giving a broader overview of the Pen Duick drift and research area. The transition between drift and hemipelagic deposits perpendicular to the Pen Duick Escarpment is indicated by the vanishing lines. The southwestern end of the profile shows the northeastern end of the SWIM1 fault.

3.1.2. Erosive features

Moats are associated with all the ridges and mud volcanoes in the study area and most of them are accompanied by contourite drift deposits (Figure 5.4). The moats along the ridges are aligned in a general NW-SE orientation, are between 1 and 5 km long, have a U-shaped profile and their depths vary between 5 and 20 m (Figure 5.3b, c, e, f and h). Moat-like incisions are observed at the base of the mud volcanoes as well (Figure 5.3g). Except for the moat along the Adamastor mud volcano, all are aligned in a NW-SE or WNW-ESE direction. The Al Idrissi, Fiuza (Figure 5.3g) and Gemini mud volcanoes have two incisions: one to the northeast and one to the southwest, although the southwestern incision along the GMV becomes a part of the Pen Duick drift system (Figure 5.4). The length of these features varies between 2 and 5 km and the depth between 20 and 80 m, with a modus of about 30 m. The moat between the Renard Ridge and the Adamastor mud volcano (Figure 5.4) is different compared to the previous ones. The western part of this moat (Figure 5.3d) cuts deeply into the underlying horizontal hemipelagic sediments, while the eastern part cuts into dipping reflectors and contains the small patch drift described in 3.1.1 (Figure 5.3e).
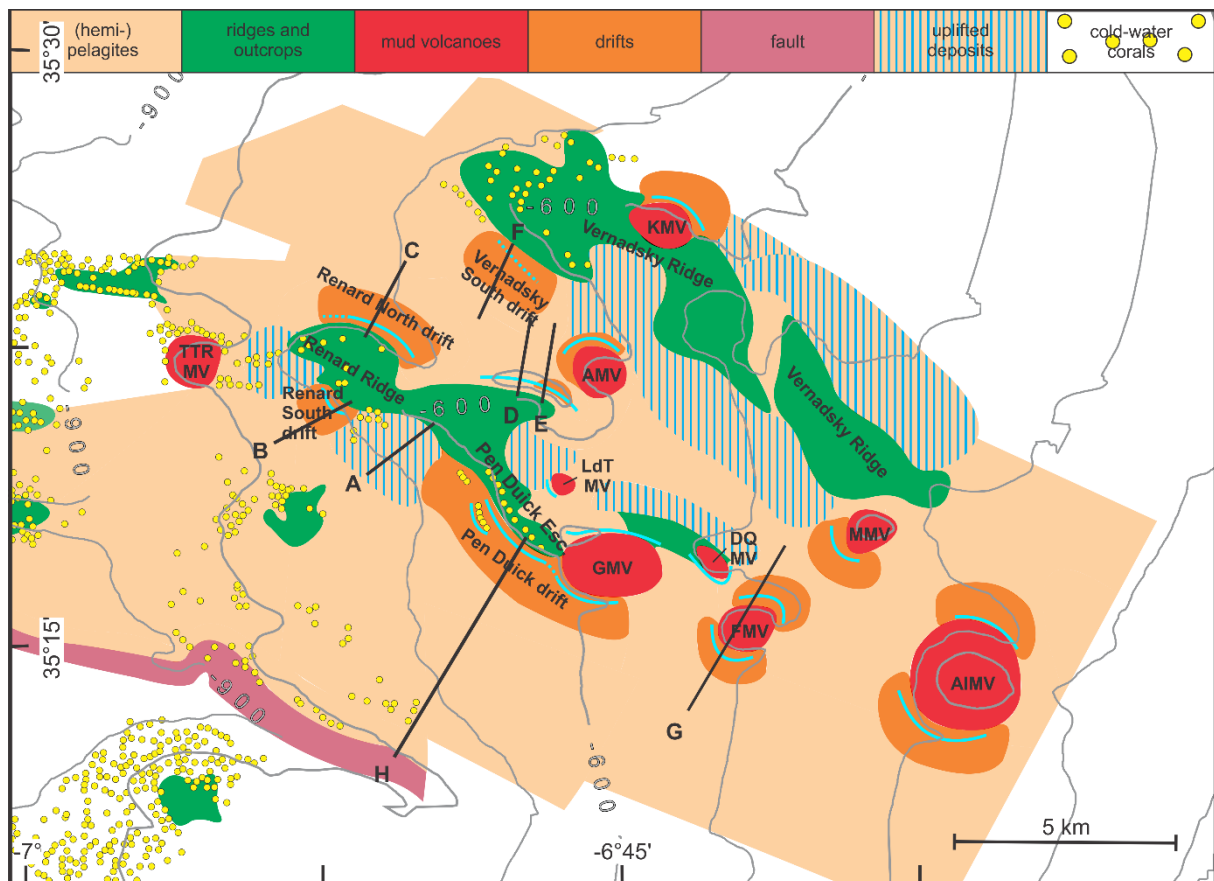
Figure 5.4: Morpho-sedimentary map of the EAMVP based on both the multibeam and seismic data. The position of the seismic profiles, displayed in Figure 5.1 and Figure 5.3, have been indicated by the white lines. All moats are displayed by a light blue line. DQ MV = Don Quijote Mud Volcano, LdT MV = Lazarillo de Tormes Mud Volcano, GMV = Gemini Mud Volcano, FMV = Fiuza Mud Volcano, MMV = Mercator Mud Volcano, KMV = Kidd Mud Volcano, AIMV = Al Idrissi Mud Volcano.

3.2. Slope gradients

The mud volcanoes have an average steepness of 8 - 10° (e.g. Gemini, dark blue colours in Figure 5.5), while the PDE displays a general higher steepness exceeding 12° and with maximum values along the eastern part of the PDE (up to 25°). The part of the Renard Ridge in between the Pen Duick drift and the Renard South drift rarely exceeds values of 7°, whereas the part along the Renard South drift has

slopes of about 15°. The northern part of the Renard Ridge, along the Renard North drift, has in general much higher slopes with average values of 20° (Figure 5.5). Between the Renard North drift and the patch drift, slopes are particularly high, averaging more than 15° and reaching more than 20° in several parts. The Vernadsky Ridge is generally less steep then the Renard Ridge with maximum values of about 17° and average values of 10-12°. Two regions display steeper slopes: the northern part, just west of Kidd mud volcano and the eastern part of the Vernadsky Ridge. Along the Vernadsky South drift, values of 10 -12° are observed (Figure 5.5).
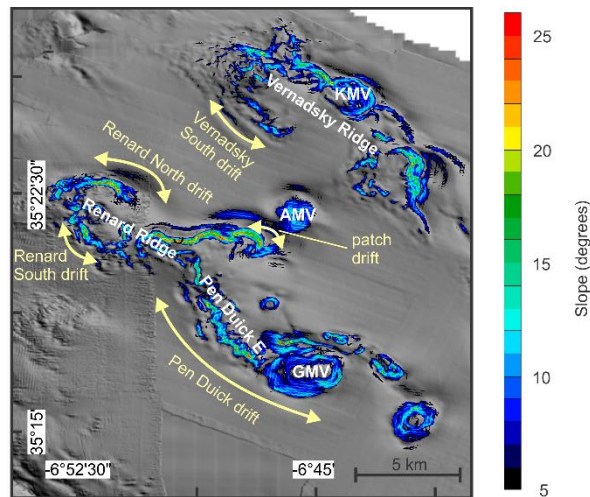
Figure 5.5: Steepness of the topographic features in the EAMVP plotted on the multibeam base map. The position of the drifts are plotted on the map. AMV = Adamastor mud volcano, GMV = Gemini mud volcano and KMV = Kidd mud volcano.

3.3. Current intensities and directions

From the surface down to about 500 m water depth, overall northward currents with speeds mostly exceeding 10 cm/s and peaks up to 15 cm/s are observed (Figure 5.6a at 300 m water depth). In terms of orientation, exceptions occur at the two easternmost stations (10 and 11) and in station 3 where a southward current is present at this depth range. Variations on these general patterns are present, but most deviating currents are very weak (Figure 5.6a & b). From about 500 m water depth, more variable and slower (2 - 8 cm/s) currents are observed (Figure 5.6c at 600 m water depth). An assessment of the deeper (>800 m water depth) currents is not possible due to the limited amount of stations at or below this depth (only stations 8 and 9). Bottom currents in the EAMVP are variable as well (Figure 5.6d). Four out of six stations show bottom current directions along the topographies. Only stations 3 and 6 deviate from this pattern, although they display significantly weaker bottom currents (<3 cm/s).

3.4. Nutrient data of bottom water masses

Bottom water Si concentrations in the EAMVP range between 0 and >20 µmol/L (Figure 5.7a). The lowest values occur close to the African continent (purple colours). From about 500 m water depth, the values increase. Between 500 and 1000 m water depth, the Si-values increase to 12 µmol/L. The highest values occur below 1500 m water depth, with peaks over 20 µmol/L. Two stations around 1400 m water depth indicate anomalous lower values of about 10 µmol/L (Figure 5.7a).

The bottom water PO_4 concentrations (Figure 5.7b) show a more or less similar trend to the Si data: low values along the African continent and high values in deeper water settings. The difference is that the highest values (up to 1.45 µmol/L) also occur close to the EAMVP at depths of 900-1000 m. A general increase from the lowest PO_4 data to these high values at 1000 m is observed across the EAMVP. At greater water depths, values between 1.1 and 1.4 µmol/L are observed.

Bottom water NO_x concentrations (Figure 5.7c) display a similar trend as the Si and PO_4 data: very low values close to the African continent (between 0 and 10 µmol/L) and very high values (>20 µmol/L) at greater water depths. Also here, a high anomaly of NO_x content is observed between 700 and 1000 m water depth (19 - 22 µmol/L), with lower values to the east (<15 µmol/L) and west (17 - 19 µmol/L). The anomaly observed in the Si data can also be observed in the NO_x data: around 1400 m water depth a value of 16 µmol/L is present.
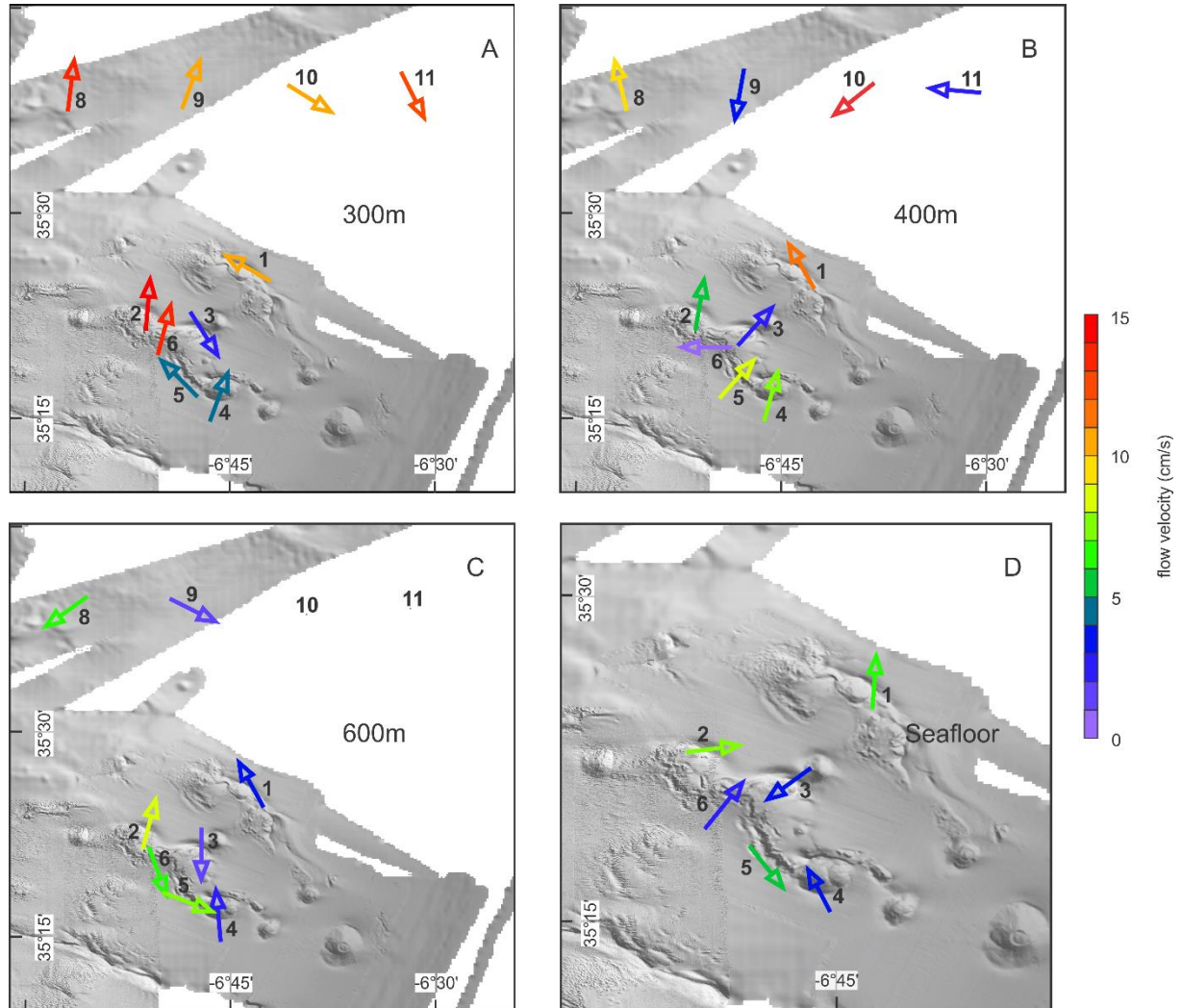
Figure 5.6: Currents in the EAMVP, measured at 300 m depth (A), 400 m (B), 600 m (C) and at the seafloor (D) by a LADCP and plotted on top of the multibeam map. Colours of the arrows correspond to average flow velocities, which range between 1 and 15 cm/s. The numbers indicate the different stations.

4. Discussion

4.1. Water masses in the EAMVP

The AAIW in the Gulf of Cádiz is described as a low-salinity, low-O_2 and nutrient-enriched water mass (Tsuchiya et al., 1992). Louarn and Morin (2011) indicated that modified Antarctic Waters in the southern Gulf of Cádiz typically have a Si-content between 10.9 and 11.9 µmol/L. These Si-values indeed occur at the outer edges of the EAMVP, around 900 m water depth (Figure 5.7). Machín et al. (2006) pointed out that NACW in the Canary Basin has Si-values of 0 - 10 µmol/L.
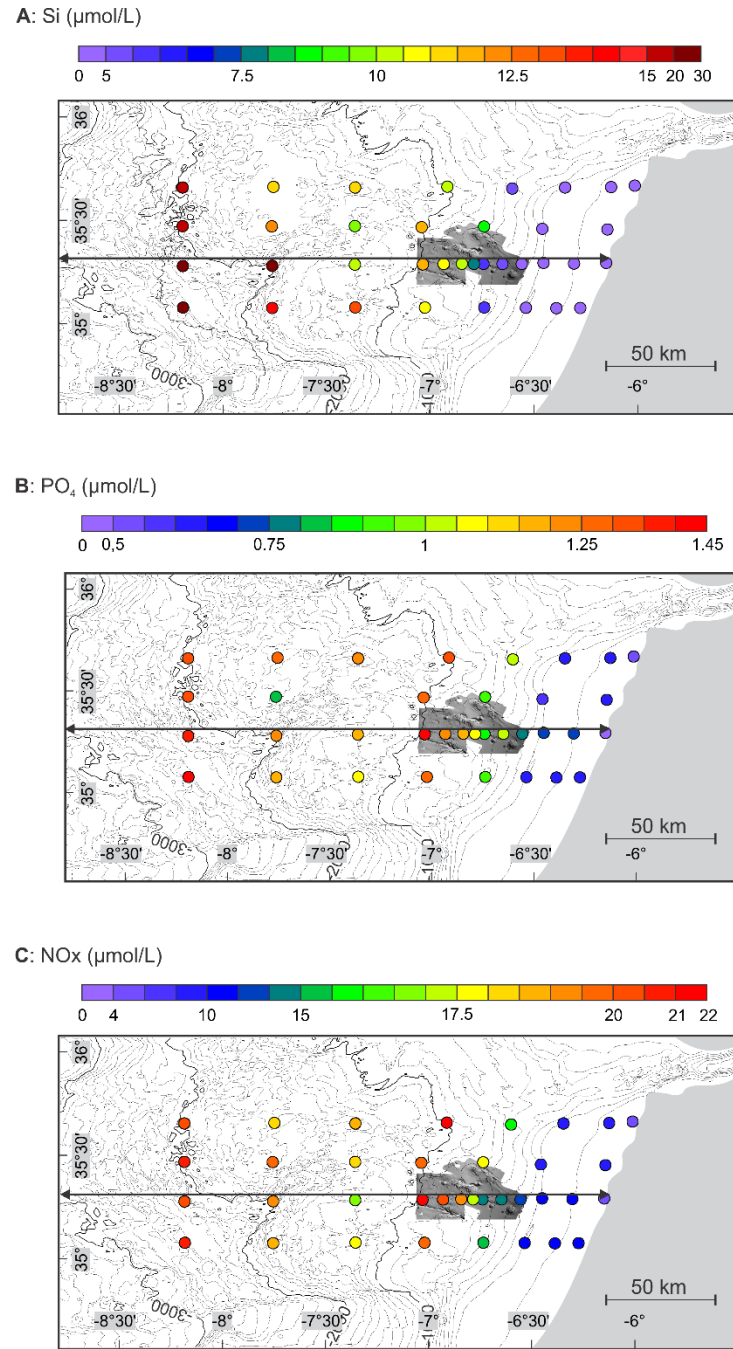
Figure 5.7: Nutrient content (Si, PO$_4$ and NO$_x$) of the bottom water mass in the EAMVP: all displayed measurements show nutrient contents of the water mass just on top of the seafloor. Depth contours every 100 m and annotated every 1000 m are indicated. The EAMVP is indicated in grey (multibeam image). The black line in the middle of each map indicates the position of the transect in Figure 5.8.

Due to the proximity of the Canary basin to the EAMVP, the same values can be used to infer the presence of NACW, which is between 0 and 600 m water depth. Below 2000 m, NADW is present with a Si-content above 15 µmol/L (Cabecadas et al., 2002; Machín et al., 2006). According to Cabecadas et al. (2002), NACW has PO$_4$ values between 0.7 and 1 µmol/L and NADW between 1 and 1.5 µmol/L. These PO$_4$ values are observed between 200 and 500 m water depth and below 1800 m water depth, respectively (Figure 5.7b). Also, the AAIW values range between 1.1 and 1.5 µmol/L, which are observed between 700 and 1300 m. NO$_x$ (Figure 5.7c) values indicate a nutrient-rich water mass between 700 and 1000 m water depth (Figure 5.7c), which is consistent with the presence of AAIW.

Mediterranean waters have PO_4 values between 0.39 and 0.7 µmol/L (with spikes up to 1.2 µmol/L) and Si-values between 10 and 15 µmol/L in the northern Gulf of Cádiz (Cabecadas et al., 2002). The nutrient data in the EAMVP also show very low values for PO_4 and Si, namely between 1200 and 1700 m water depth. These concentrations are not as low as those for pure MOW, but are remarkably lower than the surrounding values (those for NACW and AAIW). The same trend is observed for the NO_x data, lower values (Figure 5.7c) are observed around 1300 m water depth (Figure 5.7c). All of these low values are probably associated to Mediterranean waters and might indicate the position of a Mediterranean eddy (Ambar et al., 2008). Mixing with under- and overlying water masses may have caused the slightly higher nutrient concentrations values compared to unaltered MOW (Louarn and Morin, 2011). The depth of the Mediterranean waters in this region implies that they play no direct role in the drift systems in the El Arraiche area.

When combining all the nutrient datasets (Figure 5.8), NACW is present between 200 and about 550 m water depth, a mixing zone between NACW and AAIW could be present between 550 and 700 m and the AAIW itself between 700 and 1300 m. Meddies occur around 1300 m and below 1500 m, NADW is the prevailing water mass. These new data imply that the drift systems in the El Arraiche area are not only affected by the (modified) AAIW as already stated by Vandorpe et al. (2014), but also by the NACW (Figure 5.8).
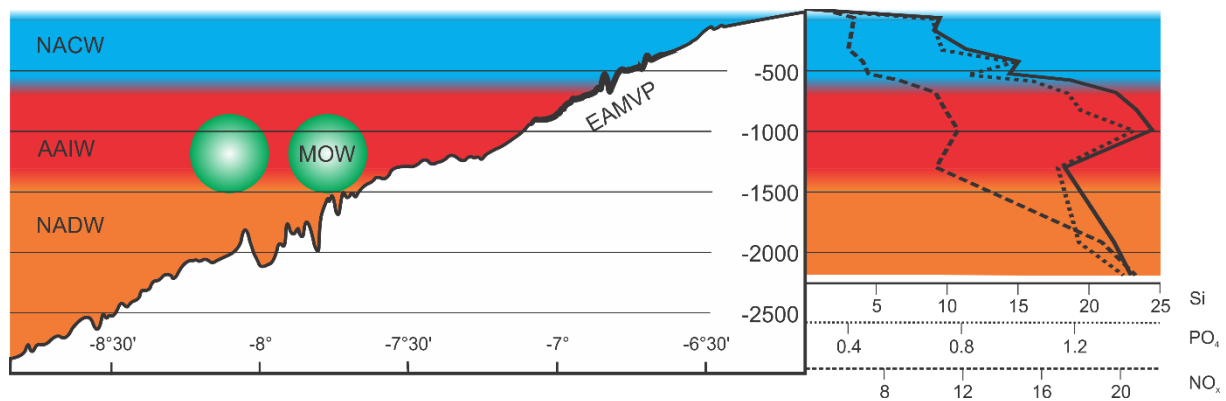
Figure 5.8: Transect along 35°20'N (see Figure 5.7 for positioning) with indication of the different water masses. The nutrient concentrations of the bottom water masses along this transect are plotted on the right and delineate the water masses. NACW is characterized by a gentle increase in nutrient concentrations, AAIW by moderate to high concentrations, MOW by low to moderate concentrations and NADW by very high concentrations. The position of the EAMVP is indicated by the thick black line on the transect. NACW: North Atlantic Central Water, AAIW: Antarctic Intermediate Water, MOW: Mediterranean Outflow Water and NADW: North Atlantic Deep Water.

4.2. Currents in the EAMVP

The LADCP data indicate that in the upper 500 m of the water column, an overall northward current is present (Figure 5.6a and b). Velocities of this current range between 2 and 15 cm/s, with the highest velocities at 200 to 300 m water depth. This is consistent with an observed northward flow at 3 mooring sites in the region (Martins and Vitorino, 2012). Some of the stations deviate from this general pattern, most likely due to the daily, weekly, monthly and annual variations present in this area (Martins and Vitorino, 2012; Mienis et al., 2012). These variations are not registered by the LADCP data, which show merely a snapshot of the hydrography. Closer to the Moroccan margin, a general southward current is observed (stations 10 and 11 in Figure 5.6a and b) and this may be the expression of the southward flow of the Azores current that enters the Gulf of Cádiz in the northwest and interacts with the upwelling waters (Martins and Vitorino, 2012).

From about 600 m water depth (Figure 5.6c), the incoherent current pattern reflects their interaction with the upper reaches of the Renard and Vernadsky Ridge. Near the El Arraiche seafloor, most of the currents are directed parallel to the topography (Figure 5.6d). This orientation is consistent with the bottom currents being deflected by (and following) the regional topography (Figure 5.9).

Internal tides up to 100 m high are reported on the GMV and both on top and at the foot of the PDE at depths of 420, 500 and 640 m by Mienis et al. (2012). In places, they result in current peaks over 30 cm/s. Their presence could be indicated by variations in temperature, salinity and current speeds (Mienis et al., 2012). Martins and Vitorino (2012) used current-meter time series to observe current variabilities dominated by semidiurnal tides (periods of 12 hours and 25 minutes) from 100 m down to at least 500 m south of, within and north of the EAMVP. All of them had roughly an east-west orientation. The basinward (westward) component of the internal tides can thus reinforce the deflected northward current consisting of a mixture of NACW and AAIW (Figure 5.9). This would create stronger bottom currents along the upper regions of the Renard Ridge. On the contrary, the shoreward (eastward) component of the internal tides has the capability to counter the westward bottom current (which follows the regional topography) and maybe even reverse it. LADCP station 5 (640 m water depth at the outer limit of the observed internal tidal waves) does indicate a 5 - 6 cm/s strong current flowing in a southeastward direction (Figure 5.6d). This may be an expression of the influence of the shoreward component of the internal tides. Longer observations are needed though to reveal these internal tides and distinguish them from the long-term bottom currents in this region. Station 6 (Figure 5.6d) is not associated to a contourite drift and shows a weak northeastward current. The small depth difference between the top of the PDE and the base at this point may cause the current to overcome the topography and continue its path (Figure 5.9). The deflected current coming from the Pen Duick drift may also be partly entrained by this flow direction.

4.3. Sedimentary features and bottom currents

4.3.1.Moats and mud volcanoes

Moats are present at the bases of all the mud volcanoes. Their shapes vary greatly, ranging from semi-circular (Fiuza) to nearly straight (Kidd). Camerlenghi et al. (1995) related moats around mud volcanoes to subsiding rims due to degassing and sediment removal. However, the seismic profiles show a clear contouritic expression within the sedimentary sequence perpendicular to the moats (Figure 5.3g). This points towards a bottom current influence, also observed by Somoza et al. (2002) in the Gulf of Cádiz. A combination of both processes, involving deepening of the subsiding rims by the action of bottom currents is most likely here, as suggested by Van Rensbergen et al. (2005). These bottom currents may result from two processes: the south to north directed northward flow of the NACW and AAIW, observed by the LADCP data (Figure 5.6a and b) or the east-west directed internal tides, reported by Martins and Vitorino (2012). Internal tidal currents are known to be able to transport sediment, as modeled by Ribbe and Holloway (2001). As all LADCP profiles are acquired below 600 m water depth in the EAMVP, the exact directions of the bottom currents in the moats of Al Idrissi, Fiuzá, Mercator and Don Quijote mud volcanoes are not known.

The Al Idrissi mud volcano has two northwest-southeast directed moats (northeast and southwest of the mud volcano) and a depositional tail on the eastern side of the volcano. Fiuza mud volcano follows almost the same trend, although there the moat is nearly circular and the tail much less pronounced (Figure 5.2). For both volcanoes, the northern moat is much deeper compared to the southern (e.g. Figure 5.3g). At the Don Quijote mud volcano, the northern moat is nearly absent, while the southern one is very prominent (Figure 5.4). A west-to-east current is inferred to be responsible for this asymmetry, since more pronounced erosion can be expected on the left side of an obstacle due to lateral asymmetry in the flow process in the northern hemisphere (Taylor, 1990; Hernández-Molina et

al., 2006). The depositional tails on the eastern sides of Al Idrissi and Fiúza mud volcano strengthen this hypothesis. The Mercator mud volcano shows a deeper southern moat and the tail is nearly absent (Figure 5.2). A more prominent subsidence on the southern side of the volcano or a dominance of east-to-west directed currents in their proximity might explain this asymmetry. Also the influence that both the Renard Ridge and Vernadsky Ridge can have on the local circulation pattern (by deflection) may contribute to the deviating sedimentological patterns. This influence might also be evidenced by the Adamastor mud volcano where the southern moat is extended and might be the result of the narrow passage between the mud volcano and the Renard Ridge. This might have caused intensified bottom currents and as a result the highly erosional channel along this part of the Renard Ridge. The Lazarillo de Tormes mud volcano has a diameter of less than 1 km and is too small to clearly differentiate a northern and southern moat.
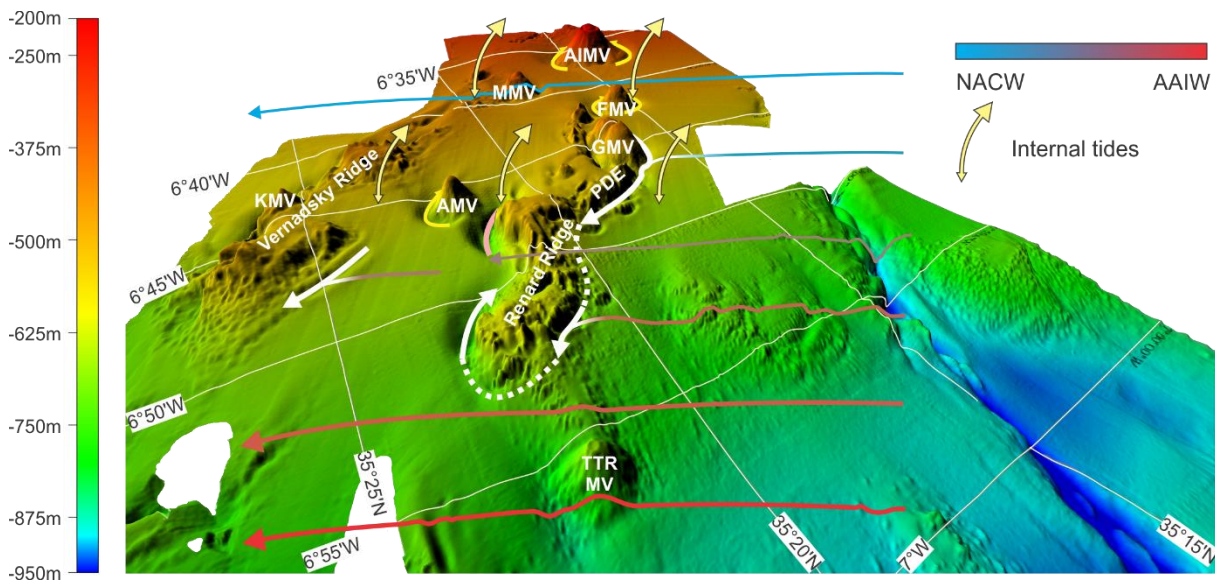
Figure 5.9: Overview of the bottom currents in the EAMVP. The northward flowing currents consist of both NACW (blue arrows) and AAIW (red arrows). Transitional colours represent mixing of the two water masses and is present in the middle of the region. Deflection of the northward currents occurs at the Renard Ridge and Vernadsky Ridge, after which the current follows the topography (white arrows). The dashed white parts are the assumed pathways, while the full lines are derived from seismic and multibeam data (Figures 5.1, 5.2 and 5.3) and are a part of a sediment drift. Light yellow colours indicate the east-west direction of the internal tides with a dominance of the eastward component. Yellow arrows indicate the flows generated by deflection of these tidal currents around the mud volcanoes. The flow of the tidal currents between Adamastor mud volcano and Renard Ridge results in a erosive channel between the two features (pink line). PDE = Pen Duick Escarpment, MMV = Mercator Mud Volcano, AMV = Adamastor Mud Volcano, AIMV = Al Idrissi Mud Volcano, FMV = Fiuzá Mud Volcano, GMV = Gemini Mud Volcano, TTR MV = TTR Mud Volcano.

In general, the moats around the mud volcanoes point towards a west-to-east directed bottom current, which is consistent with the shoreward component of the internal tides (Figure 5.9). This would imply that the shoreward component is stronger than the basinward component and the internal tides are spatially asymmetric. Spatial and temporal asymmetric internal tides have already been reported, e.g. in the South China Sea (Xu et al., 2014) or on the northern Californian margin (McPhee-Shaw et al., 2004). Turnewitsch et al. (2013) indicated that high-frequency currents can be essential to push bottom currents beyond the threshold of non-deposition/erosion/resuspension of deep-sea sediments and may thus control sediment dynamics and sedimentological patterns. Even if the currents would not be strong enough, deflection by seamounts can increase the speed by 1-10 cm/s (Turnewitsch et al., 2013). Internal tides can even be more important than the steady long-term bottom currents and as such be recorded in the geological record (Turnewitsch et al., 2013). The EAMVP may be a region where the geological record does not only constrain the long-term bottom

current flows (like the northward flow of the NACW and AAIW, Figure 5.9), but also records the high-frequency currents, in this case internal tides. That would mean that at least in the upper parts of the EAMVP the tidal currents dominate over the northward flow of NACW and AAIW as suggested by the east-west directed moats along the mud volcanoes (Figure 5.9). If a northward flow would dominate, north-south directed moats would be expected.

4.3.2.Sediment drifts

From 100 m down to 600 m water depth, a poleward current is observed (Figure 5.6) and reported (Martins and Vitorino, 2012; Mienis et al. 2012), either containing NACW or modified AAIW (Figure 5.7). Below this depth, AAIW is flowing in the same direction (Louarn and Morin, 2011). Deflection of this current against the GMV and PDE has been invoked as the driving mechanism for the Pen Duick drift (Vandorpe et al., 2014) and is consistent with the observed moats and contourite deposits (Figure 5.4). The east-west directed internal tidal currents may also play a role in shaping at least the upper parts of the Pen Duick drift, especially as Mienis et al. (2012) reported both eastward and westward directed currents in the moat along the GMV. The basinward component may enhance the bottom current along the upper reaches of the Renard Ridge, while the shoreward component may weaken or even reverse it. Bottom currents flowing along the topography are recorded in LADCP stations 4 and 5, with station 5 possibly showing the shoreward component of the internal tides (Figure 5.6). Also here, long-term records of bottom currents can reveal the nature of the currents and indicate which process dominates. For the Renard South drift, deflection of northward bottom currents is considered to be responsible for its creation, as the drift indicates a westward flowing current.

Whether the deflected current creates sediment drifts or not can largely be explained by the slope of the topography against which the current deflects: steep slopes of the southern Renard Ridge (>11°) are associated to sediment drifts while gentle ones (<11°) are not (Figure 5.5). The steeper slopes may induce a more focused, faster and thus more erosive bottom current (Borenäs et al., 2002; Wåhlin, 2004), which in turn may lead to sediment drifts at their bases. As the slope of the bounding topographies does not change drastically below or above the drift deposits (Figure 5.3a, b, c, d, e and h), the present-day slope is a good analogue for the slope at the time of deposition.

Batteen et al. (2007) modelled the Iberian and Canary Current in the Gulf of Cádiz with a terrain-following numerical model (Princeton Ocean Model). A condition was developed that indicates the maximum radius of a cape that still allows separation from the given current.

$$R < \sqrt{\frac{U}{f * \left(\frac{\nabla h}{h}\right) - \beta}}$$

In this condition, R is the radius of the cape, U the current speed, f the coriolis parameter, $\frac{\nabla h}{h}$ the slope gradient and β a constant factor (Marshall and Tansley, 2001; Batteen et al., 2007). Although this condition was intended for the large capes in the Gulf of Cádiz, it can give an approximation on how the currents will react when encountering the ridges. In the calculations, the β factor is left out of the equation as it is significantly lower than $f * \left(\frac{\nabla h}{h}\right)$ (Batteen et al., 2007). Solving the equation for U and applying the correct parameters for the tip of the Renard Ridge (a Coriolis parameter of 0.00004, a slope gradient of 0.0002 and a diameter of 3.6 km), the maximum speed by which the bottom current still turns around Renard Ridge (and does not detach) is about 10 cm/s. As measured and reported bottom currents are usually lower than 10 cm/s (Figure 5.6d; Mienis et al., 2012), it is most likely that the deflected bottom current turns around the Renard Ridge and continues its path along the northern slope. LADCP station 2 (Figure 5.6d) indeed shows an eastward bottom current. This eastward current can be responsible for the creation of the Renard North drift, which corresponds to a region of very

steep slopes (up to 25°, Figure 5.5), again indicating a topographic control on the location of the drift deposits in the EAMVP. Eastward, the moat widens and the drift deposits change into hemipelagic deposits, which indicates weakening of the bottom currents as soon as the obstacle becomes less steep (Figure 5.5).

Between Adamastor mud volcano and the Renard Ridge, a highly erosive channel is present (Figure 5.3d), while 1 km eastwards, a small patch drift is present within the channel (Figure 5.3e). Two hypotheses are brought forward to explain these features. The first hypothesis relates this to marginal valleys, as described by García et al. (2009) in the northern Gulf of Cádiz. When bottom currents encounter linear obstacles, jets at both sides of the obstacle can be formed (Marshall, 1995). The jets are considered as flow instabilities and can cause erosion on both sides of the obstacle (McCave and Carter, 1997). The Renard Ridge might destabilize the northward bottom currents and induce erosion on both sides of the ridge. Incision depths of >75 m support this hypothesis. The height of the Renard Ridge (100 m) is consistent with the diapiric ridges in the northern Gulf of Cádiz, which can be more than 150 m high (García et al., 2009). A second hypothesis relates this to the action of increased bottom currents, originating from the narrow passage between the Adamastor mud volcano and the Renard Ridge. Internal tides can propagate through this narrow passage and as a consequence increase their velocity. These increased velocities can make the current very erosive, creating the channel. If only internal tides flow through this narrow passage, with reverse flow directions every six hours, no real contourite drift can be built in this area and a solely erosive channel remains. For both hypotheses, the extrusion of mud from the Adamastor mud volcano can locally increase the sediment input, creating a small patch drift into this highly erosive channel (Figure 5.3e). Due to the non-linear shape of the Renard Ridge close to the Adamastor mud volcano and the well-reported strong internal tides in this region (Martins and Vitorino, 2012; Mienis et al., 2012), the second hypothesis seems more likely, although the first hypothesis cannot be completely ruled out.

The moat of the Vernadsky South drift is not as deep as those of the other drifts (5 m compared to >10 m in the Pen Duick drift) and the mounded part of the drift is less pronounced (Figure 5.3f), suggesting slower, less eroding bottom currents. Both the deflection of the northward current against the Vernadsky Ridge and the internal tides may explain the moat and drift deposits south of the Vernadsky Ridge. When both are flowing in the same direction, they reinforce each other. The less pronounced moat and accompanied drift can be explained by the lower slopes of the southern Vernadsky Ridge (Figure 5.5). The orientation of the small moat along the Kidd mud volcano at the northern slopes of the Vernadsky Ridge (Figure 5.4) is consistent with the shoreward component of the internal tides and the north to northwest directed currents observed in the LADCP data (Figure 5.6).

5. Conclusions

The topographic features of the El Arraiche mud volcano province interfere to a great extent with the bottom currents in the southern Gulf of Cádiz. These bottom currents are mostly flowing in a northward direction and consist of both NACW and AAIW. Deflection of the northward currents against the Renard and Vernadsky tectonic ridges induce several small sediment drifts, consisting of separated mounded drift deposits. Internal tides also play an important role in this region, where semi-diurnal tides flow in an east-west direction. These tides interfere with the mud volcanoes and create mounded drift deposits along their sides. The shoreward component seems to be stronger than the basinward component inferred from the sedimentological data. As the bottom currents flow through narrow passages between the topographic highs of the EAMVP, current velocities may increase dramatically and induce highly erosive features along their path. In the entire region, the position of the drift deposits is controlled by the steepness of the slope along which they are located. Steeper slopes induce

faster bottom currents and these in turn induce contourite deposition along the side. All of these conclusions indicate that in regions where currents are generally low, deflections against topographies and internal tides do create the possibility of enhanced bottom currents. These enhanced bottom currents can create sediment drifts which provide a high-resolution record of past environmental changes. In the EAMVP, this is very useful for the study of the prevailing CWC's, as they greatly rely on bottom currents and food supply for their growth and initiation.

References

Ambar, I., Serra, N., Neves, F., Ferreira, T., 2008. Observations of the Mediterranean Undercurrent and eddies in the Gulf of Cadiz during 2001. Journal of Marine Systems 71, 195-220.

Batteen, M.L., Martinho, A.S., Miller, H.A., McClean, J.L., 2007. A process-oriented modelling study of the coastal Canary and Iberian Current system. Ocean Modelling 18, 1-36.

Borenäs, K.M., Wåhlin, A.K., Ambar, I., Serra, N., 2002. The Mediterranean outflow splitting—a comparison between theoretical models and CANIGO data. Deep Sea Research Part II: Topical Studies in Oceanography 49, 4195-4205.

Cabecadas, G., José Brogueira, M., Goncalves, C., 2002. The chemistry of Mediterranean outflow and its interactions with surrounding waters. Deep Sea Research Part II: Topical Studies in Oceanography 49, 4263-4270.

Camerlenghi, A., Cita, M.B., Vedova, B.D., Fusi, N., Mirabile, L., Pellis, G., 1995. Geophysical evidence of mud diapirism on the Mediterranean Ridge accretionary complex. Marine Geophysical Researches 17, 115-141.

Criado-Aldeanueva, F., García-Lafuente, J., Vargas, J.M., Del Río, J., Vázquez, A., Reul, A., Sánchez, A., 2006. Distribution and circulation of water masses in the Gulf of Cadiz from in situ observations. Deep Sea Research Part II: Topical Studies in Oceanography 53, 1144-1160.

García, M., Hernández-Molina, F.J., Llave, E., Stow, D.A.V., Léon, R., Fernández-Puga, M.C., Diaz del Río, V., Somoza, L., 2009. Contourite erosive features caused by the Mediterranean Outflow Water in the Gulf of Cadiz: Quaternary tectonic and oceanographic implications. Marine Geology 257, 24-40.

Hernández-Molina, F.J., Larter, R.D., Rebesco, M., Maldonado, A., 2006. Miocene reversal of bottom water flow along the Pacific Margin of the Antarctic Peninsula: Stratigraphic evidence from a contourite sedimentary tail. Marine Geology 228, 93-116.

Louarn, E., Morin, P., 2011. Antarctic Intermediate Water influence on Mediterranean Sea Water outflow. Deep Sea Research Part I: Oceanographic Research Papers 58, 932-942.

Machín, F., Hernández-Guerra, A., Pelegrí, J.L., 2006. Mass fluxes in the Canary Basin. Progress In Oceanography 70, 416-447.

Machín, F., Pelegrí, J.L., Marrero-Díaz, A., Laiz, I., Ratsimandresy, A.W., 2006. Near-surface circulation in the southern Gulf of Cádiz. Deep Sea Research Part II: Topical Studies in Oceanography 53, 1161-1181.

Marshall, D., 1995. Influence of Topography on the Large-Scale Ocean Circulation. Journal of Physical Oceanography 25, 1622-1635.

Marshall, D.P., Tansley, C.E., 2001. An Implicit Formula for Boundary Current Separation. Journal of Physical Oceanography 31, 1633-1638.

Martins, I., Vitorino, J., 2012. Physical processes affecting the El-Arraiche mud volcano Field (NW Moroccan Margin), HERMIONE Final Meeting, Carvoeiro.

McCave, I.N., Carter, L., 1997. Recent sedimentation beneath the Deep Western Boundary Current off northern New Zealand. Deep Sea Research Part I: Oceanographic Research Papers 44, 1203-1237.

McPhee-Shaw, E.E., Sternberg, R.W., Mullenbach, B., Ogston, A.S., 2004. Observations of intermediate nepheloid layers on the northern California continental margin. Continental Shelf Research 24, 693-720.

Mienis, F., De Stigter, H.C., De Haas, H., Van der Land, C., Van Weering, T.C.E., 2012. Hydrodynamic conditions in a cold-water coral mound area on the Renard Ridge, southern Gulf of Cadiz. Journal of Marine Systems 96–97, 61-71.

Murphy, J., Riley, J.P., 1962. A modified single solution method for the determination of phosphate in natural waters. Analytica Chimica Acta 27, 31-36.

Rebesco, M., Hernández-Molina, F.J., van Rooij, D., Wåhlin, A., 2014. Contourites and associated sediments controlled by deep-water circulation processes: State of the art and future considerations. Marine Geology.

Ribbe, J., Holloway, P.E., 2001. A model of suspended sediment transport by internal tides. Continental Shelf Research 21, 395-422.

Somoza, L., Gardner, J.M., Díaz-del-Río, V., Vázquez, J.T., Pinheiro, L.M., Hernández-Molina, F.J., parties, T.A.s.s., 2002. Numerous methane gas-related sea floor structures identified in Gulf of Cadiz. Eos, Transactions American Geophysical Union 83, 541-549.

Strickland, J.D.H., Parsons, T.R., 1972. A practical handbook of seawater analysis, second ed. Fisheries Research Board of Canada, Ottawa.

Taylor, N.K., 1990. A review of the generation, trapping and shedding of eddies by flow over seamounts, Marine Science Laboratories. University college of North Wales.

Thurnherr, A.M., 2005. How to process LADCP data with the LDEO software.

Tsuchiya, M., Talley, L.D., McCartney, M.S., 1992. An eastern Atlantic section from Iceland southward across the equator. Deep Sea Research Part A. Oceanographic Research Papers 39, 1885-1917.

Turnewitsch, R., Falahat, S., Nycander, J., Dale, A., Scott, R.B., Furnival, D., 2013. Deep-sea fluid and sediment dynamics—Influence of hill- to seamount-scale seafloor topography. Earth-Science Reviews 127, 203-241.

Van Rensbergen, P., Depreiter, D., Pannemans, B., Henriet, J.-P., 2005. Seafloor expression of sediment extrusion and intrusion at the El Arraiche mud volcano field, Gulf of Cadiz. Journal of Geophysical Research: Earth Surface 110, F02010.

Vandorpe, T., Van Rooij, D., de Haas, H., 2014. Stratigraphy and paleoceanography of a topography-controlled contourite drift in the Pen Duick area, southern Gulf of Cádiz. Marine Geology 349, 136-151.

Wåhlin, A., 2004. Topographic advection of dense bottom water. Journal of Fluid Mechanics 510, 95-104.

Xu, Z., Yin, B., Hou, Y., Liu, A.K., 2014. Seasonal variability and north–south asymmetry of internal tides in the deep basin west of the Luzon Strait. Journal of Marine Systems 134, 101-112.

Zitellini, N., Gràcia, E., Matias, L., Terrinha, P., Abreu, M.A., DeAlteriis, G., Henriet, J.P., Dañobeitia, J.J., Masson, D.G., Mulder, T., Ramella, R., Somoza, L., Diez, S., 2009. The quest for the Africa-Eurasia plate boundary west of the Strait of Gibraltar. Earth and Planetary Science Letters 280, 13-50.

Chapter 6

Coral mounds

Chapter 6 – Buried coral mounds in the Atlantic Moroccan Coral Province

Abstract

Cold-water coral mounds are common seabed features in the North Atlantic Ocean, where they are mainly restricted to water depths between 200 m and 1000 m. Coral mounds consist of coral fragments and hemipelagic sediments, reflecting an often complex history of mound aggradation and erosion linked to coral vitality. In the southern Gulf of Cádiz along the Moroccan margin, a large field (extension: 1800 km^2) of 781 comparatively small buried and exposed mounds (average height: about 19.7 m) has recently been discovered. The mounds in the so-called Atlantic Moroccan Coral Province initiated on at least ten different horizons, all of them most likely related to glacial periods since the Early-Middle Pleistocene Transition. A strong link between the intensification of bottom currents and the number of coral mounds rooting on each of the identified horizons is assumed. Also a shift of the average water depth at which coral mounds initiated towards deeper regions and an accompanied increase in mound height is observed between MIS 14 and MIS 12. Finally, reduced or low sediment input is regarded as one of the main factors triggering the rather small size of coral mounds in the AMCP in comparison to other Atlantic mound provinces.

Keywords: cold-water coral mound initiation & aggradation, Atlantic Moroccan Coral Province, glacial, sediment input, bottom currents

1. Introduction

Contourite drifts are sedimentary environments with elevated sedimentation rates (Bryn et al., 2005) and are as such preferred sites for palaeoceanographic and palaeo-climate studies (Rebesco et al., 2014). However, periods of non-deposition and/or erosion are present in contourite drifts and render the record incomplete. Coral mounds baffle sediments in their coral framework (Huvenne et al., 2009; Titschack et al., 2009) and may do this even under erosive conditions (Thierens et al., 2013). Consequently, the palaeo-environmental record that can be deducted from the El Arraiche drifts systems can be improved by studying the ubiquitous coral mounds along the Atlantic Moroccan margin. A complete palaeo-environmental record of any region is hard to retrieve and the AMCP may prove valuable in achieving this goal.

As a consequence, the coral mounds (which have been briefly mentioned in the two previous chapters) will be the main focus of this chapter. Together with the sparker dataset, a 2D parasound echosounder dataset was investigated in order to describe and map all discovered coral mounds within the AMCP. The periods in which coral mound growth initiated may give additional insights regarding the palaeoceanographic and palaeo-climatic evolution of the AMCP. The results obtained by studying the seismic dataset can be used to frame the cores obtained during the "MoccoMeBo" campaign; sediment cores that will most likely improve our understanding of this region regarding the palaeo-environment.

2. Material and methods

Two datasets have been combined to investigate the buried coral mounds in the AMCP. The first dataset was obtained in 2013 during the "COMIC" campaign on board of R/V Belgica and consists of single channel reflection seismic sparker profiles (Figure 6.1) comprising 85 profiles covering nearly 650 km in total length. The energies used were 500 or 600 J, with a shooting rate of 1 or 2 seconds, depending on the water depth. The data were recorded with a 10 kHz sampling rate and a record length of 0.9 or 1.8 s, again depending on the water depth. Survey speeds were maintained at 3-4 knots. The profiles were processed in order to improve signal-to-noise ratios using the DECO RadexPro software. An Ormsby bandpass filter (75/150 Hz as low-cut ramp and 1250/1500 Hz as high-cut ramp), a swell filter, burst noise removal and spherical divergence corrections were applied.

The second dataset was collected in 2014 during the MSM36 "MoccoMeBo" campaign on board of R/V Maria S. Merian and consists of about 1430 km SBP (ATLAS PARASOUND type P70; Figure 6.1). The maximum transmission power was 70 kW with a maximum penetration of 200 m. The beam width of the primary (19.3 kHz) and secondary (3.85 kHz) frequencies was 4° by 4.5° and 4° by 5°, respectively. Maximum transmission voltage was set at 100-120 V and the receiver amplification at 15 dB. Survey speeds were kept at 2-4 knots. The sub-bottom profiles were recorded with ATLAS PARASTORE software and processed in several steps. The first step includes the transition from the *.ps3 format into the *.segy format using the ps32segy software of Dr. Hanno Keil (University Bremen). The second step was performed using the REFLEXw software (vers. 7.2.2) and consisted of a static correction, muting of the water column and applying an automatic gain control. The final processing step was performed with the DECO RadexPro software and consisted of calculating a Hilbert transform, removing burst noise and applying a spherical divergence correction.

For all coral mounds, the base horizon was mapped and correlated throughout the AMCP along the SBP and seismic profiles. Several parameters were defined for each coral mound: coordinates, width (at several cross-sections), height and the depth of the seafloor above the coral mound. Due to the 2D nature of the seismic methods, the measured widths and heights of the coral mounds have to be

considered as their minimum widths and height, as the mounds might have a far more complex shape, not represented by the 2D crosscut. As a consequence, the mound dimensions given in this paper have to be interpreted with caution, bearing in mind that the true dimensions may be deviant. The depth of the seafloor and the height of the mound were transferred from seconds TWT to meters using seismic velocities determined by a wide angle test in 2005 (location indicated as AVO, amplitude versus offset, in Figure 6.1; resulting velocities indicated in Table 6.1).
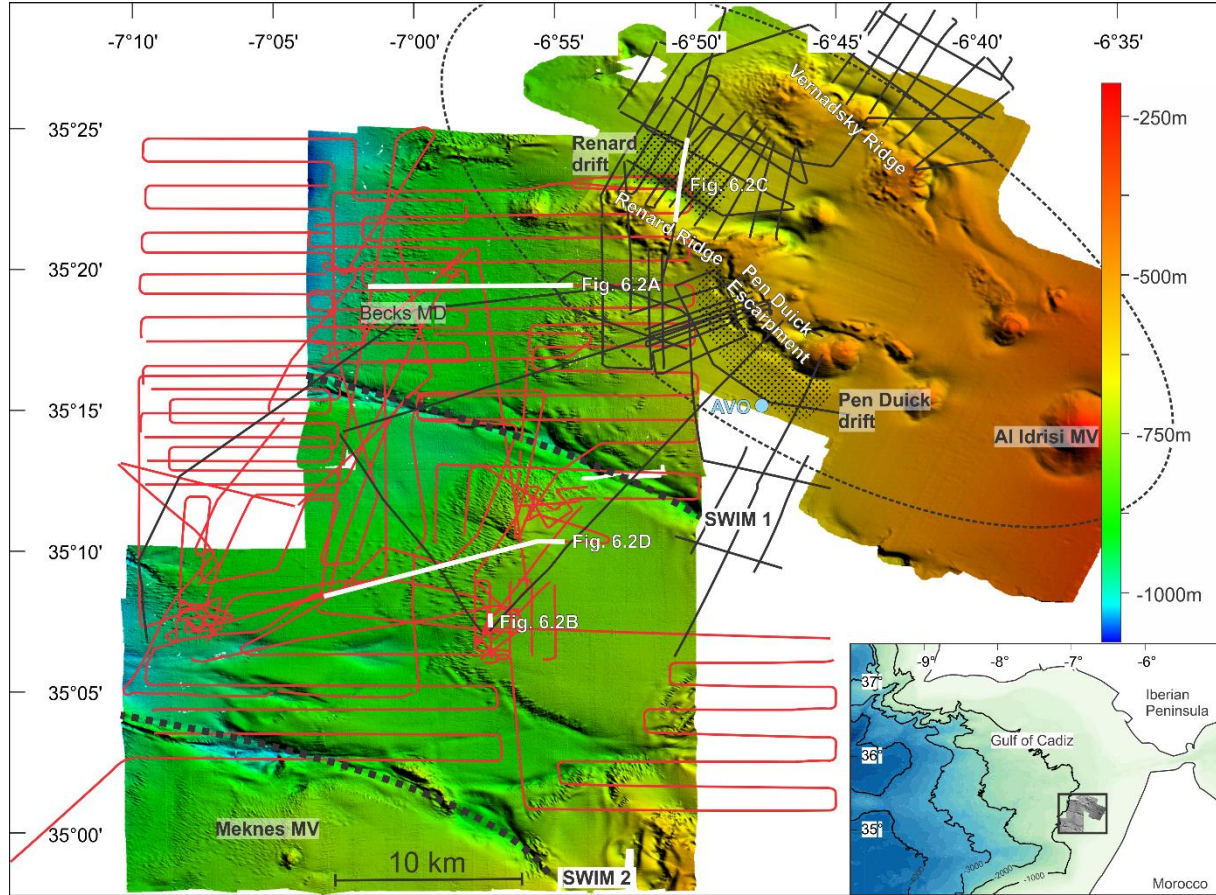
Figure 6.1: Multibeam bathymetric map of the study area along the Atlantic Moroccan margin (see overview map in the lower right inset). The SBP profiles are indicated in red and the single channel sparker reflection seismic profiles in black. The Pen Duick and Renard drifts are indicated by the dotted areas. The extent of the EAMVP (Vandorpe et al., 2016) is indicated by the thin black dashed oval. The location of the amplitude versus offset (AVO) experiment is indicated by the light blue dot. The white bold lines indicate the position of seismic profiles displayed in Figure 6.2. MD: mud diapir, MV: mud volcano, SWIM: Southwestern Iberian Margin faults.

The AVO test (Van Rooij et al., 2005) consisted of two vessels (R/V Belgica and R/V Pelagia) approaching a common point (2 km south of the Pen Duick Escarpment, Figure 6.1) and receiving the signal of each other sources. The distance between source and receiver (x) was deduced from the direct wave and an assumed average seismic velocity in the water of 1500 ms^{-1}. Besides the seafloor, five other reflectors were picked and the velocity was determined based on the following equation:

$$t^2 = t_0^2 + \frac{x^2}{v^2}$$

In this equation, v stand for velocity and t for time. t_0 for all six horizons was determined from the signal of the nearest point based on:

$$t_0^2 = t_{receiver}^2 - t_{direct}^2$$

107

The root mean square velocity was calculated based on the mapping of these horizons along the seismic line. Based on the root mean square velocity, the interval velocity could be determined using the following formula:

$$v^2_{interval} = \frac{v^2_{rms} * t_n - v^2_{rms} * t_{n-1}}{t_n - t_{n-1}}$$

From the heights of the mounds rooting on each horizon, a histogram was constructed and a log-logistic distribution fit was applied to them (e.g. for the height of mounds rooting on H3 displayed in Figure 6.3). The correlation coefficient between histogram and fit was always high (around 0.99). From the log-logistic fit, the 5% percentile, mode and 95% percentile were calculated and plotted for each horizon (Figure 6.3C).

Tsubsurface (ms TWT)	RMS velocity (m/s)	Interval-velocity (m/s)
0	1502.142	1502.142
99.1	1513.331	1609.995
215.1	1547.495	1829.109
354	1599.937	2004.367
434.4	1637.555	2204.469
749.4	1792.402	2426.758

Table 6.1: Overview of the root mean square and interval velocities used to convert the heights (seconds TWT) of the coral mounds into meters based on an AVO experiment (Van Rooij et al., 2005; location see Figure 6.1). The left column indicates the depth below seafloor of the upper boundary of the interval.

3. Results

By analyzing the seismic and SBP data, a total of 781 features, interpreted as coral mounds, were identified for the AMCP (Table 6.2). From these 781 coral mounds, 615 are fully buried by sediments and 166 are still exposed and arise several meters above the seafloor (Figure 6.2A, B, D). However, considering the limitation in penetration of the SBP (mostly less than 80 m, Figure 6.2) and the areal coverage of the surveyed areas (limited to profile lines), the ultimate number of exposed as well as buried mounds is likely considerably higher.

3.1. Seismic characteristics

Both in the reflection seismic and SBP datasets, buried mounds can be recognized due to their (almost) transparent acoustic facies (Figure 6.2). Small coral mounds (up to 20 ms TWT) appear mostly as transparent structures embedded within well-stratified sub-horizontal reflectors (Figure 6.2A, C & D), while larger coral mounds (> 20 ms TWT; Figure 6.2B) may contain small chaotic reflections and diffraction hyperbola. The mounds may affect the surrounding sediments as small moat-like structures are sometimes present (Figure 6.2) or as the overlying sediments have a mounded appearance once mound aggradation has ceased (Figure 6.2A, B & D). Within the sedimentary sequence (which can be up to 400 ms TWT), many faults are observed (Figure 6.2A, C & D). Offsets are mostly only a few ms TWT (Figure 6.2A & D), but some faults have offsets greater than 10 ms TWT (Figure 6.2C).

3.2. Horizon description

Ten horizons (H10 – H1) were identified in the sedimentary sequence of the AMCP, on which the Moroccan coral mounds (regardless if they are fully buried or are still exposed at the seafloor) have initiated in the past. These horizons were numbered from top to bottom (Figure 6.2Figure 6.3).
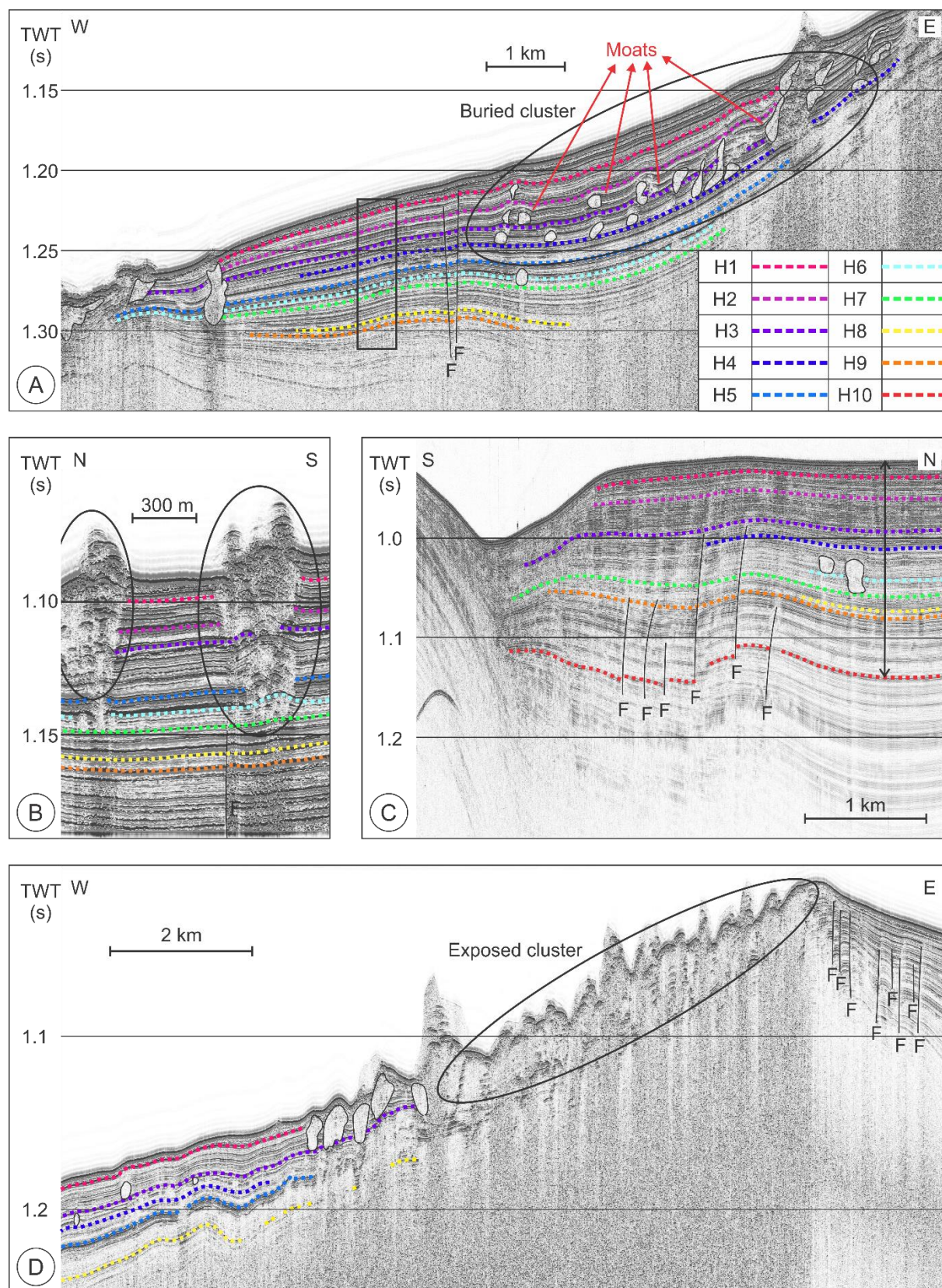
Figure 6.2: Seismic profiles (for position see Figure 6.1) with all depths indicated in s two-way-travel times. A. SBP profile extending from the Becks mud diapir towards the Renard Ridge showing nine (H1-H9) of 10 horizons identified for the study area (H1-H10; see legend for color code, which is used for all profiles shown in Figure 6.2). In the center of the profile, two near-vertical faults (F) disrupt the sedimentary sequence. Many coral mounds are delineated by a thin black line and some of them show moats. The closely-spaced buried mounds in this profile are a part of the Becks cluster, indicated in Figure 6.4. The black box indicates the part of the profile displayed in Table 6.2. B. Small part of a SBP profile in between the two SWIM faults. This profile shows two still exposed coral mounds, which display recurring phases of mound aggradation. For example, the southern mound initiated on H7 and re-started aggradation during all following horizons. Note that the width of this mound becomes progressively wider with every new re-start of aggradation. C. Sparker profile north of the Renard Ridge indicating several near-vertical faults with the lowest base horizon (H10) being displayed. D. SBP profile between the two SWIM faults showing clustered and exposed coral mounds (black oval). The eastern part of the profile is intensely faulted, while the western part is not and contains several buried mounds.

Horizon 10 is the top reflector of a package of moderate to high amplitude reflectors (Figure 6.2C). On top of this horizon, a package of low-amplitude reflectors with intermittent high amplitude reflectors is present. Due to the limited penetration of the SBP signal, H10 can only be observed on the sparker profiles. Coral mounds initiating on H10 (in total 70) were mainly identified close to the 700 m bathymetric contour line around the Vernadsky Ridge and south of the Renard Ridge. Five mounds rooting on H10 were also identified between the two SWIM faults (Figure 6.4).

Horizon 9 is the lower of two strong reflectors within a sequence of mostly low-amplitude reflectors (Figure 6.2C). It was mainly indicated by the sparker data, while it is only visible on some of the SBP profiles. The 62 coral mounds initiating on H9 mostly occur directly south of the Renard Ridge (84%) with occurrences around the Vernadsky Ridge (5) and between the SWIM faults (6) as well (Table 6.2; Figure 6.4).
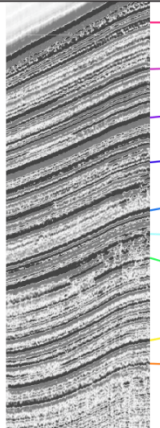
Seismic expression	Horizon	Mounds		Exposed		Average depth (m)
		amount	percentage	amount	percentage	
	1	6	0.8%	3	50.0%	716.8
	2	16	2.0%	14	87.5%	808.7
	3	135	17.3%	93	68.9%	882.7
	4	119	15.2%	37	31.1%	849.4
	5	40	5.1%	13	32.5%	834.0
	6	124	15.9%	2	1.6%	740.0
	7	66	8.5%	2	3.0%	814.4
	8	143	18.3%	2	1.4%	725.7
	9	62	7.9%	0	0%	731.4
	10	70	9.0%	0	0%	701.4

Table 6.2: Statistical evaluation of coral mounds in the AMCP. Column 1: Seismic expression of 9 of the 10 horizons based on the SBP profile of Figure 6.2A. Column 2: Number of horizons identified to act as a base for mound formation. Columns 3/4: Amount and percentage of mounds rooting on each of the 10 horizons. Columns 5/6: Amount and percentage of coral mounds still having an exposed position at the seabed surface in relation to the 10 horizons. Column 7: The average water depth where the coral mounds occur.

Horizon 8 is recognized as a strong reflector when not positioned too deep (up to 100 ms TWT below the seafloor; Figure 6.2B & D) but is far less pronounced when more sediments have been deposited on top (150-200 ms TWT; Figure 6.2C). A total of 143 coral mounds (~18% of all identified mounds in the AMCP; Table 6.2) were observed to initiate on top of H8. This is the largest number of mounds identified for any of the ten horizons. The majority of H8-mounds (~85%) occur directly around the Vernadsky Ridge and south of the Renard Ridge, while just ten mounds were identified around the

Becks mud diapir in the westernmost part of the AMCP and 14 mounds are positioned between the SWIM faults (Table 6.2; Figure 6.4).

Horizon 7 is identified as a higher-amplitude base reflector in a small package of low-amplitudes reflections. This low-amplitude package is positioned between two higher-amplitude packages (Figure 6.2A, B & C). The majority (61%) of the 66 identified coral mounds originating on H7 are found clustered in a small area between the two SWIM faults confined to a water depth of 800 m, while others are scattered over the entire AMCP (Figure 6.4).

Horizon 6 is recognized on the profiles as the lower boundary of a high amplitude interval of several reflectors, with the upper boundary of this interval being marked by H5 (Figure 6.2A & B). A total of 124 coral mounds (~16% of all identified mounds in the AMCP; Table 6.2) that initiated on H6 occur mostly (about 87%) north of the SWIM fault 1 and 16 mounds are also observed between both SWIM faults (Figure 6.4). In contrast to H6, a rather low number of coral mounds (n=40; ~5% of all identified mounds in the AMCP; Table 6.2) initiated on H5, thereby 27 mounds occur between the SWIM fault 1 and the Renard Ridge, while 13 mounds are present south of the SWIM fault 1 (Figure 6.4).

Horizon 4 is characterized by a very low amplitude reflector (Figure 6.2). Coral mounds (n=119; Table 6.2) rooting on this horizon occur everywhere in the AMCP. South of the Vernadsky Ridge, H4-mounds are confined to a water depth interval between 800 m and 1000 m, while those directly surrounding the Vernadsky Ridge occur at 650 m water depth (Figure 6.4).

Horizon 3 is the reflector with the highest amplitudes present in the sedimentary sequence in the AMCP (Figure 6.2; Table 6.2). It can be recognized throughout the area and 135 coral mounds (~17% of all identified mounds in the AMCP; Table 6.2) initiate on this horizon. The mounds rooting on H3 occur mainly in an 8 km radius around the Becks mud diapir and in a cluster between the SWIM faults (~65%), corresponding to a water depth interval of 800 m to 900 m (Figure 6.4).

Horizon 2 is recognized in the sedimentary deposits as the top of a high amplitude interval (Figure 6.2A, C), while H1 is a high-amplitude reflector, which occurs only a few ms TWT below the seafloor. The sixteen coral mounds that were identified to have initiated on H2 (2% of all identified mounds in the AMCP; Table 6.2) are all but one positioned north of the SWIM fault 1, while five of a total of six mounds identified for H1 (less than 1% of all identified mounds; Table 6.2) occur around the Vernadsky Ridge (Figure 6.4). A lot of mounds, from which the base horizon cannot be determined, are present on the steep slopes of the AMCP (Figure 6.2D). As a consequence, more mounds, rooting on several (possibly until now undiscerned) horizons are expected to be present in the AMCP.

3.3. Coral mound characteristics

Due to the limited number of coral mounds rooting on H1 (n=6) and H2 (n=16), contributing to less than 3% of all identified mounds in the AMCP (Table 6.2), they are not considered for the statistical analyses (Figure 6.3C). All other horizons show a high number of mounds rooting on them, ranging from 40 mounds identified for H5 to 143 mounds for H8 (Table 6.2).

All coral mounds in the AMCP are found within a water depth range of 600 m to 1100 m (marked by red lines in Figure 6.4). Based on the averaged present-day water depths for all coral mounds rooting on one horizon, a trend towards an increasingly deeper location is observed going from H10 (701.4 m) to H3 (882.7m), with a large exception for H6 (740 m) (Table 6.2).

Some of the larger coral mounds towered a fair amount above the palaeo-seafloor, still exhibiting a positive topography when the next initiation phase occurred, after which they were re-colonized, seemingly displaying continuous coral mound growth (e.g. several H4-mounds in the eastern part of

Figure 6.2A or the mounds displayed in Figure 6.2B). At present, 166 coral mounds still surface on the seafloor, none of which root on the deepest horizons H10 and H9. For the following three horizons (H8-H6) only 2 mounds of each horizon (1.4-3% of the total number of mounds identified per horizon) still pierce the seafloor (Table 6.2). From H5 onwards, the percentage of exposed mounds contributing to the total number of mounds strongly increases to over 30% as identified for H5 and H4, and to even ~70% of exposed mounds rooting on H3 (Table 6.2). As the base horizon for many exposed mounds is not easy to discern, the percentage of exposed mounds rooting on H2 and H1 will likely even be higher than 70%.
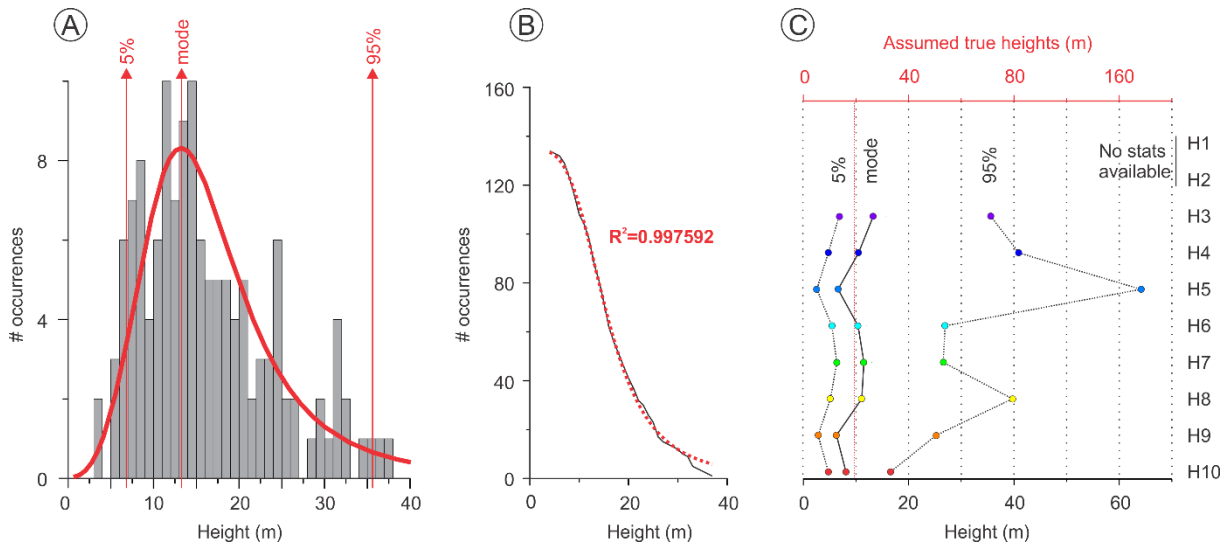
Figure 6.3: Histogram of the height of the mounds rooting on horizon 3 with indication of the log-logistic fit (red). B. Cumulative distribution of the height of the mounds of horizon 3 (black) and log-logistic fit (red). C. Evolution of the height of the mounds rooting on the different horizons based on the log-logistic fit. For the upper two horizons H1 and H2, no statistical information is calculated due to the low number of identified mounds for these horizons (respectively 6 and 16; Table 6.2). The red striped line indicates the average of the modes of the 10 horizons. The red axis on top of the plot is twice the actual measured heights and displays the assumed true heights (being 5%, mode and 95%) of the coral mounds for each horizon.

The 5th percentile (indicating the average height of the smaller mounds) and the mode have the same trend with similar values for H8, H7, H6 and H4 (between 4.7 m and 6.4 m and between 10.5 m and 11.4 m respectively) and lower values for H10, H9 and H5 (between 2.6 m and 4.8 m and between 6.3 m and 8.1 m respectively). Horizon 3 has the highest values for these parameters compared to all other horizons (6.8 m and 13.3 respectively). The 95th percentile (indicating the average height of the tallest mounds) varies differently and no clear trend is observed. H8 reveals much larger values (64.1 m) compared to the other horizons. The large variation of the 95th percentile may be caused by the skewed distribution of the heights towards smaller mounds (Figure 6.3A). The height of the coral mounds being deduced from the seismic lines has to be interpreted with caution as these lines only represent any 2D slice of a 3D volume. However, when a large number of mounds is measured, the obtained average height will be close to 50% of the real average height. As a result, an actual average height twice the obtained average height can be assumed (red axis in Figure 6.3C) and the relative changes between average heights measured for mounds rooting on the individual horizons can be discussed.

4. Discussion

4.1. Coral mound dimensions and location

The AMCP is one of the largest coral mound provinces discovered so far in the world, covering an area of over 1800 km², consisting of at least 615 buried coral mounds and 166 exposed coral mounds. In

comparison, the Campeche coral mound province in the southern Gulf of Mexico (>40 km²; Hebbeln et al., 2014), the Røst Reef (>120 km²) and the Traena Reefs (about 300 km²) along the Norwegian margin (Fosså et al., 2005) and the Magellan (about 120 km²) and Hovland (about 60 km²; Huvenne et al., 2003) coral mound provinces in the Porcupine Seabight are all considerably smaller. When comparing the density of buried coral mounds in the Magellan mound province (0.93/km²; Huvenne et al., 2003) to that of the AMCP (0.34/km², i.e. 1 mound every 2.3 km²), it is noticed that although the AMCP covers a much larger area (by a factor of 15), the density of coral mounds in this area does not differ by a similar factor (2.4).

The average mode of the individual horizons of the coral mounds in the AMCP is 19.7 m (red line in Figure 6.3C) and is among the smallest observed in the North Atlantic, in particular when compared to the Magellan, Hovland and Belgica mound provinces of the Porcupine Seabight, where average mound heights vary between 70 m and 100 m (De Mol et al., 2002; Huvenne et al., 2007), coral mounds along the Mauritanian margin with an average height of 100 m (Colman et al., 2005) and coral mounds from the western North Atlantic coral mounds of the Campeche mound province showing average heights of at least 40 m (Hebbeln et al., 2014). The overall small heights of coral mounds in the AMCP could indicate that the limited sediment supply (only a few cm/ky (Delivet, 2017) with exceptions up till 24 cm/ky in the Renard drift (Wienberg et al., 2009)) could be a very important factor inhibiting the build-up of tall coral mounds. The tallest mounds of the AMCP are found rooting on H3 (assumed mode of 26.6 m; Figure 6.3) and may result from a higher baffling capacity of the CWC framework or from the availability of more sediments (as also indicated by Glogowski et al., 2015). In both cases, sediment supply is the most important factor, indicating once more that coral mounds in the AMCP rely in a large extent on this parameter.

Thus, although a large number of coral mounds initiated in the AMCP during distinct time periods in the geological past, they rarely reached heights exceeding 40 m (Figure 6.3C). According to a simplified mound province evolution and development model presented by Kenyon et al. (2002), the ubiquitous presence of rather small coral mounds in a mound province is the result of low sedimentation rates and moderate near-bed currents, which might also be used as an explanation for the small size of the coral mounds in the AMCP.

4.2. Temporal variability of coral mound occurrence

Regarding the Atlantic coral mound realm, there are just a few areas known for which buried coral mounds were identified so far. One of the best studied areas is the Porcupine Seabight along the Irish margin, where buried mounds were found within the Magellan mound province (De Mol et al., 2002; Huvenne et al., 2003; Huvenne et al., 2007) and seem to have been originated on one single reflector (Huvenne et al., 2007; Huvenne et al., 2009). For the SW Rockall Trough, three potential/possible horizons for mound initiation were reported (van Weering et al., 2003) and in the westernmost part of the Mediterranean Sea (Alboran Sea) also three initiation horizons could be distinguished (Lo Iacono et al., 2014).

In contrast, for the AMCP, at least ten initiation events comprising distinct generations of coral mounds were identified, with several mounds restarting aggradation at one of the following horizons (Figure 6.2). Within the southern H7 coral mound of Figure 6.2B, a small package of reflectors is present within the mound immediately below H3, indicating that mound aggradation had ceased for a while between H4 and H3. However, from H3 onward, mound aggradation restarted at that location with the coral mound still piercing the present-day seafloor. This indicates that within one coral mound, several periods of coral demise and subsequent aggradation may be present. Since no absolute (coral) ages have been obtained from the Moroccan buried mounds so far, a correlation with the Quaternary Pen

Duick drift was conducted (Vandorpe et al., 2014; Figure 6.1). The most pronounced seismic stratigraphic change
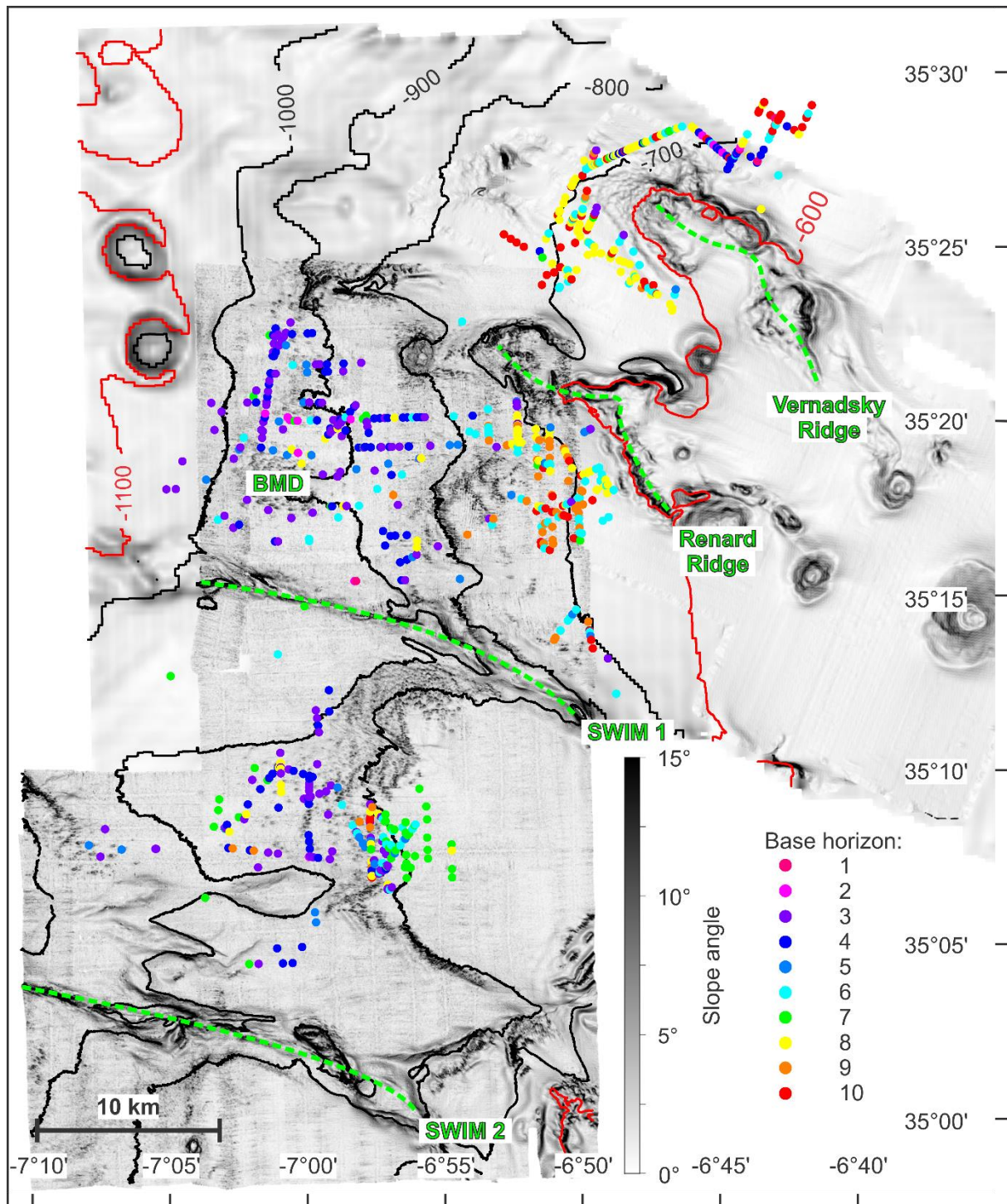
Figure 6.4: The position of the identified coral mounds (color-coded based on their base horizon, see legend) with a map of the slope angle as a background (grey scales). The 600 m and 1100 m contour lines are indicated in red. The green dashed lines indicate (from north to south) the Vernadsky Ridge, the Renard Ridge, SWIM fault 1 and SWIM fault 2. BMD: Becks mud diapir, SWIM: Southwestern Iberian Margin.

in this drift system is the transition from sheeted to mounded drift deposits since the EMPT, which is expressed by increased reflection amplitudes (Vandorpe et al., 2014). The same pattern is observed from H10 onwards as higher amplitudes are solely recognized starting from this horizon (Figure 6.2C).

As a consequence, mound formation in the AMCP most likely started right after the EMPT. Assuming that H10 coincides with the EMPT, average sedimentation rates in the Renard drift (Figure 6.1) would be 20.1 cm/ky (using the depths along the line in Figure 6.2C and the interval-velocities of Table 6.1). This rate is within the range of sedimentation rates reported by Wienberg et al. (2010), which are between 8 and 24 cm/ky.

A database of dated coral fragments (106 in total) from this region (Wienberg et al., 2009; Wienberg et al., 2010; Frank et al., 2011) shows that 75% of the obtained ages coincide with glacial periods (going back to MIS 12; Figure 6.5), implying that both the occurrence of CWC and coral mound initiation are mostly restricted to cold periods in the AMCP. Given that ten horizons (being the base for mound initiation) were discerned and that the available coral ages show that colder (glacial) periods offered more suitable environmental conditions triggering the sustained occurrence of CWC and thus the aggradation of coral mounds in the AMCP (at least during the past ~500ka; Wienberg et al., 2010), the ten identified initiation events might be assigned to cold (glacial) periods occurring since the EMPT (Lisiecki and Raymo, 2005; Figure 6.5). As discerning the base horizon of many mounds on the steeper parts of the AMCP was not possible (e.g. Figure 6.2D), more horizons may be present and more than one initiation event may have occurred in the course of one glacial cycle.
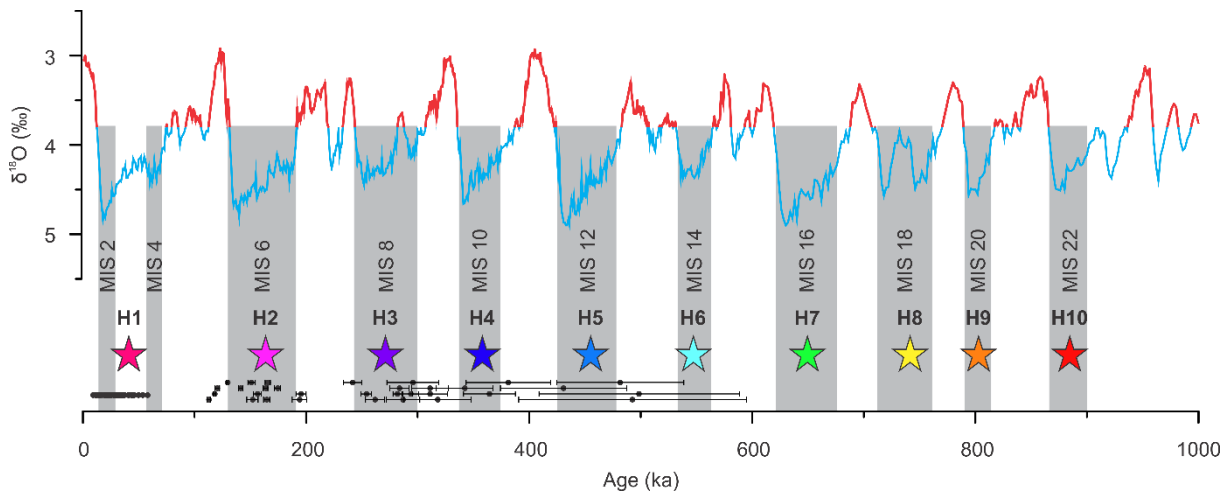
Figure 6.5: Correlation between the ten horizons (stars) acting as a base for the initiation of coral mounds and the MIS (boundaries between MIS are based on the stable oxygen isotope LR04 stack by Lisiecki and Raymo (2005)). The black dots indicate cold-water coral ages obtained from the mound-forming species Lophelia pertusa and Madrepora oculata collected from various exposed mounds in the AMCP (Wienberg et al., 2009; Wienberg et al., 2010; Frank et al., 2011).

The three horizons with the highest acoustic amplitudes (H3, H6 and H8; Figure 6.2; Table 6.2) also represent the initiation base for >50% of all coral mounds identified in the AMCP (Table 6.2). High amplitude values are usually caused by a facies change, such as a change from fine-grained (silty) to coarse-grained (sandy) sediments, inducing a difference in acoustic impedance. As Wienberg et al. (2010) indicated average grainsizes of 10 μm (at least for the last ~40 ka), facies changes may indeed result from the presence of more coarse-grained (possibly sandy) layers. These may either be derived from contouritic or turbiditic processes. Two main factors contradict a turbiditic origin for these horizons. Firstly, the three horizons (especially H3 and H8) can be observed margin-wide, which is not consistent with turbiditic deposits on continental slopes, which are expected to be focused in channels or levees (e.g. Stow and Mayall, 2000; Piper and Normark, 2009; Picot et al., 2016). And secondly, the fairly low slope angle of the margin (usually below 1°; Figure 6.4) and the low sedimentation rates (Wienberg et al., 2010), are not in favour of slope failure that could cause turbidites (Piper and Normark, 2009). Contourites and the bottom currents associated with them on the other hand are known to occur in this region (Vandorpe et al., 2016) and they usually create regionally rather

widespread horizons. This could indicate towards a bottom-current control on the number of coral mounds that initiate in a certain period. Bottom currents are known to be strongly influenced by climate (Rebesco et al., 2014), evidenced by the different pathways of the MOW during glacial and interglacial periods (Llave et al., 2006) or its variations in intensity paced by climatic changes (Toucanne et al., 2007). Also the AAIW, present within the depth ranges of the coral mounds of the AMCP (600 m to 1100 m, Figure 6.1; Vandorpe et al., 2016), has a climatic control (Makou et al., 2010; Jung et al., 2011). As a consequence, the base horizons (and hence mound initiation), which seem to be controlled by bottom currents, may be strongly climate-controlled in the AMCP.

4.3. Lateral variability and clustering of coral mound occurrence

The optimal conditions for coral mound initiation may have progressively moved towards deeper areas as the average depth for the successive horizons changes from 701.4 m for H10 to 882.7 m for H3 with the exception of H7 where the average depth is 814.4 m (Table 6.2). The largest change occurs at H5, where water depths increase rather abruptly from ~700-740 m (H10-H6) to ~830-880 m water depth (H5-H3). As most of the coral mounds rooting on H4 and H3 cluster around the Becks mud diapir or between the two SWIM faults (Figure 6.4), the optimal conditions for CWC growth and thus mound aggradation must have shifted to those deeper regions.

Clusters of buried coral mounds have been discerned in the AMCP (Figure 6.4), with all of them containing coral mounds from several horizons. Clustering of mounds is not only observed in the AMCP, but occurs in many mound provinces, e.g. in the Porcupine Seabight (De Mol et al., 2002), the Gulf of Mexico (Hebbeln et al., 2014) or off the southern Atlantic Moroccan coast (Glogowski et al., 2015). The small coral mounds can deflect bottom currents, which is evidenced by the presence of small moats around some of the buried coral mounds (Figure 6.2A), similar to the small-scale sediment drifts around the Campeche coral mounds (Hebbeln et al., 2012). Deflection of bottom currents will enhance the current speeds (Rebesco et al., 2014) and may bring more food particles and sediments to the neighboring coral mounds (Hebbeln et al., 2016). As coral mounds in many cases crosscut the subsequent base horizon (Figure 6.2), indicating they had an exposed position when the next initiation phase occurred, they could create a local more favorable environment, leading to continued coral growth in that cluster. This is evidenced by the presence of several horizons in one cluster (Figure 6.4). Moreover, besides continued coral growth in that particular cluster, the coral mound will be exposed to accelerated bottom currents (Wienberg and Titschack, 2016), making recolonization of the coral mound by CWC and renewed coral mound aggradation more likely.

5. Conclusions

With an extension of 1800 km², the AMCP along the Atlantic Moroccan margin is one of the largest coral mound provinces worldwide discovered so far. Moreover, this mound province is unique in the Atlantic realm as hundreds of exposed as well as fully buried coral mounds exist in this area, which represent different generations of coral mounds as they initiated on at least ten horizons, while for most other Atlantic mound provinces, only one single rooting horizon was indicated. The ten horizons in the AMCP could all be tentatively traced back to glacial periods since the EMPT, meaning that favorable conditions for mound initiation and subsequent aggradation occurred several times during the last 900 ka along the Atlantic Moroccan margin. As a consequence, a strong climatic control on mound initiation and aggradation can be inferred in this region.

The relatively small heights of coral mounds (~20 m) in this region might indicate that a relatively low sediment input may have prevented the development of giant mounds as found along the Irish margin. Recolonization by CWC and renewed mound aggradation was possible when coral mounds were still

exposed during the subsequent initiation phase. Clustering can intensify bottom currents locally and improve both food and sediment supply to the coral mounds.

The timing of the mound initiation, mound aggradation and coral demise cannot be determined from seismic data alone and as a consequence, datings of coral fragments from sediment cores penetrating the coral mounds are necessary to further understand the forcing mechanism. The AMCP can play a vital role in further unravelling the factors that trigger coral mound initiation and aggradation due to the ubiquitous presence of small coral mounds rooting on multiple horizons and its unique position close to contourite drifts.

References

Bryn, P., Berg, K., Stoker, M.S., Haflidason, H., Solheim, A., 2005. Contourites and their relevance for mass wasting along the Mid-Norwegian Margin. Marine and Petroleum Geology 22, 85-96.

Colman, J.G., Gordon, D.M., Lane, A.P., Forde, M.J., Fitzpatrick, J.J., 2005. Carbonate mounds off Mauritania, Northwest Africa: status of deep-water corals and implications for management of fishing and oil exploration activities, in: Freiwald, A., Roberts, J.M. (Eds.), Cold-Water Corals and Ecosystems. Springer, Berlin, Heidelberg, pp. 417-441.

De Mol, B., Van Rensbergen, P., Pillen, S., Van Herreweghe, K., Van Rooij, D., McDonnell, A., Huvenne, V., Ivanov, M., Swennen, R., Henriet, J.P., 2002. Large deep-water coral banks in the Porcupine Basin, southwest of Ireland. Marine Geology 188, 193-231.

Delivet, S., 2017. Quaternary expression of internal tidal contouritic processes along the Irish and Moroccan Atlantic margins., Deparment of Geology. Ghent University, Ghent, Belgium.

Fosså, J.H., Lindberg, B., Christensen, O., Lundälv, T., Svellingen, I., Mortensen, P.B., Alvsvåg, J., 2005. Mapping of Lophelia reefs in Norway: experiences and survey methods, in: Freiwald, A., Roberts, J.M. (Eds.), Cold-Water Corals and Ecosystems. Springer, Berlin, Heidelberg, pp. 359-391.

Frank, N., Freiwald, A., Correa, M.L., Wienberg, C., Eisele, M., Hebbeln, D., Van Rooij, D., Henriet, J.-P., Colin, C., van Weering, T., de Haas, H., Buhl-Mortensen, P., Roberts, J.M., De Mol, B., Douville, E., Blamart, D., Hatté, C., 2011. Northeastern Atlantic cold-water coral reefs and climate. Geology 39, 743-743.

Glogowski, S., Dullo, W.C., Feldens, P., Liebetrau, V., Reumont, J., Hühnerbach, V., Krastel, S., Wynn, R.B., Flögel, S., 2015. The Eugen Seibold coral mounds offshore western Morocco: oceanographic and bathymetric boundary conditions of a newly discovered cold-water coral province. Geo-Marine Letters 35, 257-269.

Hebbeln, D., Van Rooij, D., Wienberg, C., 2016. Good neighbours shaped by vigorous currents: Cold-water coral mounds and contourites in the North Atlantic. Marine Geology, 171-185.

Hebbeln, D., Wienberg, C., Beuck, L., Dehning, K., Dullo, C., Eberli, G.P., Freiwald, A., Glogowski, S., Garlichs, T., Jansen, F., Joseph, N., Klann, m., Matos, L., Nowald, N., Reyes, H., Ruhland, G., Taviani, M., Wilke, T., Wilsenack, M., Wintersteller, P., 2012. West Atlantic Cold- Water Coral Ecosystems: The west side story - Cruise No. MSM20/4 - March 14 - April 07, 2012 - Bridgetown (Barbados) - Freetown (Bahamas), in: MSM20/4, M.S.M.-B. (Ed.), DFG-Senatskommission für Ozeanographie, p. 53.

Hebbeln, D., Wienberg, C., Wintersteller, P., Freiwald, A., Becker, M., Beuck, L., Dullo, C., Eberli, G.P., Glogowski, S., Matos, L., Forster, N., Reyes-Bonilla, H., Taviani, M., 2014. Environmental forcing of the Campeche cold-water coral province, southern Gulf of Mexico. Biogeosciences 11, 1799-1815.

Huvenne, V.A.I., Bailey, W.R., Shannon, P.M., Naeth, J., di Primio, R., Henriet, J.P., Horsfield, B., de Haas, H., Wheeler, A., Olu-Le Roy, K., 2007. The Magellan mound province in the Porcupine Basin. International Journal of Earth Sciences 96, 85-101.

Huvenne, V.A.I., De Mol, B., Henriet, J.P., 2003. A 3D seismic study of the morphology and spatial distribution of buried coral banks in the Porcupine Basin, SW of Ireland. Marine Geology 198, 5-25.

Huvenne, V.A.I., Van Rooij, D., De Mol, B., Thierens, M., O'Donnell, R., Foubert, A., 2009. Sediment dynamics and palaeo-environmental context at key stages in the Challenger cold-water coral mound formation: Clues from sediment deposits at the mound base. Deep Sea Research Part I: Oceanographic Research Papers 56, 2263-2280.

Jung, S.J.A., Kroon, D., Ganssen, G., Peeters, F., Ganeshram, R., 2011. Southern Hemisphere intermediate water formation and the bi-polar seesaw. Pages News 18, 36-38.

Kenyon, N.H., Akhmetzhanov, A.M., Twichell, D.C., 2002. Sand wave fields beneath the Loop Current, Gulf of Mexico: reworking of fan sands. Marine Geology 192, 297-307.

Lisiecki, L.E., Raymo, M.E., 2005. A Plio-Pleistocene stack of 57 globally distributed benthic delta 18O records. Paleoceanography 20, PA1003.

Llave, E., Schönfeld, J., Hernández-Molina, F.J., Mulder, T., Somoza, L., Díaz del Río, V., Sánchez-Almazo, I., 2006. High-resolution stratigraphy of the Mediterranean outflow contourite system in the Gulf of Cadiz during the late Pleistocene: The impact of Heinrich events. Marine Geology 227, 241-262.

Lo Iacono, C., Gràcia, E., Ranero, C.R., Emelianov, M., Huvenne, V.A.I., Bartolomé, R., Booth-Rea, G., Prades, J., Ambroso, S., Dominguez, C., Grinyó, J., Rubio, E., Torrent, J., 2014. The West Melilla cold water coral mounds, Eastern Alboran Sea: Morphological characterization and environmental context. Deep Sea Research Part II: Topical Studies in Oceanography 99, 316-326.

Makou, M.C., Oppo, D.W., Curry, W.B., 2010. South Atlantic intermediate water mass geometry for the last glacial maximum from foraminiferal Cd/Ca. Paleoceanography 25, PA4101.

Picot, M., Droz, L., Marsset, T., Dennielou, B., Bez, M., 2016. Controls on turbidite sedimentation: Insights from a quantitative approach of submarine channel and lobe architecture (Late Quaternary Congo Fan). Marine and Petroleum Geology 72, 423-446.

Piper, D., Normark, W., 2009. Processes that initiate turbidity currents and their influence on turbidites: a marine geology perspective. Journal of sedimentary research 79, 347-362.

Rebesco, M., Hernández-Molina, F.J., van Rooij, D., Wåhlin, A., 2014. Contourites and associated sediments controlled by deep-water circulation processes: State of the art and future considerations. Marine Geology.

Stow, D.A.V., Mayall, M., 2000. Deep-water sedimentary systems: New models for the 21st century. Marine and Petroleum Geology 17, 125-135.

Thierens, M., Browning, E., Pirlet, H., Loutre, M.F., Dorschel, B., Huvenne, V.A.I., Titschack, J., Colin, C., Foubert, A., Wheeler, A.J., 2013. Cold-water coral carbonate mounds as unique palaeo-archives: the Plio-Pleistocene Challenger Mound record (NE Atlantic). Quaternary Science Reviews 73, 14-30.

Titschack, J., Thierens, M., Dorschel, B., Schulbert, C., Freiwald, A., Kano, A., Takashima, C., Kawagoe, N., Li, X., 2009. Carbonate budget of a cold-water coral mound (Challenger Mound, IODP Exp. 307). Marine Geology 259, 36-46.

Toucanne, S., Mulder, T., Schönfeld, J., Hanquiez, V., Gonthier, E., Duprat, J., Cremer, M., Zaragosi, S., 2007. Contourites of the Gulf of Cadiz: A high-resolution record of the paleocirculation of the Mediterranean outflow water during the last 50,000 years. Palaeogeography, Palaeoclimatology, Palaeoecology 246, 354-366.

Van Rooij, D., Versteeg, W., party, t.C.I.s.s., 2005. cruise report Belgica 05/12 "CADIPOR II", Gulf of Cadiz, off Larache, Morocco. RCMG internal publication, 43 pp.

van Weering, T.C.E., de Haas, H., de Stigter, H.C., Lykke-Andersen, H., Kouvaev, I., 2003. Structure and development of giant carbonate mounds at the SW and SE Rockall Trough margins, NE Atlantic Ocean. Marine Geology 198, 67-81.

Vandorpe, T., Martins, I., Vitorino, J., hebbeln, D., García, M., Van Rooij, D., 2016. Bottom currents and their influence on the sedimentation pattern in the El Arraiche Mud Volcano Province, southern Gulf of Cadiz. Marine Geology 378, 114-126.

Vandorpe, T., Van Rooij, D., de Haas, H., 2014. Stratigraphy and paleoceanography of a topography-controlled contourite drift in the Pen Duick area, southern Gulf of Cádiz. Marine Geology 349, 136-151.

Wienberg, C., Frank, N., Mertens, K.N., Stuut, J.-B., Marchant, M., Fietzke, J., Mienis, F., Hebbeln, D., 2010. Glacial cold-water coral growth in the Gulf of Cádiz: Implications of increased palaeo-productivity. Earth and Planetary Science Letters 298, 405-416.

Wienberg, C., Hebbeln, D., Fink, H.G., Mienis, F., Dorschel, B., Vertino, A., Correa, M.L., Freiwald, A., 2009. Scleractinian cold-water corals in the Gulf of Cádiz—First clues about their spatial and temporal distribution. Deep Sea Research Part I: Oceanographic Research Papers 56, 1873-1893.

Wienberg, C., Titschack, J., 2016. Framework-Forming Scleractinian Cold-Water Corals Through Space and Time: A Late Quaternary North Atlantic Perspective, in: Rossi, S., Bramanti, L., Gori, A., Orejas, C. (Eds.), Marine Animal Forests: The ecology of Benthic Biodiversity Hotspots. Springer International Publishing Switzerland.

Chapter 7

Computed tomography of contourite sequences

Campaign 7: GATEWAYS - Marion Dufresne (2013)

Chapter 7 – Analysing contourite cores using computed tomography

Abstract

Five sediment cores, retrieved within 4 different morphological settings (a sheeted drift, a confined mounded drift, a mounded elongated drift and an abrasive surface) from the northern Gulf of Cádiz and the Alboran Sea have been analysed using X-ray computed tomography (CT). A quantitative approach has been applied, resulting in a workflow that delineates several components based on the grey values histogram of each core and tracks these components throughout the core. The components have been compared to chemical and geophysical proxies as well as grainsize measurements to derive their geological significance. The highest correlations were observed between high Hounsfield Units (HU's) and coarser grains, indicating a link between elevated bottom currents and intervals of higher HU's. This observation is confirmed by the co-variation of the Zr/Al ratio, a measure for bottom current strength, and higher HU's within the cores of mounded drift systems. A continuous increase in average HU's and inferred bottom current velocities could be observed in the 5 cores, going from sheeted to mounded drifts and eventually towards the abrasive surface. This research gives an onset towards the analysis of contourite cores using CT and indicates how intervals of elevated bottom currents may be detected. Despite imperfections and the requirement of additional research, promising results have been obtained that could allow the detection of diagnostic criteria for discerning contourite intervals.

Keywords: Computed Tomography, contourites, correlation coefficient, grainsize, bottom currents

Contribution: The sediment cores have been acquired by several Spanish teams (Montera, Sagas and Contouriber), while the MSCL, XRF and texture data have been acquired by two Spanish labs (IGME, CSIC). The CT scans have been acquired and processed by TV, JG and ID. The chapter has been written by TV and revised by DVR, VC and SL.

1. Introduction

Discerning a contouritic from a turbiditic facies within sediment cores has been proven difficult in many cases (Shanmugam, 2000), especially as bottom currents may induce bottom current reworked sands (Mutti and Carminati, 2012; Shanmugam, 2012) or mixed turbidite-contourite facies (Llave et al., 2007; Hernández-Molina et al., 2009; Brackenridge et al., 2013). The facies model of Faugères and Stow (2008), based on the initial model by Faugères et al. (1984) and Gonthier et al. (1984), is solely based on sedimentological data derived from sediment cores and does not take into account other research methods, such as X-ray computed tomography (CT). However, CT data from contourite sediment cores may aid in the characterization of contourites and in the differentiation between contourite and turbidite facies. Two approaches may be applied when it comes to CT scans: a descriptive (visual) and a quantitative (analytical) approach. The former has already been applied in several contourite studies (Lucchi et al., 2002; Mulder et al., 2013; Rebesco et al., 2013; Hanebuth et al., 2015), while the latter is still in full development. Mena et al. (2015), for example, used ranges of Hounsfield units (HU) to distinguish between pelagic, hemipelagic, contouritic, turbiditic and ice-rafted debris layers. Similarly, this study focusses on the **quantitative analysis** of **CT scans** from several sediment cores in order to identify the **contourite intervals** within those cores. Consequently, a **workflow** will be created which will allow **future cores to be analysed in a similar way** (uniform workflow) and **aid in the recognition of contourite intervals**. In order to be able to characterize contourite sequences based on CT-scans, sediment cores from various contourite drifts are required, originating from different morphological and sedimentological settings. This is to make sure that a broad range of contourite facies of varying grainsizes are present within the dataset.
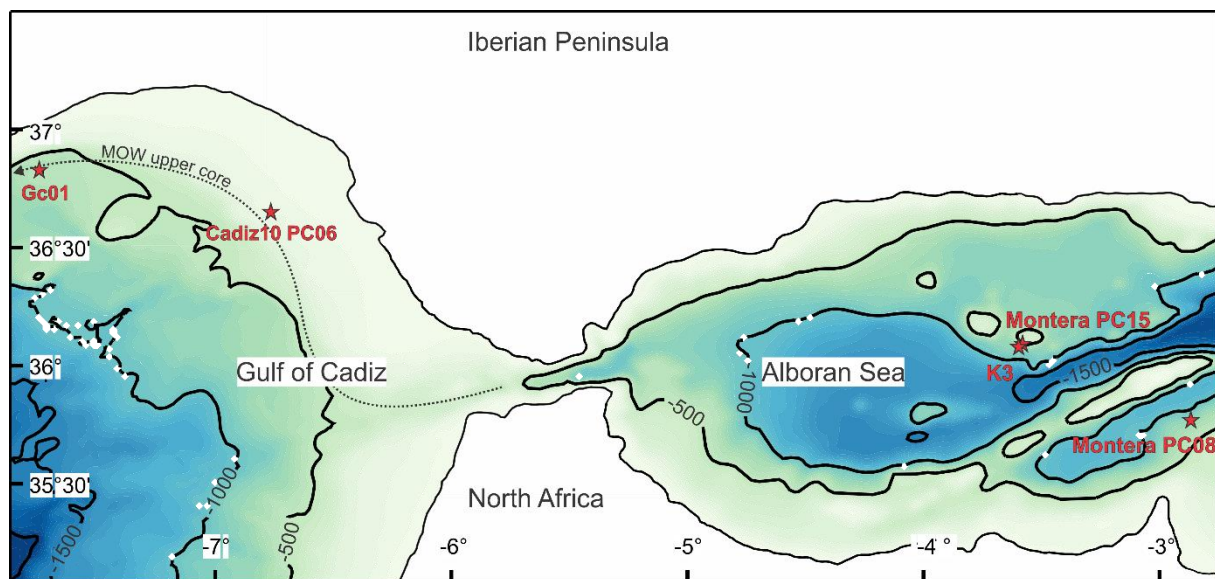
Figure 7.1: Location of the 5 investigated cores. The pathway of the MOW upper core is indicated and corresponds to Figure 2.4.

Five sediment cores are studied for this purpose (Table 7.1), three originate from the Alboran Sea and two from the Gulf of Cádiz. In the Alboran Sea (Figure 7.1), two cores were acquired from the Djibouti confined drift (Palomino et al., 2011): core Sagas K3 (hereafter called K3) from the mounded part of the contourite drift and core MONTERA PC15 (hereafter called M15) from the moat of this drift system. The Djibouti confined drift is located south of the Djibouti Ville seamount (Palomino et al., 2011) and is part of what could be called the Djibouti CDS. Both cores from this drift contain muddy to silty mud contourites; core M15 contains coarser grains (moat) compared to core K3 (mounded part). One core (MONTERA PC08; hereafter called M08) is acquired from the Tres Forcas sheeted elongated drift within

the Alboran Sea (Ercilla et al., 2016). The Tres Forcas sheeted elongated drift is located south of the Alboran ridge and is composed of muddy contourites (Vázquez and Alonso, 2012).

From the Gulf of Cádiz, two cores were analysed; core Cadiz10_PC06 (hereafter called C06) originates from the abrasive surfaces within the proximal scour and ribbons sector (Hernández-Molina et al., 2011) and is composed of coarse-grained lithologies, while core GC01 originates from the Cádiz-Albufeira drift system (Llave et al., 2001, 2007). The Cádiz-Albufeira drift is an elongated mounded drift that consists of an incisive moat (Alvarez Cabral moat) and a distinct mounded drift part (Llave et al., 2001). Within core GC01, three contourite sequences have been determined, one of which in the core's trigger (Anton et al., 2012; Lebreiro et al., 2015). Their origin is ascribed to changes in the MOW, related to the palaeoceanographic and climatic changes on a millennial scale.

These five cores make sure that several drift morphologies (confined, elongated mounded and sheeted) and lithologies (sandy, silty and muddy contourites) are represented within the dataset as well as different settings within one contourite drift (moat versus mounded part in the Djibouti contourite drift). Additionally, core C06 allows comparing a core from mainly erosive areas with cores from mainly depositional areas. The metadata of all five cores can be found in Table 7.1.

Core	Latitude	Longitude	Length	Analyses	Water depth	Main references
Cadiz10_PC06 (**C06**)	36° 18.27'N	6° 45.86'W	2.4m	XRF, GS, CT	489 m	(Hernández-Molina, 2010)
GC01 (**GC01**)	36° 49.63'N	7° 44.71'W	5.2m	XRF, MSCL, CT	566 m	(Lebreiro et al., 2015) (Anton et al., 2012)
Sagas K3 (**K3**)	36° 04.94'N	3° 35.59'W	4.5m	XRF, GS, CT	712 m	(Palomino et al., 2011) (Alonso, 2010)
Montera_PC08 (**M08**)	35° 46.10'N	2° 52.05'W	6.3m	XRF, MSCL, CT	753 m	(Alonso et al., 2014) (Vázquez and Alonso, 2012)
Montera_PC15 (**M15**)	36° 05.43'N	3° 34.81'W	5.9m	XRF, MSCL, CT	763 m	(Palomino et al., 2011) (Alonso et al., 2014)

Table 7.1: Metadata of the 5 investigated cores. Their short name (used throughout this chapter) is indicated in bold. XRF: X-ray fluorescence; MSCL: multi-sensor core logger; GS: grainsize.

2. Material and methods

The five cores were analyzed using XRF and grain-size analyses and measurements using a MSCL were performed (Table 7.1). All cores were scanned using the Avaatech XRF scanner at a resolution of 1 cm and the sediment surface was covered with an ultralene film to avoid contamination. Except for C06 (where only 10 keV was used), all cores were scanned at both 10 and 30 keV. Core GC01 has was scanned at IGME Madrid (Instituto Geológico y Minero de España), while the other 4 cores were scanned at CSIC (Consejo Superior de Investigaciones Cientificas) in Barcelona. As for the MSCL, cores GC01, M08 and M15 were logged at an interval of 1 cm with the MS and gamma density sensors. M08 and M15 were logged on board of the R/V Sarmiento de Gamboa, while GC01 was logged at IGME Madrid.

Grain-size measurements were performed on cores C06 (using the Malvern Mastersizer) and core K3 (using the Coulter LS 100 laser). For Core C06, samples (10 cm^3) were taken every 2 cm and the organic matter was removed using a 30% H_2O_2-solution for 0.5-2 hours, depending on the amount of organic matter. After the removal of the organic content, a 0.6% sodium hexametaphosphate (calgon) solution was added and the sample was put into an ultrasonic bath for 10 min in order to avoid flocculation of the finer particles and keep them in suspension. For core K3, samples of ±0.5 grams were taken on average every 7 cm and pre-treated for 1 day with a 50 ml 1M chloridic acid solution in order to remove the carbonate fraction and with a H_2O_2-solution in order to remove the organic matter. The chloridic acid was removed using a centrifuge at 5000 rpm for 3 minutes. Eventually, a 2.5% sodium

hexametaphosphate solution was added to the sample and it was put into an ultrasonic bath to avoid flocculation and keep the finer particles in suspension.

All five cores (totalling over 24 m of sediment) were scanned using the SOMATON definition flash scanner of the Ghent University hospital. A 120 kV step and rotation time of 1 second resulting in an x and y-resolution of 0.2 mm and z-resolution of 0.6 mm were set and the images were reconstructed using the "J37s medium smooth" algorithm. The analytical software package Octopus Analysis (formerly Morpho+; Brabant et al., 2011) from the Centre for X-ray Tomography of Ghent University was used in order to discern different components based on the grey-values histogram. The grey values (expressed in HU) are related to the X-ray attenuation coefficient, a measure for changes in density and average atomic number (Cnudde and Boon, 2013).

3. CT workflow

For every core (combining all slices from that core) the frequency distribution of a certain HU value was established (Figure 7.2B). Based on this distribution, single-threshold components were differentiated based on the maxima present in the distribution with their boundaries determined by the minima in between the components (Figure 7.2B).
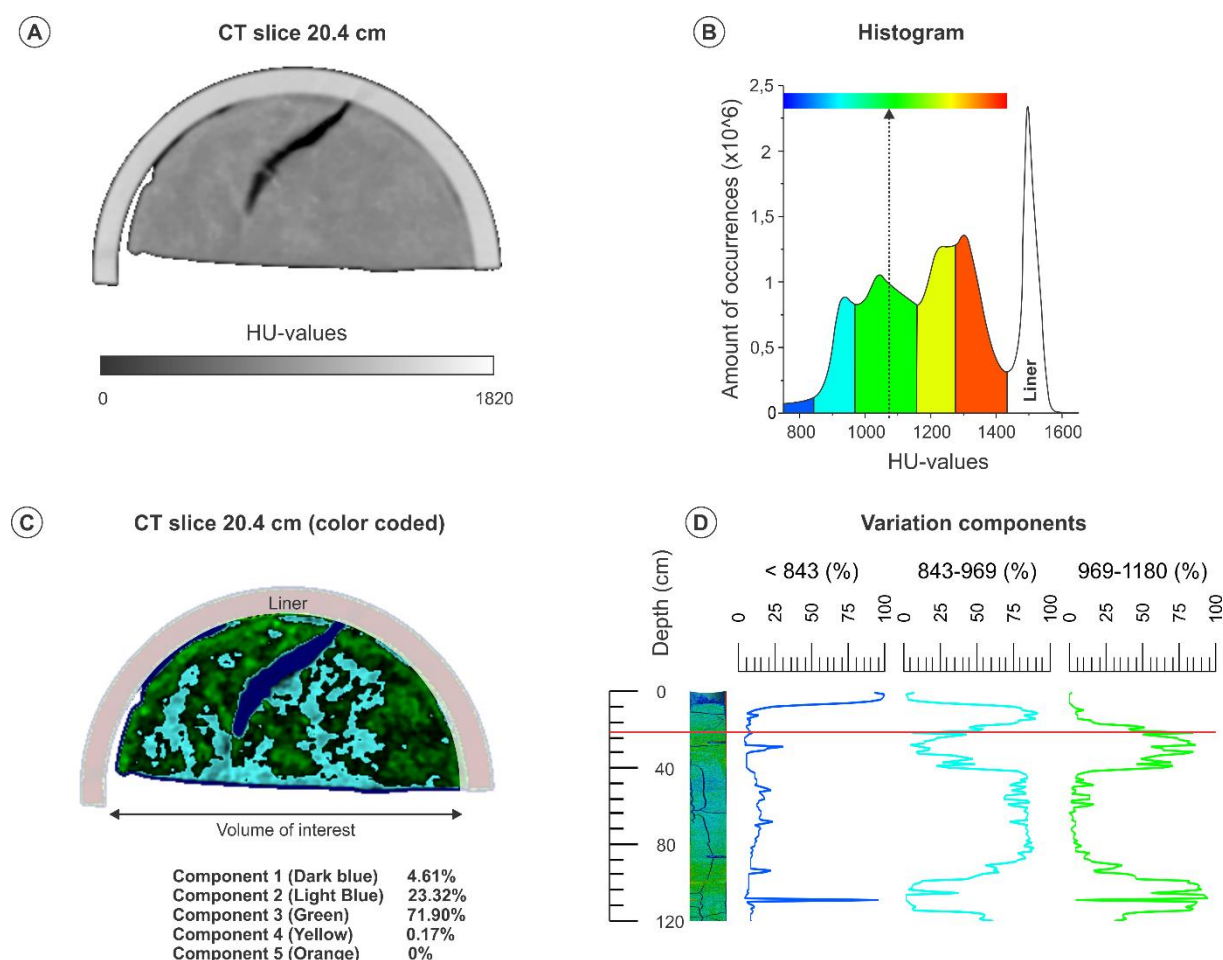
Figure 7.2: Overview of the CT workflow. In this example, the slice at 20.4 cm of core K3 has been used. A. The original slice displayed in grey values (HU). B. Frequency distribution of HU of core K3 with indication of the identified components based on the hinge points in the plot. The black dotted arrow indicates the colour of the component between 969 HU and 1180 HU. C. The slice at 20.4 cm colour coded based on the frequency distribution and indication of percentages of the components within that slice. The lin er has been made transparent and is not considered to calculate the percentages of each component. D. Overview of three components within the upper 120 cm of core K3. The red line indicates the position of the slice visualized in part A and C.

Single thresholding is a technique to delimit components in a histogram by applying one strict lower and upper boundary, whereas dual thresholding would allow to define a second interval that, if connected to the first interval, would be implemented in calculations regarding that component (Hannah et al., 1995; Figure 7.3B, C). Although single thresholding does not consider the outer limits of the component (Figure 7.3A, B); i.e. it cuts away the percentages belonging to the lowest and highest HU values; and consequently induces a small error, this method is still preferred as dual thresholding would induce overlap between the components and the cumulative percentages of each slice would surpass 100%. To assess, the extent of this error, a Gaussian distribution has been fitted to the different components. This indicates that the components always contain between 1 and 3 standard deviations of the distribution, meaning they capture between 68% and 95.3% of the Gaussian curve (Figure 7.3B). With always more than 75% of the Gaussian distribution captured, the errors remain acceptably low and the general pattern will not be obscured because of single thresholding. Also the low resolution of the medical scanner (0.2x0.2x0.6 mm) may induce a small error as multiple voxels, that contain sediments belonging to two components, will have an averaged HU-value and may thus create smoothened histograms (Figure 7.2B) which possibly obscure smaller components.
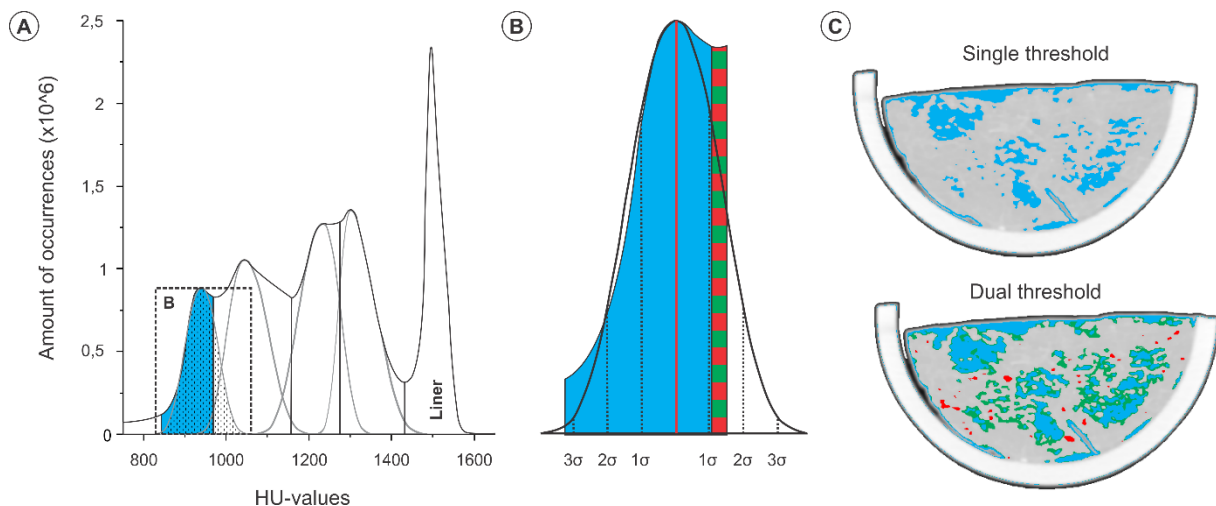
Figure 7.3: A. Gaussian curves of the different components. The Gaussian distribution of the light blue component of core K3 is dotted. B. Enlargement of the light blue component and the plots of three standard deviations of its Gaussian curve. The green-red part indicates the added part if dual thresholding would be applied. The limits for the this component are 969-987. C. Example of a slice in the upper part of core K3 indicating the single and dual threshold limits. For the dual threshold, the red regions would be rejected as they are not connected to the light blue component, the green ones would be considered.

The image displayed in Figure 7.2D and Figures 7.4 to 7.8 are created by applying an artificial rainbow colour scale between two bounding values (blue, 725 HU to red, 1435 HU; Figure 7.2B). The bounding values have been determined based on the histograms of the 5 cores and correspond to the overall lowest and highest values (Table 7.3). The image visualizes sharp boundaries, characterized by large discrepant values of HU and consequently completely different colours. Based on this colour scale, the colours of the different components (used in Figure 7.2D and Figures 7.4 to 7.8) were determined; i.e. the colour corresponding to the middle HU value of that component. For example, the green component of core K3 is bounded by 969 HU and 1180 HU, meaning that the colour is determined by the middle value (1074.5 HU), visualized by the black dotted arrow in Figure 7.2B.

The components are isolated and quantified in comparison to the total volume of interest (sediment without the liner) for each slice (Figure 7.2C). By considering all slices, the percentages of the components are obtained throughout the core (Figure 7.2D). The variation of the components is compared to selected MSCL, XRF and grain-size data by calculating a correlation matrix using principal

component analysis. This last step is executed using "SPSS Statistics 24". Which proxies are considered is determined based on several studies (Table 7.2). Depending on the focus of the study, other proxies may be used (Rothwell and Rack, 2006; Rothwell and Croudace, 2015).

Proxy	Application	References
Fe/Al	Anoxic bottom waters	Spofforth et al. (2008)
Ca/Fe	Terrigenous input variability	Nizou et al. (2011)
Ti/Al	Aeolian input variability	Jiménez-Espejo et al. (2007)
Al/Ca	Terrigenous input variability	Nizou et al. (2011)
Si/Ti	Biogenic silica variability	Agnihotri et al. (2008)
Ti/Ca	Terrigenous input variability	Tjallingii et al. (2010); Henrich et al. (2010)
S/Cl	Organic matter variability	Thomson et al. (2006)
Zr/Al	Bottom current intensity	Bahr et al. (2014)
Gamma Density	Sediment bulk density	Schultheiss and Weaver (1992)
MS	Glacial/Interglacial cycles	Rothwell and Rack (2006)
Grainsize	Sedimentary processes, sorting	McCave et al. (1995)
Sortable Silt	Paleo-current strength	McCave et al. (1995)

Table 7.2: Overview of the MSCL and XRF proxies used in this study to compare the CT-components to (Table 7.4). This list is not exhaustive, but merely sums up important proxies regarding contourites. Ti/Ca, for example, can also be used for delineating variations in ice-rafted debris input (Lebreiro et al., 2009), but is not included in the table.

4. Results

4.1. CT components & intervals

The components of all cores have been determined in a similar way as for core K3 (Figure 7.2). As a result, core C06 has 3, cores M08 and M15 have 4 and cores GC01 and K3 have 5 components (Table 7.3). By analysing the distribution of the components throughout the core, several intervals can be discerned (Figures 7.4 to 7.8).

Core	Component 1	Component 2	Component 3	Component 4	Component 5	Liner
C06	0 – 1166	1166 – 1256	1256 – 1420			1200
GC01	0 – 1040	1040 – 1174	1174 – 1231	1231 – 1315	1315 – 1429	1175 & 1575
K3	0 – 843	843 – 969	969 – 1180	1180 – 1275	1275 – **1435**	1500
M08	0 – **725**	725 – 850	850 – 1010	1010 – 1108		1150
M15	0 – 800	800 – 1036	1036 – 1120	1120 – 1234		1150

Table 7.3: Bounding HU of the different components (columns 2-6) and the main HU value (column 7) of their liners. The bold values indicate the bounding values of the rainbow colour scale (Figure 7.2B)

Overall, core C06 contains the highest HU of the five cores analysed (resulting in mostly red to orange colours when artificially coloured; Figure 7.4) and can roughly be divided into 3 intervals: bottom to 156 cm, containing very high HU (1256 – 1420 HU and > 1420 HU); 156 cm – 100 cm, containing mostly lower HU (light and dark blue component; below 1256 HU) and 100 cm – top, containing high HU(1256-1420 HU). At 156 cm, a sharp transition between two intervals is present (Figure 7.4).

Core GC01 contains moderate to high HU (resulting in mostly green and red artificial colours; Figure 7.5) and consists of several intervals with higher HU's: 420 – 370 cm, 315 – 290 cm, 175 - 150 cm and 100 – 40 cm. The latter two contain the highest HU value (over 1315 HU) and both have a sharp lower boundary (Figure 7.5).

K3 mainly consists of low to moderate HU's (resulting in light blue and green artificial colours; Figure 7.6) and one interval (242 – 208 cm) contains higher HU's (over 1180 HU; yellow and orange component) and has a fairly sharp upper boundary. The rest of the cores is composed of variations of the light blue and green artificially coloured component (Figure 7.6).

Core M08 is composed of sediment with the lowest HU's of all five cores (resulting in mostly dark and light blue artificial colours; Figure 7.7) with values usually below 1010 HU. Three big intervals can be discerned: bottom to 290 cm with varying percentages of the light blue and green component, 250 – 120 cm with mostly green and some yellow component and 120 cm – top with mainly the dark blue component. The transition between the latter two intervals is very sharp (Figure 7.7).

Core M15 is composed of sediments characterized by average HU's (resulting in overall greenish artificial colours; Figure 7.8) and contains four intervals with higher HU's: bottom – 550 cm, 405 – 376 cm; 290 – 270 cm and 125 cm – top. One interval is characterized by a fairly sharp upper boundary (376 cm; Figure 7.8).

4.2. Correlation matrix

Plotting all proxies next to the components on one figure would render the figure impossible to interpret. As a consequence, the correlation coefficients between a proxy and the CT components have been calculated. This is a measure for the covariation of both curves and can indicate whether a certain proxy might be related to that component or not. The matrix, containing all the correlation coefficients between the components of the five cores and selected proxies (Table 7.2), is displayed in Table 7.4. Based on this matrix, some proxies have been plotted on Figures 7.4 to 7.8. Except for C06, the Zr/Al ratio for all cores has been plotted as this proxy indicates variations in bottom current strength (Bahr et al., 2014), one of the most important factors for recognizing contourites.

Core C06 contains many strong (anti-) correlations, especially with grain-size fractions (Table 7.4). The two components with the lowest HU's show strong correlations with the clay and silt fractions: between 0.57 (sortable silt) and 0.73 (clay) and very strong anti-correlations with the sand fractions: between -0.51 (fine sand) and -0.64 (very fine sand). The opposite is noticed for the third component (1256 - 1420 HU): strong anti-correlations with the clay and silt fractions: either -0.82 (clay) or -0.81 (silt and sortable silt) and strong correlations with the sand fractions; between 0.50 and 0.76. Some strong correlations with XRF-proxies are observed, but they are less pronounced compared to the grain-size fractions. As a consequence, the mean grain size has been plotted in Figure 7.4.

Core GC01 has some strong (anti-) correlations between the high HU-component (orange) and several XRF-proxies, while component 2 (green) has a strong correlation with Ti/Ca and anti-correlation with Ca/Fe. As a result, the latter two proxies have been plotted in Figure 7.5.

Core K3 indicates few strong (anti-) correlations (Table 7.4). The yellow and orange component have fairly strong correlations (0.41 and 0.45 respectively) with the percentage of sand and consequently, the mean grain size has been plotted on Figure 7.6.

M08 displays numerous (anti-)correlations of the low HU component (dark blue) with many XRF-proxies, including a strong anti-correlation (-0.69) with Si/Ti. This component also has a strong anti-correlation with gamma density and a strong correlation with MS (-0.78 and 0.59 respectively). The light blue component (850 – 1010 HU) indicates a strong correlation with gamma density. Therefore, gamma density has been plotted on Figure 7.7.

The two components with the lowest HU's of core M15 have very strong (anti-) correlations with gamma density, while the component between 1036 and 1120 HU shows a very strong correlation (0.69). Consequently, gamma density has been plotted on Figure 7.8. For all XRF-proxies, very low coefficients (close to 0) are observed (Table 7.4).

Figure 7.4: Overview image for core C06 displaying from left to right the artificially coloured CT image, the grainsize distribution and the variation of the CT components throughout the core. The small black arrow on the left indicates a sharp boundary between intervals. The grey intervals refer those discussed in the text. Horizontal black dotted lines denote section boundaries.

Figure 7.5: Overview image for core GC01 displaying from left to right the artificial coloured CT image the ratios of Zr/Al, Ti/Ca and Ca/Fe and the variation of the CT components throughout the core. The grey intervals are those discussed in the text and the black dotted intervals the contourite sequences determined by Anton et al. (2012). Horizontal black dotted lines denote section boundaries.
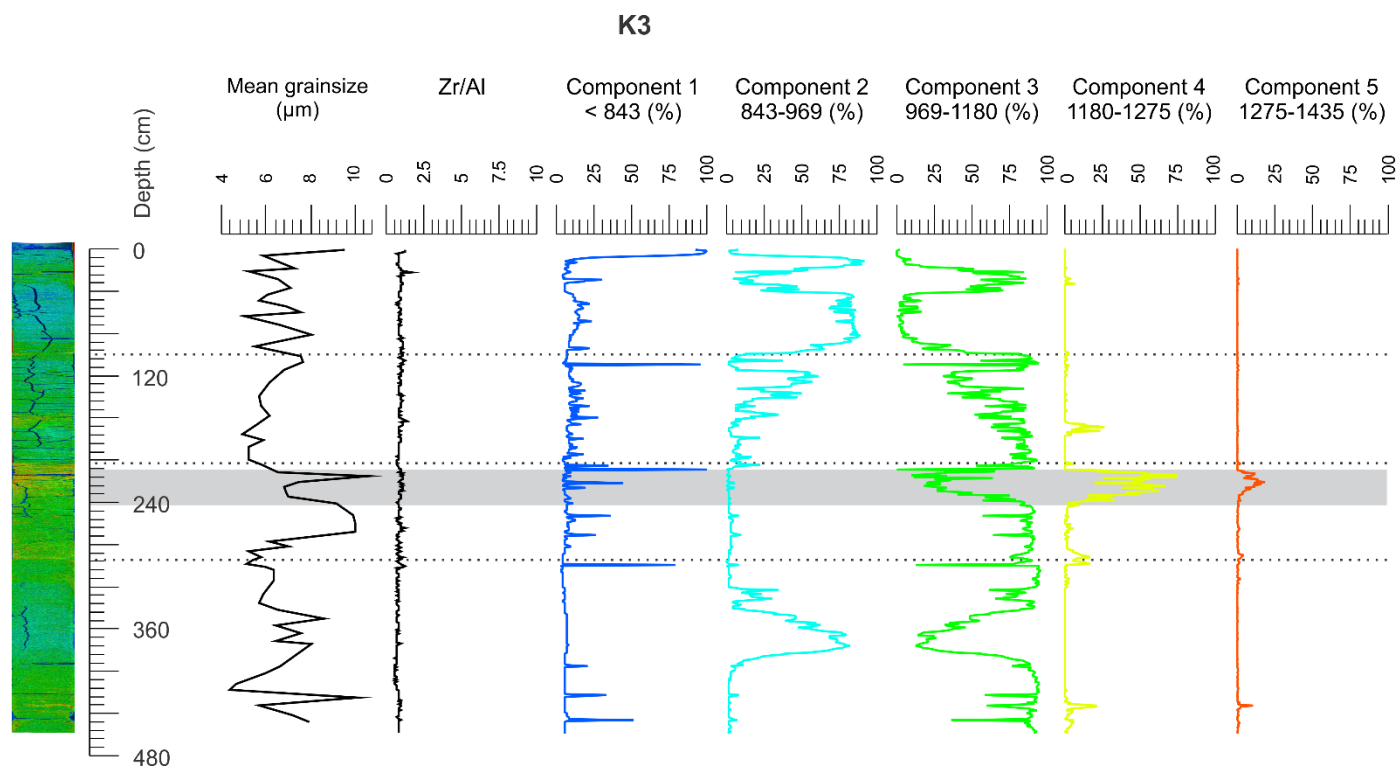
Figure 7.6: Overview image for core K3 displaying from left to right the artificial coloured CT image, the grainsize distribution (terrigenous fraction), ratio of Zr/Al and the variation of the CT components throughout the core. The grey intervals are those discussed in the text. Horizontal black dotted lines denote section boundaries.

Figure 7.7: Overview image for core M08 displaying from left to right the artificial coloured CT image, the ratio Zr/Al, the variation of gamma density (Den) and the CT components throughout the core. The grey intervals are those discussed in the text. Horizontal black dotted lines denote section boundaries.
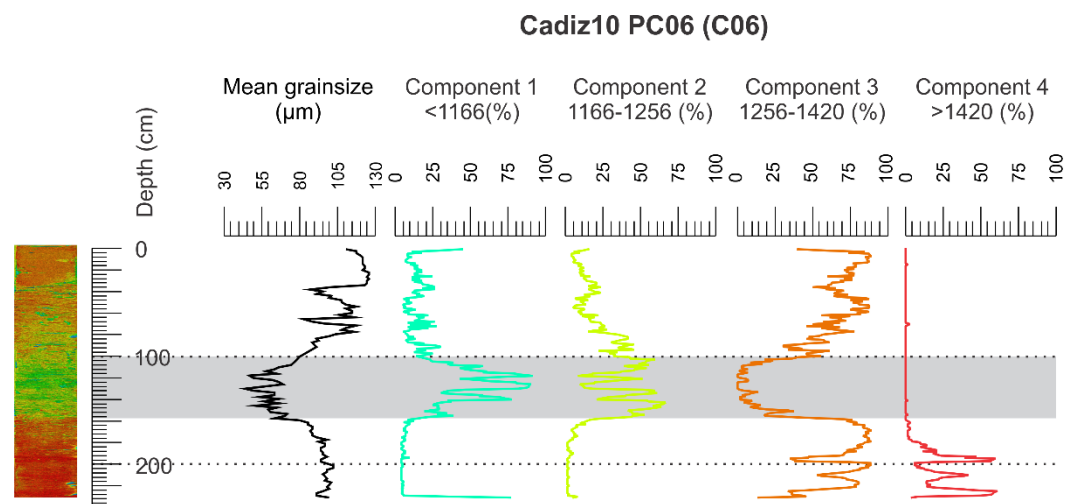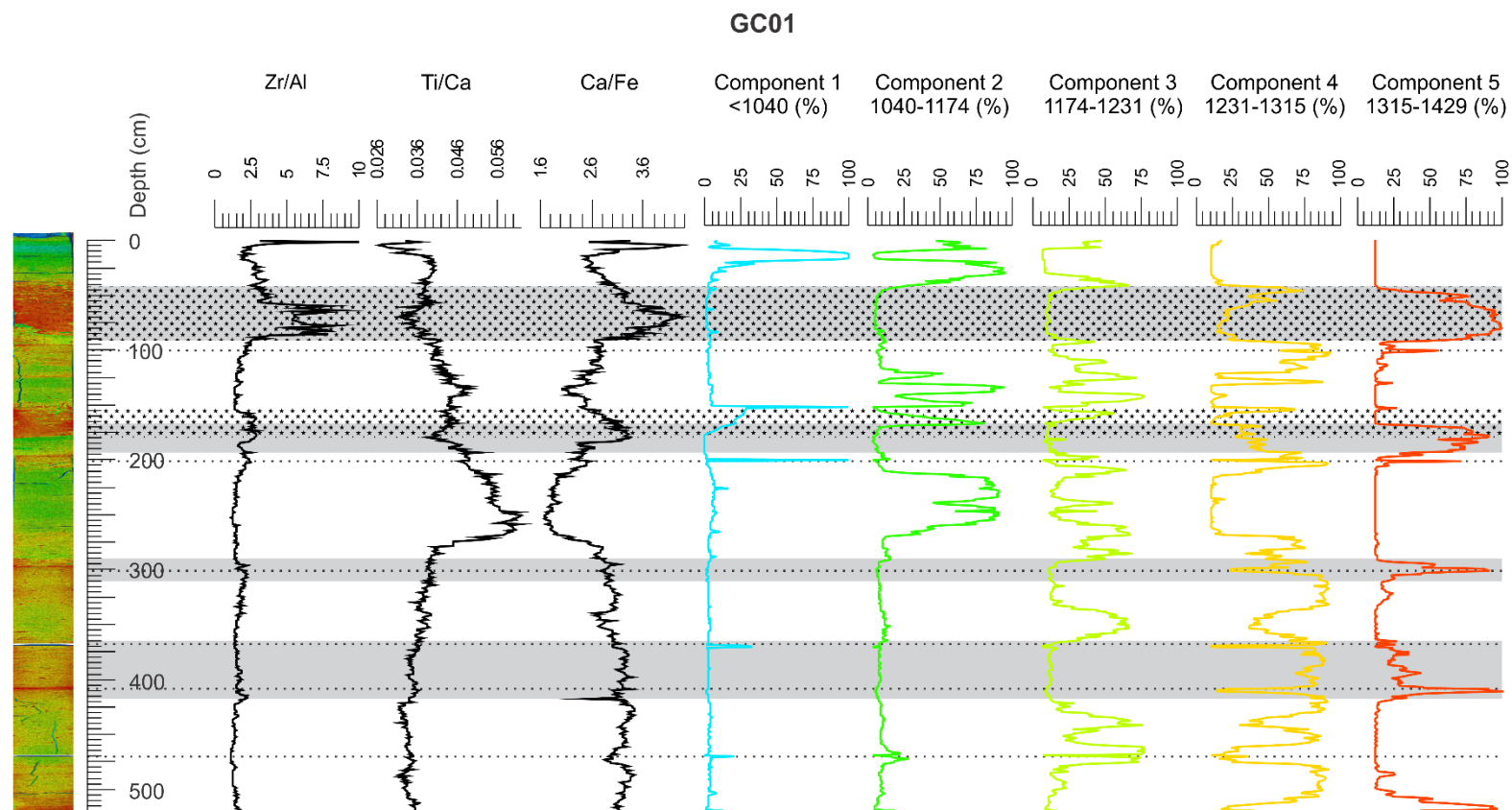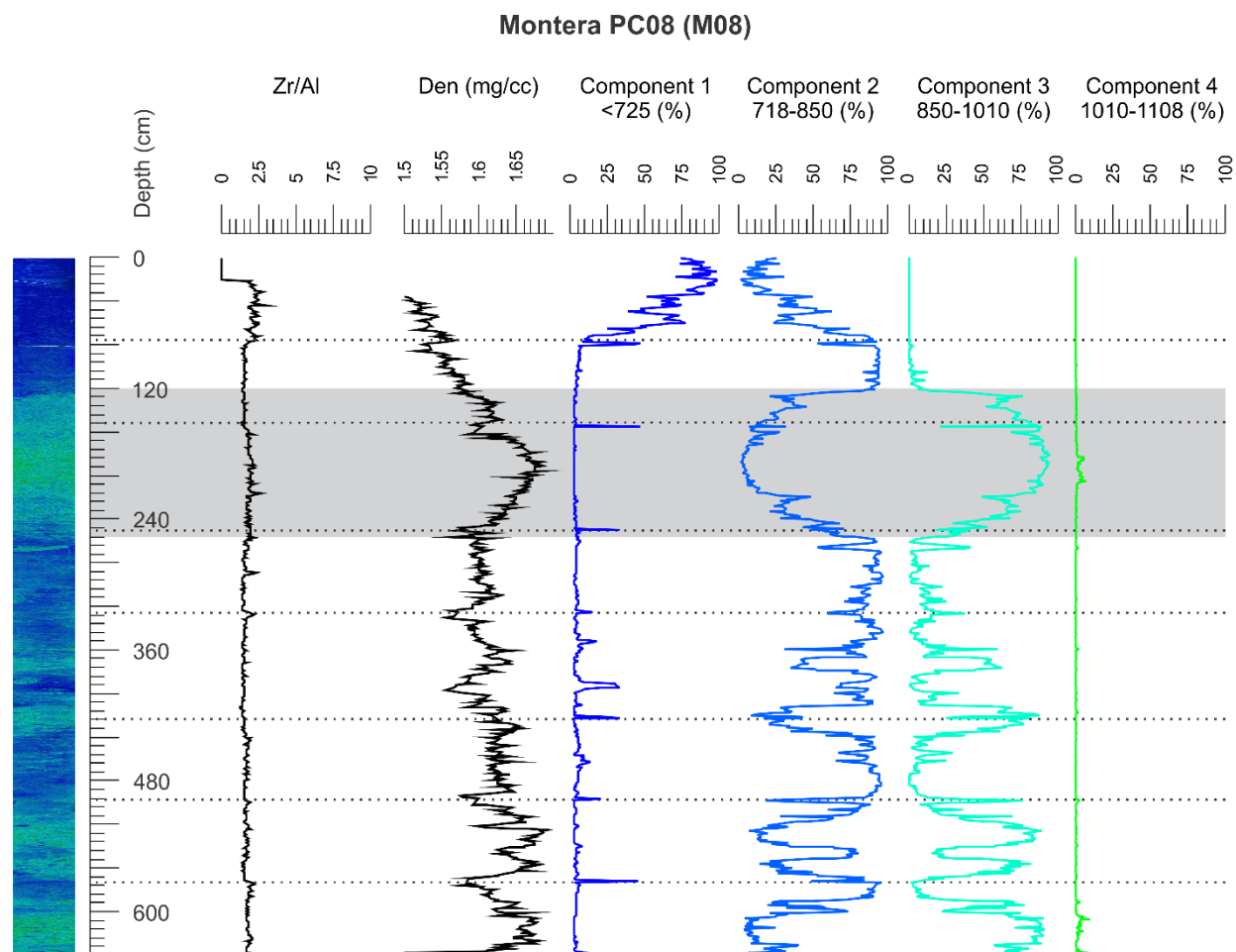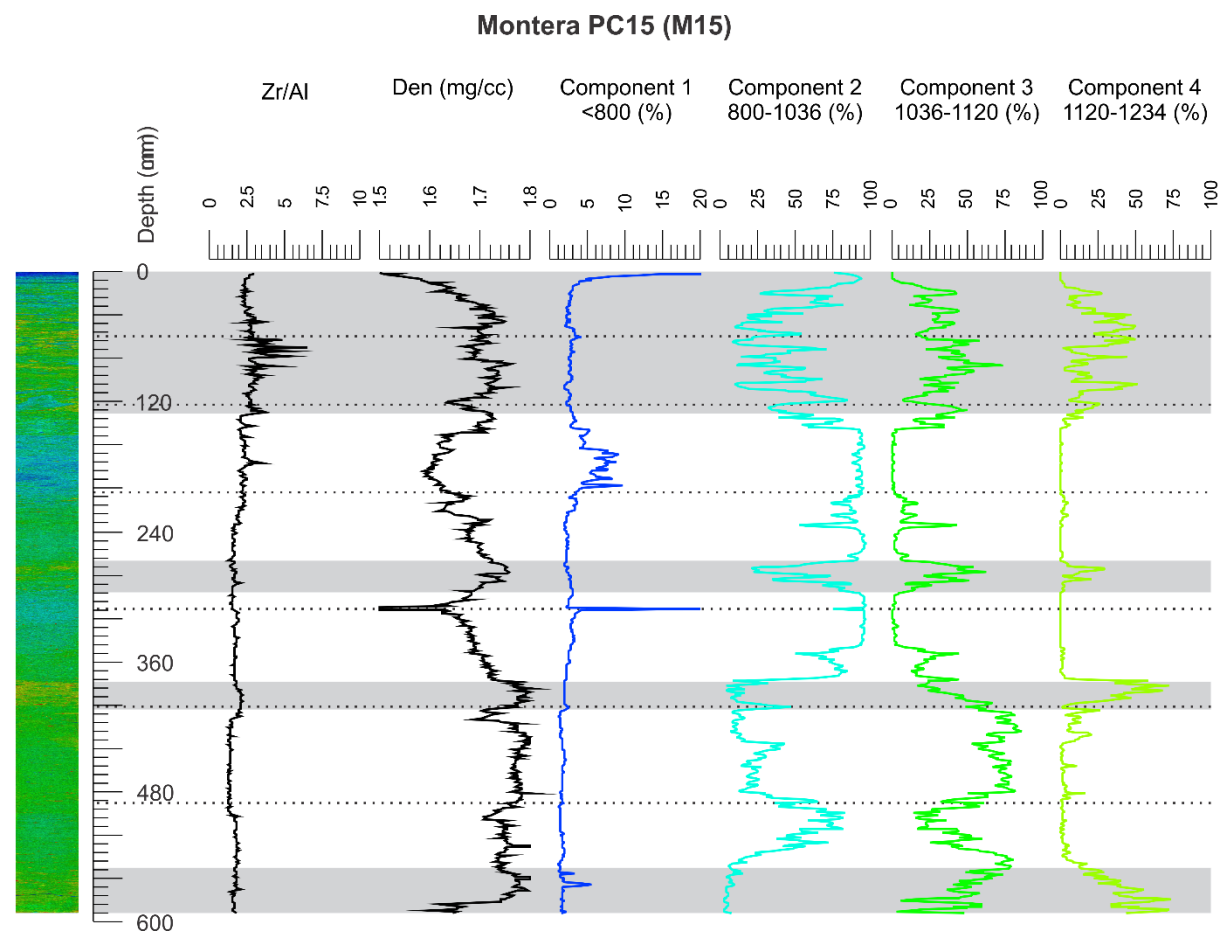
Figure 7.8: Overview image for core M15 displaying from left to right the artificially coloured CT image, the ratio Zr/Al and the variation in both gamma density (Den) and the CT components throughout the core. The grey intervals are those discussed in the results and/or discussion section. Horizontal black dotted lines denote section boundaries.

Core	C06				GC01					K3					M08				M15			
Component	<1165	1165-1256	1256-1420	>1420	<1040	1040-1174	1174-1231	1231-1315	1315-1429	<843	843-969	969-1180	1180-1275	1275-1435	<725	718-850	850-1010	1010-1108	<800	800-1036	1036-1120	1120-1234
Fe/Al	-0.10	-0.22	0.17	0.08	0.22	0.18	-0.21	-0.42	0.32	0.31	0.19	-0.36	0.13	0.01	0.48	-0.06	-0.22	-0.08	0.21	-0.07	-0.04	0.17
Ca/Fe	-0.36	-0.24	0.48	-0.18	-0.13	-0.54	-0.28	0.26	0.50	-0.29	-0.28	0.39	0.17	0.16	-0.18	-0.38	0.46	0.32	0.18	0.26	-0.28	-0.08
Ti/Al	-0.27	-0.41	0.37	0.16	0.10	0.05	-0.28	-0.39	0.54	0.32	0.19	-0.37	0.08	0.06	0.45	-0.14	-0.13	0.00	0.26	-0.09	-0.05	0.22
Al/Ca	0.50	0.49	-0.65	-0.01	-0.10	0.38	0.30	-0.10	-0.47	0.23	0.34	-0.35	-0.27	-0.25	-0.46	0.45	-0.16	-0.19	0.31	-0.08	-0.16	0.34
Si/Ti	-0.13	-0.08	0.23	-0.20	-0.25	-0.31	0.20	0.42	-0.20	-0.32	-0.24	0.41	-0.04	-0.02	-0.69	0.10	0.30	0.14	-0.28	-0.07	0.33	-0.32
Ti/Ca	0.24	0.07	-0.33	0.26	0.01	0.60	0.11	-0.44	-0.44	0.31	0.39	-0.46	-0.22	-0.21	-0.18	0.40	-0.27	-0.22	0.31	-0.08	-0.16	0.34
S/Cl	0.47	0.51	-0.60	-0.10						-0.02	-0.16	0.04	-0.07	-0.05	-0.20	0.05	0.07	0.05	0.31	-0.08	-0.15	0.34
Zr/Al					-0.01	-0.09	-0.28	-0.27	0.63	0.25	0.02	-0.28	0.26	0.21	0.33	-0.33	0.12	0.19	0.32	-0.06	-0.13	0.28
Gamma Den.					-0.35	-0.35	-0.12	0.17	0.44						-0.78	-0.24	0.69	0.38	-0.70	-0.64	0.69	0.24
Magn. Susc.					-0.17	0.00	0.23	0.03	-0.11						0.59	-0.06	-0.29	-0.20	-0.60	-0.36	0.42	0.10
%clay	0.73	0.64	-0.82	-0.20						-0.01	-0.21	0.17	-0.07	-0.10								
%silt	0.71	0.60	-0.81	-0.12						0.05	0.32	-0.25	-0.14	-0.13								
% vf sand	-0.64	-0.60	0.65	0.36																		
% fine sand	-0.64	-0.51	0.76	-0.01						-0.06	-0.17	0.11	0.41	0.45								
% m sand	-0.39	-0.27	0.50	-0.13																		
% sort. silt	0.70	0.57	-0.81	-0.07						0.02	0.05	-0.05	0.03	0.04								

Table 7.4: Overview of the correlations coefficients of the different cores and their components with the other proxy (XRF, MSCL and texture). Gamma Den. = Gamma Density. Magn. Susc. = magnetic susceptibility; vf sand = very fine sand; m sand= medium sand; sort. Silt = sortable silt.

5. Discussion

5.1. Geological significance of the correlation matrix

Caution has to be taken when interpreting the correlation coefficients from Table 7.4 as spurious correlations may arise. Spurious correlations are a side-effect of compositional data analysis (Pawlowsky-Glahn and Buccianti, 2011) and some might be present in the correlation matrix. As a consequence, the geological significance of the correlations should always be verified.

The highest correlation coefficients within the matrix occur between components of core C06 and the grain-size data (Table 7.4). Plotting the mean grain size of this core on Figure 7.4 shows that coarser grains are related to the high HU-interval (1256 - 1420 HU) and finer grains to low HU-intervals (<1166 HU and 1166 HU – 1256 HU). Consequently, low correlation coefficients are expected between clay and silt and the high HU-component (1256 – 1420 HU). The correlation matrix indeed indicates these low correlation coefficients (respectively -0.82 and -0.81; Table 7.4). This observation indicates that these coefficients of the correlation matrix are reliable and can be used for further deductions.

If the discerned components reflect geological changes, a consistent change between two proxies indicating the same geological parameter can be expected. Both Al/Ca and Ti/Ca can be used to infer changes in terrigenous input (Henrich et al., 2010; Tjallingii et al., 2010; Nizou et al., 2011) and their correlation coefficients indeed change consistently for each core (a similar trend can be observed; Figure 7.9). Ti/Al can be used to infer changes in aeolian input (Jiménez-Espejo et al., 2007; Jullien et al., 2007; Ziegler et al., 2010), which is regarded as a part of the terrigenous input. This proxy shows a far less consistent variation, especially for cores M08, GC01 and C06. The consistent variation of Ti/Ca, Al/Ca and Ti/Al in cores K3 and M15 (both from the Djibouti confined mounded drift; Figure 7.1) might indicate that in the northern Alboran Sea, aeolian input is an important factor contributing to the terrigenous input (as observed by Goudie and Middleton, 2001; Moreno et al., 2002 and Becker et al., 2005), while in the Gulf of Cádiz and southern Alboran Sea (Figure 7.1) this could be less the case. Caution has to be taken with this interpretation because if aeolian input is inferred in the northern Alboran Sea (which would be mostly originating from Sahara dust; Avila et al. (1997) and Rodríguez et al. (2001)), similar observations would be expected in the southern Alboran basin, which is located even closer to the source area.

The aforementioned examples indicate that the correlation coefficients of Table 7.4 are most likely reliable and can be used for further considerations.
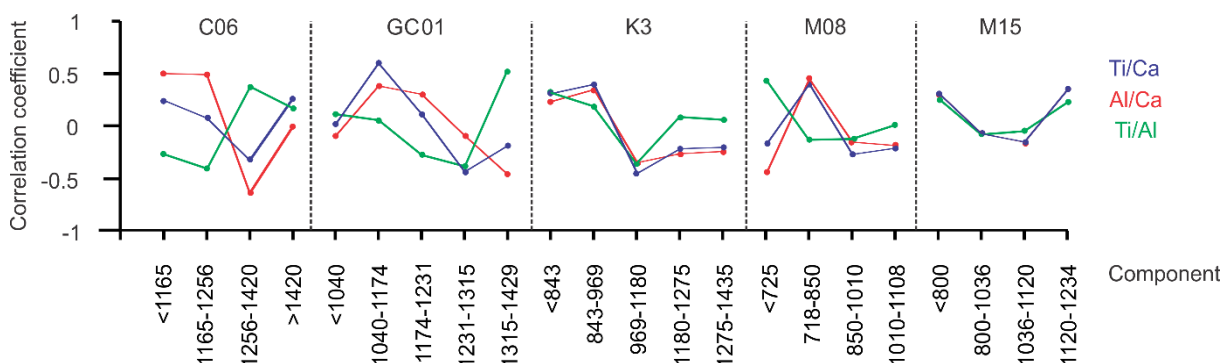

Figure 7.9: Variation of the correlation coefficients of Ti/Ca, Ti/Al and Al/Ca for the five cores. The Al/Ca of M15 is hidden below the Ti/Ca curve.

5.2. Bottom current strength and contourites

As indicated above, higher HU's are related to coarser grain sizes and vice versa for core C06. As the core is located in the pathway of the MOW upper core (Figure 7.1), the changes in prevailing high HU component could indicate changes in the strength of the MOW upper core, a phenomenon described by many authors (e.g. Cacho et al., 2000; Rogerson et al., 2012; Kaboth et al., 2016; Lofi et al., 2016). The CT scans can provide additional information on this change as the lower boundary of the interval containing finer grains (grey band in Figure 7.4) is rather abrupt, while the upper boundary is rather smooth, which may indicate that the decline of MOW strength was rather abrupt, while its increase in velocity was a more gradual process.

Grain-size data are not available for GC01, but a direct link between the Zr/Al ratio and the high HU component (1315 – 1429 HU) is observed (Figure 7.5). Bottom currents are known to increase the Zr/Al ratio, representing the relative enrichment in heavy minerals like zircon (Bahr et al., 2014), in sediments. The relatively high atomic number of Zr (40) will cause higher X-ray attenuation coefficients (Figure 7.10); the average atomic number is the most important factor controlling the Xac (Cnudde and Boone, 2013); and consequently also higher HU values. This indicates that increased percentages of the high HU-components can indeed indicate periods of elevated bottom currents. The two upper intervals of high HU and Zr/Al ratio (190 – 150 cm and 85 – 35 cm) of core GC01 almost perfectly correspond to the two contourite sequences within that core (Anton et al., 2012), furthermore strengthening the hypothesis of the link between HU and bottom currents speed. Additionally, the CT image indicates sharp lower boundaries for the two contourite intervals of core GC01, possibly indicating base-cut contourites (Figure 1.1, Stow and Faugères, 2008). A similar observation can be made for core M15: two intervals of elevated Zr/Al ratios correspond to intervals of high HU (1120 – 1234 HU) components (grey zones in Figure 7.8).
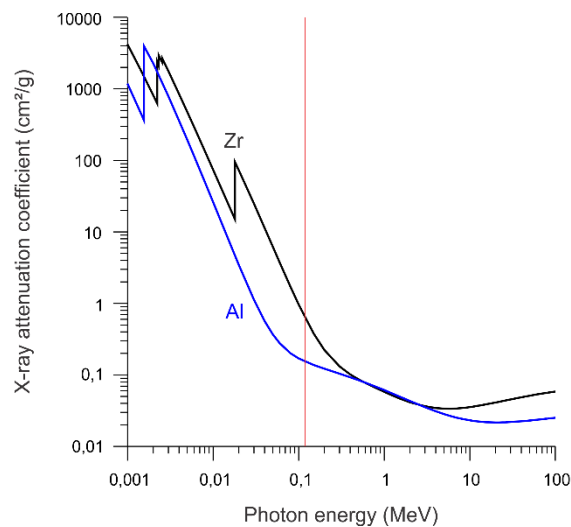
Figure 7.10: Logarithmic plot of the X-ray attenuation coefficient (with coherent scattering) versus the photon energy of the incident electrons. Both curves have been obtained from Berger et al. (2010). The red line indicates the energy level of the electrons used in the SOMATOM medical scanner.

 The three remaining peaks of the high HU component of core GC01 always coincide with the boundaries of two sections and may consequently be an artefact. One interval of slightly elevated percentages of the orange component is present between 430 cm and 345 cm (Figure 7.5), but no

corresponding higher ratios of Zr/Al are observed. Whether this interval is characterized by elevated bottom currents or not remains unknown as a consequence.

Core K3 shows one noteworthy peak of its two highest HU components (between 240 cm and 210 cm) which partly agrees to the coarsest grains measured (Figure 7.6). The correlation matrix indicates only higher correlation coefficients between the two high HU components and the sand fraction, but not between the low HU components and the silt or mud fractions (Table 7.4). As a consequence, core K3 is less conclusive when it comes to the link between bottom currents and HU, especially as the variations in Zr/Al ratio are rather small (Figure 7.6).

The five cores analysed indicate a progressive increase in HU's (imaged by the artificial colour changes in Figure 7.11) when evolving from sheeted (M08) to mounded drifts (K3, M15 and GC01) and eventually to abrasive surfaces (C06). This observation also supports the hypothesis of a link between HU-value and bottom current speed as erosive features require higher bottom currents speeds compared to mounded drift deposits, which itself require higher speeds than sheeted drift deposits (Stow et al., 2008, 2009).
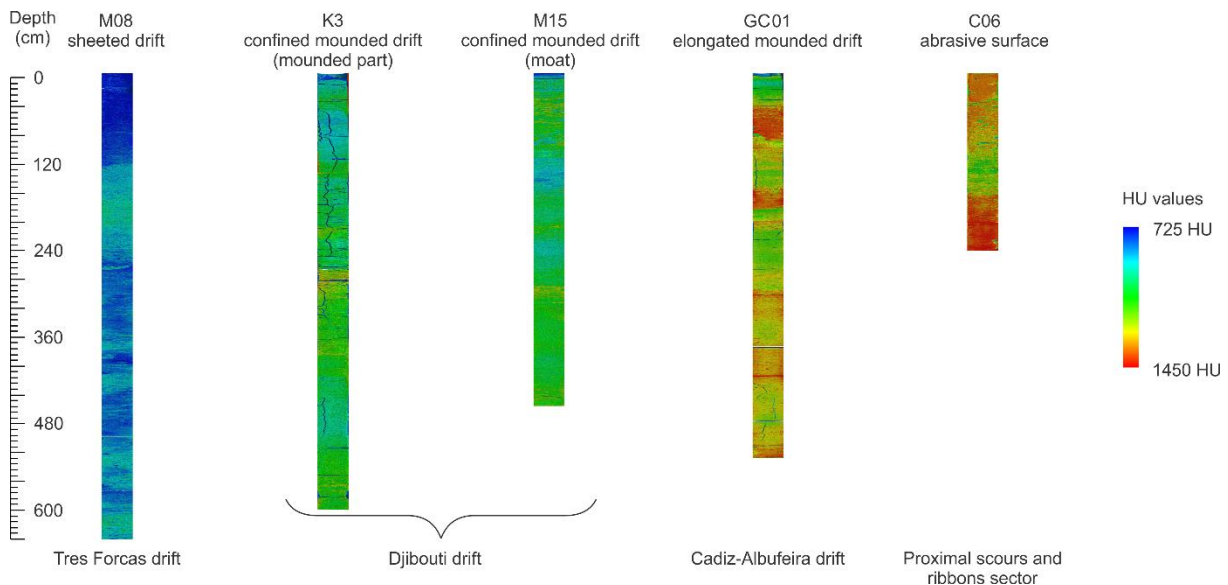
Figure 7.11: Compilation of the artificially coloured images of the five cores. The lower HU (blue colours) are present within core M08, originating from a sheeted drift, while the highest HU (red colours) are observed in C06, originating from an abrasive surface in the Gulf of Cadiz.

6. Conclusions

Quantitative analysis of CT scans of contourite cores is a very promising technique to determine intervals of elevated bottom currents in sediment cores. A workflow has been described, allowing to discern components based on the HU histogram of an individual core and link several of these components to specific MSCL and XRF proxies as well as grain-size data. A correlation matrix was developed, allowing a comparison between the CT components and a selected set of proxies based on their correlation coefficients. In general, the highest correlation coefficients were present between high HU components and the Zr/Al ratio or coarser grains.

A direct link between higher HU-values and increased bottom current velocities was detected, both within one core; intervals derived from periods of elevated bottom currents; and across sediment cores; sheeted drifts are composed of sediment characterized by generally low HU-values while mounded drift deposits contain sediments with higher HU-values.

Although the link between high HU and elevated bottom currents needs more substantiation (so far, only 5 cores have been considered) by analysing additional sediment cores from contourite drifts; the workflow may prove extremely valuable in determining intervals of elevated bottom currents without having to do a large amount of analyses (e.g. MSCL, XRF and grainsize). Also, the nature of the transition between periods of lower and elevated bottom current velocities can be visualized (in relation to base-cut or top-cut contourites) and if several cores (within the same region and/or contourite drift) have been acquired, locations with faster flowing bottom currents can be detected.

As such, the described workflow may allow the recognition of contourite intervals within sediment cores or locations of elevated bottom currents in a time- and cost-efficient way.

References

Agnihotri, R., Altabet, M.A., Herbert, T.D., Tierney, J.E., 2008. Subdecadally resolved paleoceanography of the Peru margin during the last two millennia. geochemistry, geophysics, Geosystems 9, Q05013.

Alonso, B., 2010. INFORME DE LA CAMPAÑA SAGAS bis (SDG-017). B/O SARMIENTO DE GAMBOA 9-25 de Junio de 2010.

Alonso, B., López González, N., Bozzano, G., Casas, D., Ercilla, G., Juan, C., Estrada, F., García, M., Vázquez, J.T., Cacho, I., Palomino, D., d'Acremont, E., El Moumni, B., MONTERA and MOWER teams, 2014. Djibouti Ville Drift (SW Mediterranean): Sedimentation and record of bottom-current fluctuations during the Pleistocene and Holocene, in: Van Rooij, D. (Ed.), 2nd Deep-Water Circulation Congress. VLIZ Special Publication, Ghent, Belgium, pp. 93-94.

Anton, L., Lebreiro, S., Mata, P., 2012. Origen de los depósitos contorníticos en los márgenes Ibérico y Marroquí del Gofo de Cádiz. Geo-Temas 13, 536-537.

Avila, A., Queralt-Mitjans, I., Alarcón, M., 1997. Mineralogical composition of African dust delivered by red rains over northeastern Spain. Journal of Geophysical Research: Atmospheres 102, 21977-21996.

Bahr, A., Jiménez-Espejo, F.J., Kolasinac, N., Grunert, P., Hernández-Molina, F.J., Röhl, U., Voelker, A.H.L., Escutia, C., Stow, D.A.V., Hodell, D., Alvarez-Zarikian, C.A., 2014. Deciphering bottom current velocity and paleoclimate signals from contourite deposits in the Gulf of Cádiz during the last 140 kyr: An inorganic geochemical approach. geochemistry, geophysics, Geosystems 15, 3145-3160.

Becker, J., Lourens, L.J., Hilgen, F.J., van der Laan, E., Kouwenhoven, T.J., Reichart, G.-J., 2005. Late Pliocene climate variability on Milankovitch to millennial time scales: A high-resolution study of MIS100 from the Mediterranean. Palaeogeography, Palaeoclimatology, Palaeoecology 228, 338-360.

Berger, M.J., Hubbell, J.H., Seltzer, S.M., Chang, J., Coursey, J.S., Sukumar, R., Zucker, D.S., Olsen, K., 2010. NIST Standard Reference Database 8 (XGAM). National Institute of Standards and Technology, Gaithersburg, Maryland, USA.

Brabant, L., Vlassenbroeck, J., Witte, Y.D., Cnudde, V., Boone, M.N., Dewanckele, J., Hoorebeke, L.V., 2011. Three-Dimensional Analysis of High-Resolution X-Ray Computed Tomography Data with Morpho+. Microscopy and microanalysis 17, 252-263.

Brackenridge, R.E., Hernández-Molina, F.J., Stow, D.A.V., Llave, E., 2013. A Pliocene mixed contourite–turbidite system offshore the Algarve Margin, Gulf of Cadiz: Seismic response, margin evolution and reservoir implications. Marine and Petroleum Geology 46, 36-50.

Cacho, I., Grimalt, J.O., Sierro, F.J., Shackleton, N., Canals, M., 2000. Evidence for enhanced Mediterranean thermohaline circulation during rapid climatic coolings. Earth and Planetary Science Letters 183, 417-429.

Cnudde, V., Boone, M.N., 2013. High-resolution X-ray computed tomography in geosciences: A review of the current technology and applications. Earth-Science Reviews 123, 1-17.

Ercilla, G., Juan, C., Hernández-Molina, F.J., Bruno, M., Estrada, F., Alonso, B., Casas, D., Farran, M.l., Llave, E., García, M., Vázquez, J.T., D'Acremont, E., Gorini, C., Palomino, D., Valencia, J., El Moumni, B., Ammar, A., 2016. Significance of bottom currents in deep-sea morphodynamics: An example from the Alboran Sea. Marine Geology 378, 157-170.

Faugères, J.-C., Gonthier, E., Stow, D.A.V., 1984. Contourite drift molded by deep Mediterranean outflow. Geology 12, 296-300.

Faugères, J.C., Stow, D.A.V., 2008. Contourite drifts: Nature, Evolution and Controls, in: Rebesco, M., Camerlenghi, A. (Eds.), Contourites. Elsevier, pp. 259-288.

Gonthier, E.G., Faugères, J.-C., Stow, D.A.V., 1984. Contourite facies of the Faro Drift, Gulf of Cadiz. Geological Society, London, Special Publications 15, 275-292.

Goudie, A.S., Middleton, N.J., 2001. Saharan dust storms: nature and consequences. Earth-Science Reviews 56, 179-204.

Hannah, I., Patel, D., Davies, R., 1995. The use of variance and entropic thresholding methods for image segmentation. Pattern Recognition 28, 1135-1143.

Hanebuth, T.J.J., Zhang, W., Hofmann, A.L., Löwemark, L.A., Schwenk, T., 2015. Oceanic density fronts steering bottom-current induced sedimentation deduced from a 50 ka contourite-drift record and numerical modeling (off NW Spain). Quaternary Science Reviews 112, 207-225.

Henrich, R., Cherubini, Y., Meggers, H., 2010. Climate and sea level induced turbidite activity in a canyon system offshore the hyperarid Western Sahara (Mauritania): The Timiris Canyon. Marine Geology 275, 178-198.

Hernández-Molina, F.J., 2010. Informe Científico Campaña Oceanográfica CONTOURIBER--1. 17 Septiembre-14 Octubre, 2010, B/O Sarmiento de Gamboa.

Hernández-Molina, F.J., Paterlini, M., Violante, R., Marshall, P., de Isasi, M., Somoza, L., Rebesco, M., 2009. Contourite depositional system on the Argentine Slope: An exceptional record of the influence of Antarctic water masses. Geology 37, 507-510.

Hernández-Molina, F.J., Serra, N., Stow, D.A.V., Llave, E., Ercilla, G., Van Rooij, D., 2011. Along-slope oceanographic processes and sedimentary products around the Iberian margin. Geo-Mar Lett 31, 315-341.

Jiménez-Espejo, F.J., Martínez-Ruiz, F., Finlayson, C., Paytan, A., Sakamoto, T., Ortega-Huertas, M., Finlayson, G., Iijima, K., Gallego-Torres, D., Fa, D., 2007. Climate forcing and Neanderthal extinction in Southern Iberia: insights from a multiproxy marine record. Quaternary Science Reviews 26, 836-852.

Jullien, E., Grousset, F., Malaizé, B., Duprat, J., Sanchez-Goni, M.F., Eynaud, F., Charlier, K., Schneider, R., Bory, A., Bout, V., Flores, J.A., 2007. Low-latitude "dusty events" vs. high-latitude "icy Heinrich events". Quaternary Research 68, 379-386.

Kaboth, S., Bahr, A., Reichart, G.-J., Jacobs, B., Lourens, L.J., 2016. New insights into upper MOW variability over the last 150 kyr from IODP 339 Site U1386 in the Gulf of Cadiz. Marine Geology 377, 136-145.

Lebreiro, S.M., Antón, L., Reguera, M.I., Fernández, M., Conde, E., Barrado, A.I., Yllera, A., 2015. Zooming into the Mediterranean outflow fossil moat during the 1.2–1.8 million years period (Early-Pleistocene) — An approach by radiogenic and stable isotopes. Global and Planetary Change 135, 104-118.

Lebreiro, S.M., Voelker, A.H.L., Vizcaino, A., Abrantes, F.G., Alt-Epping, U., Jung, S., Thouveny, N., Gràcia, E., 2009. Sediment instability on the Portuguese continental margin under abrupt glacial climate changes (last 60 kyr). Quaternary Science Reviews 28, 3211-3223.

Llave, E., Hernández-Molina, F.J., Somoza, L., Díaz-del-Río, V., Stow, D.A.V., Maestro, A., Alveirinho Dias, J.M., 2001. Seismic stacking pattern of the Faro-Albufeira contourite system (Gulf of Cadiz): a Quaternary record of paleoceanographic and tectonic influences. Marine Geophysical Research 22, 487-508.

Llave, E., Hernández-Molina, F.J., Somoza, L., Stow, D.A.V., Díaz Del Río, V., 2007. Quaternary evolution of the contourite depositional system in the Gulf of Cadiz. Geological Society, London, Special Publications 276, 49-79.

Lofi, J., Voelker, A.H.L., Ducassou, E., Hernández-Molina, F.J., Sierro, F.J., Bahr, A., Galvani, A., Lourens, L.J., Pardo-Igúzquiza, E., Pezard, P., Rodríguez-Tovar, F.J., Williams, T., 2016. Quaternary chronostratigraphic framework and sedimentary processes for the Gulf of Cadiz and Portuguese Contourite Depositional Systems derived from Natural Gamma Ray records. Marine Geology 377, 40-57.

Lucchi, R.G., Rebesco, M., Camerlenghi, A., Busetti, M., Tomadin, L., Villa, G., Persico, D., Morigi, C., Bonci, M.C., Giorgetti, G., 2002. Mid-late Pleistocene glacimarine sedimentary processes of a high-latitude, deep-sea sediment drift (Antarctic Peninsula Pacific margin). Marine Geology 189, 343-370.

McCave, I.N., Manighetti, B., Robinson, S.G., 1995. Sortable silt and fine sediment size/composition slicing: Parameters for palaeocurrent speed and palaeoceanography. Paleoceanography 10, 593-610.

Mena, A., Francés, G., Pérez-Arlucea, M., Aguiar, P., Barreiro-Vázquez, J.D., Iglesias, A., Barreiro-Lois, A., 2015. A novel sedimentological method based on CT-scanning: Use for tomographic characterization of the Galicia Interior Basin. Sedimentary Geology 321, 123-138.

Moreno, A., Cacho, I., Canals, M., Prins, M.A., Sánchez-Goñi, M., x, a, F., Grimalt, J.O., Weltje, G.J., 2002. Saharan Dust Transport and High-Latitude Glacial Climatic Variability: The Alboran Sea Record. Quaternary Research 58, 318-328.

Mulder, T., Hassan, R., Ducassou, E., Zaragosi, S., Gonthier, E., Hanquiez, V., Marchès, E., Toucanne, S., 2013. Contourites in the Gulf of Cadiz: a cautionary note on potentially ambiguous indicators of bottom current velocity. Geo-Marine Letters 33, 357-367.

Mutti, E., Carminati, M., 2012. Deep-Water Sands of the Brazilian Offshore Basins. AAPG Search and Discovery. article 30219 http://www.searchanddiscovery.com/documents/2012/30219mutti/ndx_mutti.pdf.

Nizou, J., Hanebuth, T.J.J., Vogt, C., 2011. Deciphering signals of late Holocene fluvial and aeolian supply from a shelf sediment depocentre off Senegal (north-west Africa). Journal of Quaternary Science 26, 411-421.

Palomino, D., Vázquez, J.-T., Ercilla, G., Alonso, B., López-González, N., Díaz-del-Río, V., 2011. Interaction between seabed morphology and water masses around the seamounts on the Motril Marginal Plateau (Alboran Sea, Western Mediterranean). Geo-Marine Letters 31, 465-479.

Pawlowsky-Glahn, V., Buccianti, A., 2011. Compositional Data Analysis: Theory and Applications. Wiley, West Sussex.

Rebesco, M., Wåhlin, A., Laberg, J.S., Schauer, U., Beszczynska-Möller, A., Lucchi, R.G., Noormets, R., Accettella, D., Zarayskaya, Y., Diviacco, P., 2013. Quaternary contourite drifts of the Western Spitsbergen margin. Deep Sea Research Part I: Oceanographic Research Papers 79, 156-168.

Rodríguez, S., Querol, X., Alastuey, A., Kallos, G., Kakaliagou, O., 2001. Saharan dust contributions to PM10 and TSP levels in Southern and Eastern Spain. Atmospheric Environment 35, 2433-2447.

Rogerson, M., Rohling, E.J., Bigg, G.R., Ramirez, J., 2012. Paleoceanography of the Atlantic-Mediterranean exchange: Overview and first quantitative assessment of climatic forcing. Reviews of Geophysics 50, RG2003.

Rothwell, R.G., Croudace, I.W., 2015. Twenty Years of XRF Core Scanning Marine Sediments: What Do Geochemical Proxies Tell Us?, in: Croudace, I.W., Rothwell, R.G. (Eds.), Micro-XRF Studies of Sediment Cores: Applications of a non-destructive Tool for the Environmental Sciences. Springer Science, Dordrecht.

Rothwell, R.G., Rack, F.R., 2006. New techniques in sediment core analysis: an introduction. Geological Society, London, Special Publications 267, 1-29.

Schultheiss, P.J., Weaver, P.P.E., 1992. Multi-sensor logging for science and industry, Proceedings of Ocean '92, Mastering the Oceans Through Technology, New-port, Rhode Island, pp. 608-613.

Shanmugam, G., 2000. 50 years of the turbidite paradigm (1950s--1990s): deep-water processes and facies models--a critical perspective. Marine and Petroleum Geology 17, 285-342.

Shanmugam, G., 2012. New perspectives on deep-water sandstones: origin, recognition, initiation and reservoir quality. Handbook of Petroleum Exploration and Production. Elsevier, Amsterdam.

Spofforth, D.J.A., Pälike, H., Green, D., 2008. Paleogene record of elemental concentrations in sediments from the Arctic Ocean obtained by XRF analyses. Paleoceanography 23, n/a-n/a.

Stow, D.A.V., Faugères, J.C., 2008. Chapter 13 Contourite Facies and the Facies Model, in: Rebesco, M., Camerlenghi, A. (Eds.), Developments in Sedimentology. Elsevier, pp. 223-256.

Stow, D.A.V., Hernández-Molina, F.J., Llave, E., Sayago-Gil, M., Díaz del Río, V., Branson, A., 2009. Bedform-velocity matrix: The estimation of bottom current velocity from bedform observations. Geology 37, 327-330.

Stow, D.A.V., Hunter, S., Wilkinson, D., Hernández-Molina, F.J., 2008. The nature of Contourite deposition, in: Rebesco, M., Camerlenghi, A. (Eds.), Developments in sedimentology: Contourites. Elsevier, Oxford, pp. 143-156.

Thomson, J., Croudace, I.W., Rothwell, R.G., 2006. A geochemical application of the ITRAX scanner to a sediment core containing eastern Mediterranean sapropel units. Geological Society, London, Special Publications 267, 65-77.

Tjallingii, R., Stattegger, K., Wetzel, A., Van Phach, P., 2010. Infilling and flooding of the Mekong River incised valley during deglacial sea-level rise. Quaternary Science Reviews 29, 1432-1444.

Vázquez, J.T., Alonso, B., 2012. INFORME CIENTÍFICO – TÉCNICO Campaña MONTERA-0412. 23 de Abril a 15 de Mayo 2012, B/O SARMIENTO DE GAMBOA.

Ziegler, M., Lourens, L.J., Tuenter, E., Reichart, G.-J., 2010. High Arabian Sea productivity conditions during MIS 13 – odd monsoon event or intensified overturning circulation at the end of the Mid-Pleistocene transition? Cimate of the past 6, 63-76.

Chapter 8

General discussion

Campaign 8: MiniMound - Belgica (2014)

Chapter 8 – General discussion.

In this chapter, the conclusions from the 4 research chapters (Chapters 4-7) are discussed into a broader framework and their results are integrated. Several question marks are put behind some of the initial definitions and classifications (Chapter 1), since it is the first time that small-scale sediment drifts resulting from deflected bottom currents are described in such detail. This resulted in new or updated definitions or classification schemes.

1. Stratigraphy

Both the Pen Duick/Renard North drift and the initiation horizons for coral mounds yielded a tentative, preliminary stratigraphy for the Atlantic Moroccan coral province (AMCP). The Pen Duick drift stratigraphy yields ages ranging from the base of the Quaternary till the present, while the coral mound stratigraphy only ranges from the Early-Middle Pleistocene transition (EMPT) till present. The oldest initiation horizon of the coral mounds coincides with the position of the EMPT boundary, inferred in the Pen Duick stratigraphy based on the increase in amplitudes of the reflections and the higher sedimentation rates in the drift.

However, from the EMPT onwards, the stratigraphies are in disagreement (Figure 8.1). Both are extremely tentative as the 10 subunits of the Pen Duick drift as well as the 10 coral mound initiation horizons were assigned to glacial MIS. And they do not coincide (Figure 8.1). Glacial MIS were chosen as most of the sediments in nearby regions, the Alboran Sea and the northern Gulf of Cádiz, were deposited during glacial periods (Hernández-Molina et al., 2002) and most of the obtained ages of coral rubble in the AMCP are from glacial periods (Wienberg et al., 2010), validating both options.

One factor that may induce errors into both stratigraphies is the absence of distinct tectonic influences on the sediment drifts of the AMCP from the EMPT onwards, especially as tectonic activity is recently considered to be more important in shaping the contourite depositional system (CDS) in the northern Gulf of Cádiz (Hernández-Molina et al., 2016) with important events at 0.9 Ma, 0.6 Ma and 0.3 Ma (Llave et al., 2007; Hernández-Molina et al., 2016). This raises the question whether these tectonic pulses also influenced the evolution of the El Arraiche sediment drifts. From the Base Quaternary discontinuity till the EMPT discontinuity, tectonic influence is noticed, but no changes could be detected in the sedimentation pattern (Figure 8.1). The 0.9 Ma event could be linked to the cessation of tectonic activity along the Renard ridge and the change from sheeted to mounded drifts (Chapter 4; (Vandorpe et al., 2014), but the 0.6 and 0.3 Ma events are not recognized in the El Arraiche sediment drifts. On top, the MIS 15 and MIS 9 discontinuities recognized in the El Arraiche sediment drifts do not evidence tectonic changes (Chapter 4; Vandorpe et al., 2014). Consequently, tectonic activity is not considered a major influencing factor for the El Arraiche drift systems and can thus not aid in refining the stratigraphy.

Without absolute ages obtained from either dating coral mounds or surrounding sediments, indicating which stratigraphy is the most probable cannot be determined. Given the tentative nature of both, it is highly likely that even both stratigraphies are wrong at one or several timeframes. A plot of the sedimentation rates derived from both stratigraphies (inset Figure 8.1) indicates that extremely high sedimentations rates (129 and 109 cm/ky) would have been present during MIS 22 and MIS 20

following the Pen Duick stratigraphy, while more moderate (41 and 91 cm/ky) ones are derived from the coral mound stratigraphy. Consequently, the coral mound stratigraphy is more probable.

One additional cautious note has to be made regarding the EMPT boundary. This boundary is the only shared one for both stratigraphies and has been derived based on the change from sheeted to mounded drift deposits in the Pen Duick drift and the coinciding increase in amplitude strength of the reflectors. The boundary was tentatively assigned an EMPT age, based on similar characteristics found all over the North Atlantic (Hernández-Molina et al., 2006; Llave et al., 2007; Van Rooij et al., 2007). The EMPT has an age of 900 ka in the North Atlantic, as Head et al. (2008) stated that the physical environment was profoundly affected by successive major glaciations from 900 ka onwards, most notably in the northern hemisphere. However, the El Arraiche mud volcano province (EAMVP) drift systems have been linked (at least partly) to the AAIW, a southern sourced water mass. Consequently, the EMPT may have a different age in the EAMVP and both stratigraphies could yield wrong ages. Absolute ages have to be obtained to clarify this matter and indicate which stratigraphy (if any) is the most correct one.
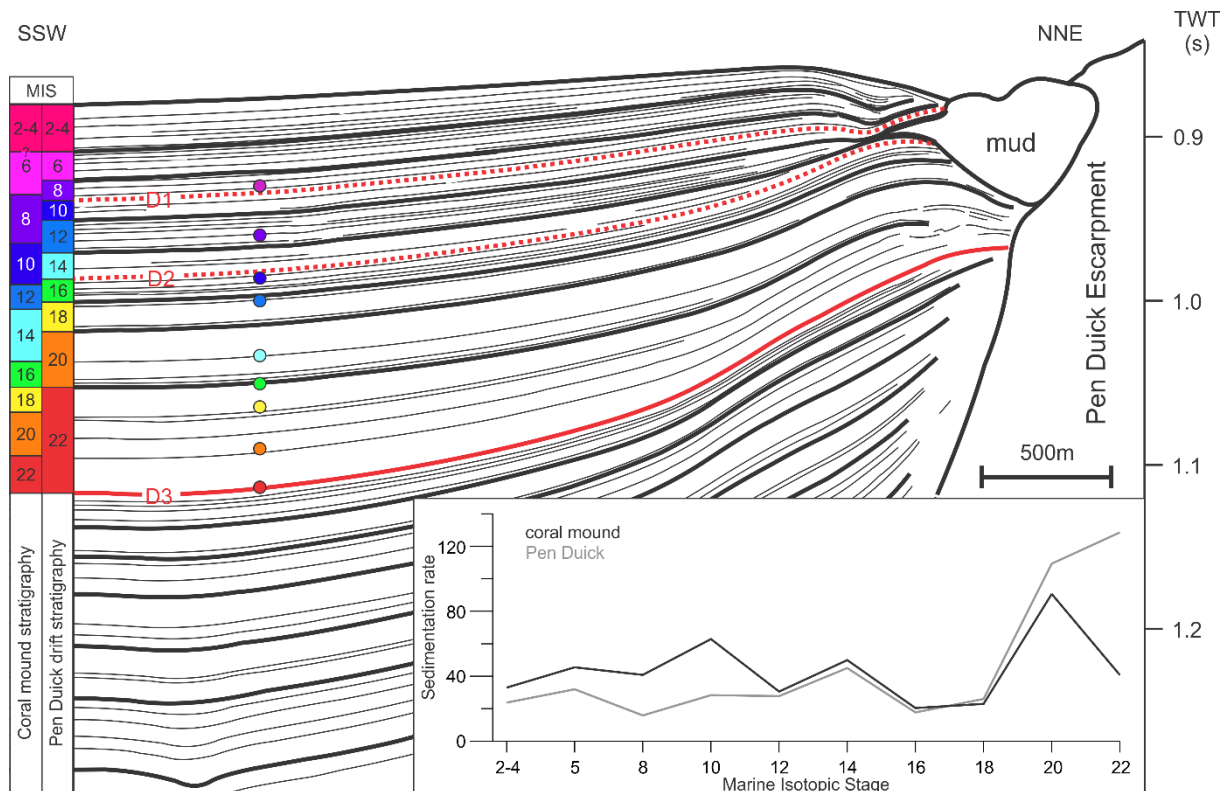
Figure 8.1: Coral mound and Pen Duick stratigraphy plotted on the same seismic profile (cfr. Figure 4.5). The dots indicate the position of the initiation horizons at the crossing of two seismic profiles. The colours of the coral mound stratigraphy are retained in order to highlight the discrepancies between both. The upper initiation horizon of the coral mounds could not be correlated on this seismic profile. The inset shows the sedimentation rates (cm/y) based on both stratigraphies.

2. Oceanography

The build-up of the Pen Duick drift is linked to the glacial AAIW, whose production is known to increase during glacial periods (Chapter 4; Vandorpe et al., 2014). This would make it by far the most northern expression of this water masses known till date; so far it was 37° S (Voigt et al., 2013), although Oppo and Curry (2005) proved its presence up till 27°S. It also implies that glacial AAIW was able to advance far more north in the northern hemisphere than previously thought and still had the capability of being involved in the build-up of sediment drifts. Nowadays though, the contourite drifts along the Renard

and Vernadsky ridges are affected by the action of northward-flowing NACW and AAIW, indicated by the nutrient content of these water masses and the gathered LADCP data (Chapter 5; Vandorpe et al., 2016). As no hemipelagic drapes are encountered in the moats of the El Arraiche sediment drifts (Figure 5.3), drift deposition might still be active at present. If this is true, the El Arraiche sediment drifts are at least maintained and possibly even build up by the combined action of two water masses, NACW and AAIW.

Most of the sediment drifts and contourite depositional systems (CDS) are related to one and the same water mass, e.g. the Cádiz CDS (Hernández-Molina et al., 2006) and the Le Danois CDS (Van Rooij et al., 2010) resulting from the MOW, the Argentine CDS resulting from the AAIW (Hernández-Molina et al., 2009; Preu et al., 2013) or the Pianosa CDS resulting from the Levantine Intermediate Water (Miramontes et al., 2016). However, some CDS's are the result of two (or more) water masses, e.g. the Alboran CDS resulting from the Western Mediterranean Deep Water, the Levantine Intermediate Water, the Winter Intermediate Water and the Atlantic Waters (Ercilla et al., 2002; Palomino et al., 2011; Ercilla et al., 2016) or the CDS in the South China Sea resulting from the action of South China Sea Intermediate and Deep Waters (Chen et al., 2013). In the EAMVP, four distinct mounded sediment drifts, i.e. Pen Duick, Renard South, Renard North and Vernadsky, might be built up by glacial AAIW (Chapter 4; Vandorpe et al., 2014) and maintained or further build up by the combined action of NACW and AAIW; both flowing in a south-north direction before being deflected by the tectonic ridges in the region (Chapter 5; Vandorpe et al., 2016). Additionally, several patch drifts along the mud volcanoes are related to the action of internal tides, resulting from the interface between these two water masses. Besides generating the patch drift, internal tides also aid in the maintenance of the sediment drifts along the tectonic ridges (Chapter 5; Vandorpe et al., 2016). The sediment drifts of the EAMVP can be combined into the El Arraiche CDS, a CDS that would result (at least partly) from the combined action of AAIW and NACW and the resulting internal tidal currents. The El Arraiche CDS may thus provide additional evidence that a CDS does not necessarily originates due to the action of a single water mass, but may be linked to two or more water masses.

The conclusions regarding internal tides support the hypothesis of Turnewitsch et al. (2013) stating that the majority of the sedimentary record may indicate more about the variability of higher-frequency flows (such as tidal currents) instead of the long-lasting net flow component. Additionally, the EAMVP might be the first regions in the world where internal tidal currents are inferred to not only aid in the generation and maintenance of sediment drifts but effectively be the sole cause for the build-up and maintenance of moats and mounded sediments due to the deflection on topographic obstacles (Chapter 5; Vandorpe et al., 2016). A similar region is the Galician margin where small-scale eddies and Kevin-Helmholtz instabilities deflecting on topographic obstacles are inferred to be responsible for the buildup of a sediment drift around the Pontevedra Outlier (Hanebuth et al., 2015; Zhang et al., 2016). In addition, in Goban Spur (Delivet et al., 2016) and the Gulf of Valencia (Ribó et al., 2015), internal tides are held responsible for the buildup of upslope-migrating sediment waves. Although sediment waves are not (yet?) considered contourite drifts (Rebesco et al., 2014), the combination of all above-mentioned observations indicates that internal tidal currents play an important role in the sedimentary record and can be responsible for the buildup of numerous drift deposits, i.e. drift deposits which may still be undiscovered or which were previously attributed to long-lasting bottom currents.

3. Coral mounds

The AMCP is so far the largest discovered coral mound province in the world, encompassing over 1800 km² and containing at least 10 stratigraphic levels at which coral mounds initiate. Buried mounds have been described before (Huvenne et al., 2007) initiating at the same horizon. However, coral mounds

initiating at different stratigraphic levels have been described for the first time in the AMCP and these levels have all been associated to glacial periods, suggesting a major climatic control on their growth. Although climatic growth cycles have been inferred before from coral-free and coral-rich layers present within one mound (Foubert et al., 2007; Rüggeberg et al., 2007; Thierens et al., 2013), the AMCP is unique as the climatic cycles can be observed as separate stratigraphic horizons. Consequently, the periods when coral mound growth was absent, palaeo-environmental conditions can still be inferred from the surrounding sediments, especially in the drift systems of the EAMVP where elevated sedimentation rates can be expected and a higher-resolution stratigraphy can be obtained. Sediment input is climate-dependent (van der Laan et al., 2012; Hodell et al., 2013) and is vital as well for the growth of the coral mounds. The small heights the coral mounds reach in this region (on average 20 m) may be ascribed to the limited sediment supply along the Moroccan Atlantic margin, which is between 8 and 24 cm/ky in the Renard North drift according to Wienberg et al. (2009) and between 8 and 14 cm/ky during glacial periods according to Van Rooij et al. (2011). During periods of coral demise, small sediment-layers developed on top of the coral mounds and possibly smoothened their positive topography. When CWC growth resumed in the next proliferation period, the coral mounds that still had a pronounced positive topography were more likely to get recolonized and experience continued coral mound growth.

The tallest mounds observed in the AMCP rarely exceed 60 meters and may contain up to 6 coral growth phases, while Challenger mound in the Porcupine Basin originates around the base of the Quaternary (unit M1a) and is 155 m high, containing a large amount of different growth phases (De Mol et al., 2002; Thierens et al., 2013). The most plausible reason why coral mounds initiated at different locations in the AMCP and did not recolonize previous mounds is that mound growth was rather small (due to the limited sediment supply) and consequently, the coral mounds did not have an exposed position anymore after a period of coral decline. As an exposed position aids in generating a larger influx of both food and sediment particles to the coral mound due to deflected bottom currents (Hebbeln et al., 2016), initiation did not necessarily start at the same location as before and a large amount of small, buried coral mounds are generated.

Bottom currents are a necessity for coral mounds as they deliver both sediment and food particles to the CWC (Hebbeln et al., 2016). However, coral mounds are also able of diverting bottom currents and inducing small-scale moats and sediment drifts along their sides. Additionally, sediment drifts are influenced by the coral mounds, illustrated by the occurrence of several hybrid mounds at the foot of the PDE, consisting of a side containing mostly CWC fragments and a side containing mostly sediments as well as by the diversion of the bottom currents and the creation of a new moat at the foot of the PDE due the presence of seven coral mounds. The interaction bottom currents/sediment drifts and coral mounds have on each other, in both ways, is clearly demonstrated in the AMCP compared to the "one way" interaction documented in the Porcupine basin (Van Rooij et al., 2007). Therefore, this region may serve as a natural laboratory for continued research regarding this relationship.

4. Patch drifts

A contourite is defined as sediment deposited or substantially reworked by the persistent action of bottom currents (Rebesco et al., 2005), while contourite drifts are regarded as sediment bodies resulting from the persistent action of bottom currents (Rebesco et al., 2014) and sediment drifts as sediment accumulations that experienced some sort of bottom current control (Stow et al., 2002). The definitions imply that there is no minimum extent to a sediment drift and that even the moats and small mounded sediments alongside the coral mounds in the AMCP may be considered sediment drifts.

Patch drifts are small, they can be smaller than 100 km² (Rebesco et al., 2014), elongated to irregular drifts characterised by a random distribution controlled by the interaction between bottom currents and irregular seafloor morphology (Hernández-Molina et al., 2006) and can have a mounded geometry (Figure 8.2A). This definition not only exactly fits the sediment drifts present around the mud volcanoes, but also those around the coral mounds and consequently, they can be categorized as such. Given the presence of many coral mounds along the Atlantic margins (Colman et al., 2005; Dorschel et al., 2005; Wheeler et al., 2007; Eisele et al., 2011; Hebbeln et al., 2014; Titschack et al., 2015), similar patch drifts most likely occur in many of these regions as well.

The morphological classification of patch drifts indicates two possible members, sheeted and mounded patch drifts with flow filaments as indicated in Figure 8.2A. The patch drifts occurring in the EAMVP indicate a different morphology, e.g. the patch drift in between the Renard Ridge and Adamastor mud has just one flow filament and contains drift deposits on one side (Figure 5.3). In addition, sheeted patch drift is not a suitable name as the morphology of the patch drift does not have a sheeted appearance (Figures 5.3 and 8.2A).
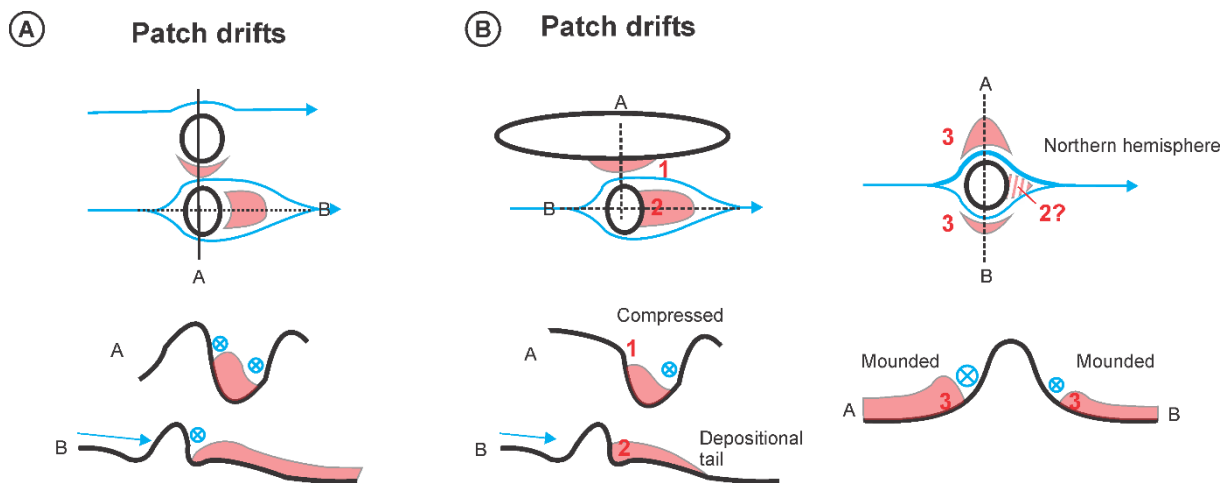
Figure 8.2: A. Original classification of patch drifts according to Rebesco et al. (2005) and Hernández-Molina et al. (2008). B. Proposed classification of patch drifts with the changes indicated by red numbers (see text for explanations).

Free-standing topographic obstacles, such as some of the mud volcanoes in the EAMVP, have two sediment drifts along their edges with a deeper moat and better-developed sediment drift on the left side of the obstacle (following the current direction), resulting from the Coriolis deflection in the northern hemisphere (Hernández-Molina et al., 2006). Similar observations can be made along the mud volcanoes in the Alboran Sea (Somoza et al., 2012) and northern Gulf of Cádiz (León et al., 2012; Palomino et al., 2016), although they were not mentioned by the authors. Patch drifts with such a morphology are not represented in the classification of contourite drifts (Rebesco et al., 2005; Hernández-Molina et al., 2008; Figure 8.2A) and should be included, especially as numerous additional similar sediment drifts will be present in the world's ocean given the ubiquitous presence of topographic obstacles on the ocean floor (Wessel et al., 2010) and the novel insight that internal tidal currents can create sediment drifts (Hanebuth et al., 2015).

Depositional tails are present at the lee side of the Al Idrissi and Mercator mud volcanoes and are absent at the other MV's. These observations indicate that depositional tails are not always present and when they are, they are attached to the topographic obstacles rather than being detached, as suggested in the classification (Rebesco et al., 2005; Hernández-Molina et al., 2008; Figure 8.2A). Attached depositional tails also seem to be present along the Tarsis and Gazul mud volcanoes (Pinheiro

et al., 2003; Palomino et al., 2016) and the Las Negras and Boabdil mud volcanoes (León et al., 2012) in the northern Gulf of Cádiz.

Considering all points outlined above, a renewed classification of patch drifts is proposed (Figure 8.2B). The main adaptations are: (1) sheeted patch drifts have a different geometry, may result from 1 flow filament and could be renamed to "compressed patch drifts" as "sheeted patch drift" does not reflect their morphology; (2) a depositional tail (if present) can also be attached to the obstacle; and (3) free-standing topographic obstacles can have moats and sediment drifts at both sides. The best developed moat and sediment drift is located at the left (right) side of the obstacle in the northern (southern) hemisphere, looking downstream (Hernández-Molina et al., 2006).

5. Tidal sediment drifts

Sediment drifts are thick and accumulative sedimentary bodies resulting from the action of bottom currents (Stow et al., 2002; Faugères and Stow, 2008). In many cases, these sedimentary bodies are extensive, reaching widths over 100 km, e.g. the Gloria sheeted drift (McCave and Tucholke, 1986). Not only sheeted drifts can be extensive, also elongated mounded drifts (e.g. the Eirik drift; Müller-Michaelis et al., 2013) and separated mounded drifts (e.g. the Feni drift; Stoker et al., 2005) can reach widths of several tens of kilometres. One might wonder where contourites end and (hemi-) pelagic sedimentation takes over, as a continuum between both exists (Rebesco et al., 2014) and a large percentage (of especially the sheeted) sediment drifts will never have experienced any direct influence of bottom currents.

The EAMVP is the first region where sediment drifts are reported resulting only from internal tidal currents (Chapter 5; Vandorpe et al., 2016). In this region, the internal tides deflect on the topographies (mud volcanoes, coral mounds and tectonic ridges), their velocities increase locally and they are capable of creating small scale sediment drifts. Around the mud volcanoes, the moats are only a few km long and the bottom current influence can be observed for just 1 – 2 km perpendicular to the moat (Figure 5.3G). Around the coral mounds, these dimensions are even much smaller, in the order of a few tens of meters and a few hundreds of meters respectively (Figure 6.2E). However, applying the definition of a sediment drift, the entire sedimentary body should be called a sediment drift, even though the bottom current influence is noticed on only a few km² (coral mounds/mud volcanoes) to maximum a few tens of km² (mud volcanoes).

Applying this concept on other regions could mean that a single topographic obstacle on an otherwise undisturbed slope could result in a contourite drift and the entire hemipelagic drape on that slope should be called a sediment drift. Given the local nature of sediment drifts resulting from the deflection of internal tidal currents on topographic obstacles, this seems a bit far-fetched. Consequently, one could argue that only the part of the sedimentary body that was directly influenced by the internal tidal currents should be called a sediment drift. Evidently, the distinction between these kinds of sediment drifts and drifts resulting from long-lasting contour-following bottom currents should then be made. Naming them "internalites" is an option as this term is already used to describe deposits resulting from internal waves (Bádenas et al., 2012). However, internalites are (so far) only recognized based on sedimentological characteristics (Bádenas et al., 2012) and not from morphological expressions, although sediment waves are acknowledged to result from the interaction between continental slopes/abyssal plains and internal waves (He et al., 2008; Delivet et al., 2016; Ribó et al., 2016). Moreover, several EAMVP sediment drifts result from the combined action of background bottom currents aided by (semi-diurnal) tidal currents (Chapter 5; Vandorpe et al., 2016). This in contrast to the internalites described by Bádenas et al. (2012) and Pomar et al. (2012), which are solely the result of internal waves. Consequently, internalites is discarded as a suitable name for the sediment

drifts of the El Arraiche CDS and the preposition "tidal" is proposed for those drifts that are build up, or at least influenced, by internal waves. This nomenclature would thus result in the occurrence of tidal mounded drifts and tidal patch drifts in the AMCP. For the tidal sediment drifts, only the part which is influenced directly by the internal tidal currents could be considered a sediment drift, significantly reducing the extent of such deposits and avoiding the unnecessary large extent of sediment drifts in this area.

6. Occurrence of contourites

In general, two main sediment drift morphologies are present in the EAMVP, sheeted and mounded drift deposits. The sheeted drift deposits nearly all initiated at the start of the Quaternary and mounded drift deposits are present from the EMPT onwards. The shift towards mounded drift deposits is accompanied by elevated bottom current velocities in the respective moats and may be linked to higher and steeper slopes of the neighbouring tectonic ridges. The steepness of the tectonic ridges (Renard and Vernadsky) plays a vital role in the build-up and maintenance of the drift deposits in the EAMVP, as a threshold of about 11° seems to exist for drift deposition (Chapter 5; Vandorpe et al., 2016).

The background bottom currents in the AMCP (below 10 cm/s) are in theory not fast enough to create sediment drifts. However, sediment drifts are present and result from the deflection of the bottom currents against the steep ridges. These results imply that drift deposition does not only occur due to the persistent action of large-scale and often long-term oceanographic processes, e.g. density-driven currents (Baringer and Price, 1997; WÅhlin and Walin, 2001), eddies (Serra et al., 2010) or secondary circulations (Faugères and Stow, 1993; McCave and Carter, 1997), but also due to the effects of small-scale deflected bottom currents, flowing along topographic features. In addition, these results indicate that bottom currents locally rapidly accelerate and decelerate, delineating regions of elevated bottom currents and accompanied sediment drifts alternating with regions of slower bottom currents and accompanied hemipelagic sediments. Similar observations have been made in the South China Sea, where a multitude of depositional and erosional features are observed due to the persistent action of bottom currents, all related to the steepness of the slope (Chen et al., 2014) or seamount (Chen et al., 2013). Also in the Alboran Sea, small-scale (<10 km in length) sediment drifts are observed around seamounts on the Motril marginal plateau (Palomino et al., 2011). The ever increasing numbers of discovered small-scale drifts, related to topographic features on the seafloor, and the existence of at least $25x10^6$ seamounts (Wessel et al., 2010), implies that a large number of yet uncharted sediment drifts may be present on the ocean floors, which may contain a wealth of information regarding the palaeoceanography and -climatology of these specific regions.

An example of such a region is the Maldives, where over 1000 coral islands and many more drowned atolls are present. The Inner Sea of the Maldives is a region where many small-scale sediment drifts can be expected as bottom currents are present (Tomczak and Godfrey, 2003; Lüdmann et al., 2013), accommodation space is provided by the average subsidence rates of 0.043 to 0.057 mm/year (Backman et al., 1988) and sediment is provided by the carbonate platform and monsoon conditions (Betzler et al., 2013). Additionally, the (drowned) atolls provide possible steep topographic features on the seafloor where elevated bottom current velocities can be expected and sediment drifts may initiate along their borders. Lüdmann et al. (2013) indeed indicated the presence of several sediment drifts and waves, close to the topographic features, confirming this hypothesis. As these authors only mapped about one third of the Inner Sea, more sediment drifts are expected, increasing the number of identified drifts. Similar regions in other parts of the world where sufficient sediment is present, bottom currents are able of transporting sediment, accommodation space is provided and steep

topographic features characterize the seafloor; might drastically increase the number of known drifts deposits and complete the map produced by Rebesco et al. (2014).

The possible presence of many additional drifts in the world's oceans is important for several purposes. First, contourites are characterized by elevated sedimentation rates and are usually fairly continuous, making them preferred sites for studies regarding ocean circulation patterns, oceanographic changes and palaeo-climatic studies (Rebesco et al., 2014); the resolution which can be achieved by studying muddy contourite deposits (e.g. Llave et al., 2006; Toucanne et al., 2007; Voelker et al., 2015) approaches that of ice-core archives. Secondly, knowledge regarding the position of contourites is beneficiary for submarine installations, as drifts are places where submarine landslides are more likely (Bryn et al., 2005) due to their low shear-strength, under-consolidation, loading, possible gas-content and their main location on slopes (Laberg and Camerlenghi, 2008). Thirdly, regions containing well-sorted coarse-grained (source rocks) or fine-grained (seals) sediments will be discovered which can become additional hydrocarbon exploration targets (Viana et al., 2007; Brackenridge et al., 2013; Lüdmann et al., 2013).

Being able to predict where possible drifts may be present (based on the position of bottom currents and topography for example) and to delineate the exact extent of drift systems (taking into consideration the limited extent of tidal drifts and patch drifts) are consequently important factors that will allow to determine the location of current-influenced sediments. Their location can result in a map that will help to locate regions where palaeo-climatic research may yield higher-resolution archives (science), regions where sediments are more prone to failure (science and industry) or regions that are a possible hydrocarbon exploration target (industry).

7. CT-based diagnostic criteria of contourites

Diagnostic criteria to discern contourites from pelagites and especially turbidites are still ambiguous and are solely based on sedimentological and lithological properties (Rebesco et al., 2005; Llave et al., 2006; Faugères and Stow, 2008). Consequently, the workflow determined in Chapter 7 may prove to be very valuable when it comes to distinguishing such deposits. It has to be noted though that turbidites are also characterized by elevated (downslope) bottom currents exceeding 100 cm/s (Southard and Cacchione, 1975; Xu et al., 2004; Piper and Normark, 2009) and are capable of creating a distinct basal discontinuity as well (Lowe, 1982), meaning they could have similar CT-characteristics as contourites and a distinction based on CT analyses (as described in Chapter 7) would not be possible.

However, contourites are capable of sorting/winnowing sediments over a prolonged period of time (Heezen, 1959; Shanmugam, 2006; Rebesco and Camerlenghi, 2008; Stow et al., 2009), e.g. causing the high Zr/Al-ratio's (Bahr et al., 2014) which help creating high HU-values (Chapter 7). Turbidites on the other hand are created within hours or days (Piper and Normark, 2009; Xu et al., 2014) and lack such a winnowing effect. Consequently, one would expect that turbidite intervals consist of sediments of varying chemistry and porosity and therefore are characterized by more averaged HU-values. Pelagites are expected to contain similar compositions compared to contourites, but to have a different texture and fabric (Stow, Ogawa, et al., 2002). The difference in texture could result in different HU-values; pelagites are usually finer-grained and are thus expected to have lower HU-values; possibly allowing to differentiate contourites from pelagites.

The hypothesis outlined above could allow to make a distinction between contourites, turbidites and pelagites based on CT analyses and could mean a significant advancement in the determination of diagnostic criteria for contourites. However, caution has to be taken given the fact that so far only five contourite cores have been analysed. To valorise the method, a large number of additional cores need

to be analysed. Preferentially, these additional sediment cores are well-described, fully-analysed in terms of grain size, chemical composition and geophysical properties and contain a succession of contourites, turbidites and (hemi-) pelagites, allowing a comparison of all three end-members within one core. In this way, the link between higher HU values and coarser grains or higher Zr/Al ratios can be verified and whether this link exists for contourites only or for turbidites as well. If additional analyses indicate that contourites indeed possess unique CT characteristics compared to turbidites and pelagites, they have to be added to the existing set of diagnostic criteria. As such, the workflow described in Chapter 7 might prove to be the missing link in the determination of contourites.

References

Backman, J., Duncan, R.A., Peterson, L.C., Baker, P.A., Baxter, A.N., Boersma, A., 1988. Mascarne Plateau - Sites 705-716. Ocean Drilling Program College Station, TX

Bádenas, B., Pomar, L., Aurell, M., Morsilli, M., 2012. A facies model for internalites (internal wave deposits) on a gently sloping carbonate ramp (Upper Jurassic, Ricla, NE Spain). Sedimentary Geology 271–272, 44-57

Bahr, A., Jiménez-Espejo, F.J., Kolasinac, N., Grunert, P., Hernández-Molina, F.J., Röhl, U., Voelker, A.H.L., Escutia, C., Stow, D.A.V., Hodell, D., Alvarez-Zarikian, C.A., 2014. Deciphering bottom current velocity and paleoclimate signals from contourite deposits in the Gulf of Cádiz during the last 140 kyr: An inorganic geochemical approach. geochemistry, geophysics, Geosystems 15, 3145-3160

Baringer, M.O.N., Price, J.F., 1997. Momentum and Energy Balance of the Mediterranean Outflow. Journal of Physical Oceanography 27, 1678-1692

Betzler, C., Fürstenau, J., Lüdmann, T., Hübscher, C., Lindhorst, S., Paul, A., Reijmer, J.J.G., Droxler, A.W., 2013. Sea-level and ocean-current control on carbonate-platform growth, Maldives, Indian Ocean. Basin Research 25, 172-196

Brackenridge, R.E., Hernández-Molina, F.J., Stow, D.A.V., Llave, E., 2013. A Pliocene mixed contourite–turbidite system offshore the Algarve Margin, Gulf of Cadiz: Seismic response, margin evolution and reservoir implications. Marine and Petroleum Geology 46, 36-50

Bryn, P., Berg, K., Stoker, M.S., Haflidason, H., Solheim, A., 2005. Contourites and their relevance for mass wasting along the Mid-Norwegian Margin. Marine and Petroleum Geology 22, 85-96

Chen, H., Xie, X., Van Rooij, D., Vandorpe, T., Huang, L., Guo, L., Su, M., 2013. Depositional characteristics and spatial distribution of deep-water sedimentary systems on the northwestern middle-lower slope of the Northwest Sub-Basin, South China Sea. Marine Geophysical Research 34, 239-257

Chen, H., Xie, X., Van Rooij, D., Vandorpe, T., Su, M., Wang, D., 2014. Depositional characteristics and processes of alongslope currents related to a seamount on the northwestern margin of the Northwest Sub-Basin, South China Sea. Marine Geology 355, 36-53

Colman, J.G., Gordon, D.M., Lane, A.P., Forde, M.J., Fitzpatrick, J.J., 2005. Carbonate mounds off Mauritania, Northwest Africa: status of deep-water corals and implications for management of fishing and oil exploration activities, in: Freiwald, A., Roberts, J.M. (Eds.), Cold-Water Corals and Ecosystems. Springer, Berlin, Heidelberg, pp. 417-441

De Mol, B., Van Rensbergen, P., Pillen, S., Van Herreweghe, K., Van Rooij, D., McDonnell, A., Huvenne, V., Ivanov, M., Swennen, R., Henriet, J.P., 2002. Large deep-water coral banks in the Porcupine Basin, southwest of Ireland. Marine Geology 188, 193-231

Delivet, S., Van Eetvelt, B., Monteys, X., Ribó, M., Van Rooij, D., 2016. Seismic geomorphological reconstructions of Plio-Pleistocene bottom current variability at Goban Spur. Marine Geology 378, 261-275

Dorschel, B., Hebbeln, D., Rüggeberg, A., Dullo, W.-C., Freiwald, A., 2005. Growth and erosion of a cold-water coral covered carbonate mound in the Northeast Atlantic during the Late Pleistocene and Holocene. Earth and Planetary Science Letters 233, 33-44

Eisele, M., Frank, N., Wienberg, C., Hebbeln, D., López Correa, M., Douville, E., Freiwald, A., 2011. Productivity controlled cold-water coral growth periods during the last glacial off Mauritania. Marine Geology 280, 143-149

Ercilla, G., Baraza, J., Alonso, B., Estrada, F., Casas, D., Farran, M., 2002. The Ceuta Drift, Alboran Sea, southwestern Mediterranean, in: Stow, D., Pudsey, C., Howe, J., Faugères, J., Viana, A. (Eds.), Deep-water contourite systems: modern drifts and ancient series, seismic and sedimentary characteristics. Geol Soc Lond Mem, pp. 155-170

Ercilla, G., Juan, C., Hernández-Molina, F.J., Bruno, M., Estrada, F., Alonso, B., Casas, D., Farran, M.l., Llave, E., García, M., Vázquez, J.T., D'Acremont, E., Gorini, C., Palomino, D., Valencia, J., El Moumni, B., Ammar, A., 2016. Significance of bottom currents in deep-sea morphodynamics: An example from the Alboran Sea. Marine Geology 378, 157-170

Faugères, J.C., Stow, D.A.V., 1993. Contourite drift types and their distribution in the North and South Atlantic Ocean basins. Sedimentary Geology 82, 189-203

Faugères, J.C., Stow, D.A.V., 2008. Contourite drifts: Nature, Evolution and Controls, in: Rebesco, M., Camerlenghi, A. (Eds.), Contourites. Elsevier, pp. 259-288

Foubert, A., Van Rooij, D., Blamart, D., Henriet, J.P., 2007. X-ray imagery and physical core logging as a proxy of the content of sediment cores in cold-water coral mound provinces: a case study from Porcupine Seabight, SW of Ireland. International Journal of Earth Sciences 96, 141-158

Hanebuth, T.J.J., Zhang, W., Hofmann, A.L., Löwemark, L.A., Schwenk, T., 2015. Oceanic density fronts steering bottom-current induced sedimentation deduced from a 50 ka contourite-drift record and numerical modeling (off NW Spain). Quaternary Science Reviews 112, 207-225

He, Y., Gao, Z., Luo, J., Luo, S., Liu, X., 2008. Characteristics of internal-wave and internal-tide deposits and their hydrocarbon potential. Petroleum Science 5, 37-44

Head, M.J., Pillans, B., Farquhar, S.A., 2008. The Early–Middle Pleistocene Transition: characterization and proposed guide for the defining boundary. Episodes 31, 255-259

Hebbeln, D., Van Rooij, D., Wienberg, C., 2016. Good neighbours shaped by vigorous currents: Cold-water coral mounds and contourites in the North Atlantic. Marine Geology, 171-185

Hebbeln, D., Wienberg, C., Wintersteller, P., Freiwald, A., Becker, M., Beuck, L., Dullo, C., Eberli, G.P., Glogowski, S., Matos, L., Forster, N., Reyes-Bonilla, H., Taviani, M., 2014. Environmental forcing of the Campeche cold-water coral province, southern Gulf of Mexico. Biogeosciences 11, 1799-1815

Heezen, B.C., 1959. Dynamic Processes of Abyssal Sedimentation: Erosion, Transportation, and Redeposition on the Deep-sea floor. Geophysical Journal of the Royal Astronomical Society 2, 142-172

Hernández-Molina, F.J., Larter, R.D., Rebesco, M., Maldonado, A., 2006. Miocene reversal of bottom water flow along the Pacific Margin of the Antarctic Peninsula: Stratigraphic evidence from a contourite sedimentary tail. Marine Geology 228, 93-116

Hernández-Molina, F.J., Llave, E., Stow, D.A.V., 2008. Continental slope contourites, in: Rebesco, M., Camerlenghi, A. (Eds.), Contourites. Elsevier, *Developments in Sedimentology*, ELSEVIER, pp. 379-407

Hernández-Molina, F.J., Llave, E., Stow, D.A.V., Garciá, m., Somoza, L., Vázquez, J.T., Lobo, F.J., Maestro, A., Díaz del Río, G., León, R., Medialdea, T., Gardner, J., 2006. The contourite depositional system of the Gulf of Cádiz: A sedimentary model related to the bottom current activity of the Mediterranean outflow water and its interaction with the continental margin. Deep Sea Research Part II: Topical Studies in Oceanography 53, 1420-1463

Hernández-Molina, F.J., Paterlini, M., Violante, R., Marshall, P., de Isasi, M., Somoza, L., Rebesco, M., 2009. Contourite depositional system on the Argentine Slope: An exceptional record of the influence of Antarctic water masses. Geology 37, 507-510

Hernández-Molina, F.J., Sierro, F.J., Llave, E., Roque, C., Stow, D.A.V., Williams, T., Lofi, J., Van der Schee, M., Arnáiz, A., Ledesma, S., Rosales, C., Rodríguez-Tovar, F.J., Pardo-Igúzquiza, E., Brackenridge, R.E., 2016. Evolution of the gulf of Cadiz margin and southwest Portugal contourite depositional system: Tectonic, sedimentary and paleoceanographic implications from IODP expedition 339. Marine Geology 377, 7-39

Hernández-Molina, F.J., Somoza, L., Vazquez, J.T., Lobo, F., Fernández-Puga, M.C., Llave, E., Díaz-del-Río, V., 2002. Quaternary stratigraphic stacking patterns on the continental shelves of the southern Iberian Peninsula: their relationship with global climate and palaeoceanographic changes. Quaternary International 92, 5-23

Hodell, D.A., Lourens, L., Stow, D.A.V., Hernández-Molina, J., Alvarez Zarikian, C.A., the Shackleton Site Project, M., 2013. The "Shackleton Site" (IODP Site U1385) on the Iberian Margin. Sci. Dril. 16, 13-19

Huvenne, V.A.I., Bailey, W.R., Shannon, P.M., Naeth, J., di Primio, R., Henriet, J.P., Horsfield, B., de Haas, H., Wheeler, A., Olu-Le Roy, K., 2007. The Magellan mound province in the Porcupine Basin. International Journal of Earth Sciences 96, 85-101

Laberg, J.S., Camerlenghi, A., 2008. Chapter 25 The Significance of Contourites for Submarine Slope Stability, in: Rebesco, M., Camerlenghi, A. (Eds.), Developments in Sedimentology. Elsevier, pp. 537-556

León, R., Somoza, L., Medialdea, T., Vázquez, J.T., González, F.J., López-González, N., Casas, D., del Pilar Mata, M., del Fernández-Puga, M.C., Giménez-Moreno, C.J., Díaz-del-Río, V., 2012. New discoveries of mud volcanoes on the Moroccan Atlantic continental margin (Gulf of Cádiz): morpho-structural characterization. Geo-Marine Letters 32, 473-488

Llave, E., Hernández-Molina, F., Stow, D.V., Fernández-Puga, M., García, M., Vázquez, J., Maestro, A., Somoza, L., Díaz del Río, V., 2007. Reconstructions of the Mediterranean Outflow Water during the quaternary based on the study of changes in buried mounded drift stacking pattern in the Gulf of Cadiz. Marine Geophysical Researches 28, 379-394

Llave, E., Hernández-Molina, F.J., Somoza, L., Stow, D.A.V., Díaz del Río, V., 2007. Quaternary evolution of the contourite depositional system in the Gulf of Cadiz. Geological Society, London, Special Publications 276, 49-79

Llave, E., Schönfeld, J., Hernández-Molina, F.J., Mulder, T., Somoza, L., Díaz del Río, V., Sánchez-Almazo, I., 2006. High-resolution stratigraphy of the Mediterranean outflow contourite system in the Gulf of Cadiz during the late Pleistocene: The impact of Heinrich events. Marine Geology 227, 241-262
Lowe, D.R., 1982. Sediment gravity flows; II, Depositional models with special reference to the deposits of high-density turbidity currents. Journal of sedimentary research 52, 279-297

Lüdmann, T., Kalvelage, C., Betzler, C., Fürstenau, J., Hübscher, C., 2013. The Maldives, a giant isolated carbonate platform dominated by bottom currents. Marine and Petroleum Geology 43, 326-340

McCave, I.N., Carter, L., 1997. Recent sedimentation beneath the Deep Western Boundary Current off northern New Zealand. Deep Sea Research Part I: Oceanographic Research Papers 44, 1203-1237

McCave, I.N., Tucholke, B.E., 1986. Deep current-controlled sedimentation in the western North Atlantic, in: McCreggor, B.A. (Ed.), The western North Atlantic region. The geological society of America, pp. 451-468

Miramontes, E., Cattaneo, A., Jouet, G., Théreau, E., Thomas, Y., Rovere, M., Cauquil, E., Trincardi, F., 2016. The Pianosa Contourite Depositional System (Northern Tyrrhenian Sea): Drift morphology and Plio-Quaternary stratigraphic evolution. Marine Geology 378, 20-42

Müller-Michaelis, A., Uenzelmann-Neben, G., Stein, R., 2013. A revised Early Miocene age for the instigation of the Eirik Drift, offshore southern Greenland: Evidence from high-resolution seismic reflection data. Marine Geology 340, 1-15

Oppo, D.W., Curry, W.B., 2005. Glacial water mass geometry and the distribution of delta 13C of CO2 in the western Atlantic Ocean. Paleoceanography 20

Palomino, D., López-González, N., Vázquez, J.-T., Fernández-Salas, L.-M., Rueda, J.-L., Sánchez-Leal, R., Díaz-del-Río, V., 2016. Multidisciplinary study of mud volcanoes and diapirs and their relationship to seepages and bottom currents in the Gulf of Cádiz continental slope (northeastern sector). Marine Geology 378, 196-212

Palomino, D., Vázquez, J.-T., Ercilla, G., Alonso, B., López-González, N., Díaz-del-Río, V., 2011. Interaction between seabed morphology and water masses around the seamounts on the Motril Marginal Plateau (Alboran Sea, Western Mediterranean). Geo-Marine Letters 31, 465-479

Pinheiro, L.M., Ivanov, M.K., Sautkin, A., Akhmanov, G., Magalhães, V.H., Volkonskaya, A., Monteiro, J.H., Somoza, L., Gardner, J., Hamouni, N., Cunha, M.R., 2003. Mud volcanism in the Gulf of Cadiz: results from the TTR-10 cruise. Marine Geology 195, 131-151

Piper, D., Normark, W., 2009. Processes that initiate turbidity currents and their influence on turbidites: a marine geology perspective. Journal of sedimentary research 79, 347-362

Pomar, L., Morsilli, M., Hallock, P., Bádenas, B., 2012. Internal waves, an under-explored source of turbulence events in the sedimentary record. Earth-Science Reviews 111, 56-81

Preu, B., Hernández-Molina, F.J., Violante, R., Piola, A.R., Paterlini, C.M., Schwenk, T., Voigt, I., Krastel, S., Spiess, V., 2013. Morphosedimentary and hydrographic features of the northern Argentine margin: The interplay between erosive, depositional and gravitational processes and its conceptual implications. Deep Sea Research Part I: Oceanographic Research Papers 75, 157-174

Rebesco, M., Camerlenghi, A., 2008. Contourites. Elsevier

Rebesco, M., Hernández-Molina, F.J., van Rooij, D., Wåhlin, A., 2014. Contourites and associated sediments controlled by deep-water circulation processes: State of the art and future considerations. Marine Geology 352, 111-154

Rebesco, M., Richard, C.S., Cocks, L.R.M., Ian, R.P., 2005. Sedimentary environments: Contourites, Encyclopedia of Geology. Elsevier, Oxford, pp. 513-528

Ribó, M., Puig, P., Muñoz, A., Lo Iacono, C., Masqué, P., Palanques, A., Acosta, J., Guillén, J., Gómez Ballesteros, M., 2016. Morphobathymetric analysis of the large fine-grained sediment waves over the Gulf of Valencia continental slope (NW Mediterranean). Geomorphology 253, 22-37

Ribó, M., Puig, P., van Haren, H., 2015. Hydrodynamics over the Gulf of Valencia continental slope and their role in sediment transport. Deep Sea Research Part I: Oceanographic Research Papers 95, 54-66

Rüggeberg, A., Dullo, C., Dorschel, B., Hebbeln, D., 2007. Environmental changes and growth history of a cold-water carbonate mound (Propeller Mound, Porcupine Seabight). International Journal of Earth Sciences 96, 57-72

Serra, N., Ambar, I., Boutov, D., 2010. Surface expression of Mediterranean Water dipoles and their contribution to the shelf/slope-open ocean exchange. Ocean Science Discussions 6, 191-209

Shanmugam, G., 2006. Chapter 8 The turbidite facies model, in: Shanmugam, G. (Ed.), Handbook of Petroleum Exploration and Production. Elsevier, pp. 283-315

Somoza, L., Medialdea, T., León, R., Ercilla, G., Vázquez, J.T., Farran, M.l., Hernández-Molina, J., González, J., Juan, C., Fernández-Puga, M.C., 2012. Structure of mud volcano systems and pockmarks in the region of the Ceuta Contourite Depositional System (Western Alborán Sea). Marine Geology 332–334, 4-26

Southard, J.B., Cacchione, D.A., 1975. Bed Configurations, in: Harms, J.C., Southard, J.B., Spearing, D.R., Walker, R.G. (Eds.), Depositional environments as interpreted from primary sedimentary structures and stratification sequences. Lecture Notes for Society of Economic Paleontologists and Mineralogists Short Course No. 2, Dallas, Texas, pp. 5-43

Stoker, M.S., Praeg, D., Hjelstuen, B.O., Laberg, J.S., Nielsen, T., Shannon, P.M., 2005. Neogene stratigraphy and the sedimentary and oceanographic development of the NW European Atlantic margin. Marine and Petroleum Geology 22, 977-1005

Stow, D.A.V., Faugères, J.-C., Howe, J.A., Pudsey, C.J., Viana, A.R., 2002. Bottom currents, contourites and deep-sea sediment drifts: current state-of-the-art. Geological Society, London, Memoirs 22, 7-20

Stow, D.A.V., Hernández-Molina, F.J., Llave, E., Sayago-Gil, M., Díaz del Río, V., Branson, A., 2009. Bedform-velocity matrix: The estimation of bottom current velocity from bedform observations. Geology 37, 327-330

Stow, D.A.V., Ogawa, Y., Lee, I.T., Mitsuzawa, K., 2002. Neogene contourites, Miura-Boso forearc basin, SE Japan, in: Stow, D.A.V., Pudsey, C., Howe, J., Faugères, J., Viana, A. (Eds.), Deep-water contourite systems: modern drifts and ancient series, seismic and sedimentary characteristics. Geol. Soc. London Mem., pp. 409-419

Thierens, M., Browning, E., Pirlet, H., Loutre, M.F., Dorschel, B., Huvenne, V.A.I., Titschack, J., Colin, C., Foubert, A., Wheeler, A.J., 2013. Cold-water coral carbonate mounds as unique palaeo-archives: the Plio-Pleistocene Challenger Mound record (NE Atlantic). Quaternary Science Reviews 73, 14-30

Titschack, J., Baum, D., De Pol-Holz, R., López Correa, M., Forster, N., Flögel, S., Hebbeln, D., Freiwald, A., 2015. Aggradation and carbonate accumulation of Holocene Norwegian cold-water coral reefs. Sedimentology 62, 1873-1898

Tomczak, M., Godfrey, J.S., 2003. Regional Oceanography. An Introduction. Daya Publishing House, Delhi

Toucanne, S., Mulder, T., Schönfeld, J., Hanquiez, V., Gonthier, E., Duprat, J., Cremer, M., Zaragosi, S., 2007. Contourites of the Gulf of Cadiz: A high-resolution record of the paleocirculation of the Mediterranean outflow water during the last 50,000 years. Palaeogeography, Palaeoclimatology, Palaeoecology 246, 354-366

Turnewitsch, R., Falahat, S., Nycander, J., Dale, A., Scott, R.B., Furnival, D., 2013. Deep-sea fluid and sediment dynamics—Influence of hill- to seamount-scale seafloor topography. Earth-Science Reviews 127, 203-241

van der Laan, E., Hilgen, F.J., Lourens, L.J., de Kaenel, E., Gaboardi, S., Iaccarino, S., 2012. Astronomical forcing of Northwest African climate and glacial history during the late Messinian (6.5–5.5 Ma). Palaeogeography, Palaeoclimatology, Palaeoecology 313–314, 107-126

Van Rooij, D., Blamart, D., De Mol, L., Mienis, F., Pirlet, H., Wehrmann, L.M., Barbieri, R., Maignien, L., Templer, S.P., de Haas, H., Hebbeln, D., Frank, N., Larmagnat, S., Stadnitskaia, A., Stivaletta, N., van Weering, T., Zhang, Y., Hamoumi, N., Cnudde, V., Duyck, P., Henriet, J.P., 2011. Cold-water coral mounds on the Pen Duick Escarpment, Gulf of Cadiz: The MiCROSYSTEMS project approach. Marine Geology 282, 102-117

Van Rooij, D., Blamart, D., Richter, T., Wheeler, A., Kozachenko, M., Henriet, J.P., 2007. Quaternary sediment dynamics in the Belgica mound province, Porcupine Seabight: ice-rafting events and contour current processes. International Journal of Earth Sciences 96, 121-140

Van Rooij, D., Iglesias, J., Hernández-Molina, F.J., Ercilla, G., Gomez-Ballesteros, M., Casas, D., Llave, E., De Hauwere, A., Garcia-Gil, S., Acosta, J., Henriet, J.P., 2010. The Le Danois Contourite Depositional System: Interactions between the Mediterranean Outflow Water and the upper Cantabrian slope (North Iberian margin). Marine Geology 274, 1-20

Vandorpe, T., Martins, I., Vitorino, J., hebbeln, D., García, M., Van Rooij, D., 2016. Bottom currents and their influence on the sedimentation pattern in the El Arraiche Mud Volcano Province, southern Gulf of Cadiz. Marine Geology 378, 114-126

Vandorpe, T., Van Rooij, D., de Haas, H., 2014. Stratigraphy and paleoceanography of a topography-controlled contourite drift in the Pen Duick area, southern Gulf of Cádiz. Marine Geology 349, 136-151

Viana, A.R., Almeida, W., Jr, Nunes, M.C.V., Bulhoes, E.M., 2007. The economic importance of contourites. Geological Society, London, Special Publications 276, 1-23

Voelker, A.H.L., Salgueiro, E., Rodrigues, T., Jimenez-Espejo, F.J., Bahr, A., Alberto, A., Loureiro, I., Padilha, M., Rebotim, A., Röhl, U., 2015. Mediterranean Outflow and surface water variability off southern Portugal during the early Pleistocene: A snapshot at Marine Isotope Stages 29 to 34 (1020–1135 ka). Global and Planetary Change 133, 223-237

Voigt, I., Henrich, R., Preu, B.M., Piola, A.R., Hanebuth, T.J.J., Schwenk, T., Chiessi, C.M., 2013. A submarine canyon as a climate archive — Interaction of the Antarctic Intermediate Water with the Mar del Plata Canyon (Southwest Atlantic). Marine Geology 341, 46-57

WÅhlin, A.K., Walin, G., 2001. Downward Migration of Dense Bottom Currents. Environmental Fluid Mechanics 1, 257-279

Wessel, P., Sandwell, D.T., Kim, S.-S., 2010. The global seamount census. Oceanography 23, 24-33

Wheeler, A.J., Beyer, A., Freiwald, A., de Haas, H., Huvenne, V.A.I., Kozachenko, M., Olu-Le Roy, K., Opderbecke, J., 2007. Morphology and environment of cold-water coral carbonate mounds on the NW European margin. International Journal of Earth Sciences 96, 37-56

Wienberg, C., Frank, N., Mertens, K.N., Stuut, J.-B., Marchant, M., Fietzke, J., Mienis, F., Hebbeln, D., 2010. Glacial cold-water coral growth in the Gulf of Cádiz: Implications of increased palaeo-productivity. Earth and Planetary Science Letters 298, 405-416

Wienberg, C., Hebbeln, D., Fink, H.G., Mienis, F., Dorschel, B., Vertino, A., Correa, M.L., Freiwald, A., 2009. Scleractinian cold-water corals in the Gulf of Cádiz—First clues about their spatial and temporal distribution. Deep Sea Research Part I: Oceanographic Research Papers 56, 1873-1893

Xu, J.P., Noble, M.A., Rosenfeld, L.K., 2004. In-situ measurements of velocity structure within turbidity currents. Geophysical Research Letters 31, n/a-n/a

Xu, Z., Yin, B., Hou, Y., Liu, A.K., 2014. Seasonal variability and north–south asymmetry of internal tides in the deep basin west of the Luzon Strait. Journal of Marine Systems 134, 101-112

Zhang, W., Hanebuth, T.J.J., Stöber, U., 2016. Short-term sediment dynamics on a meso-scale contourite drift (off NW Iberia): Impacts of multi-scale oceanographic processes deduced from the analysis of mooring data and numerical modelling. Marine Geology 378, 81-100

Chapter 9

Conclusions & outlook

Campaign 9: Alaska - Lutris (2015)

Chapter 9 – Conclusions and outlook.

The four main goals of this thesis were to

1. Investigate the region between the Strait of Gibraltar and 35°N in order to improve our understanding regarding the interaction between the position of drift systems, topographic obstacles and various oceanographic processes.
2. Unravel the spatial and temporal evolution of the drift systems in this region.
3. Make a first assessment on the amount, dimensions and initiation levels of the coral mounds in the Atlantic Moroccan coral province (AMCP) in order to investigate if a climatic and oceanographic signal can be detected.
4. Characterize typical contourite sequences using of X-ray computed tomography (CT) in order to improve the diagnostic criteria for identifying contourite facies.

The temporal evolution of the drift systems and the effect mud volcanism has on them was unravelled in Chapter 4, while the interaction between topographic obstacles, oceanographic processes and the spatial evolution of drift deposition was discussed in Chapter 5. The controlling factors for the build-up and maintenance of the ubiquitous coral mounds in the AMCP were discussed in Chapter 6, although the coral mounds themselves were mentioned already in Chapters 4 (interaction with the moat at the foot of the PDE) and 5 (mapping of all exposed coral mounds). Finally, the characterization of contourite facies (ranging from sheeted over mounded drifts to abraded surfaces) using CT scans was described in Chapter 7. A general discussion on the sediment drifts, coral mounds and CT analyses, indicating their broader applications are described in Chapter 8. Below, the main conclusions of these five chapters are highlighted and outlook-possibilities are indicated to improve, extend and apply these conclusions.

1. Conclusions

1.1. The climatic control on coral mound growth

A large amount of buried and surfacing coral mounds are present in the AMCP, making it the largest discovered coral province in the world so far. The coral mounds initiate at 10 different horizons with an onset at the start of the Early-Middle Pleistocene Transition, around 920 ka (Chapter 6). The initiation phases are linked to glacial periods, inferring a strong climatic dependence on coral mound growth. The coral mounds interact with the bottom currents which enable a larger influx of food particles and sediment to their skeleton (Chapter 6), induce small-scale mounded sediment drifts at their bases (Chapter 6) and deviate the bottom currents at the foot of the Pen Duick escarpment (Chapter 4). The AMCP is the first region in the world where the strong connection between climate changes and coral mound growth can be observed as ten different initiation horizons in the stratigraphic record (Chapters 4 and 8). The co-occurrence of sediment drifts (Chapters 4 and 5) and coral mounds makes the AMCP an ideal location to obtain a high-resolution palaeo-climatic and palaeoceanographic record, which will allow a better understanding of the temporal evolution of this region and how climate change affects these ecosystems.

1.2. The spatial and temporal evolution of the sediment drifts in the El Arraiche mud volcano province (EAMVP).

The spatial evolution of the sediment drifts in the EAMVP is influenced to a large extent by the topographic obstacles. Lateral variations along the Renard ridge occur several times; evidenced by drift deposits alternating with hemipelagic deposits; and are all linked to the steepness of the bounding topographies (Chapter 5) or the presence of topographic obstacles in the flow path of bottom currents (Chapter 4 and 5). Slopes with steepness's exceeding 11° are accompanied by sediment drifts, while more gentles ones are usually not. The mud volcanoes and even the coral mounds also induce the generation of small mounded drifts at their bases; the larger the obstacle, the more extensive the sediment drift is. When two sediment drifts are attached to a mud volcano, a more developed sediment drifts is located at the left side (looking down-current) due to Coriolis deflection (Chapter 5).

The onset of contourite deposition in the EAMVP happens at the start of the Quaternary, when sheeted drifts were formed along the Renard and Vernadsky ridges (Chapter 4). The temporal evolution of the sediment drifts is characterized by one major boundary, the Early-Middle Pleistocene discontinuity, marking the onset of mounded drift formation and coral mound growth in this region (Chapters 4 and 6). Ten subunits could be discerned, each linked to glacial marine isotopic stages (Chapter 4), yielding a tentative stratigraphy for the upper sequence. However, this stratigraphy contains some offsets compared to the stratigraphy derived from coral mound initiation in the AMCP (Chapter 6), inferring that either one or both stratigraphies contain wrong age-depth correlations (Chapter 8). Several factors contribute to the uncertainties related to the age-depth model, including the absence of clear tectonic controlling factors and the absence of absolute ages in both records (Chapter 8).

1.3. The link between oceanography and sediment drifts

Opposed to previous assumptions, Mediterranean outflow water does not play a major role in the build-up and maintenance of the sediment drifts in the EAMVP. The sediment drifts along the tectonic ridges are build up by glacial water masses, most likely glacial Antarctic Intermediate Water (gAAIW; Chapter 4 and 8), while they are maintained (or even further build up) during interglacials by a combination of North Atlantic Central Water (NACW) and AAIW (Chapter 5). Internal waves at tidal frequencies (i.e. internal tides) are created at the interface between these two water masses, resulting in alternating shore- and basin-ward currents (Chapter 5). The tidal currents aid in the maintenance of the sediment drifts along the Renard and Vernadsky ridge, while the sediment drifts along the mud volcanoes most likely originate due to deflected tidal currents with a more pronounced shore-ward component as more extensive sediment drifts are build up at the northern side of the large mud volcanoes (Chapter 5). Additionally, the passing of these tidal currents through a narrow passage between Renard ridge and Adamastor mud volcano induces the creation of a deep erosive channel with a small patch drift inside (Chapter 5).

All deposits resulting from internal waves could be called "internalites" (Bádenas et al., 2012). However, given the fact that some sediment drifts are the result of a combination of long-lasting contour-following bottom currents as well as by internal tides (Chapter 5), this term is not entirely fitting. Consequently, the preposition "tidal" has been proposed for sediment drifts resulting from both oceanographic processes, e.g. tidal patch drift or tidal mounded drift (Chapter 8).

1.4. The importance, extent and classification of sediment drifts

Several patch drifts are present in the EAMVP (Chapters 5 and 6), enabling to verify the classification proposed by Rebesco et al. (2005) and Hernández-Molina et al. (2008) for these drifts. Three main adaptations are proposed to their classification: (1) compressed patch drifts with one flow filament

should be considered, (2) a depositional tail (if present) is not detached from the topographic obstacle and (3) free-standing obstacles can have sediment drifts at both sides (Chapter 8). Based on these criteria, thousands of additional small-scale (patch) drifts may be discovered in the near future, allowing to compile a more detailed map of contourite-occurrence (Rebesco et al., 2014). These thousands of additional sediment drifts would render the map incomprehensible, leading to question the exact extent of sediment drifts, especially patch drifts. By defining the extent of patch drifts at the boundary where bottom current influence is not noticed any more in the sedimentary record, the map may even be further improved (Chapter 8). This might be beneficial for both science and industry as preferred investigation sites for palaeo-climatic and palaeoceanographic studies are easily recognized and locations where sediments are more prone to fail are mapped.

1.5. Diagnostic criteria for contourites

Based on CT analyses of 5 sediment cores from morphologically and texturally different sediment drifts, intervals of elevated bottom currents in contourite cores have been detected based on their higher Hounsfield unit (HU) values and possible erosional basal discontinuities (Chapter 7). These intervals contain either higher ratios of Zr/Al or coarser grains, both indicative of faster-flowing bottom currents. Moreover, sediment cores from different contourite areas can be compared regarding their HU values as cores from sheeted drifts have lower average HU values compared to mounded drift deposits, in turn having lower values compared to sediment cores from mainly erosional locations (Chapter 7). Although additional sediment cores from contourites, turbidites and pelagites need to be analysed to further document this link and investigate additional differences and/or pitfalls, promising results have been obtained which might lead to new and improved diagnostic criteria for distinguishing contourites (Chapter 8). Improved diagnostic criteria are required as distinguishing contourites from turbidites and pelagites is very valuable for hydrocarbon potential and palaeo-climatic studies. For the former, the differentiation is required since contourites may contain well-sorted sands and thus create suitable host rocks or create an impenetrable clay layer, which are perfect seals. For the latter, the distinction is important turbidites cannot contain a long-term palaeo record, they are created in a very short amount of time, while contourites can.

2. Outlook

2.1. Coral mounds

The AMCP is already the largest discovered coral mound province in the world so far, but its full extent is not yet precisely known, as multibeam data suggest that south and north of the AMCP additional exposed (and probably also buried) coral mounds are present (Hebbeln et al., 2008). Additional 2D and/or 3D seismic data have to be gathered across these regions in order to define the exact extent of this coral mound province and to determine whether additional levels of coral mounds initiation are present (Figure 9.1). The additional datasets will allow a better understanding of the evolution of cold-water corals under changing marine environments (climate and oceanography). This in turn can improve our understanding on how climate change will affect these organisms in the future (Freiwald et al., 2004).

The spatial and temporal evolution of the coral mounds was determined based on 2D seismic profiles (Chapter 6). In order to fully visualize the coral mounds, high-resolution 3D seismic data would be required though as they are able to display the morphology of the coral mounds most accurately and indicate exactly how many initiation horizons are present. The 3D P-cable system is a high-resolution 3D seismic imaging tool which ensures a better resolution (down to 3 m) compared to conventional 3D seismic systems and can achieve a much more accurate imaging (Petersen et al., 2010).

Consequently, it is at the moment the best method to visualize the coral mounds. Three suggested areas for 3D seismic data acquisition are indicated in Figure 9.1.

2.2. Stratigraphy

In order to determine a more precise stratigraphy of the AMCP, absolute ages have to be obtained from both the sedimentary and coral mound record. Having both records in the same region might prove valuable as hiatuses within the sediment record might be resolved by the coral mound record and vice versa. Therefore, several long sediment cores have to be obtained to be able to reconstruct a reliable stratigraphy. In 2014, several cores (up till 80 m) have been acquired during the "MoccoMebo" campaign in the AMCP (Figure 9.1), with both on- and off-mound sites. The long records might prove to be an onset towards a reliable stratigraphy, but even longer records are needed in order to penetrate the lower initiation horizons. Two options are possible to achieve this goal: the new MeBo corer, which can reach depths of 200 m (MeBo200, 2014), or requesting IODP cores, which could reach the Base Quaternary discontinuity, situated over 300 m below the seafloor. Such long records from the Pen Duick drift are required as well in order to fill in the hiatuses of the coral mound record. In addition, the elevated sedimentation rates of the Pen Duick drift, compared to the off-mound record in the hemi-pelagic area south of the EAMVP, will yield a higher-resolution stratigraphy, which will allow to assess the palaeo-environmental conditions in this region much more precisely.

2.3. Spatial variation of the sediment drifts

The link between various types of drift deposits, slope angles and bottom currents (mounded drifts are associated with elevated bottom currents, themselves related to steeper slopes of the tectonic ridges) raises the question how fast bottom current velocities are and which grain-size classes are present. The former question can be solved by acquiring long-term bottom current measurements, the latter may be resolved by acquiring sediment cores, e.g. by using a vibro-corer, gravity corer or piston corer, along strategic cross-sections in the AMCP (Figure 9.1). The analyses of these sediment cores will indicate how grain-sizes and consequently bottom currents vary spatially, but also how they vary through time.

A validation of the link between the slope angle of the obstacle and the occurrence of sediments drifts at their base (Chapter 5) is required before the concept can be applied on other regions. Regions containing several sediment drifts in close succession along topographic obstacles are suited for this purpose, e.g. the Galician margin where erosional as well as depositional features are created due to the deflection of northward flowing bottom currents on a complex basement topography (Haberkern et al., 2016).

2.4. Oceanography

The presence of internal tides raises many questions, e.g. how strong are these currents? What is their daily, weekly, monthly, yearly, etc. variability? How do they affect the slopes of the AMCP? A comprehensive work combining long-term oceanographic measurements, modelling bottom current patterns, geophysical and sedimentological research regarding internal tides and how they affect the continental slope is presented for the Gulf of Valencia (Ribó et al., 2013; Ribó et al., 2015; Ribó et al., 2016) or the Galician margin (Hanebuth et al., 2015; Zhang et al., 2016). A similar approach could be applied in the AMCP, especially as sediment waves are known to occur in the region south of the EAMVP (Figure 9.1). This means that long term (bottom) current measurements should be performed, e.g. by using moorings containing a down-ward looking ADCP, optical backscatter sensors and thermistor strings. Also, additional seismic profiles have to be acquired on the AMCP continental slope in order to visualize the sediment waves in higher detail. And sediment samples could be retrieved

from the area, indicating the grain sizes across the sediment wave field and across the sediment drifts. All of these suggestions are indicated on Figure 9.1. The numerical model applied by Zhang et al. (2016) in the Galician margin can be applied in the AMCP and can illustrate how the mud volcanoes and tectonic ridges interfere with the different bottom currents. By acquiring this extensive dataset and applying the numerical model, our understanding regarding internal tides and how they affect the ocean floor will improve significantly for this region. The concepts that will be developed by investigating the AMCP may be applied in similar settings elsewhere. As such, the AMCP can become a natural laboratory when it comes to internal tides, as it is the first regions where tidal sediment drifts are reported.
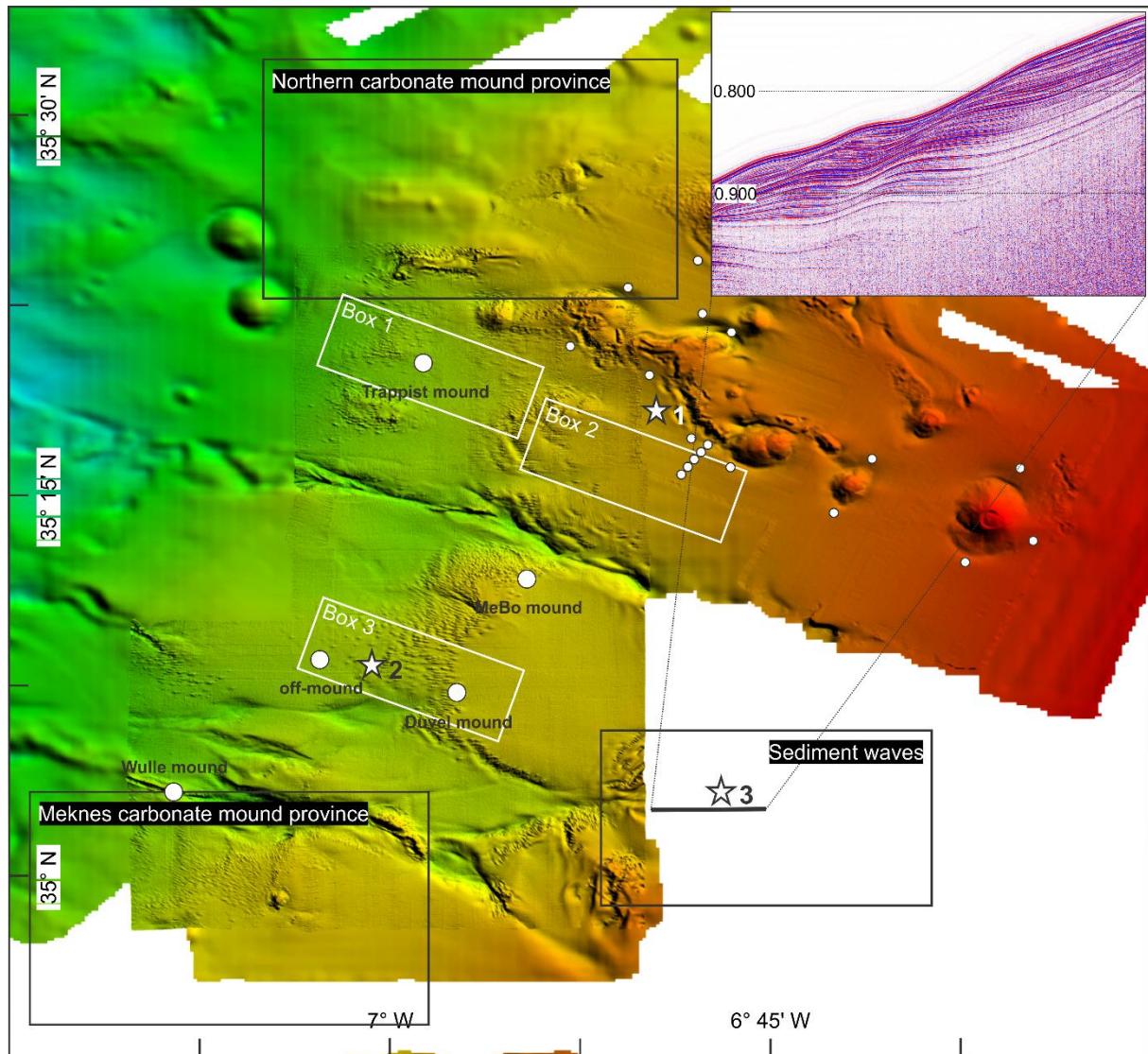

Figure 9.1: Proposed core sites, mooring stations, 2D seismic profiles and 3D seismic data locations for additional research in the AMCP. The small white dots indicate the proposed coring sites, each situated in different morpho-sedimentary regions and one transect across the Pen Duick drift. The big white dots indicate the MeBo drilling sites (Hebbeln et al., 2015).The white stars indicate the proposed sites for moorings. The sediment waves are displayed in the inset and the box around the region indicates where additional sparker seismic profiles could be acquired to examine these sediment waves. The Meknes and Northern carbonate mound province require additional sparker seismic profiles in order to investigate the buried coral mounds and determine the full extent of the AMCP.

2.5. Computed tomography and diagnostic criteria

The most important aspect concerning the CT-research in this dissertation concerns validation of the obtained results (Chapters 7 and 8). Additional sediment cores from contourites, turbidites and pelagites have to be analysed in order to find out their defining CT-characteristics and investigate the link between HU values and bottom current proxies. This should be performed ideally on sediment cores containing all three endmembers.

A second aspect that needs to be verified is the link between higher HU values and more energetic environments. Contourite cores from different morphological settings (sheeted, mounded and patch drifts as well as erosional surfaces) need to be analysed to confirm the hypothesis. By creating a large database of analysed contourite cores, general bounding values for components might be derived, rendering the histogram analysis (Chapter 7) for each core superfluous and decreasing the time required to apply the workflow immensely.

Finally, turbidites have the capability of lining up sedimentary particles, a feature preserved within sediment cores and visualized by µCT scanning (Van Daele et al., 2016). Although many contourites are associated with lower velocities compared to turbidites, generally below 50 cm/s (Stow et al., 2009) compared to velocities exceeding 100 cm/s (Piper and Normark, 2009), it might be possible that contourite sediments also contain particles that are lined-up according to the palaeo-flow direction. Similarly, µCT scans of sediment cores from contourites may indicate intervals of elevated bottom currents by sediments that are lined-up according to the prevailing flow direction. Additionally, if the sediment cores are oriented, they may indicate the palaeo-flow direction based on these µCT scans.

If contourites indeed possess unique CT-based characteristics, the set of diagnostic criteria can be expanded and differentiating them from similar deep-sea sediments will become easier. Additional research on this topic should therefore be prioritized.

References

Bádenas, B., Pomar, L., Aurell, M., Morsilli, M., 2012. A facies model for internalites (internal wave deposits) on a gently sloping carbonate ramp (Upper Jurassic, Ricla, NE Spain). Sedimentary Geology 271–272, 44-57

Freiwald, A., Fosså, J.H., Grehan, A., Koslow, T., Roberts, J.M., 2004. Cold-water Coral reefs, UNEP-WCMC, Cambridge, UK.

Haberkern, J., Schwenk, T., Hanebuth, T.J.J., Spiess, V., 2016. Morphology of small-scale contouritic depositional systems associated to topographic heights at the Galician margin (NW-Spain), 35th IGC, Cape Town, South Africa

Hanebuth, T.J.J., Zhang, W., Hofmann, A.L., Löwemark, L.A., Schwenk, T., 2015. Oceanic density fronts steering bottom-current induced sedimentation deduced from a 50 ka contourite-drift record and numerical modeling (off NW Spain). Quaternary Science Reviews 112, 207-225

Hebbeln, D., Wienberg, C., Bartels, M., Bergenthal, M., Frank, N., Gaide, S., Henriet, J.P., Kaszemeik, K., Klar, S., Klein, T., Krengel, T., Kuhnert, M., Meyer-Schack, B., Noorlander, C., Reuter, M., Rosiak, U., Schmidt, W., Seeba, H., Seiter, C., Strange, N., Terhzaz, L., Van Rooij, D., 2015. MoccoMeBo Climate-driven development of Moroccan cold-water coral mounds revealed by MeBo-drilling: Atlantic vs. Mediterranean settings - Cruise MSM36 - February 18- March 14, 2014 - Malaga (Spain) - Las Palmas (Spain), MARIA S. MERIAN -berichte, MSM36, DFG-Senatskommission für Ozeanographie, p. 47

Hebbeln, D., Wienberg, C., Participants, C., 2008. Report and preliminary results of RV Pelagia cruise 64PE284, Cold-water corals in the Gulf of Cádiz and on Coral Patch Seamont, Portimao-Portimao, 18.02-09.03.2008. Reports of the Department of Geosciences (GeoB) of the University of Bremen, University of Bremen, Germany, p. 90

Hernández-Molina, F.J., Llave, E., Stow, D.A.V., 2008. Continental slope contourites, in: Rebesco, M., Camerlenghi, A. (Eds.), Contourites. Elsevier, *Developments in Sedimentology*, ELSEVIER, pp. 379-407

MeBo200, 2014. https://www.marum.de/en/MeBo200.html,

Petersen, C.J., Bünz, S., Hustoft, S., Mienert, J., Klaeschen, D., 2010. High-resolution P-Cable 3D seismic imaging of gas chimney structures in gas hydrated sediments of an Arctic sediment drift. Marine and Petroleum Geology 27, 1981-1994

Piper, D., Normark, W., 2009. Processes that initiate turbidity currents and their influence on turbidites: a marine geology perspective. Journal of sedimentary research 79, 347-362

Rebesco, M., Hernández-Molina, F.J., van Rooij, D., Wåhlin, A., 2014. Contourites and associated sediments controlled by deep-water circulation processes: State of the art and future considerations. Marine Geology 352, 111-154

Rebesco, M., Richard, C.S., Cocks, L.R.M., Ian, R.P., 2005. Sedimentary environments: Contourites, Encyclopedia of Geology. Elsevier, Oxford, pp. 513-528

Ribó, M., Puig, P., Muñoz, A., Lo Iacono, C., Masqué, P., Palanques, A., Acosta, J., Guillén, J., Gómez Ballesteros, M., 2016. Morphobathymetric analysis of the large fine-grained sediment waves over the Gulf of Valencia continental slope (NW Mediterranean). Geomorphology 253, 22-37

Ribó, M., Puig, P., Salat, J., Palanques, A., 2013. Nepheloid layer distribution in the Gulf of Valencia, northwestern Mediterranean. Journal of Marine Systems 111–112, 130-138

Ribó, M., Puig, P., van Haren, H., 2015. Hydrodynamics over the Gulf of Valencia continental slope and their role in sediment transport. Deep Sea Research Part I: Oceanographic Research Papers 95, 54-66

Stow, D.A.V., Hernández-Molina, F.J., Llave, E., Sayago-Gil, M., Díaz del Río, V., Branson, A., 2009. Bedform-velocity matrix: The estimation of bottom current velocity from bedform observations. Geology 37, 327-330

Van Daele, M., Cnudde, V., Boone, M., Deprez, M., De Batist, M., 2016. On how X-ray (micro) computed tomography on turbidites can help us unravel paleoflow successions, directions and dynamics, EGU General Assembly 2016, Vienna, Austria

Zhang, W., Hanebuth, T.J.J., Stöber, U., 2016. Short-term sediment dynamics on a meso-scale contourite drift (off NW Iberia): Impacts of multi-scale oceanographic processes deduced from the analysis of mooring data and numerical modelling. Marine Geology 378, 81-100